Comptes Rendus
de l'Académie des sciences

1878-1535 (electronic)

Physique

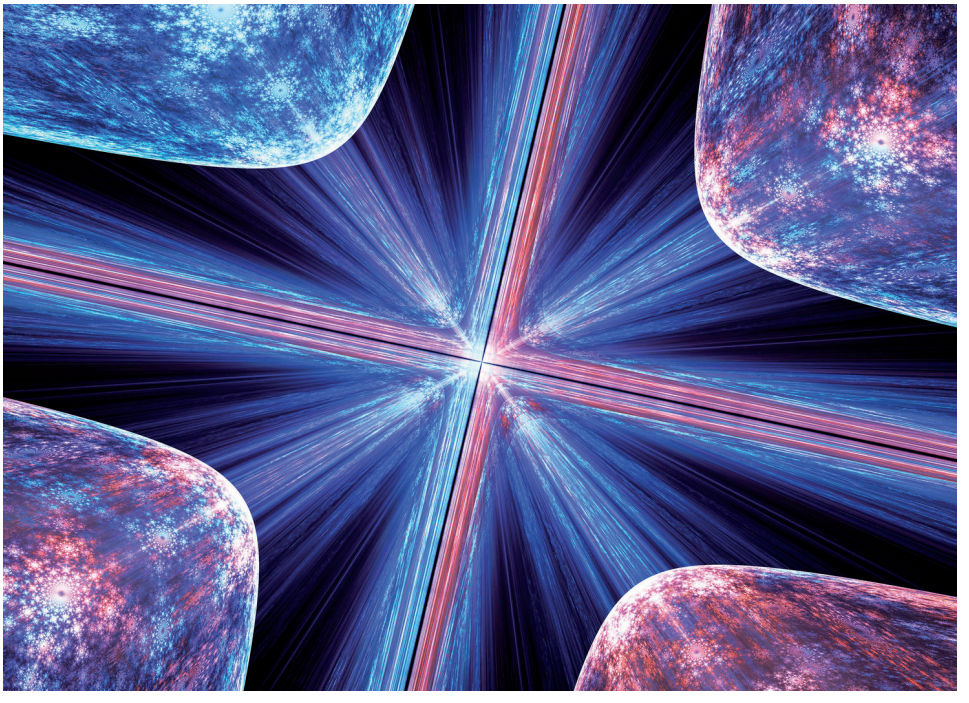

Volume 21, Special Issue 4-5, août-septembre 2020

Special issue / *Numéro thématique*
Metamaterials 1 / *Métamatériaux 1*

Guest editors / *Rédacteurs en chef invités*
Boris Gralak, Sébastien Guenneau

Académie des sciences — Paris

INSTITUT DE FRANCE
Académie des sciences

CENTRE MERSENNE

Comptes Rendus

Physique

Objective of the journal

Comptes Rendus Physique is a peer-reviewed electronic journal of international standing, covering all fields of physics and astrophysics. It publishes mainly thematic issues, but also original research articles, preliminary announcements, review articles, historical perspectives, pedagogical texts or conference proceedings, without length limit, in English or in French. It also publishes special issues devoted to certain recent and/or significant aspects of the discipline, whose authors are chosen from among the most active researchers on the subject and whose coordination is assured by guest editors.

Comptes Rendus Physique is published according to a virtuous policy of diamond open access, free for authors (no publication fees) as well as for readers (immediate and permanent open access).

About the journal

All journal's information, including the text of published articles, which is fully open access, is available from the journal website at https://comptes-rendus.academie-sciences.fr/physique/.

Author enquiries

For enquiries relating to the submission of articles, please visit this journal's homepage at https://comptes-rendus.academie-sciences.fr/physique/.

Contact

Académie des sciences
23, quai de Conti, 75006 Paris, France
Tel: (+33) (0)1 44 41 43 72
CR-Physique@academie-sciences.fr

Comptes Rendus
Physique
2020, 21, nº 4-5

Contents / *Sommaire*

Comptes Rendus
Physique
2020, 21, nº 4-5, p. 311-341
https://doi.org/10.5802/crphys.36

Metamaterials 1 / *Métamatériaux 1*

Foreword

Boris Gralak[*, a] **and Sébastien Guenneau**[b]

[a] CNRS, Aix Marseille Univ, Centrale Marseille, Institut Fresnel, Marseille, France

[b] UMI 2004 Abraham de Moivre-CNRS, Imperial College London, London SW7 2AZ, UK

E-mails: boris.gralak@fresnel.fr (B. Gralak), s.guenneau@imperial.ac.uk (S. Guenneau)

Metamaterial is a word that seems both familiar and mysterious to the layman: on the one hand, this research area born twenty years ago at the interface between physical and engineering sciences requires a high level of expertise to be investigated with advanced theoretical and experimental methods; and on the other hand electromagnetic paradigms such as negative refraction, super lenses and invisibility cloaks have attracted attention of mass media.

Even the origin and meaning of the word metamaterial (formed of the Greek prefix $\mu\varepsilon\tau\acute{\alpha}$ meaning beyond or self and the Latin suffix *materia*, meaning material) remains elusive. It seems that most researchers assume metamaterials is a term that refers to composites whose properties go beyond that found in ordinary materials, since it is well-known that the prefix "meta" appears in words like metaphysics and metaphysical. According to Martin Wegener at the Karlsruhe Institute of Technology, who played a pivotal role in the development of metamaterials, a good definition would be that « metamaterials are rationally designed composites allowing for effective medium composites that go qualitatively or quantitatively beyond those of the bulk ingredients ». However, some researchers might argue that this definition does not encompass the case of metamaterials that gain their unique properties from their structured interface, which is the case for instance of metasurfaces. Also, the emerging topic of space-time metamaterials, which in general are complex media with some periodic modulation of their properties both in space and time, can be homogeneous media just modulated in time, and thus actually not encompassed by the definition proposed by M. Wegener: indeed, a piece of glass could acquire extraordinary properties thanks to time modulations, even though it is not a composite. Therefore, looking at the existing literature and the variety of proposed definitions for what a metamaterial should be, it seems fair to say that there is not yet a "universal" definition of a metamaterial. This is especially so, because the term metamaterials is now in use across many fields of physical and engineering sciences, and it has even some applications in life and medical sciences.

Moreover, it is maybe less well-known amongst researchers working in the field of metamaterials that the prefix meta was also used in connection with mathematical logic one hundred years ago by the German mathematician David Hilbert in a research project entitled « metamathematics ». Hilbert implied that this was a project not only beyond ordinary mathematics, but also with

* Corresponding author.

self-referencing aspects (think for instance of « This sentence contains thirty-six letters », which is an example of sentence referencing itself). One can therefore argue that there is also some idea of multiple scales, and some interplay between them, in a metamaterial. Even if the first prototypes of electromagnetic metamaterials that appeared at the turn of this century, mostly consist of two scales (the scale of an elementary cell, made of resonant circuits, which is periodically arranged in space, and the scale of the overall composite consisting of hundreds of cells), the past few years have seen the emergence of hierarchical composites with multiple scales. However, it is not straightforward to identify the effective properties of hierarchical metamaterials, especially if the different scales are not well separated. And since their effective properties remain elusive, this might be another class of metamaterials, akin to Russian dolls (or Matrioshka), that is not covered by the definition of M. Wegener.

So, in these two special double volumes of the Comptes Rendus Physique, we assume a pragmatic approach, and we simply opt for the definition of metamaterials being some « complex media with rationally designed unusual properties » (but we do not claim they can be modelled as effective composites, and note that a time-modulated piece of glass is compatible with our definition). Now that we have made this word of caution, we would like to point out some important work that predates the birth of metamaterials: this field was not created ex nihilo, and as Sir Isaac Newton used to tell his mathematics students, we believe physics is like standing on the shoulder of giants to see the future. Thus, let us start by a prominent physicist and polymath.

John William Strutt, 3rd Baron Rayleigh (1842–1919) is most famous amongst the optics community for Rayleigh scattering (this explains why the sky is blue). However, Rayleigh waves that are, with Love waves, responsible for many of the earthquake disasters in human infrastructures, also bear the name of Rayleigh, who also contributed to light scattering, sound and hydrodynamic theories, color vision, elasticity theory and thermodynamics of gazes. Rayleigh's textbook, [The Theory of Sound, MacMillan and co., London, 1877], which appeared in two volumes, has been together with Augustus Edward Hough Love's monograph [Some Problems of Geodynamics, Cambridge University Press, Cambridge, 1911], an invaluable source of inspiration for generations of physicists, engineers, and mathematicians. He is viewed by many researchers in the theory of composites, as a precursor of homogenization theory, which is a branch of mathematics devoted to the analysis of partial differential equations with fast oscillating space-periodic coefficients. Lord Rayleigh, who became the second Cavendish Professor of Physics at the University of Cambridge in 1879 (following the death of James Clerk Maxwell), was awarded a Nobel Prize in Physics in 1904 for his « investigations of the densities of the most important gases and for his discovery of argon in connection with these studies », had three sons, the eldest of whom was to become Professor of Physics at Imperial College of Science and Technology in London.

Victor Veselago (1929–2018) is at the origin of the electromagnetic paradigm of negative refraction. He was a Russian physicist born in Crimea, who dedicated his life to electromagnetic waves, starting as a radio amateur during his teenage. The concept of negative refraction in isotropic media with simultaneaously negative permittivity and permeability, touched upon in the book by Sir Arthur Schuster [An Introduction to the Theory of Optics, London: Edward Arnold and Co., 1904], that mentions the possibility to have a Poynting vector opposite to the wave vector, was first put forward in a seminal paper by Veselago [Sov. Phys. Usp. 10, 509, 1968]. However, the technological breakthrough came with the discovery of Sir John Pendry and his colleagues that split ring resonators combined with thin straight wires would enable effective negative permittivity and permeability at certain microwave frequencies [Phys. Rev. Lett. 76, 4773–4776, 1996; IEEE transactions on microwave theory and techniques 47 (11), 2075–2084, 1999]. More precisely, in this seminal article Veselago showed that a plane-parallel plate of a negatively refracting medium would be an optical instrument capable of transmitting images without distortions. Maybe less

well known is Veselago's claim that under light absorption in a negatively refracting medium the light pressure changes by light attraction. In parallel to his scientific work on so-called magnetic semi-conductors, Veselago engaged an extensive pedagogical work. From 1961, he taught at the Moscow Institute of Physics and Technology (MIPT) and he delivered there the original course of the faculty cycle « The Basic Elements of Vibration Physics » and simultaneously conducted seminars and laboratory work at the Chair of General Physics. Veselago was one of the pioneers of the distribution of scientific information about the Internet in Russia: back in 1992, he already organized the mailing of the contents of scientific journals through the Internet. He invented the "Informag" system, which was useful to the Russian scientific community because of the disastrous situation with university libraries in the 90's. In 1998, Veselago organized the first reviewable electronic journal in Russia. He received a number of Russian and foreign awards for his scientific merits such as the 1976 State Prize of the former Soviet Union and in 2004 the Fock's Prize of the Russian Academy of Sciences. In 2009, Veselago received the medal of the American Optical Society for his work, which goes far beyond electrodynamics and optics. Indeed, Veselago's ideas have had tremendous significance in many fields of physics, and we shall present some of these in these two special double volumes of the Comptes Rendus Physique. Let us now present another physicist who has made landmark contributions to the field of metamaterials, which is further popularized well beyond the photonics community.

John Pendry worked as a young researcher on Low-energy electron diffraction at the Cavendish laboratory in Cambridge and after a postdoc on photoelectron spectroscopy at the Bell Labs, then in USA, in 1972–1973. He was then appointed head of the theory group at Daresbury laboratory of the Science and Engineering Research Council of the UK and then a Professor of Physics at Imperial College London in 1981. While in the Bell Labs, Pendry developed the first quantitative theory of so-called extended X-ray absorption fine structure for which he was awarded the Dirac Prize in 1996 and, as head of the theory group in Dalesbury, he published his theory of angle-resolved photoemission spectroscopy, which remains a standard model for probing the structure of the electrons in 1D and 2D crystalline structures, to this date. When he moved to Imperial College in 1981, he maintained a strong activity in his usual research area in surface science, but he also started to study the behavior of electrons in disordered media, and his scattering theory and computational methods for 1D and higher dimensional disordered media found some application in biology, relevant to conductivity of bio-molecules. All this former work led 25 years ago to his first seminal paper on photonic band structures, accompanied by the freeware he designed with his colleagues at Imperial College and the *Universidad Autonoma de Madrid* [Computer Physics Communications 85, 306–322, 1995] that made it possible to unveil extremely low plasmon polaritons in dilute metallic arrays of fibers [Phys. Rev. Lett. 76, 4773–4776, 1996], which together with the famous split ring resonators he proposed for artificial magnetism at the turn of the century [IEEE Transactions on Microwave Theory and Techniques 47, 2075, 1999], can be considered as the cornerstone of metamaterials for negative refraction. As we shall recall next, the physics of negative refraction—wherein light rays are refracted at an interface according to the Snell-Descartes laws in which the sign of one refractive index has been flipped—was introduced by the Russian physicist Veselago 30 years before Pendry proposed a route towards complex media that would make it possible. However, Pendry not only made negative refraction possible, but also negative index for evanescent waves and he further proposed that the convergent flat lens envisioned by Veselago has a theoretically unlimited resolution. As a twist to history, the so-called Rayleigh criterion (named after John William Strutt Rayleigh), which states that « two images are just resolvable when the center of the diffraction pattern of one is directly over the first minimum of the diffraction pattern of the other », could be overcome thanks to negative index, according to Pendry [Phys. Rev. Lett. 85, 3966–3969, 2000]. Pendry's article led to a scientific controversy, which has been resolved after a few years of heated debates, thanks to both experimental

and theoretical works, of physicists and mathematicians alike. Six years after his seminal paper on the perfect lens, Pendry proposed a route to invisibility via the concept of transformation optics, together with his colleagues David Schurig and David Smith at Duke University in Durham, USA [Science 312, 1780–1782, 2006]. This route known as « transformation optics » amounts to applying some geometric transformation to the Maxwell's equations, which can fortunately be written in a covariant form that avoids numerous technical difficulties that would arise for instance in the Navier equations for elasticity. However, even if Maxwell's equations behave well under a geometric transform, the invisibility cloak which results from a disc being mapped onto a ring (with the hole inside the ring being concealed to electromagnetic waves), requires the use of an anisotropic heterogeneous shell surrounding the object to cloak, and is different from the proposal of conformal optics put forward by Ulf Leohnardt at Saint-Andrews University in Scotland [Science 312, 1777–1780, 2006], which requires only some spatially varying refractive index, but at the cost of working in 2D geometries (conformal maps requiring a complex plane) and in the ray optics limit.

The research on metamaterials also benefited from important contributions by eminent researchers in physics and electrical engineering. We provide here a (non-exhaustive) list of some of them:

Sergei Tretyakov started his career as a research engineer at the Radiophysics Department of Peter the Great St. Petersburg Polytechnic University (formerly the Leningrad Polytechnic Institute in 1980). In the nineties, Tretyakov held an adjunct position at the Electromagnetics Laboratory of Helsinki University of Technology where he worked with Ismo Lindell, Ari Sihvola and Ari Viitanen with whom he published the influential book [Electromagnetic waves in chiral and bi-isotropic media, Artech House Antenna Library, Norwood, MA, USA, 1994] that presents a clear exposure of optical activity and chirality in electromagnetic media akin to metamaterials. During these years, he made important contributions to the theory of spatially dispersive media with Konstantin Simovski at the St. Petersburg Polytechnic University, where he got promoted full professor in 1996. In 2000, he moved to the Helsinki University of Technology as full professor of Radio Engineering, and was soon followed by Konstantin Simovski who holds the same position there. Tretyakov and Simovski have contributed to the career of a young generation of extremely talented research scientists, such as Pavel Belov (the present dean of the faculty of Physics at the ITMO University, formerly the Leningrad Institute of Fine Mechanics and Optics), and Mario Silveirinha (currently a professor of electrical engineering at the University of Lisbon), notably on strong spatial dispersion of wire media in the homogenization limit [Phys. Rev. B 67, 113103, 2003].

Nader Engheta received a BS degree in electrical engineering from the University of Tehran in Iran in 1978, the MS degree in electrical engineering and the Ph.D. degree in electrical engineering and physics from the California Institute of Technology (Caltech), Pasadena, California. After spending one year as a Postdoctoral Research Fellow at Caltech and four years as a Senior Research Scientist at Kaman Sciences Corporation's Dikewood Division in Santa Monica, California, he joined the faculty of the University of Pennsylvania, where he rose through the ranks and is currently H. Nedwill Ramsey Professor. He was the graduate group chair of electrical engineering from 1993 to 1997. He has made seminal contributions to the field of metamaterials, notably on epsilon-near-zero (ENZ) metamaterials that exhibit unique properties in light-matter interaction such as novel Purcell effects, plasmonic cloaking and optical nano circuitry. The plasmonic cloaking route he proposed with Andrea Alù [Phys. Rev. E 72, 016623, 2005] has led to new methods in stealth physics. He and his group have developed several areas and concepts in the fields of metamaterials and plasmonic optics, including, "extreme-parameter" metamaterials and ENZ metamaterials [Phys. Rev. B 75 (15), 155410, 2007]; He contributed to the emerging the field of graphene with the field of metamaterials and plasmonic optics in infrared regime,

providing the roadmaps for one-atom-thick optical devices and one-atom-thick information processing; microwave artificial chirality; « signal-processing » metamaterials, « digital » metamaterials and « meta-machine ». He is currently the H. Nedwill Ramsey Professor at the University of Pennsylvania, Philadelphia, Pennsylvania, USA, affiliated with the departments of Electrical and Systems Engineering, Bioengineering, materials science and engineering, and Physics and Astronomy. He is a Fellow of many international scientific and technical societies. His current research activities span a broad range of areas including nanophotonics, metamaterials, plasmonics, nano-scale optics, graphene optics, imaging and sensing inspired by eyes of certain animal species, optical nanoengineering, time-reversal symmetry breaking and non-reciprocity, microwave and optical antennas, mathematics of fractional operators, and physics and engineering of fields and waves. He has made pioneering contributions to the fields of electromagnetism and microwaves, metamaterials, transformation optics, plasmonic optics, nanophotonics, graphene photonics, nano-materials, nanoscale optics, nano-antennas and miniaturized antennas, physics and reverse-engineering of polarization vision in nature, bio-inspired optical imaging and fractional paradigm in electrodynamics.

Martin Wegener completed his PhD in physics in 1987 at Johann Wolfgang Goethe-Universität Frankfurt (Germany), he spent two years as a postdoc at AT&T Bell Laboratories in Holmdel (U.S.A.). From 1990–1995 he was professor at Universität Dortmund (Germany) and, since 1995, he has been professor at the Institute of Applied Physics of Karlsruhe Institute of Technology (KIT). Since 2001, he has held a joint appointment as department head at Institute of Nanotechnology of KIT. From 2001–2014 he was the coordinator of the DFG-Center for Functional Nanostructures (CFN) at KIT. Since 2019, he has been a co-speaker at the 3D Matter Made to Order center of excellence. His research interests comprise ultrafast optics, (extreme) nonlinear optics, near-field optics, optical laser lithography, photonic crystals, optical, mechanical, and thermodynamic metamaterials, as well as transformation physics. This research has led to various awards and honors, among which are the SPIE Prism Award 2014 for the start-up company Nanoscribe GmbH. In the past fifteen years, his research group has been particularly active in electromagnetic [Science 306, 1351–1353, 2004; Science 328, 337–339, 2010], mechanical [Applied Physics Letters 100, 191901, 2012; Phys. Rev. Lett. 108, 014301, 2012; Phys. Rev. Lett. 108, 014301, 2014; Proceedings of the National Academy of Sciences 112, 4930–4934, 2015; Science 358, 1072–1074, 2017] and thermal [Phys. Rev. Lett. 110, 195901, 2013] metamaterials. Muamer Kadic (currently assistant professor of physics at the University of Franche-Comté) has been involved in much of Wegener's work on mechanical and thermal metamaterials. Moreover, Wegener received the 2005 Descartes Prize together with Sir John Pendry, David Smith (who contributed essential articles such as the first experimental evidence of negative refraction [Phys. Rev. Lett. 84, 4184, 2000] and microwave cloaking [Science 314, 977–980, 2006]), Ekmel Ozbay and Kostas Soukoulis (who made important contributions to so-called all-angle negative refraction with photonic crystals [Nature 423 (6940), 604–605, 2004], which is a research area in photonics initiated by a theoretical paper coauthored by one of us [J. Opt. Soc. Am. A 17, 1012–1020, 2000]).

The 2005 Descartes Prize for EU research was awarded for the development of artificial structures with entirely new optical properties. Indeed, the European Union acknowledged that the research teams of these prominent researchers created and developed a novel class of artificial metamaterials, at that time called « left-handed materials », as the usual rule of thumb used to describe the triplet (**E**, **H**, **k**) should be performed with the left hand instead of the right hand as is conventional. Indeed, in ordinary isotropic media with simultaneously positive permittivity and permeability (hence a positive refractive index), the triplet (**E**, **H**, **k**) is right-handed and the wavevector k points parallel to the Poynting vector **S**, which is defined as the cross product of **E** and **H**. Whereas for simultaneously negative permittivity and permeability (hence a negative refractive index according to Veselago's seminal paper [Sov. Phys. Usp. 10, 509, 1968]), the

wavevector **k** changes direction and the triplet becomes left-handed (and **k** and **S** become antiparallel, hence the phase and group velocities point in opposite directions). Left-handed media are now known as « negative index materials » (NIMs), and their fascinating properties include negative refraction, inverse Doppler and Cerenkov effects and vacuum impedance matching possibility (so transparency) as discovered by Veselago more than 50 years ago [Sov. Phys. Usp. 10, 509, 1968]. But possibilities offered by NIMs include imaging not constrained by the diffraction limit as further pointed out by Pendry 20 years ago [Phys. Rev. Lett. 85, 3966–3969, 2000]. Fabrication of NIMs has opened up the possibility of novel applications and devices including sub-diffraction limited imaging and other subwavelength devices, as well as miniature antennas and waveguides, and artificial magnetic and bianisotropic materials. However, the 2005 Descartes prize did not foresee that electromagnetic metamaterials would find tremendous applications in other fields of physics. For instance, it was pointed out by Alexander Movchan and one of us in [Phys. Rev. B 70, 125116, 2004] that split ring resonators can be used to create low frequency stop bands in acoustics due to the fact that they behave like locally resonant structures that can be modelled by springs and masses, and thus can form the basis of negatively refracting index media in acoustics [New Journal of Physics 9, 399, 2007]. A similar claim was made by Jensen Li and Che Ting Chan around the same time [Phys. Rev. E 70, 055602, 2004]. However, it is the group of Ping Sheng which first unveiled the true potential of locally resonant sonic materials in a landmark article [Science 289, 1734–1736, 2000]. The group of Martin Wegener pushed the analogy drawn between optics and mechanics by introducing the concept of chiral mechanical metamaterials [Science 358, 1072–1074, 2017]. The latter could be the cornerstone for an elastodynamic cloak built from a Cosserat medium, as proposed by the applied mathematics group of Alexander Movchan at Liverpool University over a decade ago [Appl. Phys. Lett. 94, 061903, 2009]. Another possibility might be to approximate so-called Milton–Briane–Willis media [New Journal of Physics, 8 (10), 248, 2006] with chiral mechanical metamaterials [Phys. Rev. B 99, 214101, 2019].

Following the rise of graphene, carbon nanotubes and other two-dimensional new materials, researchers in metamaterials paid a special interest to composites similar to these two-dimensional materials. It is interesting here to note some connections with the work of Thomas Ebbessen who is a professor of physical chemistry at the University of Strasbourg in France. Ebbessen is known for his pioneering work in nanoscience. He received the 2014 Kavli Prize in Nanoscience for transformative contributions to the field of nano-optics that have broken long-held beliefs about the limitations of the resolution limits of optical microscopy and imaging, together with Stefan Hell (2014 Nobel prize in chemistry), and John Pendry. In 2019, Ebbessen was awarded the CNRS Gold medal in France. While working at the company NEC in the late eighties, Ebbesen discovered that it was possible to transmit light through subwavelength holes milled in opaque metal films under certain resonant conditions. The phenomenon, known as extraordinary optical transmission, involves surface plasmons. Surface plasmons remain a very active research area, with prominent researchers such as Stefan Maier [Plasmonics: fundamentals and applications Springer Science & Business Media, 2007], who started his carreer working with Harry Atwatter at the California Institute of Technology, notably publishing a landmark paper on Local detection of electromagnetic energy transport below the diffraction limit in metal nanoparticle plasmon waveguides [Nature Materials 2, 229–232, 2003] and who currently holds a professorship position at Imperial College London and at the Ludwig-Maximilian Universität München. We note that Stefan Maier has published numerous papers with John Pendry and Paloma Huidobro (a young and extremely talented researcher who has recently joined the group of Mario Silveirinha in Lisbon) on the control of surface plasmon polaritons using tools of transformation optics as well as optics of graphene.

Federico Capasso is another major contributor to the field of metasurfaces. He received the

doctor of Physics degree from the University of Rome in 1973 for his research on fiber optics, and he joined the Bell Labs in 1976. In 1984, he was made a Distinguished Member of Technical Staff and in 1997 a Bell Labs Fellow. He joined Harvard University as a professor in applied physics in 2003. Capasso and his collaborators made many wide-ranging contributions to semiconductor devices, pioneering the design technique known as band-structure engineering. He applied it to novel low noise quantum well avalanche photodiodes, heterojunction transistors, memory devices and lasers. Capasso and his collaborators invented and demonstrated the quantum cascade laser (QCL) [Science 264, 553–556, 1994]. Capasso's group showed that suitably designed plasmonic interfaces consisting of optically thin arrays of optical nanoantennas lead to a powerful generalization of the centuries-old laws of reflection and refraction. They form the basis of flat optics based on metasurfaces, which Capasso has popularized [Science, 334, 333–337, 2011; Nature Materials 13, 139–150, 2014] well beyond the photonics community.

Philippe Lalanne who is a Director of Research at CNRS at Institut d'Optique d'Aquitaine, can be certainly included in the pioneering researchers on metasurfaces with his seminal work on effective medium theory of sub-wavelength periodic structures [Journal of Modern Optics 43, 2063–2085, 1996] and on blazed binary subwavelength gratings [Optics Letters 23, 1081–1083, 1998]. Lalanne also brought essential contributions to electromagnetic numerical modelling with the highly improved convergence of the Fourier decomposition for periodic structures [J. Opt. Soc. Am. A 13, 779–784, 1996] and to photonics with the theory of the extraordinary optical transmission [Nature 452, 728–731, 2008]. He has been involved in computational electrodynamics and in applications of subwavelength optical structures for diffractive optics, plasmonics, photonic crystals, integrated optics and microcavities.

However, metamaterials are not only media designed with some space heterogeneity. One can also engineer properties of media by working on the time variable. Here, we would like to cite one researcher whose name is associated with time-reversal mirrors.

Mathias Fink received the Doctorat es-Sciences degree from Paris University in the area of ultrasonic focusing for real-time medical imaging under the supervision direction of Pierre Alais in 1978. In 1981, he was appointed Professor at the University of Strasbourg. After a stay as a visiting professor at the University of Irvine in the radiology department, he returned to France to become professor at the Paris Diderot University (Paris 7). In 1990 he founded the Waves and Acoustics Laboratory at Ecole Supérieure Physique Chimie Industrielle (ESPCI) in Paris, which became the Institut Langevin in 2009. In 2005, he was appointed professor at ESPCI, where he now is professor emeritus and holds the Georges Charpak chair (named after the Polish-born French physicist, who held the Joliot-Curie Chair at ESPCI and was the awarded the Nobel prize in Physics in 1992 for his invention and development of particle detectors). Fink pioneered the development of time-reversal mirrors and Time Reversal Signal Processing [Europhysics Journal Physics 15, 81, 1994; Wave Motion 20, 151, 1994; Phys. Rev. Lett. 79, 3170, 1997]. He developed many applications of this concept from ultrasound therapy, medical imaging, non-destructive testing, underwater acoustics, seismic imaging, tactile objects, to electromagnetic telecommunications. He also pioneered innovative medical imaging methods: transient elastography, supersonic shear imaging and multi-wave imaging that are now implemented by several companies. Six companies with around 400 staff have been created from his research: Echosens, Sensitive Object, Supersonic Imagine (which he cofounded notably with Charpak), Time Reversal Communications, Cardiawave, and GreenerWave. We note that Philippe Roux, a director of research at CNRS who is currently the head of Institut des Sciences de la Terre ISTERRE in Grenoble, has made important contributions to seismic metamaterials [Scientific Reports 6, 19238, 2016; Geophysical Journal International 220, 1330–1339, 2020] and is a former PhD student of Fink. Metamaterials is a small world ranging from ultrasonics to geophysics.

Another important contributor to the field of seismic metamaterials is Stéphane Brûlé, a researcher in seismic risk assesment, soil-structure interaction, who is also a senior geotechnical engineer, holder of a master's degree research from Ecole Normale Supérieure de Paris and Pierre and Marie Curie University and an engineering diploma in geotechnics of Grenoble-Alpes University in the field of soil mechanics, ground improvement and deep foundations. Brûlé is the leading author of the foundation paper for the field of seismic metamaterials [Phys. Rev. Lett. 112, 133901, 2014] that he coauthored with Emmanuel Javelaud (who was back in 2012 an engineer and researcher in Brûlés research group at Ménard), Stefan Enoch (director of research at CNRS) and one of us. He also led the first experiment on lensing of surface Rayleigh waves via negative refraction [Scientific Reports 7, 18066, 2017]. He is a member of the International Technical Committee 203 « Geotechnical Earthquake Engineering and Associated Problems », is also an active board-member of the French committee of soil mechanics (CFMS) and of the French earthquake engineering association (AFPS).

Finally, in the tracks of Lord Rayleigh, some eminent researchers working in applied mathematics and theoretical mechanics have contributed to the development of metamaterials. We have already cited many famous researchers (some of whom will appear in what follows as they are contributors to the two special double volumes). Nonetheless, we are well aware that many great scientists do not appear in our preface, and we would like to apologize for that. But trying to be more exhaustive, would lead us far beyond the scope of this preface. So let us just mention Alain Bensoussan, Jacques-Louis Lions and Georges Papanicolaou for their landmark book on homogenization theory [Asymptotic Analysis for periodic structures, North-Holland, 1978], and Habib Ammari, Allan Greenleaf, Robert Kohn, Michael Vogelius and Michael Weinstein for their seminal contribution to the mathematical theory of cloaking, and of the members of the mathematics laboratory POEMS of Anne-Sophie Bonnet Ben-Dhia at ENSTA in Palaiseau, which is a leading laboratory for the research on corners consisting of a frequency dispersive medium that share some features with the physics of black-holes. Our list is obviously far from being exhaustive and we would like to apologize for missing other eminent researchers. Let us however, pay a special attention to the work of two mathematicians, since the latest developments of spatially and temporally modulated metamaterials point towards their seminal work. Konstantin Lurie graduated with a Master of Science from the Leningrad Polytechnic Institute in 1959 and a PhD from the Physical-Technical Institute five years afterwards. He obtained the equivalent of the French « Doctorat d'Etat » from the same institute in 1972. His research has been devoted since the sixties to optimal material design. The journal papers and books he published have laid the mathematical foundation of this discipline, as we know it today. The need for optimal design comes from various technological requirements such as devices, which are produced with a better quality, less weight, at a lower cost and with faster fabrication. As explained by Lurie, there are strong ties between optimal design and physics, mechanics, biology, and natural science in general. Optimality embraces many fields such as communication systems and nanostructural design, or traffic control. We note that Andrej Cherkaev, another key player in the theory of composites, contributed a few influential works with Konstantin Lurie, and there is even a landmark work these researchers published with Graeme Milton and Marco Avellaneda on the conductivity of polycrystals and a phase-interchange inequality [Physica A: Statistical Mechanics and its Applications 157, 148–153, 1989] Lurie extrapolated these principles to material dynamics by introducing a novel concept of dynamic materials [An Introduction to the Mathematical Theory of Dynamic Materials, Springer, 2007], and in this way he has laid the mathematical foundations for metamaterials with properties variable in space and time. Space-time metamaterials has become a fast-developing area of metamaterials.

John Willis is Emeritus Professor of Theoretical Solid Mechanics in the University of Cambridge. He graduated from the Department of Mathematics at Imperial College London where

he was an Assistant Lecturer in 1962–1964, before working as a Research Associate at the Courant Institute in New-York during one year. From 1965 to 1972, he was a Director of Research at the Department of Applied Mathematics and Theoretical Physics (DAMTP) of Cambridge University, and then a Professor of Applied Mathematics in Bath University until 1994. He was back as a Professor of Theoretical Solid Mechanics at DAMTP from 1994 to 2007, as well as being Professor of Mechanics at Ecole Polytechnique from 1998 to 2004. He was Editor of the Journal of Mechanics and Physics of Solids for a quarter of a century (from 1982 to 2006). Major research interests of Willis have included static and dynamic problems for anisotropic media, problems of irradiation damage of materials, structural integrity, effective properties of composite materials (both static and dynamic), mechanics of nonlinear composites, stability of strained-layer semiconductor devices. Recent work has been on strain-gradient plasticity and the dynamics of composites (as applied to acoustic metamaterials). He was elected a Fellow of the Royal Society in 1992, a Foreign Member of the US National Academy of Engineering (2004) and a membre Associé Etranger of the French Académie des Sciences (2009). So-called Willis media, named after his seminal paper on variational and related methods for the overall properties of composites that led to new governing equations for elastodynamics waves propagating within heterogeneous media [Advances in Applied Mechanics, 21, 1–78, 1981], are an area of elastic metamaterials with very intense research activity. Besides from these groundbreaking articles, Willis published some important work on the dynamical interpretation of flutter instability in a continuous medium, [J. Mech. Phys. Solids 54, 2391–2417, 2006], as well as some landmark paper on modifications of Newton's second law and linear continuum elastodynamics, which he coauthored with Graeme Milton, another eminent mathematician [Proc. Roy. Soc. A 463, (2007), 855–880, 2007].

As we suggested with the « metamathematics » of David Hilbert, metamaterials is a subject at the interface between physics and mathematics (notwithstanding the importance of engineering sciences that will come next in the preface). We are honoured to have the polymath Graeme Milton as a contributor of the two special double volumes, who is a Distinguished Professor at the University of Utah and also a Full Professor at Courant Institute of Mathematical Sciences in New-York. When a Master student at Sydney University he published a seminal paper on Bounds on the complex dielectric constant of a composite material [Appl. Phys. Lett. 37, 300–302 (1980)], that lays the foundations of the so-called Bergmann–Milton theory of bounds. Milton's undergraduate honors' thesis was on « Theoretical studies of the transport properties of inhomogeneous media », under the direction of Ross McPhedran who introduced him to the field of composite materials, resulting in the aforementioned publication that received according to Milton more reprint requests than any of his subsequent papers. He did his Ph.D thesis on Some Exotic Models in Statistical Physics at Cornell University Physics Department with Michael Fisher, then a postdoc with Michael Cross at Caltech as a Weingart Fellow, and George Papanicolaou (who coauthored with Alain Bensoussan and Jacques-Louis Lions the classical book on homogenization theory [Asymptotic Analysis of Periodic Structures, North-Holland, New-York, 1978]) suggested he apply for an assistant professorship at the Courant Institute, where he got tenure and was promoted to Associate Professor after two years, and later to Full Professor. Twenty five years ago, he published with his colleague Andrej Cherkaev a breakthrough article entitled « Which elasticity tensors are realizable? » [Journal of Eng. Mat. and Technology 117, 483–493, 1995], that introduced a whole new class of composites with unprecedented elastic properties. So-called Pentamode media have been made a reality five years ago thanks to the group of Martin Wegener [Phys. Rev. Appl. 2, 054007, 2014]. In 1999, he became Distinguished Professor of the University of Utah Mathematics Department, and served as department chair from 2002–2005. He published another classical book [The Theory of composites, Cambridge University Press, Cambridge, 2002] that echoes that of Bensoussan, Lions and Papanicolaou. These two books will still serve as an inspiration for physicists and mathematicians working in the field of metamaterials for the years to

come.

The paradigm shifts of negative refraction and cloaking have fueled the interest in metamaterials. Thus far, we have presented prominent researchers in this field, whose works are cited in the 14 articles of these two special double volumes. However, as guest editors of the Comptes Rendus Physique, we have the great pleasure to gather in these double volumes' contributions by other highly distinguished, and extremely gifted, chemists, physicists and mathematicians who have also made landmark contributions to the field of metamaterials.

By alphabetical order, we start with Andrea Alù who graduated with a PhD from the University of Roma Tre in 2007. After spending one year as a postdoctoral research fellow working with Prof. Nader Engheta at the University of Pennsylvania, Philadelphia, in 2009 he joined the faculty of the University of Texas at Austin where he is currently a Senior Research Scientist and an Adjunct Professor. He joined the City University New-York in 2018 as a Professor and the founding director of the Photonics Initiative for its Advanced Science Research Center. He remains affiliated with the Applied Research Laboratories at the University of Texas at Austin, where he is involved in research projects on electromagnetics and acoustics. His current research interests span over a broad range of areas, including metamaterials and plasmonics, electromagnetics, optics and photonics, scattering, cloaking and transparency [Phys. Rev. E 72, 016623, 2005], nanocircuits and nanostructures modeling, miniaturized antennas and nanoantennas, radio frequency antennas and circuits, acoustic and mechanical devices and metamaterials. Alù is currently the President of the Metamorphose Virtual Institute for Artificial Electromagnetic Materials and Metamaterials, and a member of the Administrative Committee of the IEEE Antennas and Propagation Society. Since 2014, Alù has been also serving as Chief Technology Officer of Silicon Audio RF Circulator, a company that holds the exclusive license of a few inventions stemming from Alù's lab around magnetic-free technology for non-reciprocal devices.

Yuri Kivshar studied at the Kharkiv school founded by the Nobel prize laureate Lev Landau. In 1984, he received Doctor of Philosophy degree and in 1989 aged 30 he became the youngest research fellow of Verkin Institute for Low Temperature Physics and Engineering. From 1991 he worked as a scientist in USA, Finland, Spain, Germany and in 1993 was invited to the Optical Sciences Centre of Australia and later founded his own laboratory Nonlinear Physics Centre of Autralian National University. Starting from 2000 Yuri Kivshar worked in different fields of nonlinear optics and carried out research of solitons and metamaterials, nonlinear photonic crystal and composite materials theories. He made fundamental impact into self-focusing effect, metamaterials, dielectric nanoantennas, topological insulators, optic signal processing and optical communications. He also discovered series of solitons and described their dynamic properties in nearly integrable systems. In 2010, Yuri Kivshar was invited to St. Petersburg thanks to the government Megagrant program. He became a scientific leader of the International Research Centre for Nanophotonics and Metamaterials of the ITMO University (Saint-Petersburg, Russia). Throughout his exceptionally prolific career, Yuri Kivshar has made landmark contributions to many fields of physics and he also contributed to the dissemination of ideas of non-linear optics in photonic crystals and metamaterials, notably with the classical book he coauthored with Govind Agrawal [Optical solitons: from fibers to photonic crystals, Academic press, New-York, 2003]. Last, but not least, the work of Yuri Kivshar has received over 80,000 citations according to Google Scholar (with an h-index of 130) which suggests the profound impact his work has in the field of photonics. Besides from that, he has developed an amazing number of collaborations with research groupings worldwide. His extraordinary scientific life is thus reminiscent to that of the mathematician Paul Erdôs who published work with more than 500 collaborators, which prompted the creation of the Erdôs number, the number of steps in the shortest path between a mathematician and Erdős in terms of co-authorships.

Ross McPhedran completed his undergraduate studies and PhD at the University of Tasmania, before moving to Sydney in 1975 as a Queen Elizabeth II Fellow. He was appointed a Senior Lecturer in the School of Physics at Sydney University in 1984, and was promoted to a Personal Chair in 1994. His interests range over many aspects of wave theory, photonics, microstructured fibres, elastodynamics, composite science, mathematical methods and numerical algorithms. McPhedran has made seminal contributions to the field of wave science, its techniques and applications. These have provided methods of unprecedented accuracy and insights which have enabled major developments in the performance of microstructured optical fibres, composite materials, diffraction gratings, photonic and platonic crystals (the latter are crystal plates coined platonics by McPhedran perhaps in reference to Plato, the Athenian philosopher of Ancient Greece). The multipole formulation has been developed as a major tool for solving scattering problems involving electromagnetic and elastic waves with both periodic and finite systems for applications like spectroscopy and photovoltaic and photothermal energy conversion. The associated tools of lattice sums, density of state functions, mode and defect analysis have advanced understanding and methodologies of wave science. Ross McPhedran has played a pivotal role in the career of many research scientists, including one of us. He has attacked during his exceptional career problems ranging from applied physics [Physics World 26, 32, 2013] to pure mathematics [https://arxiv.org/pdf/2003.14241.pdf].

We have presented some of the prominent scientists in the physical, mathematical and engineering sciences, who in our opinion have shaped the field of metamaterials and the theory of composites in general. We do not claim to be exhaustive as the list of prominent scientists who contributed to metamaterials is vast: this list only reflects the opinion of the guest editors. However, as often in sciences, research advances are the work of many individuals and groups who contribute to the dissemination and improvement of great ideas of a happy few. Let us remind another point of history that in the late 1940s, Winston Kock from AT&T Bell Laboratories developed materials that had similar characteristics to metamaterials. In the 1950s and 1960s, artificial dielectrics were studied for lightweight microwave antennas. Then, microwave radar absorbers were researched in the 1980s and 1990s as applications for artificial chiral media. These devices can be considered as complex media with rationally designed unusual properties, so are encompassed by our definition of metamaterials (and also that of Wegener).

Since 1999, researchers who have contributed to this field of metamaterials, include pure and applied mathematicians, theoretical and applied physicists, but also chemists, biologists, mechanical engineers and also geophysicists. Therefore, electromagnetic metamaterials are just one side of the coin. Indeed, correspondences between the governing equations for electromagnetic waves and acoustic, elastodynamic and hydrodynamic waves have allowed to translate unusual phenomena first discovered in electromagnetism to other fields and find exciting applications. For instance, the invisibility cloak proposed by Pendry and his colleagues [Science 312, 1780–1782, 2006] to show the true potential of electromagnetic field control by metamaterials, has been then designed for pressure waves and it might improve the acoustics of concert halls by acoustically concealing columns. One of us has even proposed that seismic metamaterials might provide protection from earthquakes by rerouting or diverting seismic waves with a gigantic invisibility cloak akin to Pendry's cloak for electromagnetic waves. Allied to designing or creating devices, many interesting conceptual questions naturally arise, for instance one recurring question is the reciprocity principle: If light cannot reach a fictional character covered by an invisibility cloak, can he or she see the outer world? In fact, he or she would be in complete darkness if the cloak would have no eyeholes; these two defects in the cloak could then be perceived by an outer observer. Similarly, in other wave systems, one has to think of the consequences of such cloaking or devices, for instance, the invisibility region should act as a quiet zone if one were to design a cloak for acoustic or seismic waves.

Thus far, the physics of negative refraction and cloaking (i.e. of invisibility cloaks) seem dissociated topics, but they reunite in the theory of external cloaking proposed by Graeme Milton and Nicolae Nicorovici [Proc. Roy. Soc. A: Mathematical, Physical and Engineering 462, 3027–3059, 2006]. In this approach, the invisibility cloak consists of a negatively refracting shell, and what's more, the object to conceal lies outside the cloak! The design of an external cloak is radically different to Pendry's cloak, since the latter is based on anisotropic features of the shell (or cloak) surrounding the object to hide. It defies the above arguments of reciprocity principle since the fictional character is no longer surrounded by the cloak, but it lives somewhat in a space-folded region, known as a Riemann sheet, that is not sensed by light illuminating the external cloak and the fictional character. Other counterintuitive physics is that of topological insulators, which are complex media that support a host of symmetry-protected surface states, and are also encompassed by our definition of metamaterials.

The present two special double volumes of the Comptes Rendus Physique aim to draw an overview of the topic of metamaterials. This collection of fourteen articles, carried out with the cooperation of leading international experts in the field of metamaterials, includes original research as well as more review-oriented contributions. The articles cover the topics of electromagnetic, acoustic, elastic, and seismic metamaterials and are organized in two sets gathering on one side, articles more-oriented on concepts and models and on the other side, articles reporting results more related to promising potential applications. The two double volumes thus cover theoretical as well as experimental and fundamental as well as applied aspects in different areas of metamaterials from nanoscale (electrodynamics and plasmonics) to meter-scale (geophysics) media.

In the first of the two double volumes, the first set of seven articles starts by a survey of the physics of negative index materials at the frontier of macroscopic electromagnetism, by one of us. In this contribution, the new phenomena and questions brought by the negative refraction, negative index, perfect flat lens and corner structures are discussed within the frame of macroscopic electromagnetism. As a continuation, an analog of « black hole » phenomenon is highlighted in simple corner structures filled with frequency dispersive permittivity and arguments are provided to support that, in passive media, the imaginary part of the magnetic permeability can take positive and negative values.

It is followed by an article on first principle homogenization with application to wire media by Mario Silveirinha *et al.*, which presents an overview of a homogenization theory for periodic metamaterials. This *ab initio* general approach can be considered as an extension to periodic metamaterials of the frame developed in order to derive the phenomenological equations of macroscopic electromagnetism and represents a remarkable counterpart to the usual homogenization theories established in applied mathematics. The proposed approach is applied to various cases of two-dimensional and three-dimensional electromagnetic wire media allowing to highlight a variety of exotic phenomena and the effect of spatial dispersion.

The next article on transformation optics for plasmonics, by Paloma Huidobro and Antonio Fernandez-Dominguez, reviews the latest theoretical advances in the application of transformation optics for the theoretical description of sub-wavelength plasmonics structures. This article starts with an introduction to the technique of transformation optics. The technique is notably applied to the design of metasurfaces with singular geometries, obtained by mapping an infinite extended volume to a plasmonic nanoparticle, which enable broadband absorption and provide platform for investigation of spatial dispersion. The technique is also exploited to determine analytically the coupling of a quantum emitter with plasmonic nano-particles.

The article by Graeme Milton and Ross McPhedran is a review of anomalous resonance, the associated cloaking, and superlensing. The authors adopt an original and interesting viewpoint

on the history of external cloaking and the superlensing, alternative to the ones generally found in the literature, based on the discoveries of ghost sources and anomalous resonances back in 1994. This theoretical article brings a nice introduction to cloaking due to complementary media for quasistatics and fine analyses of anomalous resonances, cloaking and superlensing in the limit as the absorption goes to zero.

The next article on all-dielectric Mie-resonant metaphotonics by Nicolas Bonod and Yuri Kivshar draws the advantages of all-dielectric subwavelength structures when compared with their plasmonic counterparts. This article starts with a review on the electric and magnetic resonances with low multipolar order leading, without metals, to artificial optical magnetism and negative effective permeability. Then is shown how these resonances can be used to achieve the Kerker effect and the Kerker conditions from dielectric particles, and to design all-dielectric nanoantenna for the enhancement of the excitation strength of quantum emitters. This concept of dielectric resonances is applied to the design of all-dielectric metasurfaces for bound states in the continuum and for generating colors and holograms.

Philippe Barois *et al.* contributed a review article on bottom-up nanocolloidal metamaterials at optical frequencies. This article, mainly experimental, reports the design and the fabrication, from nanocolloidal meta-atoms assemblies, of three-dimensional metamaterials in the visible range. The metamaterials are in addition characterized in terms of effective permittivity and permeability. Both kinds of metamaterials involving plasmonic or Mie resonances are addressed, showing for each the powerfulness and drawbacks. Metasurfaces for flat optics and perfect absorbers applications are also addressed.

The last contribution of the first set of articles, by Romain Fleury, Andrea Alù and Farzad Zangeneh-Nejad, addresses the emerging topic of topological wave insulators. This review article starts with the simple one-dimensional example of the Su–Schrieffer–Heeger (SSH) model and then turns to two-dimensional situations, discussing classical wave analogues of Chern, quantum Hall, spin-Hall, Valley-Hall, and Floquet topological insulators. The most recent developments are also reviewed. This article draws a remarkable interdisciplinary research topic with the transposition of concepts, originally discovered in condensed matter systems, to classical wave physics: photonics, microwaves, phononics, acoustics and mechanics.

In the second double volume, the second set of seven articles, where promising applications are reported, is opened with a contribution on tunable metasurface-based waveplates by Nader Engheta and Nasim Estakhri. The authors propose an innovative type of waveplate, for full control on phase retardation and light polarization, consisting of two symmetric metasurfaces separated by a varying distance. The metastructures are designed by inverse design topology optimization. Several numerical examples are shown, including metastructures designed from a genetic algorithm and compatible with currently available fabrication techniques in the visible range.

The following article is a survey in the visible range of dispersion and efficiency engineering of metasurfaces by Benfeng Bai *et al.* Metasufaces allow the manipulation of electromagnetic waves from the strong resonant behaviors of varied meta-atoms arranged in a subwavelength lattice. After introducing metasurfaces, their advantages and drawbacks, the authors review the recent endeavors in solving the limitations of metasurfaces due to their dispersion and low efficiency. The dispersion and efficiency of metasurfaces are engineered according to the specific applications: ultra-highly sensitive sensing, field modulation, nonlinear interactions, full-color imaging, holographic display…

Metasurfaces are again considered in the article on metasurfaces for thin antenna applications by Massimiliano Casaletti *et al.* In this contribution, metasurfaces are considered for microwaves, where standard circuit technologies can be used for easy fabrication and integration. The authors review the latest progress in metasurface antenna design, where metasurfaces are exploited to

miniaturize the profile, increase the bandwidth, and control the radiation pattern in the near- and far-field regions.

The next article, by S. Anantha Ramakrishna *et al.*, focuses on the properties of waveguides filled with anisotropic metamaterials. The authors show how metamaterials based waveguides offer a whole new range of novel features exploiting anisotropic permittivity and permeability that can have vanishing or even sign-shifting eigenvalues. Zero-index and hyperbolic waveguides lead to modes with fractional and even imaginary orders. They may have potential applications in near-field optical microscopy, Laser amplification, harmonic generation, or self-phase modulation that can occur over short lengths of the waveguide.

The article by Vicent Romero-Garcia *et al.* initiates the series of contributions on classical waves other than electromagnetic with a survey on the design of acoustic metamaterials made of Helmholtz resonators for perfect absorption. The authors first report a robust technique for the design of acoustic metamaterials based on the analysis of the zeros and poles of the eigenvalues of the scattering matrix in the plane of complex frequencies. Then several examples of perfectly absorbing one-dimensional structures and membranes are reviewed. In particular, the possibility to obtain perfect absorption by some defined critical coupling conditions is discussed in detail.

That article on acoustic metamaterials is followed by the review article on the theory and design of metamaterials in mechanics by the metamaterial group of Muamer Kadic at FEMTO-ST. In this article, the authors present the general procedure of designing elastic metamaterials based on masses and springs. It is shown that using this simple approach, any set of effective properties can be designed, including linear elastic metamaterials—defined by bulk modulus, shear modulus, mass density—and nonlinear metamaterials—with instabilities or programmable parts. The designs and the corresponding numerical calculations to illustrate different constitutive behaviors are presented.

The last article of the second special double volume by Stéphane Brûlé at DGI-Ménard Inc and one of us is on the role of seismic metamaterials on soil dynamics. The article actually focuses its attention on control of soils structured by an array of boreholes (that are more akin to photonic crystals than metamaterials, as they essentially work in the Bragg regime), that have been shown to allow for shielding and focusing effects. Some previously unpublished experimental results show the potential for energy harvesting of ambient seismic noise of the array of boreholes. The authors further proposed to bridge the field of time-modulated media and seismic metamaterials in order to generate some new effects leading notably to a concept of analogue seismic computer and some internet of things using seismic ambient noise on a geophysics scale.

In conclusion, these two special double volumes of the Comptes Rendus Physique touch upon many topical subjects in the physics of acoustic, elastic, electromagnetic metamaterials, which were discovered less than a quarter of a century ago. These two double volumes cover theoretical as well as experimental aspects in these different areas from nanoscale (optics and plasmonics) to meter-scale (civil engineering in seismics) passing through microwaves, acoustics and mechanics. Emerging topics like topological insulators and numerous promising applications from metasurfaces have been addressed. The fourteen articles constituting these two double volumes give a comprehensive survey of recent advances in this mature field. Much remains to be discovered and doubtless the future will be exciting, we hope that the present collection of articles will help foster theoretical and experimental efforts in metamaterials. We stress that all these contributions promise to revolutionize ways of controlling the propagation of sound, light, and any particular form of waves at macroscopic and microscopic scales. Indeed, potential applications range from subwavelength lensing and optical waveguides, to biosensors and full control of light ellipticity, to enhanced excitation strength of quantum emitter and nonlinear interactions, to flat optics and holographic display, to

perfect absorption in acoustics and metasurface antenna, to underwater camouflaging and electromagnetic invisibility, to manipulation of visible light and protection from harmful physical waves (e.g., tsunamis and earthquakes).

We would like to convey our warmest thanks to all authors, who are the principal architects of this special volume of the Comptes Rendus Physique published by the French Academy of Sciences, for their excellent scientific contribution and their willingness to share their knowledge of the mathematics and physics of metamaterials. The assistance and professionalism of the teams of the Centre Mersenne and the Comptes Rendus of the Académie of Sciences is also greatly acknowledged. Last, but not least, we are deeply indebted to Denis Gratias, for his keen interest in the topic of metamaterials and his constant encouragements through the preparation of this volume, especially during the final stage which occurred during the covid-19 pandemic in Europe. We hope that you will enjoy reading these articles and find them as inspirational as we did.

Préface

Le mot « métamatériau » semble à la fois familier et mystérieux au profane : d'une part, ce domaine de recherche né il y a vingt ans à l'interface entre sciences physiques et sciences de l'ingénieur nécessite un haut niveau d'expertise pour être approfondi avec des méthodes théoriques et expérimentales avancées ; et d'autre part, les paradigmes électromagnétiques tels que la réfraction négative, les super lentilles et les capes d'invisibilité ont attiré l'attention des médias de masse.

Il s'avère que même l'origine et la signification du mot métamatériau (formé du préfixe grec $\mu\varepsilon\tau\acute{\alpha}$ signifiant au-delà ou soi et du suffixe latin *materia*, signifiant matériel) restent insaisissables. Il nous semble que la plupart des chercheurs supposent que les métamatériaux sont une notion qui fait référence aux composites dont les propriétés vont au-delà de celles trouvées dans les matériaux ordinaires, car il est bien connu que le préfixe « méta » apparaît dans des mots comme métaphysique. Selon Martin Wegener du Karlsruhe Institute of Technology, qui a joué un rôle central dans le développement des métamatériaux, une définition appropriée serait que « les métamatériaux sont des composites rationnellement conçus permettant des propriétés effectives qui vont qualitativement ou quantitativement au-delà de ceux du mélange des ingrédients les constituant ». Cependant, certains chercheurs pourraient argumenter que cette définition n'englobe pas le cas des métamatériaux qui tirent leurs propriétés uniques de leur interface structurée, ce qui est le cas par exemple des métasurfaces. De plus, le sujet émergent des métamatériaux spatio-temporels, qui sont en général des milieux complexes avec une certaine modulation périodique de leurs propriétés à la fois dans l'espace et dans le temps, peuvent être des mlieux homogènes simplement modulés dans le temps, et donc en fait non couverts par la définition proposée par Wegener : en effet, un morceau de verre pourrait acquérir des propriétés extraordinaires grâce aux modulations temporelles, même s'il ne s'agit pas d'un composite. Par conséquent, en regardant la littérature existante et la variété des définitions proposées pour ce qu'un métamatériau devrait être, il semble juste de dire qu'il n'y a pas encore de définition « universelle » d'un métamatériau. Ceci est particulièrement vrai, car le terme métamatériaux est maintenant utilisé dans de nombreux domaines des sciences physiques et de l'ingénierie, et il a même des applications dans les sciences de la vie et les sciences médicales.

Par ailleurs, il est peut-être moins connu parmi les chercheurs travaillant dans le domaine des métamatériaux que le préfixe « méta » a également été utilisé par le mathématicien allemand David Hilbert en relation avec la logique mathématique il y a cent ans dans un projet

de recherche intitulé « métamathématiques ». Hilbert a laissé entendre qu'il s'agissait d'un projet non seulement au-delà des mathématiques ordinaires, mais aussi avec des aspects d'auto-référencement (pensez par exemple à « Cette phrase contient trente-six lettres », qui est un exemple d'auto-référence de phrase). On peut donc affirmer qu'il y a aussi une idée d'échelles multiples, et une certaine interaction entre elles, dans un métamatériau. Même si les premiers prototypes de métamatériaux électromagnétiques apparus au tournant de ce siècle se composent majoritairement de deux échelles (l'échelle d'une cellule élémentaire, constituée de circuits résonants, qui est périodiquement disposée dans l'espace, et l'échelle du composite global constitué de centaines de cellules), ces dernières années ont vu l'émergence de composites hiérarchiques à échelles multiples. Cependant, il n'est pas simple d'identifier les propriétés effectives des métamatériaux hiérarchiques, surtout si les différentes échelles ne sont pas bien séparées. Et comme leurs propriétés effectives restent insaisissables, cela pourrait être une autre classe de métamatériaux, semblable aux poupées russes (ou Matrioshka), qui n'est pas couverte par la définition de M. Wegener.

Ainsi, dans ces deux doubles volumes spéciaux des Comptes Rendus Physique, nous supposons une approche pragmatique, et nous optons simplement pour la définition des métamatériaux comme étant des « milieux complexes aux propriétés inhabituelles rationnellement conçues » (mais nous ne prétendons pas qu'ils peuvent être modélisés comme des composites aux propriétés effectives, et notez qu'un morceau de verre modulé dans le temps est compatible avec notre définition). Maintenant que nous avons fait cette précision, nous tenons à souligner certains travaux importants antérieurs à la naissance des métamatériaux : ce domaine n'a pas été créé ex nihilo, et comme Sir Isaac Newton avait l'habitude de le dire à ses étudiants en mathématiques, nous pensons que faire de la physique revient à se tenir sur l'épaule de géants pour voir l'avenir. Ainsi, commençons par un physicien et un polymathe de premier plan.

John William Strutt, 3ème baron Rayleigh (1842–1919) est célèbre dans la communauté de l'optique pour la diffusion Rayleigh (ce phénomène explique pourquoi le ciel est bleu). Cependant, les ondes de Rayleigh qui sont, avec les ondes de Love, responsables de nombreuses catastrophes sismiques dans les infrastructures humaines, portent également le nom de Rayleigh, qui a également contribué à la diffusion de la lumière, aux théories sonores et hydrodynamiques, à la vision des couleurs, à la théorie de l'élasticité et à la thermodynamique des gaz. Le livre de Rayleigh, [The Theory of Sound, MacMillan and co., London, 1877], paru en deux volumes, a été accompagné de la monographie d'Augustus Edward Hough Love [Some Problems of Geodynamics, Cambridge University Press, Cambridge, 1911], une source d'inspiration inestimable pour des générations de physiciens, d'ingénieurs et de mathématiciens. Il est considéré par de nombreux chercheurs en théorie des composites comme un précurseur de la théorie de l'homogénéisation, qui est une branche des mathématiques consacrée à l'analyse d'équations aux dérivées partielles avec des coefficients périodiques spatialement et oscillant rapidement. Lord Rayleigh, qui est devenu le deuxième professeur Cavendish de physique à l'Université de Cambridge en 1879 (suite à la mort de James Clerk Maxwell), a reçu un prix Nobel de physique en 1904 pour ses « recherches sur les densités des gaz les plus importants et pour sa découverte de l'argon en relation avec ces études » et a eu trois fils, dont l'aîné deviendra professeur de physique à l'Imperial College of Science and Technology de Londres.

Victor Veselago (1929–2018) est à l'origine du paradigme électromagnétique de la réfraction négative. Il était un physicien russe né en Crimée, qui a consacré sa vie aux ondes électromagnétiques, en commençant comme radioamateur pendant son adolescence. Le concept de réfraction négative dans les milieux isotropes avec permittivité et perméabilité simultanément négatives, abordé dans le livre de Sir Arthur Schuster [An Introduction to the Theory of Optics, London: Edward Arnold and Co., 1904], qui mentionne la possibilité d'avoir un vecteur de Poynting opposé au vecteur d'onde, a été proposé pour la première fois dans un article fondateur de

Veselago [Sov. Phys. Usp. 10, 509, 1968]. Cependant, comme mentionné ci-dessus, la percée technologique est venue avec la découverte de Sir John Pendry et de ses collègues que des résonateurs à anneaux fendus combinés à des fils droits et minces permettraient une permittivité et une perméabilité effectives négatives à certaines fréquences micro-ondes [Phys. Rev. Lett. 76, 4773–4776, 1996 ; IEEE transactions on microwave theory and techniques 47 (11), 2075–2084, 1999]. Plus précisément, dans l'article fondateur de 1968, Veselago a montré qu'une simple lame à faces parallèles d'un milieu d'indice de réfraction négatif serait un instrument optique capable de transmettre des images sans distorsions. Une affirmation de Veselago peut-être moins connue est selon laquelle sous absorption de lumière dans un milieu à réfraction négative, la pression lumineuse change par attraction lumineuse. Parallèlement à ses travaux scientifiques sur les semiconducteurs dits magnétiques, Veselago a engagé un vaste travail pédagogique. À partir de 1961, il enseigne à l'Institut de physique et de technologie de Moscou (MIPT) et y donne le cours original du cycle universitaire « Les éléments de base de la physique des vibrations » et dirige simultanément des séminaires et des travaux de laboratoire à la Chaire de physique générale. Veselago a été l'un des pionniers de la diffusion d'informations scientifiques sur Internet en Russie : en 1992, il organisait déjà l'envoi par Internet du contenu des revues scientifiques. Il a inventé le système « Informag », qui a été utile à la communauté scientifique russe en raison de la situation désastreuse des bibliothèques universitaires dans les années 90. En 1998, Veselago a organisé la première revue électronique à comité de lecture en Russie. Il a reçu un certain nombre de prix russes et étrangers pour ses recherches scientifiques tels que le prix d'État 1976 de l'ex-Union soviétique et en 2004 le prix Fock de l'Académie des sciences de Russie. En 2009, Veselago a reçu la médaille de l'American Optical Society pour son travail, qui va bien au-delà de l'électrodynamique et de l'optique. En effet, les idées de Veselago ont eu une importance considérable dans de nombreux domaines de la physique, et nous en présenterons quelques-unes ces deux doubles volumes spéciaux des Comptes Rendus Physique. Nous présentons maintenant un autre physicien qui a apporté des contributions majeures dans le domaine des métamatériaux, qui est encore popularisé bien au-delà de la communauté photonique.

John Pendry a travaillé comme jeune chercheur sur la diffraction d'électrons à basse énergie au laboratoire Cavendish de Cambridge et après un post-doctorat en spectroscopie photoélectronique aux Bell Labs aux USA, en 1972–1973. Il a ensuite été nommé directeur du groupe de théorie au laboratoire de Daresbury du Science and Engineering Research Council du Royaume-Uni, puis professeur de physique à l'Imperial College de Londres en 1981. Alors qu'il travaillait aux Bell Labs, Pendry a développé la première théorie quantitative de la structure fine d'absorption des rayons X étendue pour laquelle il a reçu le prix Dirac en 1996 et, en tant que chef du groupe de théorie à Dalesbury, il a publié sa théorie de la spectroscopie de photoémission résolue en angle, qui reste à ce jour un modèle standard pour sonder la structure des électrons dans les structures cristallines 1D et 2D. Lorsqu'il a pris son poste actuel de professeur à l'Imperial College en 1981, il a maintenu une forte activité dans son domaine de recherche familier en science des surfaces, mais il a également commencé à étudier le comportement des électrons dans des milieux désordonnés, et a développé sa théorie de la diffusion et ses méthodes de calcul pour des structures désordonnées en 1D et en dimension supérieure. Ces milieux ont trouvé une application en biologie relevant de la conductivité des biomolécules. Tous ces travaux antérieurs ont conduit il y a 25 ans à son premier article fondateur sur les structures de bandes photoniques, accompagné du logiciel gratuit qu'il a conçu avec ses collègues de l'Imperial College et de l'*Universidad Autonoma de Madrid* [Computer Physics Communications 85, 306–322, 1995] qui a rendu possible de dévoiler des plasmons polaritons à des fréquences extrêmement faibles dans des réseaux de fibres métalliques diluées [Phys. Rev. Lett. 76, 4773–4776, 1996], qui, avec les célèbres résonateurs à anneau fendu, qu'il a proposés pour le magnétisme artificiel au tournant du siècle [IEEE Transactions on Microwave Theory and Techniques 47, 2075, 1999], peuvent être considérés comme la

pierre angulaire des métamatériaux pour la réfraction négative. Comme nous le rappellerons ensuite, la physique de la réfraction négative — dans laquelle les rayons lumineux sont réfractés à une interface selon la loi de Snell-Descartes dans laquelle le signe d'un indice de réfraction a été inversé — a été introduite par le physicien russe Veselago 30 ans avant que Pendry propose une voie vers des milieux complexes qui la rendraient possible. Cependant, Pendry a non seulement rendu possible la réfraction négative, mais aussi un indice négatif pour les ondes évanescentes et il a en outre proposé que la lentille plate convergente envisagée par Veselago ait une résolution théoriquement illimitée. Comme un pied de nez à l'histoire, le célèbre critère de Rayleigh (d'après John William Strutt Rayleigh), qui stipule que « deux images sont simplement résolubles lorsque le centre du diagramme de diffraction de l'une est directement sur le premier minimum du diagramme de diffraction de l'autre », pourrait être dépassé grâce à un indice négatif, selon Pendry [Phys. Rev. Lett. 85, 3966–3969, 2000]. L'article de Pendry a conduit à une controverse scientifique, qui s'est résolue après quelques années de débats houleux, grâce à des travaux expérimentaux et théoriques, de physiciens comme de mathématiciens. Six ans après son article fondateur sur la lentille parfaite, Pendry a proposé une voie vers l'invisibilité *via* le concept de l'optique de transformation, avec ses collègues David Schurig et David Smith de l'Université Duke à Durham, USA [Science 312, 1780–1782, 2006]. Cette technique dite de l'« optique de transformation » revient à appliquer une certaine transformation géométrique aux équations de Maxwell, qui peuvent s'écrire sous une forme covariante évitant de nombreuses difficultés techniques qui se poseraient par exemple dans les équations de Navier pour l'élasticité. Cependant, même si les équations de Maxwell sont invariantes après une transformation géométrique, la cape d'invisibilité qui résulte de la transformation d'un disque en un anneau (le trou à l'intérieur de l'anneau étant dissimulé aux ondes électromagnétiques), nécessite l'utilisation d'une coque hétérogène anisotrope entourant l'objet à masquer. Une classe différente de capes d'invisibilité, basée sur l'optique conforme, a été proposée par Ulf Leohnardt à l'Université de Saint-Andrews au Royaume-Uni [Science 312, 1777–1780, 2006]. Cette deuxième solution ne nécessite que quelques indices de réfraction spatialement variables, mais au prix de travailler en géométrie 2D (les transformations conformes nécessitant un plan complexe) et dans la limite de l'optique des rayons.

La recherche sur les métamatériaux a également bénéficié d'importantes contributions d'éminents chercheurs en physique et en génie électrique. Nous fournissons ici une liste (non exhaustive) de certains d'entre eux.

Sergei Tretyakov a commencé sa carrière comme ingénieur de recherche au Département de radiophysique de l'Université polytechnique Pierre le Grand de Saint-Pétersbourg (anciennement Institut polytechnique de Leningrad en 1980). Dans les années 90, Tretyakov a occupé un poste auxiliaire au laboratoire d'électromagnétique de l'Université de technologie d'Helsinki où il a travaillé avec Ismo Lindell, Ari Sihvola et Ari Viitanen avec qui il a publié l'influent ouvrage [Ondes électromagnétiques dans les milieux chiraux et bi-isotropes, Artech House Antenna Library, Norwood, MA, USA, 1994] qui expose une présentation claire de l'activité optique et de la chiralité dans des milieux électromagnétiques apparentés aux métamatériaux. Au cours de ces années, il a apporté d'importantes contributions à la théorie des milieux spatialement dispersifs avec Konstantin Simovski à l'Université polytechnique de Saint-Pétersbourg, où il a été promu professeur en 1996. En 2000, il a rejoint l'Université de technologie d'Helsinki en tant que professeur de Radio Engineering, et fut rapidement suivi par Konstantin Simovski qui y occupe également un poste de professeur. Tretyakov et Simovski ont contribué à la carrière d'une génération de jeunes chercheurs extrêmement talentueux, tels que Pavel Belov (le doyen de la faculté de physique de l'Université ITMO) et Mario Silveirinha (actuellement professeur d'électrotechnique à l'Université de Lisbonne), notamment reconnus pour leurs travaux sur la forte dispersion spatiale des milieux filaires dans la limite d'homogénéisation [Phys. Rev. B 67, 113103, 2003].

Nader Engheta a été diplômé en génie électrique de l'Université de Téhéran en Iran en 1978,

puis a obtenu une maîtrise en génie électrique et un doctorat en génie électrique et physique du California Institute of Technology (Caltech), Pasadena, Californie. Après avoir passé un an en tant que chercheur postdoctoral à Caltech et quatre ans en tant que chercheur principal à la division Dikewood de Kaman Sciences Corporation à Santa Monica, en Californie, il a rejoint la faculté de l'Université de Pennsylvanie, où il est actuellement Professeur H. Nedwill Ramsey et où il a été président du groupe d'études supérieures en génie électrique de 1993 à 1997. Il a apporté des contributions fondamentales au domaine des métamatériaux, notamment sur les métamatériaux à indice proche de zéro (ou métamatériaux ENZ pour *epsilon-near-zero* en anglais) qui présentent des propriétés uniques dans l'interaction lumière-matière, comme les nouveaux effets de Purcell, le camouflage plasmonique et les nano-circuits optiques. L'exploitation de la plasmonique pour rendre des objets « invisibles » ou « transparents », qu'il a proposée dès 2005 avec Andrea Alù [Phys. Rev. E 72, 016623, 2005], a conduit à de nouvelles méthodes en physique furtive. Avec son groupe, il a développé plusieurs domaines et concepts dans les domaines des métamatériaux et de l'optique plasmonique, notamment les métamatériaux « à paramètres extrêmes » et les métamatériaux ENZ [Phys. Rev. B 75 (15), 155410, 2007] ; il a contribué à l'émergence du domaine du graphène dans le domaine des métamatériaux et de l'optique plasmonique en régime infrarouge, fournissant les feuilles de route pour les dispositifs optiques d'un atome d'épaisseur et le traitement de l'information avec ces dispositifs ; il a joué un rôle déterminant dans les thématiques de la chiralité artificielle par micro-ondes, des métamatériaux « traitement du signal », des métamatériaux « numériques » et des « méta-machines ». Il est actuellement professeur H. Nedwill Ramsey à l'Université de Pennsylvanie, Philadelphie, Pennsylvanie, États-Unis, affilié aux départements de génie électrique et des systèmes, de bio-ingénierie, de science et d'ingénierie des matériaux, et de physique et d'astronomie. Il est membre de nombreuses sociétés scientifiques et techniques internationales. Ses activités de recherche actuelles couvrent un large éventail de domaines, notamment la nanophotonique, les métamatériaux, la plasmonique, l'optique à l'échelle nanométrique, l'optique au graphène, l'imagerie et la détection inspirées par les yeux de certaines espèces animales, la nano-ingénierie optique, la rupture de symétrie d'inversion de temps et la non-réciprocité, les antennes optiques et micro-ondes, les mathématiques des opérateurs fractionnaires, et la physique et l'ingénierie des champs et des ondes. Il a apporté des contributions pionnières dans les domaines de l'électromagnétisme et des micro-ondes, des métamatériaux, de l'optique de transformation, de l'optique plasmonique, de la nanophotonique, de la photonique du graphène, des nanomatériaux, de l'optique à l'échelle nanométrique, des nanoantennes et des antennes miniaturisées, de la physique et de l'ingénierie inverse de la vision de polarisation dans la nature, de l'imagerie optique bio-inspirée et du paradigme fractionnaire en électrodynamique.

Martin Wegener a obtenu son doctorat en physique en 1987 à Johann Wolfgang Goethe-Universität Frankfurt (Allemagne), puis il a passé deux ans en tant que chercheur au AT&T Bell Laboratories à Holmdel (États-Unis). De 1990 à 1995, il était professeur à l'Universität Dortmund (Allemagne) et, depuis 1995, il est professeur à l'Institut de physique appliquée de l'Institut de technologie de Karlsruhe (KIT). Depuis 2001, il occupe un poste conjoint en tant que chef de service à l'Institut de nanotechnologie du KIT. De 2001 à 2014, il était le coordinateur du DFG-Center for Functional Nanostructures (CFN) au KIT. Depuis 2019, il est co-conférencier au centre d'excellence 3D Matter Made to Order. Ses intérêts de recherche comprennent l'optique ultrarapide, l'optique non-linéaire (extrême), l'optique en champ proche, la lithographie laser optique, les cristaux photoniques, les métamatériaux optiques, mécaniques et thermodynamiques, ainsi que la physique des transformations. Cette recherche a débouché sur différents prix et distinctions, parmi lesquels le SPIE Prism Award 2014 pour la start-up Nanoscribe GmbH. Au cours des quinze dernières années, son groupe de recherche a été particulièrement actif dans les thématiques des métamatériaux électromagnétiques [Science 306, 1351–1353, 2004; Sci-

ence 328, 337–339, 2010], mécaniques [Appl. Phys. Lett. 100, 191901, 2012; Phys. Rev. Lett. 108, 014301, 2012; Phys. Rev. Lett. 108, 014301, 2014; Proceedings of the National Academy of Sciences 112, 4930–4934, 2015; Science 358, 1072–1074, 2017] et thermiques [Phys. Rev. Lett. 110, 195901, 2013]. Muamer Kadic (actuellement enseignant-chercheur en physique à l'Université de Franche-Comté) a participé à de nombreux travaux de Wegener sur les métamatériaux mécaniques et thermiques. Wegener a de plus reçu le prix Descartes 2005 avec Sir John Pendry, David Smith (qui a rédigé des articles essentiels tels que la première preuve expérimentale de la réfraction négative [Phys. Rev. Lett. 84, 4184, 2000] et du camouflage micro-ondes [Science 314, 977–980, 2006]), Ekmel Ozbay et Kostas Soukoulis (qui ont apporté d'importantes contributions à la réfraction négative dite à tous angles avec des cristaux photoniques [Nature 423 (6940), 604–605, 2004], qui est un domaine de recherche en photonique initiée par un article théorique co-écrit par l'un de nous [J. Opt. Soc. Am. A 17, 1012–1020, 2000]).

Le prix Descartes 2005 de la recherche européenne a été décerné pour le développement de structures artificielles aux propriétés optiques entièrement nouvelles. En effet, l'Union européenne a reconnu que les équipes de recherche de ces éminents chercheurs ont créé et développé une nouvelle classe de métamatériaux artificiels, à l'époque appelés « matériaux gauchers », étant donné que la règle de base habituelle utilisée pour décrire le triplet (**E**, **H**, **k**) doit être effectuée avec la main gauche au lieu de la main droite comme c'est conventionnel. En effet, dans les milieux isotropes ordinaires à permittivité et perméabilité simultanément positives (d'où un indice de réfraction positif), le triplet (**E**, **H**, **k**) est direct droitier et le vecteur d'onde **k** est parallèle au vecteur de Poynting **S**, qui est défini comme le produit vectoriel de **E** et **H**. Alors que pour une permittivité et une perméabilité simultanément négatives (d'où un indice de réfraction négatif selon l'article fondateur de Veselago [Sov. Phys. Usp. 10, 509, 1968]), le vecteur d'onde **k** change de direction et le triplet (**E**, **H**, **k**) devient indirect (et **k** et **S** deviennent antiparallèles, et donc les vitesses de phase et de groupe pointent dans des directions opposées). Les milieux main-gauche sont maintenant généralement dénommés « matériaux à indice négatif » (NIM pour *negative index materials* en anglais), et leurs propriétés fascinantes comprennent la réfraction négative, les effets Doppler et Cerenkov inverses et la possibilité d'adaptation de l'impédance du vide (donc la transparence) comme l'a découvert Veselago il y a plus de 50 ans [Sov. Phys. Usp. 10, 509, 1968]. Mais les possibilités offertes par les NIM incluent également l'imagerie non limitée par la limite de diffraction comme l'a souligné Pendry il y a 20 ans [Phys. Rev. Lett. 85, 3966–3969, 2000]. La fabrication de NIM a ouvert la possibilité à de nouvelles applications et de nouveaux dispositifs, comme l'imagerie haute résolution et d'autres dispositifs sous-longueur d'onde, ainsi que des antennes et guides d'ondes miniatures, et des matériaux artificiels magnétiques et bianisotropes. Cependant, le prix Descartes 2005 ne mentionnait pas que les métamatériaux trouveraient d'énormes applications dans d'autres domaines de la physique. Par exemple, il a été souligné par Alexander Movchan et l'un de nous dans [Phys. Rev. B 70, 125116, 2004] que les résonateurs à anneau fendu peuvent être utilisés pour créer des bandes interdites basse fréquence en acoustique en raison du fait qu'ils se comportent comme des structures localement résonantes qui peuvent être modélisées par des ressorts et des masses, et peuvent donc former la base de milieux d'indice de réfraction négatif en acoustique [New Journal of Physics 9, 399, 2007]. Une découverte similaire a été faite par Jensen Li et Che Ting Chan à peu près au même moment [Phys. Rev. E 70, 055602, 2004]. Cependant, c'est le groupe de Ping Sheng qui a dévoilé pour la première fois le véritable potentiel des matériaux sonores localement résonants dans un article marquant [Science 289, 1734–1736, 2000]. Le groupe de Martin Wegener a poussé l'analogie établie entre l'optique et la mécanique en introduisant le concept de métamatériaux mécaniques chiraux [Science 358, 1072–1074, 2017]. Ce dernier pourrait être la pierre angulaire d'une cape élastodynamique construite à partir d'un milieu Cossérat, comme proposé par le groupe de mathématiques appliquées d'Alexander Movchan à l'Université de Liv-

erpool il y a plus de dix ans [Appl. Phys. Lett. 94, 061903, 2009]. Une autre possibilité pourrait être d'approcher les milieux dits Milton–Briane–Willis [New Journal of Physics, 8 (10), 248, 2006] avec des métamatériaux mécaniques chiraux [Phys. Rev. B 99, 214101, 2019].

Suite à l'essor du graphène, des nanotubes de carbone et autres nouveaux matériaux bidimensionnels, les chercheurs en métamatériaux ont porté un intérêt particulier à des composites qui s'apparentaient à ces matériaux bidimensionnels. Il est intéressant de noter ici quelques liens avec les travaux de Thomas Ebbessen qui est professeur de chimie physique à l'Université de Strasbourg en France. Ebbessen est connu pour ses travaux pionniers dans le domaine des nanosciences. Il a reçu le prix Kavli 2014 en nanosciences pour ses contributions transformatrices au domaine de la nano-optique qui ont brisé des certitudes de longue date sur les limites de résolution de la microscopie optique et de l'imagerie, avec Stefan Hell (prix Nobel de chimie 2014), et John Pendry. En 2019, Ebbessen a reçu la médaille d'or du CNRS en France. Alors qu'il travaillait pour la société NEC à la fin des années quatre-vingt, Ebbesen a découvert qu'il était possible, dans certaines conditions de résonance, de transmettre la lumière à travers des trous de dimension sous-longueur d'onde fraisés dans des films métalliques opaques. Le phénomène, connu sous le nom de transmission optique extraordinaire, implique des plasmons de surface. Les plasmons de surface restent un domaine de recherche très actif, avec d'éminents chercheurs comme Stefan Maier [Plasmonics: fundamentals and applications Springer Science & Business Media, 2007], qui a commencé sa carrière en travaillant avec Harry Atwatter au California Institute of Technology, publiant notamment un article qui fait date sur la détection locale du transport d'énergie électromagnétique sous la limite de diffraction dans les guides d'ondes plasmoniques à nanoparticules métalliques [Nature Materials 2, 229–232, 2003] et qui occupe actuellement un poste de professeur à l'Imperial College de Londres et à la Ludwig-Maximilian Universität München. Notons que Stefan Maier a publié de nombreux articles avec John Pendry et Paloma Huidobro (une jeune chercheuse extrêmement talentueuse qui a récemment rejoint le groupe de Mario Silveirinha à Lisbonne) sur le contrôle des polaritons de plasmon de surface à l'aide d'outils de transformation optique ainsi que sur l'optique de graphène.

Federico Capasso est un contributeur majeur dans le domaine des métasurfaces. Il a reçu le doctorat en physique de l'Université de Rome en 1973 pour ses recherches sur la fibre optique, et il a rejoint les Bell Labs en 1976. En 1984, il a été nommé membre distingué du personnel technique et, en 1997, Bell Labs *Fellow*. Il a rejoint l'Université de Harvard en tant que professeur de physique appliquée en 2003. Capasso et ses collaborateurs ont apporté de nombreuses contributions de grande envergure aux dispositifs à semi-conducteurs, avec des travaux pionniers sur la technique de conception connue sous le nom d'« ingénierie de structure de bande ». Il l'a appliqué à de nouvelles photodiodes à cascade quantique à faible bruit, à des transistors à hétérojonction, à des dispositifs de mémoire et à des lasers. Capasso et ses collaborateurs ont inventé et démontré le laser à cascade quantique (QCL) [Science 264, 553–556, 1994]. Le groupe de Capasso a montré que des interfaces plasmoniques, astucieusement conçues et constituées de réseaux optiquement minces de nano-antennes optiques, conduisaient à une puissante généralisation des lois séculaires de la réflexion et de la réfraction. Ces structures sont au fondement de l'optique planaire basée sur les métasurfaces, que Capasso a popularisé [Science, 334, 333–337, 2011 ; Nature Materials 13, 139–150, 2014] bien au-delà de la communauté photonique.

Philippe Lalanne, qui est Directeur de Recherche CNRS à l'Institut d'Optique d'Aquitaine, peut certainement être inclus dans les chercheurs pionniers sur les métasurfaces avec ses travaux qui font date sur la théorie des milieux effectifs des structures périodiques sous-longueur d'onde, 1996] et sur des réseaux binaires blazés sous-longueur d'onde [Optics Letters 23, 1081–1083, 1998]. Lalanne a également apporté des contributions essentielles à la modélisation numérique électromagnétique en améliorant la convergence de la décomposition

de Fourier pour les structures périodiques [J. Opt. Soc. Am. A 13, 779–784, 1996] et à la photonique avec la théorie de la transmission optique extraordinaire [Nature 452, 728–731, 2008]. Il a été impliqué dans l'électrodynamique computationnelle et dans les applications de structures optiques sous-longueur d'onde pour l'optique diffractive, la plasmonique, les cristaux photoniques, l'optique intégrée et les microcavités.

Comme déjà mentionné, les métamatériaux ne peuvent se résumer à des composites rationnellement conçus avec une certaine hétérogénéité spatiale. On peut également concevoir les propriétés des matériaux en exploitant la variable de temps. Ici, nous voudrions citer un chercheur dont le nom est associé aux miroirs à inversion temporelle.

Mathias Fink a obtenu en 1978 le Doctorat en Sciences de l'Université de Paris dans le domaine de la focalisation ultrasonore pour l'imagerie médicale en temps réel sous la direction de Pierre Alais. En 1981, il est nommé professeur à l'Université de Strasbourg. Après un séjour en tant que professeur invité à l'Université d'Irvine dans le département de radiologie, il revient en France pour devenir professeur à l'Université Paris Diderot (Paris 7). En 1990, il fonde le Laboratoire Ondes et Acoustique de l'Ecole Supérieure Physique Chimie Industrielle (ESPCI) à Paris, laboratoire qui composera l'Institut Langevin en 2009. En 2005, il est nommé professeur à l'ESPCI, où il est aujourd'hui professeur émérite et titulaire de la chaire Georges Charpak (du nom du physicien français d'origine polonaise, qui a occupé la chaire Joliot-Curie à l'ESPCI et a reçu le prix Nobel de physique en 1992 pour son invention et le développement de détecteurs de particules). Fink a été le pionnier du développement de miroirs à inversion temporelle et du traitement du signal par inversion temporelle [Europhysics Journal Physics 15, 81, 1994 ; Wave Motion 20, 151, 1994 ; Phys. Rev. Lett. 79, 3170, 1997]. Il a développé de nombreuses applications de ce concept, de la thérapie par ultrasons, l'imagerie médicale, les tests non destructifs, l'acoustique sous-marine, l'imagerie sismique, les objets tactiles, jusqu'aux télécommunications électromagnétiques. Il a également été le pionnier des méthodes d'imagerie médicale innovantes : élastographie transitoire, imagerie par cisaillement supersonique et imagerie multi-ondes qui sont maintenant mises en œuvre par plusieurs entreprises. Six entreprises comptant environ 400 employés ont été créées à partir de ses recherches : Echosens, Sensitive Object, Supersonic Imagine (qu'il a cofondée notamment avec Charpak), Time Reversal Communications, Cardiawave et GreenerWave. Notons que Philippe Roux, directeur de recherche au CNRS et actuellement directeur de l'Institut des Sciences de la Terre ISTERRE à Grenoble, a apporté d'importantes contributions aux métamatériaux sismiques [Rapports Scientifiques 6, 19238, 2016 ; Geophysical Journal International 220, 1330–1339, 2020] et est un ancien doctorant de Fink. Les métamatériaux sont un petit monde allant de l'ultrasonique à la géophysique.

Un autre contributeur important dans le domaine des métamatériaux sismiques est Stéphane Brûlé, chercheur en évaluation du risque sismique, interaction sol-structure, qui est également ingénieur géotechnique en chef, titulaire d'un master recherche de l'Ecole Normale Supérieure de Paris et de l'Université Pierre et Marie Curie et diplômé ingénieur en géotechnique de l'Université Grenoble-Alpes dans le domaine de la mécanique des sols, de l'amélioration des sols et des fondations profondes. Brûlé est l'auteur principal de l'article fondateur pour le domaine des métamatériaux sismiques [Physical Review Letters 112, 133901, 2014] qu'il a co-écrit avec Emmanuel Javelaud (qui était en 2012 ingénieur et chercheur dans le groupe de recherche de Brûlé chez Ménard), Stefan Enoch (directeur de recherche au CNRS) et l'un de nous. Il a également dirigé la première expérience de focalisation des ondes de Rayleigh de surface par réfraction négative [Scientific Reports 7, 18066, 2017]. Il est membre du Comité technique international 203 « Génie géotechnique sismique et problèmes associés », est également membre du Comité français de mécanique des sols (CFMS) et de l'Association française du génie parasismique (AFPS).

Enfin, dans les traces de Lord Rayleigh, d'éminents chercheurs travaillant en mathématiques

appliquées et en mécanique théorique ont contribué au développement des métamatériaux. Nous avons déjà cité de nombreux chercheurs célèbres (dont certains apparaîtront dans la suite car ils sont contributeurs de ces deux doubles volumes spéciaux). Néanmoins, nous sommes bien conscients que de nombreux grands scientifiques n'apparaissent pas dans notre préface, et nous tenons à nous en excuser. Mais essayer d'être plus exhaustif nous conduirait bien au-delà de la portée de cette préface. Mentionnons donc simplement Alain Bensoussan, Jacques-Louis Lions et Georges Papanicolaou pour leur livre historique sur la théorie de l'homogénéisation [Analyse asymptotique pour les structures périodiques, Hollande du Nord, 1978], et Habib Ammari, Allan Greenleaf, Robert Kohn, Michael Vogelius et Michael Weinstein pour leur contribution fondamentale à la théorie mathématique du camouflage, et des membres du laboratoire de mathématiques POEMS d'Anne-Sophie Bonnet Ben-Dhia à l'ENSTA à Palaiseau, laboratoire de référence pour les travaux de recherche sur les coins constitués d'un matériau dispersif en fréquence qui partagent certaines caractéristiques avec la physique des trous noirs. Notre liste est évidemment loin d'être exhaustive et nous tenons à nous excuser d'avoir manqué d'autres chercheurs éminents. Portons cependant une attention particulière au travail de deux mathématiciens, car les derniers développements des métamatériaux modulés spatialement et temporellement pointent vers leur travail fondateur. Konstantin Lurie a obtenu une maîtrise en sciences de l'Institut polytechnique de Leningrad en 1959 et un doctorat de l'Institut physico-technique cinq ans plus tard. Il a obtenu l'équivalent du « Doctorat d'Etat » du même institut en 1972. Ses recherches se consacrent depuis les années 60 à la conception optimale des matériaux. Les journaux et livres qu'il a publiés ont jeté les bases mathématiques de cette discipline telle que nous la connaissons aujourd'hui. Le besoin d'une conception optimale provient de diverses exigences technologiques telles que des dispositifs, qui sont produits avec une meilleure qualité, moins de poids, à moindre coût et avec une fabrication plus rapide. Comme l'explique Lurie, il existe des liens étroits entre la conception optimale et la physique, la mécanique, la biologie et les sciences naturelles en général. L'optimalité englobe de nombreux domaines tels que les systèmes de communication et la conception nanostructurale ou le contrôle du trafic. On note qu'Andrej Cherkaev, autre acteur clé de la théorie des composites, a contribué à quelques travaux avec Konstantin Lurie, y compris un travail historique que ces chercheurs ont publié avec Graeme Milton et Marco Avellaneda sur la conductivité des polycristaux et une inégalité d'échange de phase [Physica A: Statistical Mechanics and its Applications 157, 148–153, 1989]. Lurie a extrapolé ces principes à la dynamique des matériaux en introduisant un nouveau concept de matériaux dynamiques [An Introduction to the Mathematical Theory of Dynamic Materials, Springer, 2007], et de cette manière il a jeté les bases mathématiques de métamatériaux aux propriétés variables dans l'espace et le temps. Les métamatériaux spatio-temporels sont devenus un domaine en développement rapide des métamatériaux.

John Willis est professeur émérite de mécanique théorique des solides à l'Université de Cambridge. Il est diplômé du département de mathématiques de l'Imperial College de Londres où il a été assistant-conférencier en 1962–1964, avant de travailler en tant qu'associé de recherche au Courant Institute de New-York pendant un an. De 1965 à 1972, il a été directeur de recherche au Département de mathématiques appliquées et de physique théorique (DAMTP) de l'Université de Cambridge, puis professeur de mathématiques appliquées à l'Université de Bath jusqu'en 1994. Il était de retour en tant que professeur de mécanique théorique des solides à la DAMTP de 1994 à 2007, ainsi que professeur de mécanique à l'Ecole Polytechnique de 1998 à 2004. Il a été rédacteur en chef du Journal of Mechanics and Physics of Solids pendant un quart de siècle (de 1982 à 2006). Les principaux intérêts de recherche de Willis ont inclus les problèmes statiques et dynamiques pour les milieux anisotropes, les problèmes de dommages par irradiation des matériaux, l'intégrité structurelle, les propriétés efficaces des matériaux composites (à la fois statiques et dynamiques), la mécanique des composites non

linéaires, la stabilité des dispositifs semi-conducteurs à couche contrainte. Des travaux récents ont porté sur la plasticité du gradient de déformation et la dynamique des composites (appliquée aux métamatériaux acoustiques). Il a été élu Fellow de la Royal Society en 1992, membre étranger de la US National Academy of Engineering (2004) et membre Associé Etranger de l'Académie des Sciences (2009). Les milieux dits de Willis, du nom de son article fondateur sur les méthodes variationnelles et connexes pour les propriétés globales des composites qui ont conduit à de nouvelles équations de gouvernance pour les ondes élastodynamiques se propageant dans des milieux hétérogènes [Advances in Applied Mechanics, 21, 1–78, 1981], sont un domaine des métamatériaux élastiques avec une activité de recherche très intense. Willis a publié des travaux importants sur l'interprétation dynamique de l'instabilité du flottement (flutter) dans un milieu continu, [J. Mech. Phys. Solids 54, 2391–2417, 2006], ainsi qu'un article de référence sur les modifications de la deuxième loi de Newton et de l'élastodynamique continue linéaire, qu'il a co-écrit avec Graeme Milton, un autre mathématicien éminent [Proc. Roy. Soc. A 463, (2007), 855–880, 2007].

Comme nous l'avons suggéré avec les « métamathématiques » de David Hilbert, les métamatériaux sont un sujet à l'interface entre la physique et les mathématiques (nonobstant l'importance des sciences de l'ingénieur qui sera montrée ensuite dans la préface). Nous sommes honorés d'avoir le polymathe Graeme Milton comme contributeur de ce volume spécial, actuellement professeur émérite à l'Université de l'Utah et également professeur au Courant Institute of Mathematical Sciences à New-York. Lorsqu'il était étudiant en Master à l'Université de Sydney, il a publié un article fondateur sur les limites sur la constante diélectrique complexe d'un matériau composite [Appl. Phys. Lett. 37, 300–302 (1980)], qui jette les bases de la théorie des limites dite de Bergmann-Milton. La thèse de Milton portait sur « Les études théoriques des propriétés de transport des supports inhomogènes », sous la direction de Ross McPhedran qui l'introduisit dans le domaine des matériaux composites, aboutissant à la publication susmentionnée qui a reçu selon Milton plus de demandes de réimpression que tout autre de ses articles ultérieurs. Il a fait sa thèse de doctorat sur certains modèles exotiques en physique statistique au département de physique de l'Université Cornell avec Michael Fisher, puis un post-doctorat avec Michael Cross à Caltech en tant que Weingart Fellow, et George Papanicolaou (qui a co-écrit avec Alain Bensoussan et Jacques-Louis Lions le livre classique sur la théorie de l'homogénéisation [Asymptotic Analysis of Periodic Structures, North-Holland, New-York, 1978]) lui a suggéré de postuler pour un poste de professeur adjoint au Courant Institute, où il a obtenu son poste et a été promu professeur associé après deux ans, puis professeur. Il y a 25 ans, il publiait avec son collègue Andrej Cherkaev un article de rupture intitulé « Quels tenseurs d'élasticité sont réalisables ? » [Journal of Eng. Mat. and Technology 117, 483–493, 1995], qui a introduit une toute nouvelle classe de composites aux propriétés élastiques sans précédent. Les médias dits « Pentamode » sont devenus réalité il y a six ans grâce au groupe de Martin Wegener [Phys. Rev. Appl. 2, 054007, 2014]. En 1999, il est devenu professeur émérite du département de mathématiques de l'Université de l'Utah et a été directeur de ce département de 2002 à 2005. Il a publié un ouvrage qui est devenu un classique [The Theory of composites, Cambridge University Press, Cambridge, 2002] qui fait écho à celui de Bensoussan, Lions et Papanicolaou. Ces deux livres serviront encore d'inspiration aux physiciens et mathématiciens travaillant dans le domaine des métamatériaux pour les années à venir.

Les changements de paradigmes de la réfraction négative et du camouflage ont alimenté l'intérêt pour les métamatériaux. Jusqu'à présent, nous avons présenté d'éminents chercheurs dans ce domaine, dont les travaux sont cités dans les 14 articles de ces deux doubles volumes spéciaux. Cependant, en tant que rédacteurs invités des Comptes Rendus Physique, nous avons le grand plaisir de réunir dans ce volume spécial les contributions d'autres chimistes, physiciens et mathématiciens distingués et extrêmement talentueux qui ont également apporté des contri-

butions majeures au domaine des métamatériaux.

Par ordre alphabétique, nous commençons par Andrea Alù qui a obtenu un doctorat de l'Université de Roma Tre en 2007. Après avoir passé un an en tant que chercheur postdoctoral à travailler avec le professeur Nader Engheta à l'Université de Pennsylvanie, Philadelphie, en 2009, il a rejoint la faculté de l'Université du Texas à Austin où il est actuellement chercheur principal et professeur associé. Il a rejoint la City University New-York en 2018 en tant que professeur et directeur fondateur de la Photonics Initiative pour l'Advanced Science Research Center. Il reste affilié au Laboratoire de recherche appliquée de l'Université du Texas à Austin, où il est impliqué dans des projets de recherche sur l'électromagnétisme et l'acoustique. Ses sujets actuels de recherche couvrent un large éventail de domaines, y compris les métamatériaux et la plasmonique, l'électromagnétique, l'optique et la photonique, la diffusion, le camouflage et la transparence [Phys. Rev. E 72, 016623, 2005], la modélisation des nanocircuits et des nanostructures, les antennes miniaturisées et les nanoantennes, les antennes circuits en radio-fréquence, les dispositifs acoustiques et mécaniques en métamatériaux. Alù est l'actuel président de l'Institut virtuel européen METAMORPHOSE pour « *Les matériaux électromagnétiques artificiels et les métamatériaux* », et membre du comité administratif de l'IEEE Antennas and Propagation Society. Depuis 2014, Alù est également directeur de la technologie chez Silicon Audio RF Circulator, une société qui détient la licence exclusive de quelques inventions issues du laboratoire d'Alù autour de la technologie non-magnétique pour les dispositifs non réciproques.

Yuri Kivshar a étudié à l'école de Kharkiv fondée par le lauréat du prix Nobel Lev Landau. En 1984, il a obtenu un doctorat en sciences et en 1989, à 30 ans, il est devenu le plus jeune chercheur du Verkin Institute for Low Temperature Physics and Engineering. À partir de 1991, il a travaillé comme scientifique aux États-Unis, en Finlande, en Espagne, en Allemagne et en 1993, il a été invité à l'Optical Sciences Center of Australia et a ensuite fondé son propre laboratoire Nonlinear Physics Center de l'Australian National University. À partir de 2000, Yuri Kivshar a travaillé dans différents domaines de l'optique non linéaire et a mené des recherches sur les solitons et les métamatériaux, les cristaux photoniques non linéaires et les théories des matériaux composites. Ses recherches ont eu un impact fondamental sur l'effet d'auto-focalisation, les métamatériaux, les nano-antennes diélectriques, les isolateurs topologiques, le traitement du signal optique et les communications optiques. Il a également découvert des séries de solitons et décrit leurs propriétés dynamiques dans des systèmes presque intégrables. En 2010, Yuri Kivshar a été invité à Saint-Pétersbourg grâce au programme gouvernemental Megagrant. Il est devenu un responsable scientifique du Centre international de recherche en nanophotonique et métamatériaux de l'Université ITMO (Saint-Pétersbourg, Russie). Tout au long de sa carrière exceptionnellement prolifique, Yuri Kivshar a apporté des contributions majeures à de nombreux domaines de la physique et il a également contribué à la diffusion d'idées d'optique non linéaire dans les cristaux photoniques et les métamatériaux, notamment à travers l'ouvrage devenu un classique qu'il a co-écrit avec Govind Agrawal [Solitons optiques : des fibres aux cristaux photoniques, Academic press, New-York, 2003]. Enfin, le travail de Yuri Kivshar a reçu plus de 80 000 citations selon Google Scholar (avec un h-index de 130), ce qui suggère le profond impact de son travail dans le domaine de la photonique. Par ailleurs, il a développé un nombre incroyable de collaborations avec des groupes de recherche dans le monde entier. Son extraordinaire vie scientifique rappelle ainsi celle du mathématicien Paul Erdôs qui a publié des travaux avec plus de 500 collaborateurs, ce qui a suscité la création du nombre d'Erdôs, le nombre d'étapes du chemin le plus court entre un mathématicien et Erdős en termes de co-paternités.

Ross McPhedran a terminé ses études de premier cycle et son doctorat à l'Université de Tasmanie, avant de déménager à Sydney en 1975 en tant que boursier de la reine Elizabeth II. Il a été nommé professeur assistant à la School of Physics (École de physique) de Sydney

University en 1984 et a été promu à une chaire personnelle en 1994. Ses intérêts couvrent de nombreux aspects de la théorie des ondes, de la photonique, des fibres microstructurées, de l'élastodynamique, de la science des composites, des méthodes mathématiques et des algorithmes numériques. McPhedran a apporté des contributions fondamentales au domaine de la science des ondes, ses techniques et ses applications. Ses travaux ont fourni des méthodes d'une précision et d'une compréhension sans précédent qui ont permis des développements majeurs dans les performances des fibres optiques microstructurées, des matériaux composites, des réseaux de diffraction, des cristaux photoniques et platoniques (ces derniers sont des plaques minces périodiques baptisées platoniques par McPhedran peut-être en référence à Platon, le philosophe athénien de la Grèce antique). La formulation multipolaire a été développée comme un outil majeur pour résoudre les problèmes de diffraction impliquant des ondes électromagnétiques et élastiques avec des systèmes périodiques infinis et finis pour des applications telles que la spectroscopie et la conversion d'énergie photovoltaïque et photothermique. Les outils associés des « *lattice sums* », de la densité des fonctions d'état, de l'analyse des modes et des défauts ont une compréhension et des méthodologies avancées de la science des ondes. Ross McPhedran a joué un rôle central dans la carrière de nombreux chercheurs scientifiques, dont l'un d'entre nous. Il s'est attaqué au cours de sa carrière exceptionnelle à des problèmes allant de la physique appliquée [Physics World 26, 32, 2013] aux mathématiques pures [https://arxiv.org/pdf/2003.14241.pdf].

Nous avons présenté quelques-uns des scientifiques éminents des sciences physiques, mathématiques et de l'ingénierie, qui à notre avis ont façonné le domaine des métamatériaux et la théorie des composites en général. Nous ne prétendons pas être exhaustifs car la liste des scientifiques éminents qui ont contribué aux métamatériaux est vaste : cette liste ne reflète que l'opinion des éditeurs invités. Cependant, comme souvent en sciences, les avancées de la recherche sont l'œuvre de nombreux individus et groupes qui contribuent à la diffusion et à l'amélioration des grandes idées de quelques heureux élus. Rappelons un autre point de l'histoire : à la fin des années 1940, Winston Kock d'AT&T Bell Laboratories a développé des matériaux qui avaient des caractéristiques similaires aux métamatériaux. Dans les années 1950 et 1960, des diélectriques artificiels ont été étudiés pour des antennes micro-ondes légères. Par la suite, les absorbeurs de radar à micro-ondes ont été étudiés dans les années 1980 et 1990 comme applications pour les milieux chiraux artificiels. Ces dispositifs peuvent être considérés comme des milieux complexes avec des propriétés inhabituelles rationnellement conçues, ils sont donc englobés par notre définition des métamatériaux (et aussi celle de Wegener).

Depuis 1999, les chercheurs qui ont contribué à ce domaine des métamatériaux comprennent des mathématiciens purs et appliqués, des physiciens théoriques et appliqués, mais aussi des chimistes, des biologistes, des ingénieurs en mécanique et aussi des géophysiciens. Par conséquent, les métamatériaux électromagnétiques ne sont qu'un côté de la médaille. En effet, les correspondances entre les équations régissant les ondes électromagnétiques et les ondes acoustiques, élastodynamiques et hydrodynamiques ont permis de traduire des phénomènes inhabituels découverts en électromagnétisme vers d'autres domaines et de trouver des applications passionnantes. Par exemple, la cape d'invisibilité proposée par Pendry et ses collègues [Science 312, 1780–1782, 2006] pour montrer le véritable potentiel du contrôle du champ électromagnétique par les métamatériaux, a ensuite été conçue pour les ondes de pression et pourrait améliorer l'acoustique des salles de concert par des colonnes acoustiquement dissimulées. L'un de nous a même proposé que les métamatériaux sismiques puissent fournir une protection contre les tremblements de terre en détournant les ondes sismiques avec une gigantesque cape d'invisibilité semblable à la cape proposée par Pendry pour les ondes électromagnétiques. Associées à la conception ou à la création de dispositifs, de nombreuses questions conceptuelles intéressantes se posent naturellement, par exemple la question récurrente

du principe de réciprocité : si la lumière ne peut atteindre un personnage fictif couvert par une cape d'invisibilité, peut-il voir le monde extérieur ? En fait, il ou elle serait dans l'obscurité totale si la cape n'avait pas de trous pour les yeux ; ces deux défauts de la cape pourraient alors être perçus par un observateur extérieur. De même dans d'autres systèmes d'ondes, il faut penser aux conséquences de tels capes ou dispositifs, par exemple, la région d'invisibilité devrait agir comme une zone de calme si l'on devait concevoir une cape pour les ondes acoustiques ou sismiques.

Jusqu'à présent, les physiques de la réfraction négative et du camouflage (c'est-à-dire des capes d'invisibilité) semblent dissociées, mais elle se retrouvent dans la théorie du camouflage externe proposée par Graeme Milton et Nicolae Nicorovici [Proc. Roy. Soc. A : Mathematical, Physical and Engineering 462, 3027–3059, 2006]. Dans cette approche, la cape d'invisibilité consiste en une coquille à réfraction négative et, de plus, l'objet à dissimuler se trouve à l'extérieur du manteau ! La conception d'une cape externe est radicalement différente de celle proposée par Pendry, puisque cette dernière est basée sur les caractéristiques anisotropes de la coquille (ou cape) entourant l'objet à cacher. Elle défie les arguments du principe de réciprocité mentionnés ci-dessus, puisque le personnage fictif n'est plus entouré par la cape, mais il vit pour ainsi dire dans une région repliée dans l'espace, appelée feuille de Riemann, qui n'est pas détectée par la lumière qui éclaire la cape externe et le personnage fictif. Une autre physique contre-intuitive est celle des isolants topologiques, qui sont des milieux complexes qui supportent une foule d'états de surface protégés grâce à des propriétés topologiques, et qui sont également englobés par notre définition des métamatériaux.

Ces deux doubles volumes spéciaux des Comptes Rendus Physique ont pour but de faire un tour d'horizon de la thématique des métamatériaux. Cet ensemble de quatorze articles, réalisé avec la coopération d'experts internationaux de premier plan dans le domaine des métamatériaux, comprend des recherches originales ainsi que des contributions plus orientées vers des revues de l'état de l'art. Les articles couvrent les sujets des métamatériaux électromagnétiques, acoustiques, élastiques et sismiques et sont organisés en deux ensembles rassemblant d'une part, des articles plus orientés sur les concepts et les modèles et, d'autre part, des articles rapportant des résultats plus liés à des applications potentielles prometteuses. Ces deux volumes doubles couvrent donc les aspects théoriques aussi bien qu'expérimentaux, et fondamentaux aussi bien qu'appliqués, dans différents domaines des métamatériaux, depuis les milieux à l'échelle nanométrique (électrodynamique et plasmonique) jusqu'aux milieux à l'échelle du mètre (géophysique).

Dans le premier des deux volumes doubles, la première série de sept articles commence par une présentation de la physique des matériaux à indice négatif à la frontière de l'électromagnétisme macroscopique, par l'un de nous. Dans cette contribution, les nouveaux phénomènes et questions apportés par la réfraction négative, les indices négatifs, la lentille plate parfaite et les structures en coin sont discutés dans le cadre de l'électromagnétisme macroscopique. Dans le prolongement, un analogue du phénomène de « trou noir » est mis en évidence dans de simples structures en coin remplies d'un matériau de permittivité avec dispersion en fréquence et des arguments sont fournis pour soutenir que, dans les milieux passifs, la partie imaginaire de la perméabilité magnétique peut prendre des valeurs positives et négatives.

Il est suivi d'un article sur l'homogénéisation avec une application aux milieux filaires par Mario Silveirinha *et al.*, qui présente un aperçu d'une théorie d'homogénéisation pour les métamatériaux périodiques. Cette approche générale *ab initio* peut être considérée comme une extension aux métamatériaux périodiques du cadre développé pour établir les équations de l'électromagnétisme macroscopique et représente une approche physique remarquable aux théories d'homogénéisation habituelles établies en mathématiques appliquées. L'approche proposée est appliquée à divers cas de milieux filaires électromagnétiques, bidimensionnels et tridi-

mensionnels, permettant de mettre en évidence une variété de phénomènes exotiques et notamment l'effet de la dispersion spatiale.

L'article suivant sur l'optique de transformation pour la plasmonique, par Paloma Huidobro et Antonio Fernandez-Dominguez, passe en revue les dernières avancées théoriques dans l'application de l'optique de transformation pour la description théorique des structures plasmoniques sous-longueur d'onde. Cet article commence par une introduction à la technique de l'optique de transformation. La technique est notamment appliquée à la conception de métasurfaces à géométries singulières, obtenues en cartographiant un volume infini étendu sur une nanoparticule plasmonique, qui permettent une absorption large bande et fournissent une plateforme pour l'étude de la dispersion spatiale. La technique est également exploitée pour déterminer analytiquement le couplage d'un émetteur quantique avec des nanoparticules plasmoniques.

L'article de Graeme Milton et Ross McPhedran est un état de l'art de la résonance anormale, du camouflage associé et de la super focalisation. Les auteurs adoptent un point de vue original et intéressant sur l'histoire du camouflage externe et de la super focalisation, alternatif à ceux que l'on trouve généralement dans la littérature, basé sur la découverte en 1994 des notions de sources fantômes et de résonances anormales. Cet article théorique apporte une belle introduction au camouflage dû à des milieux complémentaires en régime quasi-statique avec des analyses fines des résonances anormales, du camouflage et de la super focalisation dans la limite lorsque l'absorption tend vers zéro.

L'article suivant sur la métaphotonique tout diélectrique à base de résonances de Mie, par Nicolas Bonod et Yuri Kivshar, tire les avantages des structures sous-longueur d'onde tout diélectrique par rapport à leurs homologues plasmoniques. Cet article commence par une revue des résonances électriques et magnétiques à faible ordre multipolaire conduisant, sans métaux, à un magnétisme optique artificiel et à une perméabilité effective négative. Ensuite, il est montré comment ces résonances peuvent être utilisées pour obtenir l'effet Kerker et les conditions de Kerker à partir de particules diélectriques, ou concevoir une nanoantenne tout diélectrique pour l'amélioration de la force d'excitation des émetteurs quantiques. Ce concept de résonances diélectriques est appliqué à la conception de métasurfaces tout diélectriques pour « les états liés dans le continuum » (*bound states in the continuum* en anglais) et pour générer des couleurs et des hologrammes.

Philippe Barois *et al.* apportent une contribution sous forme d'un article de synthèse sur les métamatériaux nanocolloïdaux « ascendants » (*bottom-up* en anglais) aux fréquences optiques. Cet article, principalement expérimental, rend compte de la conception et de la fabrication, à partir d'assemblages de méta-atomes nanocolloïdaux, de métamatériaux tridimensionnels dans le domaine du visible. Les métamatériaux sont en outre caractérisés en termes de permittivité et de perméabilité effectives. Les deux types de métamatériaux impliquant des résonances plasmoniques ou de Mie sont abordés, montrant pour chacun leurs avantages et leurs inconvénients. Les métasurfaces pour les optiques plates et les applications d'absorbeurs parfaits sont également abordées.

La dernière contribution de cette première série d'articles, par Romain Fleury, Andrea Alù et Farzad Zangeneh-Nejad, aborde le sujet émergent des isolants topologiques. Cet article de synthèse commence par l'exemple canonique, monodimensionnel, du modèle Su–Schrieffer–Heeger (SSH), avant d'aborder des situations bidimensionnelles, en présentant des analogues d'ondes classiques des isolants topologiques de Chern, de Hall quantique, de spin-Hall, de Valley-Hall et de Floquet. Les développements les plus récents sont également passés en revue. Cet article dessine un sujet de recherche interdisciplinaire remarquable avec la transposition de concepts, découverts à l'origine dans les systèmes de matière condensée, à la physique des ondes classiques en photonique, micro-ondes, phononique, acoustique et

mécanique.

Dans le second volume double, la deuxième série de sept articles, où des applications prometteuses sont présentées, commence avec une contribution sur les lames d'onde accordables basées sur des métasurfaces, par Nader Engheta et Nasim Estakhri. Les auteurs proposent une classe de lames d'onde innovantes, pour un contrôle total du retard de phase et de la polarisation de la lumière, constituées de deux métasurfaces symétriques séparées par une distance variable. Les métastructures sont conçues par des méthodes inverses de type optimisation de topologie. Plusieurs exemples numériques sont présentés, dont des métastructures conçues à partir d'un algorithme génétique et compatibles avec les techniques de fabrication actuellement disponibles dans le domaine du visible.

L'article suivant est une étude dans le domaine visible de l'ingénierie de la dispersion et de l'efficacité des métasurfaces, par Benfeng Bai *et al.* Les métasufaces permettent la manipulation d'ondes électromagnétiques à partir du comportement fortement résonant de méta-atomes variés disposés sur un réseau sous-longueur d'onde. Après une introduction sur les métasurfaces, leurs avantages et leurs inconvénients, les auteurs passent en revue les efforts récents pour surmonter les limitations des métasurfaces en raison de leur dispersion et de leur faible efficacité. La dispersion et l'efficacité des métasurfaces sont contrôlées et adaptées en fonction des applications spécifiques : détection ultra-très sensible, modulation de champ, interactions non linéaires, image en couleur, affichage holographique ...

Les métasurfaces sont à nouveau au cœur de l'article sur les métasurfaces pour les applications d'antennes de faible épaisseur, par Massimiliano Casaletti *et al.* Dans cette contribution, les métasurfaces sont considérées pour les micro-ondes, où les technologies standard des circuits imprimés peuvent être utilisées pour une fabrication et une intégration faciles. Les auteurs passent en revue les derniers progrès dans la conception d'antennes à métasurface, où les métasurfaces sont exploitées pour miniaturiser le profil, augmenter la bande passante et contrôler le diagramme de rayonnement dans les régions de champ proche et lointain.

L'article suivant, par S. Anantha Ramakrishna *et al.*, se concentre sur les propriétés des guides d'ondes remplis de métamatériaux anisotropes. Les auteurs montrent comment les guides d'ondes à base de métamatériaux offrent une toute nouvelle gamme de nouvelles fonctionnalités exploitant la permittivité et la perméabilité anisotropes qui peuvent avoir des valeurs propres de proches de zéro ou même avec changement de signe. Les guides d'ondes à indice proche de zéro et hyperboliques conduisent à des modes avec des ordres fractionnaires et même imaginaires. Ils peuvent avoir des applications potentielles dans la microscopie optique en champ proche, l'amplification laser, la génération d'harmoniques ou l'auto-modulation de phase qui peuvent se produire sur de courtes longueurs du guide d'ondes.

L'article de Vicent Romero-Garcia *et al.* est la première contribution sur les ondes classiques autres qu'électromagnétiques avec une étude sur la conception de métamatériaux acoustiques constitués de résonateurs de Helmholtz pour une absorption parfaite. Les auteurs présentent tout d'abord une technique robuste pour la conception de métamatériaux acoustiques basée sur l'analyse, dans le plan des fréquences complexes, des zéros et des pôles des valeurs propres de la matrice de diffraction. Ensuite, plusieurs exemples de structures et de membranes unidimensionnelles parfaitement absorbantes sont passés en revue. En particulier, la possibilité d'obtenir une absorption parfaite sous certaines conditions de couplage critiques spécifiques est discutée en détail.

Cet article sur les métamatériaux acoustiques est suivi de l'article de revue sur la théorie et la conception des métamatériaux en mécanique, par le groupe de recherche en métamatériaux de Muamer Kadic. Dans cet article, les auteurs présentent la procédure générale de conception de métamatériaux élastiques à partir de masses et de ressorts. Il est montré qu'en utilisant cette approche simple, tout un ensemble de propriétés effectives peut être conçu, y compris les

métamatériaux élastiques linéaires — définis par le module de masse, le module de cisaillement et la densité de masse — et les métamatériaux non linéaires — avec des instabilités ou des éléments programmables. Les *designs* et les calculs numériques correspondants pour illustrer différents comportements constitutifs sont présentés.

Le dernier article du second double volume spécial, par Stéphane Brûlé de la société Ménard et l'un de nous, porte sur le rôle des métamatériaux sismiques sur la dynamique des sols. L'article porte sur le contrôle des sols structurés par un réseau de trous de forage (qui s'apparentent plus à des cristaux photoniques qu'à des métamatériaux, car ils fonctionnent essentiellement dans le régime de Bragg), dont il a été démontré qu'ils permettent des effets de miroirs réfléchissants et de focalisation. Certains résultats expérimentaux inédits montrent le potentiel de récupération d'énergie du bruit sismique ambiant du réseau de forages. Les auteurs ont en outre proposé de jeter un pont entre le domaine des milieux modulés dans le temps et des métamatériaux sismiques afin de générer de nouveaux effets conduisant notamment à un concept d'ordinateur sismique analogique et d'Internet des objets utilisant le bruit sismique ambiant à l'échelle géophysique.

En conclusion, ces deux doubles volumes spéciaux des Comptes Rendus Physique abordent de nombreux sujets d'actualité en physique des métamatériaux acoustiques, élastiques et électromagnétiques, découverts il y a moins d'un quart de siècle. Ce volume couvre aussi bien les aspects théoriques qu'expérimentaux dans ces différents domaines de l'échelle nanométrique (optique et plasmonique) à l'échelle du mètre (génie civil en sismique) en passant par les micro-ondes, l'acoustique et la mécanique. Des sujets émergents tels que les isolants topologiques et de nombreuses applications prometteuses des métasurfaces ont été abordés. Les quatorze articles constituant ces deux volumes doubles donnent un aperçu complet des progrès récents dans ce domaine mature. Il reste encore beaucoup à découvrir et l'avenir sera sans aucun doute passionnant. Nous espérons que cette collection d'articles contribuera à stimuler les efforts théoriques et expérimentaux en métamatériaux. Nous soulignons que toutes ces contributions promettent de révolutionner les moyens de contrôler la propagation du son, de la lumière et de toute forme particulière d'ondes à des échelles macroscopiques et microscopiques. En effet, les applications potentielles vont de la lentille sous-longueur d'onde et des guides d'ondes optiques, aux biocapteurs et au contrôle total de l'ellipticité de la lumière, à l'exaltation des émetteurs quantiques et aux interactions non linéaires, à l'optique planaire et à l'affichage holographique, à l'absorption parfaite en acoustique et aux antennes de métasurface, au camouflage sous-marin et à l'invisibilité électromagnétique, à la manipulation de la lumière visible et à la protection contre les ondes physiques délétères (par exemple, les tsunamis et les tremblements de terre).

Nous remercions chaleureusement tous les auteurs, qui sont les principaux architectes de ce volume spécial des Comptes Rendus Physique publié par l'Académie des Sciences, pour leurs excellentes contributions scientifiques et leur volonté de partager leurs connaissances des mathématiques et de la physique des métamatériaux. L'assistance et le professionnalisme des équipes du Centre Mersenne et des Comptes Rendus de l'Académie des Sciences sont également vivement remerciés. Enfin, nous sommes profondément redevables à Denis Gratias, pour son vif intérêt pour le sujet des métamatériaux et ses encouragements constants à travers la préparation de ce volume, en particulier lors de la dernière étape qui a eu lieu lors de la pandémie de covid-19 en Europe. Nous espérons que vous apprécierez la lecture de ces articles et que vous les trouverez aussi inspirants que nous.

Boris Gralak is a 1997 graduate engineer of Ecole Polytechnique, received in 2001 the PhD degree of Universtité d'Aix-Marseille in *Mathematical physics and modelling*, and then worked for 3 years from 2001 to 2004 as researcher in Amsterdam at the research institute AMOLF of Nederlands organization for scientific research (NWO). He is presently Directeur de recherche at Centre national de la recherche scientifique (CNRS) and works at Institut Fresnel in Marseille, France. His main research interests include the mathematical analysis of equations of macroscopic electromagnetism, the modelling of electromagnetic metamaterials, and the design of optical devices.
Boris Gralak est ingénieur de l'Ecole Polytechnique diplômé en 1997, a obtenu en 2001 le diplôme de doctorat de l'Université d'Aix-Marseille en *Physique mathématique et modélisation*, puis a travaillé pendant 3 ans de 2001 à 2004 comme chercheur à Amsterdam à l'institut de recherche AMOLF de l'organisation néerlandaise pour la recherche scientifique (NWO). Il est actuellement directeur de recherche au Centre national de la recherche scientifique (CNRS) et travaille à l'Institut Fresnel à Marseille en France. Ses principaux intérêts de recherche sont l'analyse mathématique des équations de l'électromagnétisme macroscopique, la modélisation des métamatériaux électromagnétiques et la conception de dispositifs optiques.

Sébastien Guenneau is a Director of Research at the Centre National de la Recherche Scientifique who joined the CNRS-Imperial Abraham de Moivre Unité Mixte Internationale in 2019, after working as a lecturer in the Department of Mathematical Sciences at Liverpool University (2004–2005; 2007–2009) and as a CNRS researcher at the Institut Fresnel in Marseille (2006–2019). His main research interests lie in the physics of metamaterials for an enhanced control of wave and diffusion phenomena (including negative refraction and cloaking), in homogenization of multi-scale periodic and quasi-periodic media, and in finite element models of acoustic, electromagnetic, hydrodynamic and elastodynamic waves.
Sébastien Guenneau est directeur de recherche au Centre National de la Recherche Scientifique. Il a rejoint l'Unité Mixte Internationale CNRS-Impérial Abraham de Moivre en 2019, après avoir travaillé comme chargé de cours au Département des Sciences Mathématiques de l'Université de Liverpool (2004–2005 ; 2007–2009) et en tant que chercheur CNRS à l'Institut Fresnel de Marseille (2006–2019). Ses principaux axes de recherche résident dans la physique des métamatériaux pour un contrôle accru des phénomènes ondulatoires et des processus diffusifs (y compris la réfraction négative et le camouflage), dans l'homogénéisation de milieux périodiques et quasi-périodiques multi-échelles, et dans les modèles d'éléments finis en acoustique, électromagnétisme, hydrodynamique et élastodynamique.

Boris Gralak
CNRS, Aix Marseille Univ
Centrale Marseille, Institut Fresnel
Marseille, France
boris.gralak@fresnel.fr

Sébastien Guenneau
UMI 2004 Abraham de Moivre-CNRS
Imperial College London
London SW7 2AZ, UK
s.guenneau@imperial.ac.uk

Comptes Rendus
Physique
2020, 21, nº 4-5, p. 343-366
https://doi.org/10.5802/crphys.29

Metamaterials 1 / *Métamatériaux 1*

Negative index materials: at the frontier of macroscopic electromagnetism

Matériaux d'indice négatif : à la frontière de l'électromagnétisme macroscopique

Boris Gralak[a]

[a] CNRS, Aix Marseille Univ, Centrale Marseille, Institut Fresnel, Marseille, France
E-mail: boris.gralak@fresnel.fr

Abstract. The notions of negative refraction and negative index, introduced by V. Veselago more than 50 years ago, have appeared beyond the frontiers of macroscopic electromagnetism and purely formal during 30 years, until the work of J. Pendry in the late 1990s. Since then, the negative index materials and the metamaterials displayed extraordinary properties and spectacular effects which have tested the domain of validity of macroscopic electromagnetism. In this article, several of these properties and phenomena are reviewed. First, mechanisms underlying the negative index and negative refraction are briefly presented. Then, it is shown that the frame of the time-harmonic Maxwell's equations cannot describe the behavior of electromagnetic waves in the situations of the perfect flat lens and corner reflector due to the presence of essential spectrum at the perfect -1 index frequency. More generally, it is shown that simple corner structures filled with frequency dispersive permittivity have a whole interval of essential spectrum associated with an analog of "black hole" phenomenon. Finally, arguments are provided to support that, in passive media, the imaginary part of the magnetic permeability can take positive and negative values. These arguments are notably based on the exact expression, for all frequency and wave vector, of the spatially-dispersive effective permittivity tensor of a multilayered structure.

Résumé. Les notions de réfraction négative et d'indice négatif, imaginées par V. Veselago il y a plus de 50 ans, ont semblé au-delà des frontières de l'électromagnétisme macroscopique et sont restées purement formelles pendant 30 ans, jusqu'aux travaux de J. Pendry à la fin des années 1990. Depuis lors, les matériaux à indice négatif et les métamatériaux ont montré des propriétés extraordinaires et des effets spectaculaires qui ont mis à l'épreuve le domaine de validité de l'électromagnétisme macroscopique. Dans cet article, plusieurs de ces propriétés et phénomènes sont passés en revue. Tout d'abord, les mécanismes sous-jacents aux indices négatifs et à la réfraction négative sont brièvement présentés. Ensuite, il est montré que le cadre des équations de Maxwell harmoniques en temps ne peut pas décrire le comportement des ondes électromagnétiques dans les situations de la lentille plate et du réflecteur en coin parfaits en raison de la présence de spectre essentiel à la fréquence où l'indice prend la valeur -1. Plus généralement, il est montré que de simples structures en coin remplies d'une permittivité dispersive en fréquence ont un intervalle entier de spectre essentiel associé à un analogue du phénomène de « trou noir ». Enfin, des arguments sont fournis pour soutenir que, dans les milieux passifs, la partie imaginaire de la perméabilité magnétique peut prendre des valeurs positives et négatives. Ces arguments reposent notamment sur l'expression exacte, pour toutes les fréquences et tous les vecteurs d'onde, du tenseur de permittivité effective avec dispersion spatiale d'une structure multicouche.

Keywords. Negative index, Metamaterials, Frequency dispersion, Corner mode, Spatial dispersion, Passivity, Permeability.

Mots-clés. Indice négatif, Métamatériaux, Dispersion en fréquence, Mode de coin, Dispersion spatiale, Passivité, Perméabilité.

1. Introduction

The notion of negative index of refraction has been introduced more than 50 years ago by V. Veselago [1]. The refraction at an interface separating two media with positive and negative refractive indices is subject to the usual Snell–Descartes law:

$$n_1 \sin\phi_1 = n_2 \sin\phi_2. \tag{1}$$

Consequently, if the refractive indices n_1 and n_2 of the two media have opposite sign, e.g. $n_1 > 0$ and $n_2 < 0$, then the refraction angles ϕ_1 and ϕ_2 have also opposite sign, so that the ray is negatively refracted at the interface (see Figure 1). In macroscopic electromagnetism, media with negative refractive index can be modelled by magnetodielectric materials with simultenously negative values of the dielectric permittivity ε and magnetic permeability μ [1]. In such media, the wave vector $\boldsymbol{k}$ has opposite direction from the Poynting vector $\boldsymbol{S} = \boldsymbol{E} \times \boldsymbol{H}$, and the triplet formed by the electric field $\boldsymbol{E}$, the induction field $\boldsymbol{H}$ and the wave vector $\boldsymbol{k}$ is left-handed. Thus V. Veselago also coined a medium with negative refractive index a "left-handed material" [1].

Since no material can be found in nature with simultaneously negative values of the permittivity ε and permeability μ, the notion of negative refractive index has appeared beyond the frontiers of macroscopic electromagnetism and thus remained purely formal for thirty years, until the work of J. Pendry in 1999. In [2], J. Pendry *et al.* showed that *"microstructures built from nonmagnetic conducting sheets exhibit an effective magnetic permeability μ_{eff}, which can be tuned to values not accessible in naturally occurring materials"*, paving the way towards artificial magnetism, negative index materials and, more generally, metamaterials with extraordinary properties. Since then, the notion of negative index material has opened a vast range of possibilities and has tested the domain of validity of macroscopic electromagnetism.

In this paper, a brief overview of the electromagnetic negative index materials is presented through the mechanisms underlying the negative index of refraction, the negative index and the proposal of the perfect -1 index lens. The fundamental role of frequency dispersion in negative index materials and metamaterials is shown. Then, the spectral properties of corner structures with frequency dispersive permittivity are analyzed and an analog of "black hole" phenomenon is discussed. Finally, the key role of spatial dispersion (or non-locality) in effective permeability and metamaterials is highlighted. In particular the question on the sign of the imaginary part of the permeability in passive media is addressed. The new phenomena and questions brought by these topics within the frame of the macroscopic electromagnetism will be discussed.

2. Mechanisms underlying negative index materials

Media with negative refractive index have appeared unavailable since no natural medium may have simultaneously permittivity ε and permeability μ with real part taking negative values. Indeed, negative values of the permittivity occur in metals at frequencies around the visible range while, in the same range, the values of the permeability must be restricted around that of vaccum permeability [3]. The range of possible macroscopic electromagnetic responses has been first extended with the works on the so-called *bounds* on the effective parameters of composite

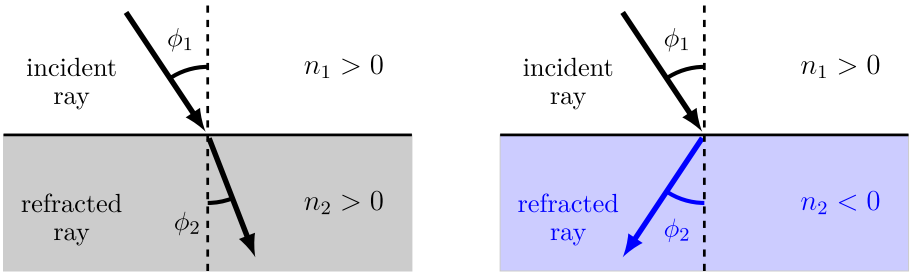

Figure 1. Refraction at an interface separating two media with positive refractive indices (left) and with positive and negative refractive indices (right).

materials, for instance on the effective permeability [4] and permittivity [5–8]. For given permittivity constants and volume fractions of the components constituting a composite, such *bounds* characterize the set of possible macroscopic responses and identify the microstructure producing the extreme effective parameters in this set, see the book of G. Milton [9] for an extensive presentation of the *bounds* of composites. These works on bounds offered new possibilities in terms of achievable values of permittivity and anisotropy. These works have been however restricted to the quasistatic regime in the frame of classical homogenization [10], where the effective parameters result from an averaging process. In this frame, the range of frequencies with negative values of permittivity cannot be significantly extended and, moreover, the effective permeability remains equal to the vacuum permeability as soon as the components constituting the composite are non-magnetic, leaving the negative refractive index unachievable in theory and in practice.

The fundamental steps that led to the negative indices have been completed thanks to the works of J. Pendry and his colleagues. Back in 1996, they proposed three-dimensional network structures made of thin metallic wires and showed theoretically, numerically and experimentally that such structures exhibit metallic behavior with low plasma frequency in the range of GHz [11, 12]. In such structures, the plasma frequency of the original metal ω_p, which is proportional to the ratio $\sqrt{N/m_{\text{eff}}}$ of the electron density N and the electron effective mass m_{eff}, is made lower using two mechanisms: (i) the electron density N is reduced since the fraction of metal in the wires network is lower than in the bulk metal and (ii) the electron effective mass m_{eff} is enhanced by confining the electrons in the thin wires. With these mechanisms, the effective plasma frequency is strongly reduced and the metallic behavior encountered in the visible range is extended to the Ghz range, which allows effective permittivity with negative values in a new range of frequencies. Then, in 1999, these physicists proposed structures made of the so-called *split rings* that exhibit resonant effective magnetic permeability in the GHz range [2]. Here, the magnetic response is induced by loops of current in the rings. In addition, this magnetic response is enhanced by introducing a thin split which makes the *split ring* equivalent to a *LC* resonator, the capacitance C resulting from the thin split and the inductance L resulting from the ring. The resonance is essential since it enhances the effective magnetic response and thus offers the possibility to address negative values of the effective permeability. Finally, combining these conducting non-magnetic *split ring* resonators with thin wires, D. Smith *et al.* proposed a composite medium with simultaneously negative permittivity and permeability in the GHz range [13]: this work enabled the experimental demonstration in the Ghz range of a negative refractive index [14], the extraordinary electromagnetic property imagined by V. Veselago in 1968 [1].

It is stressed that, in this new kind of metallic composites proposed by J. Pendry and his colleagues, the microstructure induces resonances in the effective electric and magnetic responses, which makes the nature of the underlying mechanism different from the one encountered so far

in classical homogenization and in the *bounds* of composites. Hence this new kind of composites offering extraordinary properties has been coined *metamaterials* in 2001 [15].

The implementation of metallic resonant composites operating at frequencies higher than Ghz appeared difficult and remains challenging, notably in the visible range, because of the requirements on the dimensions of the nanostructures and the presence of absorption in metals. However, in the visible and the near-infrared, purely dielectric periodic strutures, or photonic crystals [16, 17], have been exploited to obtain negative refraction at in interface separating such a structure and a homogeneous medium [18, 19]. In that case the resonance is not produced by the solely resonator itself (e.g. a *split ring*) but by the interaction between the dielectric particles periodically arranged. This resonant interaction requires that the distance between the particles be comparable to the wavelength, which results in severe limitations to consider a photonic crystal as an effectif homogeneous medium. Nevertheless, their ability to induce negative refraction in the visible range may have important consequences.

The mechanism leading to negative refraction with photonic crystals exploits the richness, in such periodic structures, of the dispersion law, i.e. the relationship $\omega(\boldsymbol{k})$ between the frequency ω and the Bloch wave vector $\boldsymbol{k}$. Indeed, the propagation of electromagnetic waves is governed by the group velocity $\boldsymbol{v}_g$ [20–22] defined as the gradient of the dispersion law: $\boldsymbol{v}_g = \partial_{\boldsymbol{k}}\omega(\boldsymbol{k})$. At an interface separating a homogeneous medium from a photonic crystal, the tangential component $\boldsymbol{k}^{\parallel}$ of the (Bloch) wave vector $\boldsymbol{k}$, parallel to the interface, is conserved according to the invariance of the periodic structure under the discrete set of lattice translations $\{\pm\boldsymbol{a}, \pm 2\boldsymbol{a}, \pm 3\boldsymbol{a}, \ldots\}$. Therefore, if the group velocity $\boldsymbol{v}_g$ has opposite direction from the wave vector $\boldsymbol{k}$, then this invariance of the tangential component $\boldsymbol{k}^{\parallel}$ of the wave vector results in the sign change of the tangential component $\boldsymbol{v}_g^{\parallel}$ at the interface. Such a situation, where the group velocity $\boldsymbol{v}_g$ and the Bloch wave vector $\boldsymbol{k}$ have opposite signs, can be realized thanks to the folding of the dispersion law in photonic crystals, as represented on Figure 2. Detailed analyses and numerical demonstrations of negative refraction of electromagnetic waves in photonic crystals can be found in [18, 19, 21], and experimental verification in [23].

The discovery of metamaterials and of their extraordinary properties stimulated the development of new homogenization techniques and effective medium theories, beyond the classical homogenization operating in the quasistatic limit, i.e. where the size of the microstructure tends to zero [10]. Indeed, classical homogenization results in an averaging process which cannot report properties like artificial magnetism and negative refractive index from purely dielectric constituents. For instance, the analysis of metamaterials with negative permittivity and permeability [24] has shown that the effective parameters of such structures are not quasistatic. Hence, in addition to the seminal works of J. Pendry [2, 11, 12], several new techniques have been proposed in applied mathematics and theoretical physics, extending the notion and validity of homogenization and of effective medium theory to new situations, see reference [25] for a review in 2009. The classical two-scale homogenization technique [26] has been extended to high-contrast inclusions [27] and led to the prediction of effective permeability. The retrieval method, based on the extraction of constitutive parameters from Fresnel reflexion and transmission coefficients, has been investigated for layered metamaterials [28, 29]. The classical quasistatic limit as been also overcome in the case of periodic metamaterials made of dielectric meta-atoms, by an approach relating the macroscopic fields to the microscopic fields averaged over the Floquet unit cell [30–32], which can be considered as an extension to periodic arrays of meta-atoms of the classical derivation of macroscopic Maxwell's equations [33]. Also, perturbative expansions with respect to the frequency have been proposed: when starting from the quasistatic limit [34], it has been shown that the first order in frequency reports magnetoelectric coupling while the second order in frequency reports effective magnetism (the higher orders bringing refined corrections to all these parameters), a mechanism similar to the expansion on the wave vector [3, 35]; and when

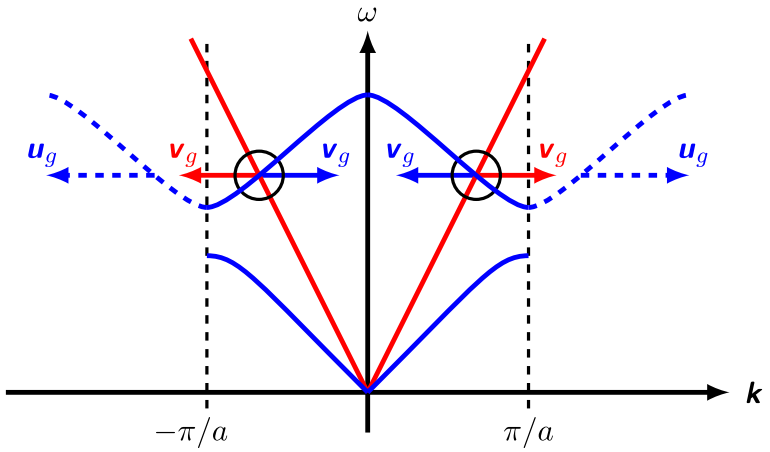

Figure 2. Effect of the folding of the dispersion law on group velocity. The red cone represents the dispersion law in a homogeneous medium with positive index: the group velocity $\boldsymbol{v}_g$ and the wave vector $\boldsymbol{k}$ in abscissa point in the same direction. The blue curve represents the dispersion law in a photonic crystals: if the dispersion law is unfolded (dotted blue curve) then the group velocity $\boldsymbol{u}_g$ and the wave vector $\boldsymbol{k}$ both point in the same direction; if the dispersion law is folded (continuous blue curve) then the group velocity $\boldsymbol{v}_g$ and the wave vector $\boldsymbol{k}$ point in opposite directions. At the couple $(\omega, \boldsymbol{k})$ indicated by the black circle, the folded dispersion law must be considered and the photonic crystal generates negative refraction.

starting from higher bands, it has been shown [36, 37] that the structure can be homogenized using the two-scale homogenization, leading to the notion of high frequency homogenization.

These non-asymptotic techniques revealed the importance of the effect of the physical boundaries of metamaterials and periodic structures [38–45]. They also highlighted the crucial role of the non-locality or *spatial dispersion* [29–32, 35, 42, 46, 47] in metamaterials and negative refractive index structures. In general, the modelling of metamaterials and periodic composites with techniques beyond the classical quasistatic limit, results unavoidably in the definition of effective parameters depending on $(\omega, \boldsymbol{k})$, the frequency (*frequency dispersion*) and the wave vector (*spatial dispersion*). Frequency and spatial dispersions are inherent to metamaterials and negative refractive media, which generated numerous questions and investigations on the *causality principle* and *passivity* of effective parameters [48–53]. In the next sections, these questions related to the dispersion are addressed.

3. The perfect lens and the spectral properties of frequency dispersive structures with negative permittivity

The most spectacular devices based on metamaterials are probably the perfect lens [54] and the invisibility cloak [55–57] proposed by J. Pendry. These propositions generated numerous interesting discussions and investigations in the community of classical electrodynamics. For the invisibility, the possibility to perfectly hide an obstacle implies that the solution to Maxwell's equations is strictly the same outside the invisibility cloak, independently of the obstacle inside the cloak, to that one would have in the absence of scattering object and cloak (so in free space). As a consequence, if the invisibility cloak is causal and passive, then the perfect invisibility can occur only at isolated frequencies [58]. Indeed, let $\boldsymbol{E}(\boldsymbol{x}, \omega)$ and $\boldsymbol{E}_0(\boldsymbol{x}, \omega)$ be the time-harmonic

electric fields oscillating at the frequency ω in the presence of the cloak, respectively with and without the obstacle. For perfect invisibility, these two electric fields are equal for position vector $\boldsymbol{x}$ outside the cloak: $\boldsymbol{E}(\boldsymbol{x},\omega) = \boldsymbol{E}_0(\boldsymbol{x},\omega)$. As for causal and passive media these electric fields are analytic functions of the frequency (as soon as ω has positive imaginary part) [59], they must be equal either for isolated frequencies ω, or for all real frequencies. Perfect invisibility is therefore only achieved at isolated frequencies and is impossible over a frequency interval. These arguments show that a causal and passive invisibility cloak must be a frequency dispersive structure.

Frequency dispersion is also an important dimension of negative index materials and the perfect lens. In 1968, V. Veselago introduced the notion of negative index of refraction and showed that a simple plate of such a medium with thickness d "can focus at a point the radiation from a point source located at a distance $l < d$" [1]. In 2000, J. Pendry extended this flat lens to negative index material including evanescent waves, and concluded that it makes a perfect lens with infinite resolution [54], beyond the diffraction limit. This perfect lens and the many potential applications have been debated in the literature with intense discussions about the infinite resolution and the underlying arguments [60–63], the divergence of the field [64], the causality principle [64, 65], and even about the existence of negative index [65, 66]. The difficulty comes from the presence of a singularity in the Green's function and the solution of the time-harmonic Maxwell's equations at the frequency ω_1 of the perfect -1 index, where the relative permittivity and permeability take simultaneously the value -1: $\varepsilon(\omega_1) = -\varepsilon_0$ and $\mu(\omega_1) = -\mu_0$, where ε_0 and μ_0 are respectively the permittivity and the permeability in vacuum. This singularity is unusual since, in mathematics, it appears at the frequency ω_1 which is an eigenvalue with infinite degeneracy of the operator associated to the Maxwell's equations [67], i.e. at a frequency in the *essential spectrum* of Maxwell's equations. In physics, the strategy may be to consider the *low absorption limit*: a small absorption is introduced, e.g. $\varepsilon^{(\gamma)} = -\varepsilon_0 + \mathrm{i}\gamma$ and $\mu^{(\gamma)} = -\mu_0 + \mathrm{i}\gamma$ with $\gamma > 0$, so that the time-harmonic Maxwell's equations are well posed for $\gamma > 0$ [63], and then the limit $\gamma \downarrow 0$ is taken. However, the solution of time-harmonic Maxwell's equations does not converge when the absorption γ tends to zero. Therefore the *low absorption limit* fails in the situation of the flat lens at the frequency ω_1 of the perfect -1 index. In other words, one can conclude that the solution to the time-harmonic Maxwell's equations does not exist at the frequency ω_1 in the case of the perfect lens. Such situations where the time-harmonic Maxwell's equations have no solutions have been also uncountered with active (or gain) media [68–70].

The absence of solutions to the time-harmonic Maxwell's equations generated difficulties to analyze the behavior of the perfect flat lens, to the point of even questioning the possibility and the existence of perfect negative index media. The solution to all these difficulties lies in rigorously taking into account the frequency dispersion.

It has been noticed by V. Veselago in his seminal article [1] that the permittivity and the permeability must depend on frequency in negative index media. This requirement, which is a consequence of the *causality principle* and the *passivity*, can be established from the generalized expression of the Kramers–Kronig relations [59, 67, 71, 72] corresponding to the Herglotz–Nevanlinna representation theorem [73]. For a complex frequency ω with positive imaginary part, $\mathrm{Im}\,\omega > 0$, this generalized Kramers–Kronig expression of the permittivity is [67]

$$\varepsilon(\boldsymbol{x},\omega) = \varepsilon_0 - \int_{\mathbb{R}} \mathrm{d}\nu \frac{\sigma(\boldsymbol{x},\nu)}{\omega^2 - \nu^2}, \quad \sigma(\boldsymbol{x},\nu) = \mathrm{Im}\,\frac{\nu\varepsilon(\boldsymbol{x},\nu)}{\pi} \geq 0, \tag{2}$$

where the relation $\sigma(\boldsymbol{x},\nu) \geq 0$ is a consequence of the passivity [67]. Notice that the quantity $\sigma(\boldsymbol{x},\nu)$ is a generalized function of ν and may contain Dirac contributions (for instance in the non-aborptive case [67, 73]). This passivity requirement for real frequency ν can be extended

to complex frequencies ω with positive imaginary part, since the imaginary part of the integral multiplied by ω in the expression above is positive:

$$\operatorname{Im}\omega\varepsilon(\boldsymbol{x},\omega) \geq \operatorname{Im}\omega\varepsilon_0. \tag{3}$$

Let ω_1 be a real frequency at which the imaginary part of the permittivity vanishes. Then $\sigma(\boldsymbol{x},\omega_1) = 0$ and the integral in the expression

$$\omega_1\varepsilon(\boldsymbol{x},\omega_1) = \omega_1\varepsilon_0 - \int_{\mathbb{R}} \mathrm{d}\nu \frac{\sigma(\boldsymbol{x},\nu)}{\omega_1 - \nu}, \tag{4}$$

is well-defined and real. Considering the derivative of this equation and using that $\sigma(\boldsymbol{x},\nu) \geq 0$, the following well-known inequality [1, 3] is obtained: if $\operatorname{Im}\varepsilon(\boldsymbol{x},\omega_1) = 0$, then

$$\operatorname{Re}\frac{\partial\,\omega\varepsilon}{\partial\omega}(\boldsymbol{x},\omega_1) \geq \varepsilon_0 \quad\Longleftrightarrow\quad \operatorname{Re}\varepsilon(\boldsymbol{x},\omega_1) \geq \varepsilon_0 - \operatorname{Re}\frac{\partial\varepsilon}{\partial\omega}(\boldsymbol{x},\omega_1). \tag{5}$$

This inequality means that, if the permittivity $\varepsilon(\boldsymbol{x},\omega_1)$ takes at the frequency ω_1 a real value less than the vacuum permittivity ε_0, then the derivative of the permittivity with respect to the frequency cannot vanish at the frequency ω_1. This corresponds precisely to the case of negative index materials and, more generally, to the situations offered by metamaterials for which the effective permittivity (and possibly the effective permeability) takes negative values or values below ε_0. Therefore, the frequency dispersion must be considered in negative index media and in metamaterials (for instance for effective refractive index below unity, also called ultra-refraction). Otherwise, the absence of frequency dispersion introduces contradictions with the causality principle or the passivity requirement.

A canonical approach for frequency dispersion has been established in 1998 by A. Tip with the *auxiliary field formalism* [71]. This formalism has been originally introduced to define a proper frame for macroscopic Maxwell's equations in absorptive and frequency dispersive dieletric media, for their quantized version [71, 74], and for the generalization of the density of states and the description of the atomic decay in absorptive and frequency dispersive structures [71, 75]. This formalism is based on the introduction of auxiliary fields so that macroscopic Maxwell's equations can be written equivalently as a unitary time evolution equation involving both electromagnetic and auxiliary fields: the new augmented system satisfies an overall energy conservation and the frequency dependence of the permittivity is transferred to the auxiliary fields. In other words, this general technique transforms a time-dependent and non self-adjoint dissipative operator into a time-independent and self-adjoint augmented operator. In 2005, A. Figotin and J. Schenker have shown that this *auxiliary field formalism* introduced by A. Tip is precisely the unique minimal self-adjoint extension of the dissipative Maxwell's equations [76]. This canonical formalism has been extended to magnetodielectric materials in order to describe frequency dispersive negative index materials [67]. It has been shown that the time evolution of a system comprising a perfect -1 index material, i.e. with a frequency ω_1 at which $\varepsilon(\boldsymbol{x},\omega_1) = -\varepsilon_0$ and $\mu(\boldsymbol{x},\omega_1) = -\mu_0$ (for $\boldsymbol{x}$ in the -1 index material), is well-defined since the electromagnetic energy remains finite at all times as soon as this is the case at the initial time: hence the compatibility of the existence of perfect negative index materials with causality principle and passivity has been unambiguously established using the canonical extension of Maxwell's equations [67].

In the case of the flat lens with perfect -1 index at the frequency ω_1, the Green's function has a pole at the frequency ω_1 [67, 77, 78] and the time-harmonic Maxwell's equations has no solution at the oscillating frequency ω_1: the time-harmonic frame fails in the case of the flat lens with perfect -1 index (or perfect negative index). However, according to the canonical frame of the *auxiliary field formalism*, the solution to (time-dependent) Maxwell's equations is well-defined at all time if it is the response to an external current source [67] as in Figure 3. The long-time behavior of such a solution can be considered for a current source turned on at an initial

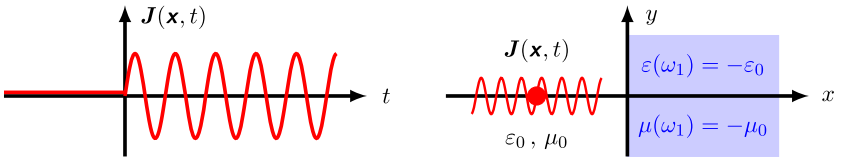

Figure 3. An external current source $\boldsymbol{J}(\boldsymbol{x},t)$ swithed on at the intial time $t=0$ and then oscillating at the frequency ω_1. This source is located at the vicinity of a plane interface separating the vacuum from a medium with perfect -1 index at the frequency ω_1.

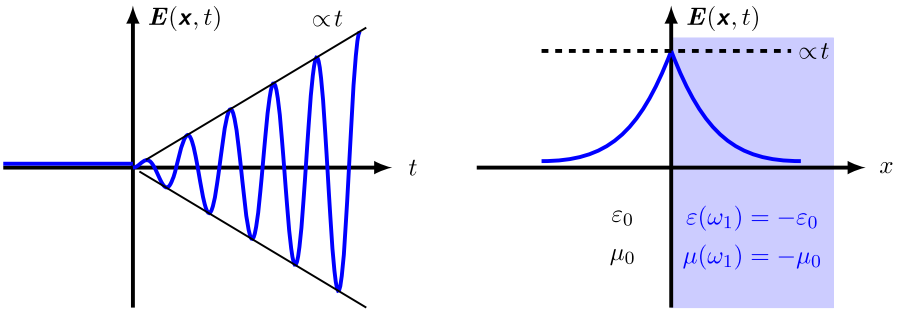

Figure 4. The reponse of the external current source swithed on at the intial time $t=0$ and then oscillating at the frequency ω_1. The amplitude of the evanescent waves at the plane interface separating the vacuum from the perfect -1 index medium (see right panel) is linearly increasing with time (see left panel).

time and then oscillating with the operating frequency ω_1 [67, 77, 78]. In the case of a single plane interface separating a perfect -1 index medium and vacuum ("single interface" case), it has been shown that the evanescent components of this time-dependent solution have their amplitude increasing linearly with time [77–79], see Figure 4. Consequently, this solution does not converge for long times to the solution to the corresponding time-harmonic problem: the *limiting amplitude principle* is not valid in this case [79]. The situation is similar in the case of the perfect flat lens (two plane interfaces delimiting a -1 index layer from vacuum, or "two interfaces" case), leading to the conclusion that the image of a point source by the perfect -1 flat lens is not a point image [77,78]. An analyzis based on the calculation of the spectral projector [79] provided the complete characterization of the spectral properties in the "single interface" case. In particular the presence of *essential spectrum* in Maxwell's equations has been highligthed at the -1 frequency ω_1 which is an eigenvalue with infinite degeneracy [67, 79].

It turns out that the extraordinary property of the perfect -1 index and the induced phenomena in the perfect flat lens are related to the presence of *essential spectrum* in Maxwell's equations. Thus the complete characterization of the spectral properties of frequency dispersive and negative index structures appears to be an important issue. For instance, a perfect corner reflector made of two orthogonal planes delimiting positive and negative index media makes a cavity that traps light and where the density of states appears to be infinite [80–83]. This infinite density of states has been related to the existence of an infinite number of modes at the -1 index frequency [80, 83], i.e. the -1 index frequency is also included in the essential spectrum as an eigenvalue with infinite degeneracy in this case of the perfect corner reflector. Next, further investigations have shown that two dimensional Maxwell's systems with corners delimiting a medium with positive permittivity (e.g. vacuum) from a medium with negative permittivity (and—or—a

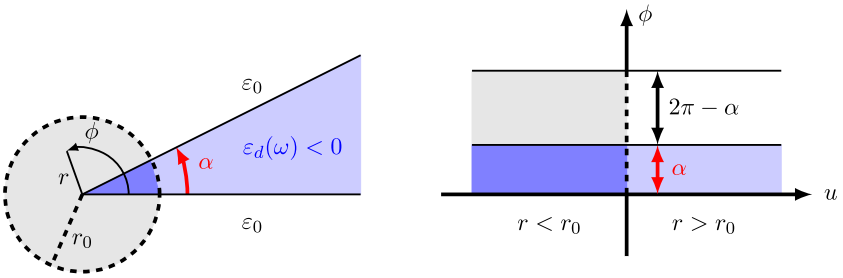

Figure 5. Left: a two-dimensional corner structure of angle α delimiting a frequency dispersive medium of permittivity $\varepsilon_d(\omega)$. Right: the 2π-periodic one-dimensional layered structure obtained after the change of variable $r \longmapsto u = \ln(r/r_0)$ and the assumption considering that the modes are localized in the vicinity of the corner.

negative permeability) bring up *essential spectrum* for an interval of negative values of the permittivity around $-\varepsilon_0$ (or around the permittivity ratio -1) [84–87]: for example, in the case of a 90 degrees corner, there is *essential spectrum* for the permittivity interval $[-3\,\varepsilon_0, -\varepsilon_0/3]$. This *essential spectrum* is associated with an analog of "black hole" phenomenon occurring in the vicinity of a corner which behaves like an unbouded domain. Such unusual effect and spectral properties, originally reported in the case of the negative index perfect corner reflectors, appears to be omnipresent in Maxwell's systems with corners delimiting a frequency dispersive medium [88]. Indeed, let the permittivity $\varepsilon_d(\omega)$ of the frequency dispersive medium be given by the Drude–Lorentz model:

$$\varepsilon_d(\omega) = \varepsilon_0 - \varepsilon_0 \frac{\Omega^2}{\omega^2 + \mathrm{i}\gamma\omega - \nu^2}, \tag{6}$$

where Ω, ν and γ are positive real constants. Then, there always exists a complex frequency ω_1 at which $\varepsilon_d(\omega_1) = -\varepsilon_0$: $\omega_1 = -\mathrm{i}\gamma/2 \pm \sqrt{\nu^2 + \Omega^2/2 - \gamma^2/4}$. And, for example, in the case of a 90 degrees corner, the permittivity interval $[-3\,\varepsilon_0, -\varepsilon_0/3]$ is spanned for the following range of complex frequencies

$$\left[-\mathrm{i}\gamma/2 \pm \sqrt{\nu^2 + \Omega^2/4 - \gamma^2/4}, -\mathrm{i}\gamma/2 \pm \sqrt{\nu^2 + 3\Omega^2/4 - \gamma^2/4} \right]. \tag{7}$$

If the permittivity is given by a more general expression, for instance a finite sum of Drude–Lorentz contributions, then the number of segments in the complex plane of frequencies, generally curved, increases like the degree of the polynomials involved in the permittivity expression. Hence the intervals of *essential spectrum* appear unavoidable in frequency dispersive systems with corners.

The main arguments exhibiting the presence of *essential spectrum* can be the following [85]: let α in $]0, 2\pi[$ be the angle of a two-dimensional corner filled with a dispersive mediumof permittivity $\varepsilon_d(\omega)$ and $\boldsymbol{x} = (r, \phi)$ the considered cylindrical coordinates (see Figure 5). The permittivity of the system is independent of the radial variable r: $\varepsilon(\boldsymbol{x}, \omega) = \varepsilon(\phi, \omega)$, $\varepsilon(\phi, \omega) = \varepsilon_d(\omega)$ for an azimuthal variable ϕ in $[0, \alpha]$ and $\varepsilon(\phi, \omega) = \varepsilon_0$ for ϕ in $[\alpha, 2\pi]$. In the time-harmonic regime, the magnetic field component $H(r, \phi, \omega)$ of the transverse magnetic waves is the solution to the Helmholtz equation

$$\frac{1}{r}\frac{\partial}{\partial r} r \frac{\partial H}{\partial r} + \frac{\varepsilon}{r^2}\frac{\partial}{\partial \phi}\frac{1}{\varepsilon}\frac{\partial H}{\partial \phi} + \omega^2 \varepsilon \mu_0 H = 0, \tag{8}$$

where the dependence on (r,ϕ,ω) has been omitted. Then the change of variable $r \longmapsto u = \ln(r/r_0)$ is performed in this Helmholtz equation (see Figure 5). The magnetic field component $\tilde{H}(u,\phi,\omega) = H(r_0 e^u,\phi,\omega)$ is now solution to

$$\frac{\partial^2 \tilde{H}}{\partial^2 u} + \varepsilon \frac{\partial}{\partial \phi} \frac{1}{\varepsilon} \frac{\partial \tilde{H}}{\partial \phi} = -r_0^2 e^{2u} \omega^2 \varepsilon \mu_0 \tilde{H}, \tag{9}$$

where the dependence on (u,ϕ,ω) has been omitted. Assuming that the modes generated by the corner are localized in the circle of radius r_0, i.e. $\tilde{H}(u,\phi,\omega) \approx 0$ for u positive, and choosing the radius r_0 small enough, then the right hand side in (9) can be neglected and set to zero. Next, a Fourier decomposition $\tilde{H}(u,\phi,\omega) \longmapsto \hat{H}(k,\phi,\omega)$ is applied, and the resulting equation is exactly that for a periodic one-dimensional layered structure (see Figure 5):

$$\varepsilon \frac{\partial}{\partial \phi} \frac{1}{\varepsilon} \frac{\partial \hat{H}}{\partial \phi} - k^2 \hat{H} = 0. \tag{10}$$

Hence, the existence of a mode 2π-periodic with respect to the azimuthal variable ϕ is subject to the following condition [89]:

$$\cosh[k\alpha]\cosh[k(2\pi-\alpha)] + \frac{1}{2}\left[\frac{\varepsilon_0}{\varepsilon_d(\omega)} + \frac{\varepsilon_d(\omega)}{\varepsilon_0}\right]\sinh[k\alpha]\sinh[k(2\pi-\alpha)] = 1. \tag{11}$$

For $k = 0$ the equality is achieved but the solution is trivial (constant) and yields vanishing electric field. Hence the existence of a corner mode is subject to a solution for $k \neq 0$. The function on the left hand side is made of two terms: the first term with the cosh functions starts from 1 at $k = 0$ and then is growing to $+\infty$; thus the second term with the sinh functions must decrease towards $-\infty$, which requires a real negative value for $\varepsilon_d(\omega)$. Since the factor in front of the sinh functions has absolute value greater than 1 (except in the case $\varepsilon_d(\omega) = -\varepsilon_0$ where it equals 1), the sum of the two terms in the left hand side tends to $-\infty$ for large values of k. Therefore, to obtain a solution $k \neq 0$ to (11), it is enough that the second derivative at $k = 0$ of the function on the left hand side be positive. This second derivative is

$$\alpha(2\pi-\alpha)\left[\frac{\alpha}{2\pi-\alpha} + \frac{2\pi-\alpha}{\alpha} + \frac{\varepsilon_0}{\varepsilon_d(\omega)} + \frac{\varepsilon_d(\omega)}{\varepsilon_0}\right], \tag{12}$$

which is positive if and only if

$$\frac{\varepsilon_d(\omega)}{\varepsilon_0} \in [-I_\alpha, -1/I_\alpha], \quad I_\alpha = \max\left\{\frac{\alpha}{2\pi-\alpha}, \frac{2\pi-\alpha}{\alpha}\right\}. \tag{13}$$

Notice that, for $\alpha = \pi$, i.e. when the corner becomes a plane interface, the number $I_\alpha = 1$ and the interval reduces to the point -1. In that case, one can check that the condition (11) is achieved for all k if $\alpha = \pi$ and $\varepsilon_d(\omega) = -\varepsilon_0$. The radial dependence of the corner modes is given by

$$r \longmapsto \exp[\mathrm{i}k \ln r/r_0] \tag{14}$$

which is oscillating with spatial frequency tending to infinity when $r \longrightarrow 0$. As a result, the electric field, deduced from the derivative, has a singularity like $1/r$ and then is not square integrable, i.e. is not finite energy. This behavior, represented on Figure 6, is different from the previous results reported in the textbooks [90] where only dielectric materials with positive permittivity and conducting materials have been considered, leading to the strongest singularity in $1/\sqrt{r}$ and to finite energy fields [90, Sections 5.2, 5.3 and 9.7.5]. In the present case of negative permittivity, the corner modes have infinite energy and are then "generalized eigenvectors" associated with the *essential spectrum* corresponding to the frequencies ω such that the ratio $\varepsilon_d(\omega)/\varepsilon_0$ is in the interval $[-I_\alpha, -1/I_\alpha]$ [88]. The radial dependence of these corner modes, with oscillations with spatial period tending to zero, makes an analog of "black hole" phenomenon occuring at the corner (see Figure 6). Indeed, the modes appear to propagate infinitely slowly and to accumulate energy when approaching the corner as if they were trapped by the corner which would behave

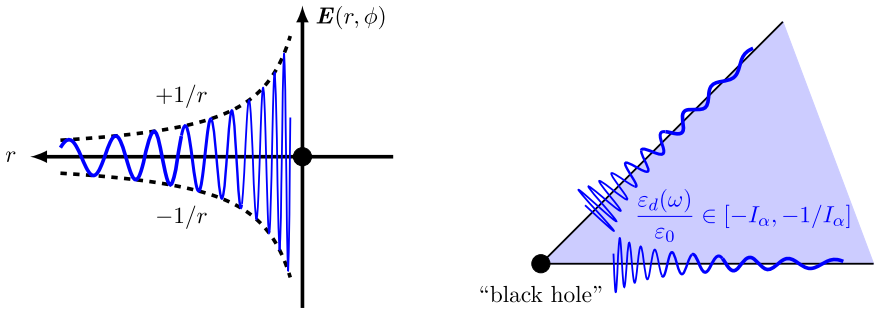

Figure 6. Left: the radial dependence of the electric field of a corner mode with amplitude increasing like $1/r$ and spatial frequency tending to infinity like $\ln(1/r)$ when $r \longrightarrow 0$. Right: a representation of the electric field of a corner mode at the vicinity of the corner.

like a semi-infinite open space. Finally, notice that it can be shown that there is no *essential spectrum* associated with the corner of angle α outside the interval $[-I_\alpha, -1/I_\alpha]$ using a "T-coercivity" argument [84–87].

This new and extraordinary behavior of corner modes exhibited in systems with negative permittivity (and—or—negative permeability) raises numerous challenging questions in applied mathematics (e.g. three-dimensional corners [81]), in physics with the analog of "black hole" phenomenon and in numerical modelling. In particular, it is stressed that the presence of the *essential spectrum* implies difficulties in the computation of modes of dispersive structures, with the lack of convergence in a frequency domain around the *essential spectrum* where the permittivity takes real negative values [91–93]. This unavoidable perturbation of numerical computation represents a challenging task in the method of quasi-normal modes expansion [92,93]. The introduction of perfectly matched layers at the corners [94] could be a promising way to address this task.

The perfect flat lens [54] and its generalization such as the perfect corner reflector [80, 82, 83] highlighted situations where, at the perfect -1 index frequency ω_1, the frame of the time-harmonic Maxwell's equations has no solutions and thus appears inappropriate to describe the behavior of electromagnetic waves. Such In addition, the presence of *essential spectrum* has been identified at the perfect -1 index frequency ω_1 which is an eigenvalue with infinite degeneracy for the perfect flat lens and corner reflector. Recently, it has been shown that more conventional structures like frequency dispersive corners also display *essential spectrum* [84–87] for a whole interval of frequencies for which there is no solution to the time-harmonic Maxwell's equations. However, it has been shown that the *auxiliary field formalism* introduced by A. Tip [71] provides a canonical approach for all these extraordinary situations with perfect negative index [67], metamaterials and negative permittivity where the frequency dispersion plays a vital role. In particular, it is stressed that this *auxiliary field formalism* offers the possibility to analyze rigorously a negative permittivity corner which makes an analog of "black hole" phenomenon.

4. Spatial dispersion and the imaginary part of the effective permeability

The modelling of metamaterials and negative index materials highlighted the role of spatial dispersion (or non-locality) [29–32, 35, 42, 46, 47] in composites displaying effective permeability. It makes sense since, in usual bulk materials, the magnetic properties can be derived from the electric permittivity tensor $\underline{\underline{\varepsilon}}(\boldsymbol{k}, \omega)$ depending on the frequency ω and the wave vector $\boldsymbol{k}$ [3,35,95]. Indeed, consider the Maxwell's equations in a homogeneous and isotropic magnetodielectric

medium with permittivity $\varepsilon(\omega)$ and permeability $\mu(\omega)$. For monochromatic plane-waves with space-time dependence in $\exp[\mathrm{i}(\boldsymbol{k}\cdot\boldsymbol{x}-\omega t)]$ these equations become

$$\boldsymbol{k}\times\boldsymbol{E}=\omega\mu(\omega)\boldsymbol{H},\quad \boldsymbol{k}\times\boldsymbol{H}=-\omega\varepsilon(\omega)\boldsymbol{E}, \tag{15}$$

and, after eliminating the field $\boldsymbol{H}$,

$$\boldsymbol{k}\times\frac{1}{\omega\mu(\omega)}\,\boldsymbol{k}\times\boldsymbol{E}+\omega\varepsilon(\omega)\boldsymbol{E}=\boldsymbol{0}. \tag{16}$$

This last equation can be written

$$\boldsymbol{k}\times\frac{1}{\omega\mu_0}\,\boldsymbol{k}\times\boldsymbol{E}+\boldsymbol{k}\times\left[\frac{1}{\omega\mu(\omega)}-\frac{1}{\omega\mu_0}\right]\boldsymbol{k}\times\boldsymbol{E}+\omega\varepsilon(\omega)\boldsymbol{E}=\boldsymbol{0}. \tag{17}$$

Thus, defining the dielectric tensor

$$\omega\underline{\underline{\varepsilon}}(\boldsymbol{k},\omega)=\omega\varepsilon(\omega)-\left[\frac{1}{\omega\mu(\omega)}-\frac{1}{\omega\mu_0}\right]\left(k^2-\boldsymbol{k}\boldsymbol{k}\right), \tag{18}$$

where $k^2=\boldsymbol{k}\cdot\boldsymbol{k}$ and $\boldsymbol{k}\boldsymbol{k}$ is the rank-two tensor acting as $\boldsymbol{k}\boldsymbol{k}\cdot\boldsymbol{E}=(\boldsymbol{k}\cdot\boldsymbol{E})\boldsymbol{k}$, the Equation (16) is equivalent to

$$\boldsymbol{k}\times\frac{1}{\omega\mu_0}\,\boldsymbol{k}\times\boldsymbol{E}+\omega\underline{\underline{\varepsilon}}(\boldsymbol{k},\omega)\cdot\boldsymbol{E}=\boldsymbol{0} \tag{19}$$

for isotropic permeability $\mu(\omega)$. Hence a magnetodielectric medium can be described by only the electric permittivity tensor $\underline{\underline{\varepsilon}}(\boldsymbol{k},\omega)$. Conversely, the permeability $\mu(\omega)$ can be derived from the permittivity tensor. Let P_{lg} and $P_{\mathrm{tr}}=1-P_{\mathrm{lg}}$ be the orthogonal projections on the subspaces parallel (or *longitudinal*) and perpendicular (or *transverse*) to the vector $\boldsymbol{k}$:

$$P_{\mathrm{lg}}=\frac{\boldsymbol{k}\boldsymbol{k}}{k^2},\quad P_{\mathrm{tr}}=1-\frac{\boldsymbol{k}\boldsymbol{k}}{k^2}. \tag{20}$$

For isotropic permittivity $\varepsilon(\omega)$ and permeability $\mu(\omega)$, the permittivity tensor (18) can be decomposed on these subspaces

$$\underline{\underline{\varepsilon}}(\boldsymbol{k},\omega)=\varepsilon_{\mathrm{lg}}(\boldsymbol{k},\omega)P_{\mathrm{lg}}+\varepsilon_{\mathrm{tr}}(\boldsymbol{k},\omega)P_{\mathrm{tr}}, \tag{21}$$

where $\varepsilon_{\mathrm{lg}}(\boldsymbol{k},\omega)=\varepsilon(\omega)$ and $\varepsilon_{\mathrm{tr}}(\boldsymbol{k},\omega)=\varepsilon(\omega)-[1/\mu(\omega)-1/\mu_0]\,k^2/\omega^2$ are the longitunal and transverse components of the tensor. Hence, the permeability can be retrieved from the permittivity tensor according to the well-known relation [3, 35]

$$\frac{1}{\omega\mu(\omega)}=\frac{1}{\omega\mu_0}+\lim_{k\to0}\frac{\omega\varepsilon_{\mathrm{lg}}(\boldsymbol{k},\omega)-\omega\varepsilon_{\mathrm{tr}}(\boldsymbol{k},\omega)}{k^2}. \tag{22}$$

Notice that this relation between the permeability and the permittivity tensor with spatial dispersion is established for bulk infinite media which are not delimited by boundaries.

Although the two descriptions of magnetodielectric media seem to be equivalent, the introduction of spatial dispersion and the gathering, in the permittivity tensor, of all the magnetic and dielectric properties of the materials, break the symmetry between the fields $\boldsymbol{E}$ and $\boldsymbol{H}$ in the Maxwell's equations. However, the symmetry between these fields and between the permittivity and permeability is widely used in textbooks of classical electrodynamics [3, 33, 90]. In particular, the Kramers–Kronig relations and the passivity requirement for the permittivity are generally also considered as valid for the permeability: for instance, it is generally considered that the imaginary of permittivity is positive [3, Section 80], $\mathrm{Im}\,\mu(\omega)\geq0$, which becomes for all frequency ω with positive imaginary part

$$\mathrm{Im}\,\omega\mu(\omega)\geq\mathrm{Im}\,\omega\mu_0. \tag{23}$$

Nevertheless, it turns out that the behaviors of the permittivity and the permeability are different in the static regime [3, 33]: unlike the static permittivity $\varepsilon(0)$ (i.e. $\varepsilon(\omega)$ at the limit $\omega\to0$), which always takes real value greater than ε_0, the static permeability $\mu(0)$ (i.e. $\mu(\omega)$ at the limit $\omega\to0$) can take real values either greater (paramagnetic media) or less (diamagnetic media) than μ_0.

This alternative for the static permeability seems in contradiction with the causality principle and the passivity. Indeed, the generalized Kramers–Kronig relation (4) applied to the permeability implies

$$\mu(0) = \mu_0 + \frac{2}{\pi}\int_0^\infty \mathrm{d}\nu\, \frac{\operatorname{Im}\mu(\nu)}{\nu}, \tag{24}$$

which requires for $\mu(0)$ to be greater than μ_0 if $\operatorname{Im}\mu(\omega) \geq 0$ for all positive real frequency ω [48]. In the textbook [3], this contradiction is explained by the frequency range where the macroscopic magnetic permeability makes sense, which is limited to the relatively low frequencies. Consequently, it is specified in [3, Section 82] that the Kramers–Kronig relations like (4) and (24) must be modified for the magnetic permeability. Hence the requirement on the imaginary part of the permeability, $\operatorname{Im}\mu(\omega) \geq 0$, has been confirmed in reference [3].

The introduction of metamaterials and negative index materials with effective permeability led to revisit these statements. Indeed, it has been found that the effective parameters of metamaterials present anomalous dispersion: in [96], "*the resonant behavior of the effective magnetic permeability is accompanied by an antiresonant behavior of the effective permittivity*" and "*the imaginary parts of the effective permittivity and permeability are opposite in sign*". These numerical results first generated some controversy [97, 98], but next the anomalous dispersion and the possibility for negative imaginary part of the effective permeability have been confirmed by several studies, which generated a series of investigations. For instance, fundamental questions on the Poynting vector and the energy have been adressed [48,49], the validity of the Kramers–Kronig relations for the magnetic permeability has been examined [51], the validity of the causality principle and the physical meanining of the metamaterials constitutive parameters has been analyzed [50, 52].

Hereafter, the objective is to bring arguments supporting that the imaginary part of the magnetic permeability $\mu(\omega)$ in passive media can take both positive and negative values, i.e. that the relation (23) is not valid. In contrast, these arguments support that the Kramers–Kronig relations make sense for the permeability. Since these claims are in contradiction with the electrodynamics based on the symmetry between, in one hand, the electric field $\boldsymbol{E}$ and the permittivity $\varepsilon(\omega)$ and, in the other hand, the magnetic induction field $\boldsymbol{H}$ and the permeability $\mu(\omega)$, the description with the dielectric tensor $\underline{\underline{\varepsilon}}(\boldsymbol{k},\omega)$ and spatial dispersion is considered.

First, a simple model with spatial dispersion is considered, the hydrodynamical model [99, 100], with the permittivity tensor expression

$$\underline{\underline{\varepsilon}}(\boldsymbol{k},\omega) = \varepsilon_0 - \varepsilon_0\,\frac{\Omega^2}{\omega^2 + \mathrm{i}\omega\gamma - \omega_0^2 - v^2k^2}\,P_{\mathrm{lg}} - \varepsilon_0\,\frac{\Omega^2}{\omega^2 + \mathrm{i}\omega\gamma - \omega_0^2}\,P_{\mathrm{tr}}. \tag{25}$$

Using the relation (22), it is possible to define from this model the magnetic permeability

$$\frac{1}{\omega\mu(\omega)} = \frac{1}{\omega\mu_0} - \omega\varepsilon_0\,\frac{\Omega^2 v^2}{(\omega^2 + \mathrm{i}\omega\gamma - \omega_0^2)^2}, \tag{26}$$

and to obtain for the imaginary part at real frequency

$$\operatorname{Im}\frac{1}{\omega\mu(\omega)} = \varepsilon_0\,\frac{2\gamma\Omega^2 v^2\omega^2(\omega^2 - \omega_0^2)}{[(\omega^2 - \omega_0^2)^2 + \omega^2\gamma^2]^2}. \tag{27}$$

This result clearly shows that the imaginary part of the obtained permeability can take both positive and negative values, depending on ω^2 is smaller or larger than ω_0^2. In addition, from the expression (26) of the permeability, the following identity, similar to the relation (24), is derived

$$\int_0^\infty \mathrm{d}\nu \operatorname{Im}\frac{1}{\nu\mu(\nu)} = \frac{\pi}{2}\left[\frac{1}{\mu(0)} - \frac{1}{\mu_0}\right] = 0, \tag{28}$$

where it has been used that $\mu(0) = \mu_0$ to obtain that the integral vanishes. This last identity confirms that the imaginary part of the permeability must take positive and negative values.

The same results can be obtained starting from a general permittivity tensor $\underline{\underline{\varepsilon}}(\boldsymbol{k},\omega)$, provided the asymptotic behavior at large complex frequencies with positive imaginary part,

$$\underline{\underline{\varepsilon}}(\boldsymbol{k},\omega) \underset{|\omega|\to\infty}{\longrightarrow} \varepsilon_0 - \frac{\Omega^2}{\omega^2}, \tag{29}$$

is independent of the wave vector $\boldsymbol{k}$ [101]. In combination with the analytic properties of the permittivity in the half plane of complex frequencies with positive imaginray parts, this asymptotic behavior implies the identity, or *sum rule*,

$$\int_0^\infty \mathrm{d}\nu \,\mathrm{Im}\, \nu\underline{\underline{\varepsilon}}(\boldsymbol{k},\nu) = \frac{\pi\Omega^2}{2}, \tag{30}$$

also independent of the wave vector $\boldsymbol{k}$ [101, 102]. Since the permeability (22) is defined from the term quadratic in $\boldsymbol{k}$ in the tensor $\underline{\underline{\varepsilon}}(\boldsymbol{k},\omega)$, its imaginary part must be subject to [101, 102]

$$\int_0^\infty \mathrm{d}\nu \,\mathrm{Im}\, \frac{1}{\nu\mu(\nu)} = 0. \tag{31}$$

Thus, starting from a general permittivity tensor, it can be shown that the imaginary part of the permeability must take positive and negative values. It is stressed that these last arguments, implying that $\mu(0) = \mu_0$, exclude the existence of media with magnetic properties in the static regime, i.e. with $\mu(0) \neq \mu_0$. This limitation can be however overtaken considering a permittivity tensor $\underline{\underline{\varepsilon}}(\boldsymbol{k},\omega)$ with an essential singularity at the point $(\boldsymbol{k},\omega) = (0,0)$ [101]. A simple example is the hydrodynamical Drude model, i.e. the expression (25) with ω_0 set to 0, which leads to the permeability

$$\frac{1}{\mu(\omega)} = \frac{1}{\mu_0} - \varepsilon_0 \frac{\Omega^2\nu^2}{(\omega+\mathrm{i}\gamma)^2}, \tag{32}$$

corresponding to a diamagnetic medium with $\mu(0) < \mu_0$. Notice that, in that case, the imaginary part of $\omega \longmapsto \omega\mu(\omega)$ is negative for all real frequency ω, i.e. its sign does not change. A paramagnetic medium could be obtained by inverting the $(\boldsymbol{k},\omega)$-dependence of the longitudinal and transverse components of the permittivity tensor in the expression (25). In addition, it is stressed that another possibility to overpass the limitation (31) may be to consider an asymptotic behavior different from the one (29) considered in [101].

The possibility for the imaginary part of the permeability to take positive and negative values is now investigated through the effective permeability of a composite medium. Here, a stack of non-magnetic homogeneous layers is considered. Indeed, the simplicity of such a structure makes it possible to define exactely, using the retrieval method, an effective permeability for all frequencies and wave vectors. In addition, it has been shown that the effective parameters of a multilayered structure present the suitable properties to ensure the causality principle and the passivity requirement [53]. Hence, this composite medium is a good candidate to investigate the sign of the imaginary part of the effective permeability.

A stack of non-magnetic homogeneous layers of total thickness h with a plane of symmetry at mid-height is considered (see left panel in Figure 7). The space variable in the stacking direction is denoted by x. The multilayered structure is located between the planes $x = -h$ and $x = 0$ and is described by the frequency dispersive and isotropic permittivity $\varepsilon(x,\omega)$, the magnetic permeability being set to the permeability of vacuum μ_0. Outside the multilayered structure, i.e. for $x < -h$ and $x > 0$, the permittivity is set to ε_0. In practice, $\varepsilon(x,\omega)$ is piecewise constant with respect to z and, according to the symmetry of the structure, $\varepsilon(-x,\omega) = \varepsilon(x-h,\omega)$. The structure (and the permittivity) is invariant under translations in the plane parallel to the layers and thus a two-dimensional Fourier decomposition is performed in these tangential directions: the two-component wave vector resulting from this Fourier decomposition is denoted by $\boldsymbol{k}_\parallel$ and $k_\parallel = \sqrt{\boldsymbol{k}_\parallel \cdot \boldsymbol{k}_\parallel}$ is its norm. Then, the time-harmonic Maxwell's equations become a set of two independent scalar equations for the electric and magnetic fields components orthogonal

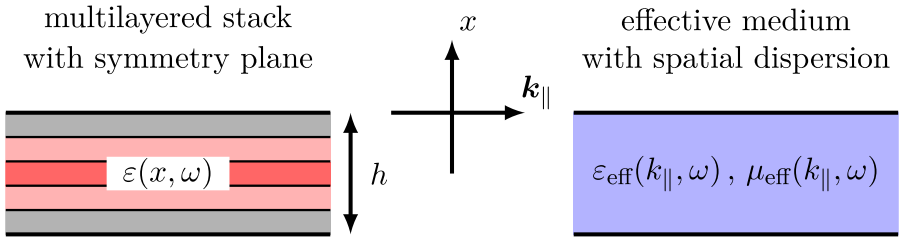

Figure 7. Left: the considered multilayered structure with a plane of symmetry described by the frequency dependent and isotropic permittivity $\varepsilon(x,\omega)$. Right: the equivalent effective medium described by the effective permittivity $\varepsilon_{\text{eff}}(k_{\|},\omega)$ and permeability $\mu_{\text{eff}}(k_{\|},\omega)$.

to both $\boldsymbol{k}_{\|}$ and the stacking direction. Let $U^e(x,k_{\|},\omega)$ and $U^m(x,k_{\|},\omega)$ be these components of the electric and magnetic fields: for $w=e,m$, the Maxwell's equations take the form

$$\frac{\partial}{\partial x}\frac{1}{\xi^w(x,\omega)}\frac{\partial}{\partial x}U^w(x,k_{\|},\omega)+\frac{\omega^2\mu_0\varepsilon(x,\omega)-k_{\|}^2}{\xi^w(x,\omega)}U^w(x,k_{\|},\omega)=0, \tag{33}$$

where $\xi^e(x,\omega)=\mu_0$ and $\xi^m(x,\omega)=\varepsilon(x,\omega)$. The solutions to these equations can be determined from the 2×2 transfer matrices $T^e(k_{\|},\omega)$ and $T^m(k_{\|},\omega)$ relating the values of the fields' tengential components parallel to the layers at the planes $x=0$ and $x=-h$ [41,53]. For $w=e,m$, the general expression of these transfer matrices is [53]

$$T^w(k_{\|},\omega)=\begin{bmatrix}A^w(k_{\|},\omega) & B^w(k_{\|},\omega)\\ C^w(k_{\|},\omega) & A^w(k_{\|},\omega)\end{bmatrix}, \tag{34}$$

where the coefficents are analytic functions in the half plane of complex frequencies ω with positive imaginary part and are related by the identity

$$A^w(k_{\|},\omega)^2-B^w(k_{\|},\omega)C^w(k_{\|},\omega)=1. \tag{35}$$

Each transfer matrix $T^e(k_{\|},\omega)$ and $T^m(k_{\|},\omega)$ is thus determined by two independent parameters. In particular, defining, for $w=e,m$,

$$\begin{aligned}k_{\perp}^w(k_{\|},\omega)&=\frac{1}{\mathrm{i}h}\ln\left[A^w(k_{\|},\omega)+\mathrm{i}\sqrt{1-A^w(k_{\|},\omega)^2}\right],\\ X^w(k_{\|},\omega)&=\sqrt{\frac{B^w(k_{\|},\omega)}{C^w(k_{\|},\omega)}},\end{aligned} \tag{36}$$

the transfer matrices (34) can be equivalently expressed as

$$T^w(k_{\|},\omega)=\begin{bmatrix}\cos\left[k_{\perp}^w(k_{\|},\omega)h\right] & \mathrm{i}\sin\left[k_{\perp}^w(k_{\|},\omega)h\right]X^w(k_{\|},\omega)\\ \mathrm{i}\sin\left[k_{\perp}^w(k_{\|},\omega)h\right]/X^w(k_{\|},\omega) & \cos\left[k_{\perp}^w(k_{\|},\omega)h\right]\end{bmatrix}. \tag{37}$$

It is stressed that the imaginary part of the parameter $k_{\perp}^w(k_{\|},\omega)$ cannot vanish for frequencies ω with postive imaginary part [53], otherwise this would allow the existence of Bloch modes in the one-dimensional system resulting from the periodic stacking of the multilayered structure [53, 103]. The sign of the imaginary part of $k_{\perp}^w(k_{\|},\omega)$ can be chosen positive, i.e.

$$\operatorname{Im}\omega>0 \quad\Longrightarrow\quad \operatorname{Im}k_{\perp}^w(k_{\|},\omega)>0, \tag{38}$$

which fix the sign of the square root in the definition (36) of the second parameter $X^w(k_{\|},\omega)$. This remarkable property (38) ensures that the definition (36) preserves in the domain $\operatorname{Im}\omega>0$ the analytic property of the parameters $k_{\perp}^w(k_{\|},\omega)$ and $X^w(k_{\|},\omega)$ since $A^w(k_{\|},\omega)$ cannot take the values ±1 and $B^w(k_{\|},\omega)$ and $C^w(k_{\|},\omega)$ cannot vanish.

The transfer matrices and thus the four independent parameters $k_\perp^w(k_\parallel,\omega)$ and $X^w(k_\parallel,\omega)$ fully determine the solution to Maxwell's equations outside the multilayered structure. For instance, the fields reflected and transmitted by the multilayered structure can be expressed from these four parameters. Thus, these parameters can be used to define an homogeneous effective medium that will lead to the same solutions to Maxwell's equations outside the multilayered structure. Notice that this procedure corresponds to the retrieval method [28, 29]. The homogeneous effective medium must be described by four effective parameters with the $(k_\parallel,\omega)$-dependence. According to the symmetry of the structure, let $\varepsilon_{\text{eff}}(k_\parallel,\omega)$ and $\mu_{\text{eff}}(k_\parallel,\omega)$ be the effective anisotropic permittivity and permeability defined by, for $w = e, m$,

$$\xi_{\text{eff}}^w(k_\parallel,\omega) = \begin{bmatrix} \xi_\parallel^w(k_\parallel,\omega) & 0 & 0 \\ 0 & \xi_\parallel^w(k_\parallel,\omega) & 0 \\ 0 & 0 & \xi_\perp^w(k_\parallel,\omega) \end{bmatrix}, \quad \xi^e = \mu, \quad \xi^m = \varepsilon, \tag{39}$$

where $\xi_\parallel^w(k_\parallel,\omega)$ are the components in the plane parallel to the layers and $\xi_\perp^w(k_\parallel,\omega)$ are the components in the stacking direction. In this effective medium, the Maxwell's equations for the components $U^e(x,k_\parallel,\omega)$ and $U^m(x,k_\parallel,\omega)$ of the electric and magnetic fields become

$$\frac{\partial^2}{\partial x^2} U^w(x,k_\parallel,\omega) + \left[\omega^2\mu_\parallel(k_\parallel,\omega)\varepsilon_\parallel(k_\parallel,\omega) - k_\parallel^2 \frac{\xi_\parallel^w(k_\parallel,\omega)}{\xi_\perp^w(k_\parallel,\omega)}\right] U^w(x,k_\parallel,\omega) = 0, \tag{40}$$

where $\xi^e = \mu$ and $\xi^m = \varepsilon$. The transfer matrices $T_{\text{eff}}^e(k_\parallel,\omega)$ and $T_{\text{eff}}^m(k_\parallel,\omega)$ corresponding to a layer of the effective medium with thickness h are, for $w = e, m$,

$$T_{\text{eff}}^w(k_\parallel,\omega) = \begin{bmatrix} \cos\left[k_{\text{eff}}^w(k_\parallel,\omega)h\right] & \mathrm{i}\sin\left[k_{\text{eff}}^w(k_\parallel,\omega)h\right] X_{\text{eff}}^w(k_\parallel,\omega) \\ \mathrm{i}\sin\left[k_{\text{eff}}^w(k_\parallel,\omega)h\right] / X_{\text{eff}}^w(k_\parallel,\omega) & \cos\left[k_{\text{eff}}^w(k_\parallel,\omega)h\right] \end{bmatrix}, \tag{41}$$

where

$$\begin{aligned} k_{\text{eff}}^w(k_\parallel,\omega) &= \sqrt{\omega^2\mu_\parallel(k_\parallel,\omega)\varepsilon_\parallel(k_\parallel,\omega) - k_\parallel^2\xi_\parallel^w(k_\parallel,\omega)/\xi_\perp^w(k_\parallel,\omega)}, \\ X_{\text{eff}}^w(k_\parallel,\omega) &= \omega\xi_\parallel^w(k_\parallel,\omega)/k_{\text{eff}}^w(k_\parallel,\omega). \end{aligned} \tag{42}$$

As a final step, the identification of the transfer matrices of the multilayered structure with the ones of the effective medium provides the four equations $k_{\text{eff}}^w(k_\parallel,\omega) = k_\perp^w(k_\parallel,\omega)$ and $X_{\text{eff}}^w(k_\parallel,\omega) = X^w(k_\parallel,\omega)$, with $w = e, m$. These four equations define the following components of the effective permittivity and permeability:

$$\begin{aligned} &\omega\varepsilon_\parallel(k_\parallel,\omega) = k_\perp^m(k_\parallel,\omega)X^m(k_\parallel,\omega), \\ &\frac{1}{\omega\varepsilon_\perp(k_\parallel,\omega)} = \frac{k_\perp^e(k_\parallel,\omega)X^e(k_\parallel,\omega) - k_\perp^m(k_\parallel,\omega)/X^m(k_\parallel,\omega)}{k_\parallel^2}, \\ &\omega\mu_\parallel(k_\parallel,\omega) = k_\perp^e(k_\parallel,\omega)X^e(k_\parallel,\omega), \\ &\frac{1}{\omega\mu_\perp(k_\parallel,\omega)} = \frac{k_\perp^m(k_\parallel,\omega)X^m(k_\parallel,\omega) - k_\perp^e(k_\parallel,\omega)/X^e(k_\parallel,\omega)}{k_\parallel^2}. \end{aligned} \tag{43}$$

The components $\mu_\parallel(k_\parallel,\omega)$ and $\mu_\perp(k_\parallel,\omega)$ of the effective permeability $\mu_{\text{eff}}(k_\parallel,\omega)$ have been defined for a non vanishing parallel wave vector $\boldsymbol{k}_\parallel$ while the definition (22) is at the limit $k \longrightarrow 0$. However, it is possible to define a permeability depending upon the wave vector as [101]

$$\frac{1}{\omega\mu(\boldsymbol{k},\omega)} = \frac{1}{\omega\mu_0} + \frac{\omega\varepsilon_{\text{lg}}(\boldsymbol{k},\omega) - \omega\varepsilon_{\text{tr}}(\boldsymbol{k},\omega)}{k^2}, \tag{44}$$

which preserves the equivalence of the descriptions of an isotropic medium by $\varepsilon(\omega)$ and $\mu(\omega)$ and by the permittivity tensor $\underline{\underline{\varepsilon}}(\boldsymbol{k},\omega)$ with expression (18).

It is stressed that the four functions $\varepsilon_\parallel(k_\parallel,\omega)$, $1/\varepsilon_\perp(k_\parallel,\omega)$, $\mu_\parallel(k_\parallel,\omega)$ and $1/\mu_\perp(k_\parallel,\omega)$ defining the effective parameters, are analytic with respect to the frequency ω in the upper half complex plane of ω with positive imaginary part. This is a consequence of the analytic properties of the

parameters $k_\perp^w(k_\parallel,\omega)$ and $X^w(k_\parallel,\omega)$ which follow from the relation (38). Also, for the parameters $1/\varepsilon_\perp(k_\parallel,\omega)$ and $1/\mu_\perp(k_\parallel,\omega)$ the numerators vanish when $k_\parallel \longrightarrow 0$ since in that case the solutions of two equations for e and m waves are identical, which implies $k_\perp^e(0,\omega) = k_\perp^m(0,\omega)$ and $X^e(0,\omega) = 1/X^m(0,\omega)$. Hence the effective parameters have the analytic properties required by the causality principle and the derivation of the Kramers–Kronig relations.

The consequences of the passivity on the effective parameters should be derived from the relation $\operatorname{Im}\omega\varepsilon(x,\omega) \geq \operatorname{Im}\omega\varepsilon_0$. Let the multilayered structure be periodically stacked so that it fills all the semi-infinite space $x<0$: $\varepsilon(x,\omega) = \varepsilon(x-h,\omega)$ for $x<0$ and $\varepsilon(x,\omega) = \varepsilon_0$ for $x>0$. Let $\boldsymbol{e}_\perp$ be the unit vector in the stacking direction x and $\nabla(\boldsymbol{k}_\parallel)$ the differential operator $(\mathrm{i}\boldsymbol{k}_\parallel + \boldsymbol{e}_\perp\partial/\partial x)$ after the Fourier decomposition in the plane parallel to the layers. After the Fourier decomposition, the Helmhotz operator $\mathsf{H}(\omega)$ for the multilayered stack is

$$\mathsf{H}(\boldsymbol{k}_\parallel,\omega)\boldsymbol{E}(x) = -\nabla(\boldsymbol{k}_\parallel)\times\frac{1}{\omega\mu_0}\nabla(\boldsymbol{k}_\parallel)\times\boldsymbol{E}(x) + \omega\varepsilon(x,\omega)\boldsymbol{E}(x), \tag{45}$$

where the $(\boldsymbol{k}_\parallel,\omega)$-dependence of the electric field has been omitted. Let $\mathsf{H}_{\mathrm{eff}}(\boldsymbol{k}_\parallel,\omega)$ be the Helmhotz operator of the effective structure which coincides with (45) except for the domain $x<0$ where $\varepsilon(x,\omega)$ and μ_0 are replaced by $\varepsilon_{\mathrm{eff}}(k_\parallel,\omega)$ and $\mu_{\mathrm{eff}}(k_\parallel,\omega)$. An electromagnetic source $\boldsymbol{J}(x)$ outside the composite is considered, i.e. $\boldsymbol{J}(x)=0$ if $x<0$. The electric field generated by this source in presence of the multilayered structure is the solution to

$$\mathsf{H}(\boldsymbol{k}_\parallel,\omega)\boldsymbol{E}(x) = \boldsymbol{J}(x), \tag{46}$$

and the electric field generated by this source in presence of the effective structure is the solution to

$$\mathsf{H}_{\mathrm{eff}}(\boldsymbol{k}_\parallel,\omega)\boldsymbol{E}_{\mathrm{eff}}(x) = \boldsymbol{J}(x). \tag{47}$$

The two electric fields are identical outside the multilayered structure: $\boldsymbol{E}(x) = \boldsymbol{E}_{\mathrm{eff}}(x)$ if $x>0$. Thus, defining the inner product by

$$\big\langle \boldsymbol{E},\boldsymbol{J}\big\rangle = \int_{\mathbb{R}} \mathrm{d}x\,\overline{\boldsymbol{E}(x)}\cdot\boldsymbol{J}(x), \tag{48}$$

the identity $\big\langle \boldsymbol{E}_{\mathrm{eff}},\boldsymbol{J}\big\rangle = \big\langle \boldsymbol{E},\boldsymbol{J}\big\rangle$ holds for all source $\boldsymbol{J}(x)$ vanishing for $x<0$, and takes the form

$$\big\langle \boldsymbol{E}_{\mathrm{eff}}, \mathsf{H}_{\mathrm{eff}}(\boldsymbol{k}_\parallel,\omega)\boldsymbol{E}_{\mathrm{eff}}\big\rangle = \big\langle \boldsymbol{E}, \mathsf{H}(\boldsymbol{k}_\parallel,\omega)\boldsymbol{E}\big\rangle. \tag{49}$$

Notice that the integrals are well-defined as soon as the imaginary part of the frequency is strictly positive: $\operatorname{Im}\omega > 0$. In order to take the limit $\operatorname{Im}\omega \longrightarrow 0$, it is assumed that there is a material in the multilayered stack with absorption, i.e. $\operatorname{Im}\omega\varepsilon(x,\omega) > 0$ at some $x<0$. Then, considering the imaginary part, the identity (49) implies for real frequencies ω

$$\operatorname{Im}\big\langle \boldsymbol{E}_{\mathrm{eff}}, \mathsf{H}_{\mathrm{eff}}(\boldsymbol{k}_\parallel,\omega)\boldsymbol{E}_{\mathrm{eff}}\big\rangle = \big\langle \boldsymbol{E}, \operatorname{Im}\omega\varepsilon(\omega)\,\boldsymbol{E}\big\rangle > 0. \tag{50}$$

Notice that the integrals over x in this relation (50) reduce to the domain $x<0$. Let P^e and $P^m = 1 - P^e$ be the orthogonal projections on the electric and magnetic waves:

$$P^e = 1 - \frac{\boldsymbol{k}_\parallel\boldsymbol{k}_\parallel}{k_\parallel^2} - \boldsymbol{e}_\perp\boldsymbol{e}_\perp, \quad P^m = \frac{\boldsymbol{k}_\parallel\boldsymbol{k}_\parallel}{k_\parallel^2} + \boldsymbol{e}_\perp\boldsymbol{e}_\perp, \tag{51}$$

where the rank-two tensors act as $\boldsymbol{k}_\parallel\boldsymbol{k}_\parallel\cdot\boldsymbol{E} = (\boldsymbol{k}_\parallel\cdot\boldsymbol{E})\boldsymbol{k}_\parallel$ and $\boldsymbol{e}_\perp\boldsymbol{e}_\perp\cdot\boldsymbol{E} = (\boldsymbol{e}_\perp\cdot\boldsymbol{E})\boldsymbol{e}_\perp$. For $x<0$ the electric field $\boldsymbol{E}_{\mathrm{eff}}(x)$ is the solution to $\mathsf{H}_{\mathrm{eff}}(\boldsymbol{k}_\parallel,\omega)\boldsymbol{E}_{\mathrm{eff}}(x)=0$ and thus, for $w=e,m$,

$$\nabla(\boldsymbol{k}_\parallel)\times P^w\cdot\boldsymbol{E}_{\mathrm{eff}}(x) = \mathrm{i}\boldsymbol{k}^w\times\boldsymbol{E}_{\mathrm{eff}}(x), \quad \boldsymbol{k}^w = \boldsymbol{k}_\parallel - k_\perp^w(k_\parallel,\omega)\boldsymbol{e}_\perp, \tag{52}$$

where the $(k_\parallel,\omega)$-dependence of the vectors $\boldsymbol{k}^w(k_\parallel,\omega)$ is omitted. Notice that the minus sign in front of the component along $\boldsymbol{e}_\perp$ has been chosen according to the condition (38) in order to

ensure the exponential decrease of the transmitted field at the limit $x \longrightarrow -\infty$. Hence, for $x < 0$, it is obtained

$$\begin{aligned}\mathsf{H}_{\text{eff}}(\boldsymbol{k}_\parallel,\omega)\boldsymbol{E}_{\text{eff}}(x) = {} & \omega\varepsilon_{\text{eff}}(k_\parallel,\omega)\boldsymbol{E}_{\text{eff}}(x) \\ & + \boldsymbol{k}^e\times\frac{1}{\omega\mu_{\text{eff}}(k_\parallel,\omega)}\,\boldsymbol{k}^e\times P^e\cdot\boldsymbol{E}_{\text{eff}}(x) \\ & + \boldsymbol{k}^m\times\frac{1}{\omega\mu_{\text{eff}}(k_\parallel,\omega)}\,\boldsymbol{k}^m\times P^m\cdot\boldsymbol{E}_{\text{eff}}(x). \end{aligned} \tag{53}$$

Considering, for $w = e, m$, the operation $\boldsymbol{k}^w\times$ as a rank-two antisymmetric tensor, the relation (50) implies that the rank-two tensor

$$\omega\varepsilon_{\text{eff}}(k_\parallel,\omega) + \boldsymbol{k}^e\times\frac{1}{\omega\mu_{\text{eff}}(k_\parallel,\omega)}\,\boldsymbol{k}^e\times P^e + \boldsymbol{k}^m\times\frac{1}{\omega\mu_{\text{eff}}(k_\parallel,\omega)}\,\boldsymbol{k}^m\times P^m \tag{54}$$

has positive imaginary part. Since $P^m\cdot\boldsymbol{k}^m = \boldsymbol{k}^m$ and $P^e\cdot\boldsymbol{k}^m = 0$, the contraction of the tensor above by $\boldsymbol{k}^m$ and its complex conjugate $\overline{\boldsymbol{k}}^m$ provides the relation

$$\operatorname{Im}\omega\overline{\boldsymbol{k}}^m\cdot\varepsilon_{\text{eff}}(k_\parallel,\omega)\cdot\boldsymbol{k}^m = k_\parallel^2\operatorname{Im}\omega\varepsilon_\parallel(k_\parallel,\omega) + |k_\perp^m|^2\operatorname{Im}\omega\varepsilon_\perp(k_\parallel,\omega) > 0. \tag{55}$$

Thus a condition forcing the imaginary part of the effective permittivity components to be positive is obtained. On the other hand, there is no condition on the imaginary part of the effective permeability. Indeed, some arguments lead to the conclusion that the imaginary part of the effective permeability $\omega\mu_{\text{eff}}(k_\parallel,\omega)$ must take positive and negative values.

As pointed out when it has been defined (43), the inverse effective permeability $1/\mu_{\text{eff}}(k_\parallel,\omega)$ is an analytic function in the upper half plane of complex frequencies ω with positive imaginary part (notice that $\omega\mu_\parallel(k_\parallel,\omega)$ cannot vanish as well as $k_\perp^e(k_\parallel,\omega)$ and $X^e(k_\parallel,\omega)$). This follows from the analytic properties of the permittivity $\varepsilon(x,\omega)$ of the multilayered structure and the contruction of the effective parameters. In addition, since the permittivity $\varepsilon(x,\omega)$ tends to that of vacuum ε_0 when $|\omega|\to\infty$, all the effective parameters tend as well to ε_0 and μ_0. Hence the relation (24) deduced from the Kramers–Kronig relations is true for the inverse effective permeability at $k_\parallel = 0$:

$$\frac{1}{\mu_{\text{eff}}(0,0)} = \frac{1}{\mu_0} + \frac{2}{\pi}\int_0^\infty \mathrm{d}\nu\operatorname{Im}\frac{1}{\nu\mu_{\text{eff}}(0,\nu)}. \tag{56}$$

And, more generally, the same relation is obtained when the wave vector $k_\parallel$ is set to $k_\parallel^2 = \omega^2\varepsilon_0\mu_0 u_\parallel^2$ with $u_\parallel^2 < 1$, which corresponds to an excitation at a fixed angle. Next, it is used that the quasistatic limit provides $\mu_{\text{eff}}(0,0) = \mu_0$ since the starting multilayered structure is non-magnetic: the relation (56) becomes

$$\int_0^\infty \mathrm{d}\nu\operatorname{Im}\frac{1}{\nu\mu_{\text{eff}}(0,\nu)} = 0. \tag{57}$$

Hence it can be concluded that the imaginary part of the effective permeability $\mu_{\text{eff}}(0,\nu)$ must take positive and negative values. Notice that, if the permittivity $\varepsilon(x,\omega)$ of the multilayered structure is well-defined for all frequency ω, then the inverse effective permeability $1/\mu_{\text{eff}}(k_\parallel,\omega)$ is also exactely and well-defined for all frequency ω. Thus, in the present case, contrary to the situation described in [3, Section 82], the Kramers–Kronig relations and the integrals (56) and (57) make sense.

Finally, it can be checked that the Kramers–Kronig relations and the resulting sum rules are consistent for the effective permittivity. According to the analytic properties of the inverse effective permittivity, the relation (56) is true for $\varepsilon_{\text{eff}}(k_\parallel,\omega)$:

$$\frac{1}{\varepsilon_{\text{eff}}(0,0)} = \frac{1}{\mu_0} + \frac{2}{\pi}\int_0^\infty \mathrm{d}\nu\operatorname{Im}\frac{1}{\nu\varepsilon_{\text{eff}}(0,\nu)}. \tag{58}$$

The value of the effective permittivity of the multilayered structure at the quasistatic limit is given by [34]

$$\varepsilon_{\parallel}(0,0) = \int_{-h}^{0} \mathrm{d}x\, \varepsilon(x,0), \quad \frac{1}{\varepsilon_{\perp}(0,0)} = \int_{-h}^{0} \mathrm{d}x\, \frac{1}{\varepsilon(x,0)}. \tag{59}$$

Since the permittivity of the multilayered structure takes real values greater ε_0 at the static limit [3], then this is also the case for the effective permittivity: $\varepsilon_{\parallel}(0,0) > \varepsilon_0$ and $\varepsilon_{\perp}(0,0) > \varepsilon_0$. These relations are consistent with the sum rule (59) and the condition (55) on the imaginary part of the effective permittivity.

These arguments confirm the lack of symmetry between the permittivity $\varepsilon(\omega)$ and the permeability $\mu(\omega)$. In that case it is relevant to consider the Maxwell's equations with spatial dispersion. In this article, the exact and explicit expression of the effective parameters of a multilayered structure has been derived for all the frequencies ω and wave vector $\boldsymbol{k}_{\parallel}$. According to (53), the expression of the corresponding effective permittivity tensor with spatial dispersion takes the form

$$\omega \underline{\underline{\varepsilon}}_{\mathrm{eff}}(\boldsymbol{k},\omega) = \omega \mathscr{E}_{\mathrm{eff}}(\boldsymbol{k},\omega) + \boldsymbol{k}\times \left[\frac{1}{\omega \mathscr{U}_{\mathrm{eff}}(\boldsymbol{k},\omega)} - \frac{1}{\omega\mu_0} \right] \boldsymbol{k}\times, \tag{60}$$

where the "permittivity part" $\mathscr{E}_{\mathrm{eff}}(\boldsymbol{k},\omega)$ and the "permeability part" $\mathscr{U}_{\mathrm{eff}}(\boldsymbol{k},\omega)$ should be expressed from $\varepsilon_{\mathrm{eff}}(k_{\parallel},\omega)$ and $\mu_{\mathrm{eff}}(k_{\parallel},\omega)$. The coefficients of the tensor $\underline{\underline{\varepsilon}}_{\mathrm{eff}}(\boldsymbol{k},\omega)$ depending on $(\boldsymbol{k},\omega)$ are different from the effective parameters depending on $(k_{\parallel},\omega)$ in the rank-two tensor (54) because they do not take into account the dispersion laws for $w = e,m$: $\boldsymbol{k}(\omega) = \boldsymbol{k}_{\parallel} \pm k_{\perp}^{w}(k_{\parallel},\omega)\boldsymbol{e}_{\perp}$. Thus the following functions are introduced for $w = e,m$:

$$K^{w}(k,\omega) = \sqrt{k^2 - k_{\perp}^{w}(k_{\parallel},\omega)^2}, \tag{61}$$

where the sign of the square root will not play a role since all the coefficients and parameters used here depend on the square of $k_{\parallel}$ (the starting equations (33) and (40) depend on $k_{\parallel}^2$). Defining the "permittivity part" as

$$\mathscr{E}_{\mathrm{eff}}(\boldsymbol{k},\omega) = \varepsilon_{\mathrm{eff}}(K^{e}(k,\omega),\omega)P^{e} + \varepsilon_{\mathrm{eff}}(K^{m}(k,\omega),\omega)P^{m}, \tag{62}$$

it is obtained for $w = e,m$ that $K^{w}(k,\omega)$ equals $k_{\parallel}$ and $\mathscr{E}_{\mathrm{eff}}(\boldsymbol{k},\omega)P^{w}$ equals $\varepsilon_{\mathrm{eff}}(k_{\parallel},\omega)P^{w}$ when the dispersion law is complied at $\boldsymbol{k}(\omega) = \boldsymbol{k}_{\parallel} \pm k_{\perp}^{w}(k_{\parallel},\omega)\boldsymbol{e}_{\perp}$. Similarly, using that the rank-two antisymmetric tensor $\boldsymbol{k}\times$ acting on P^{m} gives P^{e} acting on $\boldsymbol{k}\times$, the "permeability part" of the tensor can be defined as

$$\mathscr{U}_{\mathrm{eff}}(\boldsymbol{k},\omega) = \mu_{\mathrm{eff}}(K^{e}(k,\omega),\omega)P^{m} + \mu_{\mathrm{eff}}(K^{m}(k,\omega),\omega)P^{e}. \tag{63}$$

Notice that the projections P^{e} and P^{m}, defined by (51), depend on the vector $\boldsymbol{k}_{\parallel}$ and, consequently, the "permittivity part" $\mathscr{E}_{\mathrm{eff}}(\boldsymbol{k},\omega)$ and the "permeability part" $\mathscr{U}_{\mathrm{eff}}(\boldsymbol{k},\omega)$ depend on the vector $\boldsymbol{k}$ although the effective parameters only depend on the norm $k_{\parallel}$. Finally, substituing the expressions (62) and (63) in (60), the effective permittivity tensor is given by

$$\omega \underline{\underline{\varepsilon}}_{\mathrm{eff}}(\boldsymbol{k},\omega) = \omega \underline{\underline{\varepsilon}}^{e}_{\mathrm{eff}}(\boldsymbol{k},\omega)P^{e} + \omega \underline{\underline{\varepsilon}}^{m}_{\mathrm{eff}}(\boldsymbol{k},\omega)P^{m}, \tag{64}$$

where, for $w = e,m$,

$$\omega \underline{\underline{\varepsilon}}^{w}_{\mathrm{eff}}(\boldsymbol{k},\omega) = \omega\varepsilon_{\mathrm{eff}}(K^{w}(k,\omega),\omega) + \boldsymbol{k}\times \left[\frac{1}{\omega\mu_{\mathrm{eff}}(K^{w}(k,\omega),\omega)} - \frac{1}{\omega\mu_0} \right] \boldsymbol{k}\times. \tag{65}$$

Hence the effective permittivity tensor $\underline{\underline{\varepsilon}}_{\mathrm{eff}}(\boldsymbol{k},\omega)$ has been constructed for all frequency ω and wave vector $\boldsymbol{k}$. This exact and explicit expression of an anisotropic permittivity tensor with spatial dispersion could be the starting point of further investigations on spatial disper-

sion in macroscopic electromagnetism. As a first result, it has been shown that the imaginary part of the effective permeability of a passive multilayered structure must take positive and negative values.

5. Conclusion

The advent of negative index materials opened questions that have tested the domain of validity of macroscopic electromagnetism. The existence of a negative index of refraction appeared as unreachable during more than 30 years until the introduction of microstructured resonant media and metamaterials. Then, considerable progress has been made in the engineering and the design of microstructured media reporting extraordinary properties. In this article, several mechanisms leading to negative index and negative refraction have been briefly reviewed: the original ideas developed by J. Pendry and his colleagues with the design of microstructured metallic media displaying electric and magnetic resonances; the exploitation of the richness of the dispersion law in dielectric photonic crystals to obtain negative refraction; and the development of numerous non-asymptotic homogenization techniques and effective medium modellings for composite media. All these advances over the last twenty years are now particularly exploited in the design of metasurfaces [104, 105] and topological insulators [106, 107]. They have also been extended to other classical waves equations in acoustics, mechanics and hydrodynamics [108].

Then, it has been seen how the extraordinary properties of negative index materials and metamaterials must be associated with frequency dispersion and spatial dispersion. In addition, it has been shown that the time-harmonic Maxwell's equations cannot describe properly systems like the perfect negative index flat lens or corner reflector. On the other hand, the introduction of the *auxiliary field formalism* provides a canonical approach to describe frequency dispersive negative index structures. It has been shown that the spectacular effects in the perfect flat lens and corner reflector are associated to the presence, at the prefect -1 index frequency, of essential spectrum in the Maxwell's equations. More generally, the presence of intervals of essential spectrum has been highligthed in corner structures at frequencies where frequency dispersive permittivity takes negative values. This essential spectrum generated by the corner is associated with an analog of "black hole" phenomenon, the corner behaving like an unbounded domain. This raises challenging and fascinating questions in applied mathematics (e.g. in the case of three-dimensional corners), in physics with the analog of "black hole" phenomenon and in numerical modelling for the computation of modes of dispersive structure (e.g. in the quasi-normal modes expansion). In particular, the canonical formalism for dissipative and frequency dispersive Maxwell's equations, the *auxiliary fields formalism*, offers the opportunity to analyze rigorously an analog of "black hole" phenomenon.

In the last section, it has been shown how the effective permittivity, which has been intensively analyzed for negative index materials and metamaterials, highlighted ambiguities in the passivity requirement and Kramers–Kronig relations for the permeability. In this article, several arguments have been reported to support that, in a passive medium, the imaginary part of the permeability can take positive and negative values. This statement is in contradiction with the usual presentation of macroscopic electromagnetism where the permittivity and the permeability are introduced in a symmetric way, and thus in passive media both have positive imaginary part. The approach considered here was to define the permeability from the permittivity with spatial dispersion, which breaks the symmetry between the permittivity and the permeability. The effective permeability of a passive and non-magnetic multilayered structure has been derived exactly for all frequency and wave vector: in that case, it has been shown that the effective permeability is subject to the Kramers–Kronig relations and has imaginary part taking positive and negative values. In addition, the full effective anisotropic permittivity tensor with spatial dispersion has been

derived explicitely for all frequency and wave vector and could be the starting point of further investigations on spatial dispersion in macroscopic electromagnetism.

Acknowledgements

Sébastien Guenneau is gratefully acknowledged for his precious support. Anne-Sophie Bonnet-BenDhia, Maxence Cassier, Lucas Chesnel, Christophe Hazard and Sandrine Paolantoni are gratefully acknowledged for the fruitful discussions.

References

[1] V. G. Veselago, "The electrodynamics of substances with simultaneously negative values of ε and μ", *Sov. Phys. Usp.* **10** (1968), p. 509.
[2] J. B. Pendry, A. J. Holden, W. J. Robbins, D. J. Stewart, "Magnetism from conductors and enhanced nonlinear phenomena", *IEEE Trans. Microw. Theory Tech.* **47** (1999), p. 2075.
[3] L. D. Landau, E. M. Lifshitz, L. P. Pitaevskiĭ, *Electrodynamics of Continuous Media*, 2nd ed., Courses of Theoretical Physics, vol. 8, Robert Maxwell, M. C., 1984.
[4] Z. Hashin, S. Shtrikman, "A variational approach to the theory of the effective magnetic permeability of multiphase materials", *J. Appl. Phys.* **33** (1962), p. 3125.
[5] D. J. Bergman, "The dielectric constant of a composite material—a problem in classical physics", *Phys. Rep.* **43** (1978), p. 377.
[6] G. W. Milton, "Bounds on the complex dielectric constant of a composite material", *Appl. Phys. Lett.* **37** (1980), p. 300.
[7] G. W. Milton, "Bounds on the complex permittivity of a two-component composite material", *J. Appl. Phys.* **52** (1981), p. 5286.
[8] G. W. Milton, "Bounds on the electromagnetic, elastic, and other properties of two-component composites", *Phys. Rev. Lett.* **46** (1981), p. 542.
[9] G. W. Milton, *The Theory of Composites*, Cambridge University Press, Cambridge, 2002.
[10] A. Bensoussan, J.-L. Lions, G. Papanicolaou, *Asymptotic Analysis for Periodic Structures*, American Mathematical Society Chelsea Publishing, Providence, RI, 2011.
[11] J. B. Pendry, A. J. Holden, W. J. Stewart, I. Youngs, "Extremely low frequency plasmons in metallic mesostructures", *Phys. Rev. Lett.* **76** (1996), p. 4773.
[12] J. B. Pendry, A. J. Holden, D. J. Robins, W. J. Stewart, "Low frequency plasmons in thin-wire structures", *J. Phys.: Condens. Matter.* **10** (1998), p. 4785.
[13] D. R. Smith, W. J. Padilla, D. C. Vier, N. C. Nemat-Nasser, S. Schultz, "Composite medium with simultaneously negative permeability and permittivity", *Phys. Rev. Lett.* **84** (2000), p. 4184.
[14] R. A. Shelby, D. R. Smith, S. Schultz, "Experimental verification of a negative index of refraction", *Science* **292** (2001), p. 77.
[15] R. M. Walser, "Electromagnetic metamaterials", in *Proc. SPIE, Complex Mediums II: Beyond Linear Isotropic Dielectr* (A. Lakhtakia, W. S. Weiglhofer, I. J. Hodgkinson, eds.), SPIE, San Diego, CA, USA, 2001, p. 4467.
[16] E. Yablonovitch, "Inhibited spontaneous emission in solid-state physics and electronics", *Phys. Rev. Lett.* **58** (1987), article ID 002059.
[17] J. Sajeev, "Strong localization of photons in certain disordered dielectric superlattices", *Phys. Rev. Lett.* **58** (1987), article ID 002486.
[18] B. Gralak, S. Enoch, G. Tayeb, "Anomalous refractive properties of photonic crystals", *J. Opt. Soc. Am. A* **17** (2000), p. 1012.
[19] M. Notomi, "Theory of light propagation in strongly modulated photonic crystals: Refractionlike behavior in the vicinity of the photonic band gap", *Phys. Rev. B* **62** (2000), article ID 10696.
[20] P. Yeh, "Electromagnetic propagation in birefringent layered media", *J. Opt. Soc. Am.* **69** (1979), article ID 000742.
[21] B. Gralak, S. Enoch, G. Tayeb, "Superprism effects and EBG antenna applications", in *Metamaterials: Physics and Engineering Explorations, Chapter 10* (N. Engheta, R. W. Ziolkowski, eds.), John Wiley and Sons, Hoboken, NJ, USA.
[22] B. Gralak, M. Cassier, G. Demésy, S. Guenneau, "Electromagnetic waves in photonic crystals: laws of dispersion, causality and analytical properties", in *Compendium of Electromagnetic Analysis — From Electrostatics to Photonics, Volume 4: Optics and Photonics I, Chapter 4*, World Scientific, Hackensack, NJ, USA, 2020, Editor-in-chief I. Tsukerman.
[23] E. Cubukcu, K. Aydin, E. Ozbay, S. Foteinopoulou, C. M. Soukoulis, "Negative refraction by photonic crystals", *Nature* **423** (2003), p. 604.

[24] C. R. Simovski, P. A. Belov, S. He, "Backward wave region and negative material parameters of a structure formed by lattices of wires and split-ring resonators", *IEEE Trans. Antennas Propag.* **51** (2003), article ID 002582.
[25] C. R. Simovski, "Material parameters of metamaterials (a review)", *Opt. Spectrosc.* **107** (2009), article ID 000726.
[26] V. V. Zhikov, "On an extension of the method of two-scale convergence and its applications", *Sb. Math.* **191** (2000), p. 973.
[27] G. Bouchitté, D. Felbacq, "Homogenization near resonances and artificial magnetism from dielectrics", *C. R. Math.* **339** (2004), p. 377.
[28] D. R. Smith, S. Schultz, P. Markos, C. M. Soukoulis, "Determination of effective permittivity and permeability of metamaterials from reflection and transmission coefficients", *Phys. Rev. B* **65** (2002), article ID 195104.
[29] C. R. Simovski, S. A. Tretyakov, "Local constitutive parameters of metamaterials from an effective-medium perspective", *Phys. Rev. B* **75** (2007), article ID 195111.
[30] M. G. Silveirinha, "Metamaterial homogenization approach with application to the characterization of microstructured composites with negative parameters", *Phys. Rev. B* **75** (2007), article ID 115104.
[31] M. G. Silveirinha, "Generalized lorentz-lorenz formulas for microstructured materials", *Phys. Rev. B* **76** (2007), article ID 245117.
[32] A. Alù, "First-principles homogenization theory for periodic metamaterials", *Phys. Rev. B* **84** (2011), article ID 075153.
[33] J. D. Jackson, *Classical Electrodynamics*, 3rd ed., Whiley, New York, 1998.
[34] Y. Liu, S. Guenneau, B. Gralak, "Artificial dispersion via high-order homogenization: magnetoelectric coupling and magnetism from dielectric layers", *Proc. R. Soc. A* **469** (2013), article ID 20130240.
[35] V. M. Agranovich, Y. N. Gartstein, "Spatial dispersion and negative refraction of light", *Usp. Phys. Nauk. (UFN)* **176** (2006), article ID 001051.
[36] R. V. Craster, J. Kaplunov, A. V. Puchugin, "High-frequency homogenization for periodic media", *Proc. R. Soc. A* **466** (2010), article ID 002341.
[37] R. V. Craster, J. Kaplunov, E. Nolde, S. Guenneau, "High-frequency homogenization for checkerboard structures: defect modes, ultrarefraction, and all-angle negative refraction", *J. Opt. Soc. Am. A* **28** (2011), article ID 001032.
[38] P. A. Belov, C. R. Simovski, "Boundary conditions for interfaces of electromagnetic crystals and the generalized ewald-oseen extinction principle", *Phys. Rev. B* **73** (2006), article ID 045102.
[39] M. Silveirinha, "Additional boundary condition for the wire medium", *IEEE Trans. Antennas Propag.* **54** (2006), article ID 001766.
[40] W. Smigaj, B. Gralak, "Validity of the effective-medium approximation of photonic crystals", *Phys. Rev. B* **77** (2008), article ID 235445.
[41] R. Pierre, G. Gralak, "Appropriate truncation for photonic crystals", *J. Mod. Opt.* **55** (2008), article ID 001759.
[42] C. R. Simovski, "On electromagnetic characterization and homogenization of nanostructured metamaterials", *J. Opt.* **13** (2011), article ID 103001.
[43] V. A. Markel, J. C. Schotland, "Homogenization of Maxwell's equations in periodic composites: Boundary effects and dispersion relations", *Phys. Rev. E* **85** (2012), article ID 066603.
[44] V. A. Markel, I. Tsukerman, "Current-driven homogenization and effective medium parameters for finite samples", *Phys. Rev. B* **88** (2013), article ID 125131.
[45] I. Tsukerman, "Classical and non-classical effective medium theories: New perspectives", *Phys. Lett. A* **381** (2017), article ID 001635.
[46] A. Demetriadou, J. Pendry, "Taming spatial dispersion in wire metamaterial", *J. Phys.: Condens. Matter.* **20** (2008), article ID 295222.
[47] A. I. Cabuz, D. Felbacq, D. Cassagne, "Spatial dispersion in negative-index composite metamaterials", *Phys. Rev. A* **77** (2008), article ID 013807.
[48] V. A. Markel, "Can the imaginary part of permeability be negative?", *Phys. Rev. E* **78** (2008), article ID 026608.
[49] M. G. Silveirinha, "Poynting vector, heating rate, and stored energy in structured materials: A first-principles derivation", *Phys. Rev. B* **80** (2009), article ID 235120.
[50] A. Alù, "Restoring the physical meaning of metamaterial constitutive parameters", *Phys. Rev. B* **83** (2011), article ID 081102(R).
[51] M. G. Silveirinha, "Examining the validity of Kramers–Kronig relations for the magnetic permeability", *Phys. Rev. B* **83** (2011), article ID 165119.
[52] A. Alù, A. D. Yaghjian, R. A. Shore, M. G. Silveirinha, "Causality relations in the homogenization of metamaterials", *Phys. Rev. B* **84** (2011), article ID 054305.
[53] Y. Liu, S. Guenneau, B. Gralak, "Causality and passivity properties of effective parameters of electromagnetic multilayered structures", *Phys. Rev. B* **88** (2013), article ID 165104.
[54] J. B. Pendry, "Negative refraction makes a perfect lens", *Phys. Rev. Lett.* **85** (2000), p. 3966-3969.
[55] J. B. Pendry, D. Shurig, D. R. Smith, "Controlling electromagnetic fields", *Science* **312** (2006), p. 1780.

[56] D. Shuring, J. J. Mock, B. J. Justice, S. A. Cummer, J. B. Pendry, A. F. Starr, D. R. Smith, "Metamaterial electromagnetic cloak at microwave frequencies", *Science* **314** (2006), p. 977.
[57] U. Leonhard, "Optical conformal mapping", *Science* **312** (2006), p. 1777.
[58] M. Cassier, G. W. Milton, "Bounds on Herglotz functions and fundamental limits of broadband passive quasistatic cloaking", *J. Math. Phys.* **58** (2017), article ID 071504.
[59] B. Gralak, "Analytic properties of the electromagnetic Green's function", *J. Math. Phys.* **58** (2017), article ID 071501.
[60] G. W. 't Hooft, "Comment on "Negative refraction makes a perfect lens"", *Phys. Rev. Lett.* **87** (2001), article ID 249701.
[61] J. M. Williams, "Some problems with negative refraction", *Phys. Rev. Lett.* **87** (2001), article ID 249703.
[62] N. Garcia, M. Nieto-Vesperinas, "Left-handed materials do not make a perfect lens", *Phys. Rev. Lett.* **88** (2002), article ID 207403.
[63] M. Nieto-Vesperinas, "Problem of image superresolution with a negative-refractive-index slab", *J. Opt. Soc. Am. A* **21** (2004), article ID 000491.
[64] D. Maystre, S. Enoch, "Perfect lenses made with left-handed materials: Alice's mirror?", *J. Opt. Soc. Am. A* **21** (2004), p. 122.
[65] I. Stockman, "Criterion for negative refraction with low optical losses from a fundamental principle of causality", *Phys. Rev. Lett.* **98** (2007), article ID 177404.
[66] P. M. Valanju, R. M. Walser, A. P. Valanju, "Wave refraction in negative-index media: Always positive and very inhomogeneous", *Phys. Rev. Lett.* **88** (2002), article ID 187401.
[67] B. Gralak, A. Tip, "Macroscopic Maxwell's equations and negative index materials", *J. Math. Phys.* **51** (2010), article ID 052902.
[68] A. V. Dorofeenko, A. A. Zyablovsky, A. A. Pukhov, A. A. Lisyansky, A. P. Vinogradov, "Light propagation in composite materials with gain layers", *Phys.-Usp.* **55** (2012), article ID 001080.
[69] H. O. Hagenvik, J. Skaar, "Fourier–Laplace analysis and instabilities of a gainy slab", *J. Opt. Soc. Am. B* **32** (2015), article ID 001947.
[70] H. O. Hagenvik, M. E. Malema, J. Skaar, "Fourier theory of linear gain media", *Phys. Rev. A* **91** (2018), article ID 043826.
[71] A. Tip, "Linear absorptive dielectric", *Phys. Rev. A* **57** (1998), article ID 004818.
[72] J.-M. Combes, B. Gralak, A. Tip, "Spectral properties of absorptive photonic crystals", in *Contemporary Mathematics*, Waves in Periodic and Random Media, vol. 339, American Mathematical Society, Providence, RI, 2003, p. 1.
[73] M. Cassier, P. Joly, M. Kachanovska, "Mathematical models for dispersive electromagnetic waves: an overview", *Comput. Math. Appl.* **74** (2017), article ID 002792.
[74] A. Tip, L. Knöll, S. Scheel, D.-G. Welsch, "Equivalence of the Langevin and auxiliary-field quantization methods for absorbing dielectrics", *Phys. Rev. A* **63** (2001), article ID 043806.
[75] C.-A. Guerrin, B. Gralak, A. Tip, "Singularity of the dyadic Green's function for heterogeneous dielectrics", *Phys. Rev. E* **75** (2007), article ID 056601.
[76] A. Figotin, J. H. Schenker, "Spectral theory of time dispersive and dissipative systems", *J. Stat. Phys.* **118** (2005), article ID 000199.
[77] R. E. Collin, "Frequency dispersion limits resolution in veselago lens", *Progr. Electromagn. Res. B* **19** (2010), p. 233.
[78] B. Gralak, D. Maystre, "Negative index materials and time-harmonic electromagnetic field", *C. R. Phys.* **13** (2012), article ID 000786.
[79] M. Cassier, C. Hazard, P. Joly, "Spectral theory for Maxwell's equations at the interface of a metamaterial. Part I: Generalized Fourier transform", *Commun. Partial Differ. Equ.* **42** (2017), article ID 001707.
[80] S. Guenneau, B. Gralak, J. B. Pendry, "Perfect corner reflector", *Opt. Lett.* **30** (2005), article ID 001204.
[81] S. Guenneau, A. C. Vutha, S. A. Ramakrishna, "Negative refraction in 2d checkerboards related by mirror antisymmetry and 3d corner lenses", *New J. Phys.* **7** (2005), article ID 000164.
[82] S. Guenneau, S. A. Ramakrishna, S. Enoch, S. Chakrabarti, G. Tayeb, B. Gralak, "Cloaking and imaging effects in plasmonic checkerboards of negative ε and μ and dielectric photonic crystal checkerboards", *Photon. Nanostruct.-Fundam. Appl.* **10** (2007), article ID 000083.
[83] B. Gralak, S. Guenneau, "Transfer matrix method for point sources radiating in classes of negative refractive index materials with 2n-fold antisymmetry", *Waves Random Complex Media* **17** (2007), article ID 000581.
[84] A.-S. Bonnet-Ben Dhia, L. Chesnel, P. Ciarlet Jr., "T-coercivity for scalar interface problems between dielectrics and metamaterials", *J. Math. Mod. Num. Anal.* **46** (2012), article ID 001363.
[85] A.-S. Bonnet-Ben Dhia, L. Chesnel, X. Claeys, "Radiation condition for a non-smooth interface between a dielectric and a metamaterial", *Math. Models Methods Appl. Sci.* **23** (2013), article ID 001629.
[86] A.-S. Bonnet-Ben Dhia, L. Chesnel, P. Ciarlet Jr., "Two-dimensional Maxwell's equations with sign-changing coefficients", *Appl. Numer. Math.* **79** (2014), article ID 000029.
[87] A.-S. Bonnet-Ben Dhia, L. Chesnel, P. Ciarlet Jr., "T-coercivity for the Maxwell problem with sign-changing coefficients", *Commun. Part Differ. Equ.* **37** (2014), article ID 001007.

[88] C. Hazard, S. Paolantoni, "Spectral analysis of polygonal cavities containing a negative-index material", *Annales Henri Lebesgue* **3** (2020), p. 1161-1193.
[89] P. Yeh, *Optical Waves in Layered Media*, John Wiley and Sons, New York, 1988.
[90] J. G. Van Bladel, *Electromagnetic Fields*, 2nd ed., IEEE Press Series on Electromagnetic Wave Theory, Whiley-Interscience, Hoboken, NJ, USA, 2007.
[91] Y. Brûlé, B. Gralak, G. Demésy, "Calculation and analysis of the complex band structure of dispersive and dissipative two-dimensional photonic crystals", *J. Opt. Soc. Am. B* **33** (2016), article ID 000691.
[92] P. Lalanne, W. Yan, A. Gras, C. Sauvan, J.-P. Hugonin, M. Besbes, G. Demésy, M. D. Truong, B. Gralak, F. Zolla, A. Nicolet, F. Binkowski, L. Zschiedrich, S. Burger, J. Zimmerling, R. Remis, P. Urbach, H. T. Liu, T. Weiss, "Quasinormal mode solvers for resonators with dispersive materials", *J. Opt. Soc. Am. A* **36** (2019), article ID 000686.
[93] G. Demésy, N. Nicolet, B. Gralak, C. Geuzaine, C. Campos, J. E. Roman, "Non-linear eigenvalue problems with GetDP and SLEPc: Eigenmode computations of frequency-dispersive photonic open structures", *Comput. Phys. Commun.* **257** (2020), article ID 107509.
[94] A.-S. Bonnet-Ben Dhia, C. Carvalho, L. Chesnel, P. Ciarlet Jr., "On the use of Perfectly Matched Layers at corners for scattering problems with sign-changing coefficients", *J. Comput. Phys.* **322** (2016), article ID 000224.
[95] V. Veselago, L. Braginsky, V. Shklover, C. Hafner, "Negative refractive index materials", *J. Comput. Theor. Nanosci.* **3** (2006), p. 1.
[96] T. Koschny, P. Markos, D. R. Smith, C. M. Soukoulis, "Resonant and antiresonant frequency dependence of the effective parameters of metamaterials", *Phys. Rev. E* **68** (2003), article ID 065602(R).
[97] R. A. Depine, A. Lakhtakia, "Comment i on "resonant and antiresonant frequency dependence of the effective parameters of metamaterials"", *Phys. Rev. E* **70** (2004), article ID 048601.
[98] A. L. Efros, "Comment ii on "resonant and antiresonant frequency dependence of the effective parameters of metamaterials"", *Phys. Rev. E* **70** (2004), article ID 048602.
[99] A. D. Boardman, *Electromagnetic Surface Modes*, Whiley, New York, 1982.
[100] A. I. Fernández-Domínguez, A. Wiener, F. J. García-Vidal, S. A. Maier, J. B. Pendry, "Transformation-optics description of nonlocal effects in plasmonic nanostructures", *Phys. Rev. lett.* **108** (2012), article ID 106802.
[101] A. A. Rukhadze, V. P. Silin, "Electrodynamics of media with spatial dispersion", *Usp. Fiz. Nauk* **74** (1961), article ID 000223.
[102] D. Forcella, C. Prada, R. Carminati, "Causality, nonlocality, and negative refraction", *Phys. Rev. Lett.* **1180** (2017), article ID 134301.
[103] A. Tip, A. Moroz, J.-M. Combes, "Band structure of absorptive photonic crystals", *J. Phys. A: Math. Gen.* **33** (2000), article ID 006223.
[104] N. Yu, F. Capasso, "Flat optics with designer metasurfaces", *Nat. Mater.* **13** (2014), article ID 000139.
[105] D. Lin, P. Fan, E. Hasman, M. L. Brongersma, "Dielectric gradient metasurface optical elements", *Science* **345** (2014), article ID 000298.
[106] M. C. Rechtsman, J. M. Zeuner, Y. Plotnik, Y. Lumer, D. Podolsky, F. Dreisow, A. Szameit, "Photonic floquet topological insulators", *Nature* **496** (2013), article ID 000196.
[107] C. L. Fefferman, J. P. Lee-Thorp, M. I. Weinstein, "Honeycomb Schrödinger operators in the strong binding regime", *Commun. Pure Appl. Math.* **71** (2018), article ID 001178.
[108] R. C. Craster, S. Guenneau, *Metamaterials and Plasmonics, Volume 2: Elastic, Acoustic, and Seismic Metamaterials*, World Scientific Series in Nanoscience and Nanotechnology, World Scientific Publishing, London, UK, 2017.

Comptes Rendus
Physique
2020, 21, nº 4-5, p. 367-388
https://doi.org/10.5802/crphys.4

Metamaterials 1 / *Métamatériaux 1*

First principles homogenization of periodic metamaterials and application to wire media

Homogénéisation ab-initio de métamatériaux périodiques et applications aux réseaux périodiques de fils métalliques

Sylvain Lannebère [a], Tiago A. Morgado [a] and Mário G. Silveirinha [*, b, a]

[a] Department of Electrical Engineering, University of Coimbra and Instituto de Telecomunicações, 3030-290 Coimbra, Portugal

[b] University of Lisbon – Instituto Superior Técnico, Department of Electrical Engineering, 1049-001 Lisboa, Portugal

E-mails: sylvain.lannebere@co.it.pt (S. Lannebère), tiago.morgado@co.it.pt (T. A. Morgado), mario.silveirinha@co.it.pt (M. G. Silveirinha)

Abstract. Here, we present an overview of a first principles homogenization theory of periodic metamaterials. It is shown that in a rather general context it is possible to formally introduce effective parameters that describe the time evolution of macroscopic (slowly-varying in space) initial states of the electromagnetic field using an effective medium formalism. The theory is applied to different types of "wire metamaterials" characterized by a strong spatial dispersion in the long wavelength limit. It is highlighted that the spatial dispersion may tailor in unique ways the wave phenomena in wire metamaterials leading to exotic tunneling effects and broadband lossless anomalous dispersion.

Résumé. Nous présentons une revue d'une théorie ab-initio d'homogénéisation de métamatériaux périodiques. Nous montrons dans un cadre général qu'il est possible d'introduire formellement des paramètres effectifs qui décrivent l'évolution temporelle d'états initiaux (états à variation spatiale lente) du champ électromagnétique en faisant appel à un formalisme de type milieu effectif. Cette théorie est appliquée à différents types de métamatériaux constitués de réseaux périodiques de fils métalliques et qui ont par ailleurs la particularité d'être caractérisés par une forte dispersion spatiale dans la limite des grandes longueurs d'onde. Il est souligné que les effets de la dispersion spatiale peuvent mener à un contrôle sans précédent des phénomènes ondulatoires dans ces métamatériaux, notamment avec la possibilité d'effets tunnel exotiques ou encore de dispersion anormale sans perte et large bande.

* Corresponding author.

Keywords. Homogenization, Effective medium, Wire medium, Metamaterials, Spatial dispersion.
Mots-clés. Homogénéisation, Milieu effectif, Réseaux de fils métalliques, Métamatériaux, Dispersion spatiale.

1. Introduction

The interactions between waves and matter play a fundamental role in most physical processes. It is usually rather challenging to characterize exactly the wave propagation in macroscopic systems formed by a large number of identical elements, e.g., in periodic or random composite materials, due to the complexity of the wave phenomena at the microscopic level. Fortunately, in many instances, the detailed microscopic behavior of a wave is of very limited practical interest. Instead, one can resort to effective medium theories that provide a simplified description of the wave phenomena in terms of a limited set of parameters. Effective medium theories are particularly successful when the wavelength is large with respect to the characteristic spatial period of the composite material. In this case, the material may be regarded as a continuum, and the homogenization formalism gives a simplified and insightful picture of the wave propagation.

Effective medium theories have a long history [1]. In the case of light waves, the concepts of "permittivity" and "permeability" of a material are as old as the electromagnetism itself. Similarly, in semiconductor theory the effects of a periodic electrostatic potential associated with the ionic lattice can be modeled by an effective electron mass [2]. In the last two decades, the interest in effective medium theories has been renewed by the emergence of the field of metamaterials [3–28]. Metamaterials are composite media formed by properly shaped dielectric or metallic inclusions embedded in a host medium, which are designed to exhibit extraordinary behavior such as a negative index of refraction [29], subwavelength imaging [30, 31] or other applications [32]. Usually, in metamaterials the radiation wavelength λ is only moderately larger than the lattice constant a, typically 5–10 times. This contrasts with natural media where the ratio, λ/a, is several orders of magnitude larger than that value, even at optical frequencies. This property imposes restrictions on the application of classical homogenization theories to artificial materials [5, 7, 18, 19] due to the emergence of spatial dispersion.

In a spatially dispersive material the electric displacement vector in a given point of space cannot be written exclusively in terms of the macroscopic electric field at the same point, but ultimately may depend on the distribution of the electric field in a neighborhood that encompasses many unit cells [33]. This non-locality of the electromagnetic response has many important and nontrivial repercussions on the physical properties of a material [34].

The objective of this review article is to present an up to date comprehensive description of a general homogenization procedure first developed in the context of electromagnetic metamaterials [7] and later generalized to semiconductor superlattices [35]. The effective medium theory is applicable to a wide range of periodic physical systems and takes into account both spatial and frequency dispersion [10, 36]. We illustrate the application of the formalism to "wire media". This class of metamaterials is particularly interesting, not only because it allows for an analytic treatment that describes almost exactly the actual microscopic response of the metamaterial, but also because of the richness of the wave phenomena it enables.

The review article is organized as follows: in Section 2 we describe the general homogenization scheme of Ref. [35] that uses as a starting point a time-domain perspective. In Section 3, we focus our analysis on nonmagnetic and periodic electromagnetic metamaterials and explain how to

find the effective response in the frequency domain. The homogenization approach is applied to wire media in Section 4. The nonlocal effective models for different wire medium topologies are presented in Section 4.1. In Section 4.2, it is shown that the nonlocality of wire metamaterials emerges naturally from a quasi-static model with additional state variables that describe the internal degrees of freedom of the metamaterial. Some subtleties arising from the nonlocality of the electromagnetic response, such as the definition of the Poynting vector and the need for Additional Boundary Conditions (ABCs) are discussed in Sections 4.3 and 4.4, respectively. Finally, in Section 5 we describe some exotic wave phenomena due to the spatial dispersion in two distinct wire medium configurations.

2. Effective medium theory

In this section, we present the fundamentals of the homogenization method originally developed in Refs. [7, 35, 36]. We adopt the general perspective of Refs. [35, 36] where the effective medium parameters are defined in such a way that they describe exactly the time-evolution of any macroscopic (slowly-varying in space) initial wave packet.

2.1. *Microscopic theory*

We consider a generic periodic in space physical system whose dynamics is characterized by a one-body Schrödinger-type equation of the form:

$$\hat{H}\psi = \mathrm{i}\hbar\frac{\partial}{\partial t}\psi. \tag{1}$$

Here, $\hat{H}$ is the operator that determines the time evolution of the system and ψ is the state-vector that describes the state of the system. In general ψ is a multi-component vector (a spinor). Evidently, this type of formulation is suitable to characterize the propagation of electron waves in a bulk semiconductor or in semiconductor or graphene superlattices, and in such a context $\hat{H}$ is the system Hamiltonian, ψ is the wave function and $\hbar$ is the reduced Planck constant [35, 37–39].

Importantly, the propagation of light can also be described using a similar formulation. Indeed, the Maxwell's equations can be written in a compact form as [35]

$$\begin{pmatrix} 0 & \mathrm{i}\nabla\times\mathbf{1}_{3\times3} \\ -\mathrm{i}\nabla\times\mathbf{1}_{3\times3} & 0 \end{pmatrix}\cdot\mathbf{f} = \mathrm{i}\frac{\partial\mathbf{g}}{\partial t}, \tag{2}$$

where $\mathbf{f} = (\mathbf{e} \quad \mathbf{h})^T$ is a six-element vector with components determined by the microscopic electric and magnetic fields and $\mathbf{g} = (\mathbf{d} \quad \mathbf{b})^T$ is a six-element vector with components determined by the electric displacement and the magnetic induction fields. In electromagnetic metamaterials the $\mathbf{f}$ and $\mathbf{g}$ fields are related by a space-dependent material matrix $\mathbf{M} = \mathbf{M}(\mathbf{r})$ through the constitutive relation $\mathbf{g} = \mathbf{M}\cdot\mathbf{f}$. In conventional isotropic media the material matrix is simply:

$$\mathbf{M} = \begin{pmatrix} \varepsilon\mathbf{1}_{3\times3} & 0 \\ 0 & \mu\mathbf{1}_{3\times3} \end{pmatrix}, \tag{3}$$

where ε and μ are the permittivity and permeability, respectively. Hence, by defining $\hat{H}$ as:

$$\hat{H} = \hbar\begin{pmatrix} 0 & \mathrm{i}\nabla\times\mathbf{1}_{3\times3} \\ -\mathrm{i}\nabla\times\mathbf{1}_{3\times3} & 0 \end{pmatrix}\cdot\mathbf{M}^{-1} \tag{4}$$

and identifying the state vector with the $\mathbf{g}$ field, $\psi = \mathbf{g}$, the Maxwell's equations can be expressed as in (1). It should be noted that in the electromagnetic case $\hat{H}$ is unrelated to the energy of the system, and should be simply regarded as an operator that describes the time evolution of the classical electromagnetic field. Moreover, in the previous discussion it is implicit that the

relevant materials are nondispersive, i.e., the permittivity ε and the permeability μ are frequency independent. Yet, the formalism can be generalized to dispersive media, as it is always possible to get rid of the material dispersion with additional variables [40–42]. For lossy media, the $\hat{H}$ operator is non-Hermitian.

2.2. *Spatial averaging and the envelope function*

The envelope function is intuitively the slowly varying part, in space, of the state vector ψ. It is defined here as:

$$\Psi(\mathbf{r}, t) \equiv \left\{\psi(\mathbf{r}, t)\right\}_{\text{av}}, \tag{5}$$

where $\{\,\}_{\text{av}}$ is a linear operator that performs a spatial averaging. The averaging operator is completely determined by the response to plane waves, characterized by the function $F(\mathbf{k})$ such that

$$\left\{\mathrm{e}^{\mathrm{i}\mathbf{k}\cdot\mathbf{r}}\right\}_{\text{av}} = F(\mathbf{k})\mathrm{e}^{\mathrm{i}\mathbf{k}\cdot\mathbf{r}}. \tag{6}$$

Thus, the action of the averaging operator on a generic plane wave with wave vector $\mathbf{k}$ yields another plane wave with the same wave vector, but with a different amplitude given by $F(\mathbf{k})$. Because of the linearity of the operator $\{\,\}_{\text{av}}$, its action on a generic function is determined by Fourier theory and is given by a spatial convolution. The envelope function can be explicitly written as:

$$\Psi(\mathbf{r}, t) = \int \mathrm{d}^N\mathbf{r}' f(\mathbf{r}')\psi(\mathbf{r}-\mathbf{r}', t), \tag{7}$$

where N is the space dimension (e.g., $N = 3$ for a three-dimensional metamaterial). The weight function f is the inverse Fourier transform of F so that:

$$f(\mathbf{r}) = \frac{1}{(2\pi)^N}\int \mathrm{d}^N\mathbf{k} F(\mathbf{k})\mathrm{e}^{\mathrm{i}\mathbf{k}\cdot\mathbf{r}}. \tag{8}$$

Related ideas have been developed by Russakov in the context of macroscopic electromagnetism [43]. It is assumed that the averaging operator corresponds to an ideal low pass spatial filter such that:

$$F(\mathbf{k}) = \begin{cases} 1, & \mathbf{k} \in \text{B.Z.} \\ 0, & \text{otherwise.} \end{cases} \tag{9}$$

In this article the set B.Z. stands for the first Brillouin zone of the periodic lattice, but sometimes other choices can be relevant [36]. The envelope function $\Psi(\mathbf{r}, t)$ has no significant spatial fluctuations on the scale of a unit cell, i.e., the microscopic fluctuations are filtered out by the averaging operator. Hence, $\Psi(\mathbf{r}, t)$ determines the macroscopic state vector. In general, we say that a given state vector ψ is macroscopic when it stays invariant under the operation of spatial averaging:

$$\psi(\mathbf{r}) = \left\{\psi(\mathbf{r})\right\}_{\text{av}}, \quad \text{(macroscopic state vector)}. \tag{10}$$

Importantly, a macroscopic state cannot be more localized in space than the characteristic period of the material.

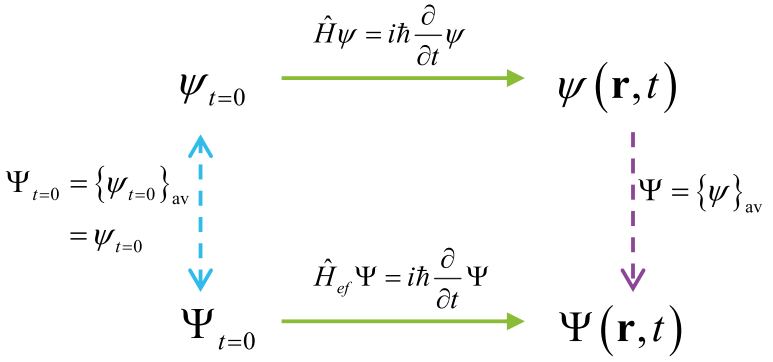

Figure 1. Schematic relation between the time evolutions determined by the macroscopic and microscopic Hamiltonians: for an initial macroscopic state the effective medium formulation ensures that $\Psi = \{\psi\}_{\text{av}}$ for $t > 0$. Reprinted with permission [37].

2.3. *The effective Hamiltonian*

The effective Hamiltonian is the operator that describes the time evolution of the envelope function. Specifically, suppose that the initial state vector is macroscopic, so that $\psi_{t=0} = \Psi_{t=0}$. In general, the time evolution of an initial macroscopic state does not yield a macroscopic state at a later time instant, i.e., $\psi(\mathbf{r}, t) \neq \Psi(\mathbf{r}, t)$ for $t > 0$. We define the effective Hamiltonian $\hat{H}_{\text{ef}}$ such that $\Psi(\mathbf{r}, t)$ calculated using $\hat{H}_{\text{ef}}$ is coincident with the spatially-averaged microscopic state vector $\{\psi(\mathbf{r}, t)\}_{\text{av}}$, where $\psi(\mathbf{r}, t)$ is determined by the microscopic Hamiltonian $\hat{H}$ [35,37]. These ideas are illustrated in the diagram of Figure 1.

The time evolution of the macroscopic state vector is determined by a generalized Schrödinger equation:

$$\left(\hat{H}_{\text{ef}}\Psi\right)(\mathbf{r}, t) = \mathrm{i}\hbar\frac{\partial}{\partial t}\Psi(\mathbf{r}, t). \tag{11}$$

From the definition of the effective Hamiltonian it is clear that it must ensure that:

$$\left\{\hat{H}\psi\right\}_{\text{av}} = \hat{H}_{\text{ef}}\Psi. \tag{12}$$

Because of linearity, the action of the effective Hamiltonian on the wave function can be expressed as a convolution in space and in time [35]:

$$\left(\hat{H}_{\text{ef}}\Psi\right)(\mathbf{r}, t) = \int \mathrm{d}^N\mathbf{r}' \int_0^t \mathrm{d}t'\, \mathbf{h}_{\text{ef}}(\mathbf{r} - \mathbf{r}', t - t') \cdot \Psi(\mathbf{r}', t'). \tag{13}$$

Note that the kernel $\mathbf{h}_{\text{ef}}$ is a function of $\mathbf{r} - \mathbf{r}'$. We shall see below that this is possible because the spatial averaging operation essentially eliminates the spatial granularity of the system. In general, the kernel $\mathbf{h}_{\text{ef}}(\mathbf{r}, t)$ is represented by a square matrix $[\mathbf{h}_{\sigma,\sigma'}]$ because Ψ is a multi-component vector. In the photonic case the dimension of $\mathbf{h}_{\text{ef}}$ is $S = 6$. Equation (13) shows that the effective Hamiltonian depends on the past history ($0 < t' < t$) and on the surroundings ($\mathbf{r}' \neq \mathbf{r}$) of the observation point, rather than just on the instantaneous and local value of Ψ. It is convenient to introduce the Fourier transform of $\mathbf{h}_{\text{ef}}(\mathbf{r}, t)$ defined as:

$$\mathscr{H}_{\text{ef}}(\mathbf{k}, \omega) = \int \mathrm{d}^N\mathbf{r} \int_0^{+\infty} \mathrm{d}t\, \mathbf{h}_{\text{ef}}(\mathbf{r}, t)\mathrm{e}^{\mathrm{i}\omega t}\mathrm{e}^{-\mathrm{i}\mathbf{k}\cdot\mathbf{r}}. \tag{14}$$

The Fourier transform is bilateral in space and unilateral in time. The unilateral Fourier transform in time can also be regarded as a Laplace transform. In the Fourier domain, the action of the effective Hamiltonian reduces to a simple multiplication:

$$\left(\hat{H}_{\text{ef}}\Psi\right)(\mathbf{k}, \omega) = \mathscr{H}_{\text{ef}}(\mathbf{k}, \omega) \cdot \Psi(\mathbf{k}, \omega). \tag{15}$$

Here, $\Psi(\mathbf{k},\omega)$ is the Fourier transform of the macroscopic state vector,

$$\Psi(\mathbf{k},\omega) = \int \mathrm{d}^N\mathbf{r} \int_0^{+\infty} \mathrm{d}t\, \Psi(\mathbf{r},t)\mathrm{e}^{\mathrm{i}\omega t}\mathrm{e}^{-\mathrm{i}\mathbf{k}\cdot\mathbf{r}}, \tag{16}$$

and $(\hat{H}_{\mathrm{ef}}\Psi)(\mathbf{k},\omega)$ is defined similarly. The integral in $\mathbf{r}$ is over all space. Note that for now the system is assumed to be periodic and unbounded, so that the effect of boundaries is disregarded. The convergence of the unilateral Fourier transform is guaranteed in the upper-half frequency plane, $\mathrm{Im}(\omega) > 0$.

The function $\mathscr{H}_{\mathrm{ef}}(\mathbf{k},\omega)$ completely determines the effective Hamiltonian. Because of the properties of the spatial averaging operator, it is possible to enforce that:

$$\mathscr{H}_{\mathrm{ef}}(\mathbf{k},\omega) = 0, \quad \text{when } \mathbf{k} \notin \text{B.Z.} \tag{17}$$

This property ensures that the effective Hamiltonian is a smoothened version of the microscopic Hamiltonian. In the following subsections, it is explained how $\mathscr{H}_{\mathrm{ef}}(\mathbf{k},\omega)$ can be calculated for $\mathbf{k} \in$ B.Z.

2.3.1. *Calculation of $\mathscr{H}_{\mathrm{ef}}(\mathbf{k},\omega)$ with a time domain approach*

Let us consider an initial macroscopic state of the form $\psi_{t=0} \sim \mathrm{e}^{\mathrm{i}\mathbf{k}\cdot\mathbf{r}}\mathbf{u}_l$ where the wavevector $\mathbf{k}$ can take any value in the B.Z. Here, $(\mathbf{u}_l)$ represents a basis of unit vectors that generates the S-dimensional vector space wherein ψ is defined. Because of the periodicity of the system, the microscopic time evolution of this initial state yields a state vector $\psi(\mathbf{r},t)$ with the Bloch property. In fact, $\psi(\mathbf{r},t)\mathrm{e}^{-\mathrm{i}\mathbf{k}\cdot\mathbf{r}}$ is a periodic function in space for any fixed t. For the same reason, $\hat{H}\psi$ has also the Bloch property. Crucially, the operation of spatial averaging only retains spatial harmonics with wave vector inside the B.Z., and hence it follows that the dependence of $\{\psi\}_{\mathrm{av}}$ and $\{\hat{H}\psi\}_{\mathrm{av}}$ on the spatial coordinates is of the form $\mathrm{e}^{\mathrm{i}\mathbf{k}\cdot\mathbf{r}}$ for any time instant. In other words, within the effective medium approach the time evolution of a plane wave-type initial state yields another plane wave-type state, such that the homogenized structure behaves as a continuum. Moreover, for Bloch modes it is possible to write:

$$\{\psi\}_{\mathrm{av}}(\mathbf{r},t) = \psi_{\mathrm{av}}(t)\cdot\mathrm{e}^{\mathrm{i}\mathbf{k}\cdot\mathbf{r}}, \tag{18a}$$

$$\{\hat{H}\psi\}_{\mathrm{av}}(\mathbf{r},t) = \left(\hat{H}\psi\right)_{\mathrm{av}}(t)\cdot\mathrm{e}^{\mathrm{i}\mathbf{k}\cdot\mathbf{r}}, \tag{18b}$$

with

$$\psi_{\mathrm{av}}(t) = \frac{1}{V_{\mathrm{cell}}}\int_\Omega \mathrm{d}^N\mathbf{r}\,\psi(\mathbf{r},t)\mathrm{e}^{-\mathrm{i}\mathbf{k}\cdot\mathbf{r}}, \tag{19a}$$

$$\left(\hat{H}\psi\right)_{\mathrm{av}}(t) = \frac{1}{V_{\mathrm{cell}}}\int_\Omega \mathrm{d}^N\mathbf{r}\,\hat{H}\psi(\mathbf{r},t)\mathrm{e}^{-\mathrm{i}\mathbf{k}\cdot\mathbf{r}}, \tag{19b}$$

where Ω represents the unit cell and V_{cell} is the respective volume. Taking now into account that $\Psi = \{\psi\}_{\mathrm{av}}$ and $\hat{H}_{\mathrm{ef}}\Psi = \{\hat{H}\psi\}_{\mathrm{av}}$, and substituting (18) into (13), it is seen after straightforward manipulations that:

$$\left(\hat{H}\psi\right)_{\mathrm{av}}(\omega) = \mathscr{H}_{\mathrm{ef}}(\mathbf{k},\omega)\cdot\psi_{\mathrm{av}}(\omega). \tag{20}$$

In the above, $\psi_{\mathrm{av}}(\omega)$ and $(\hat{H}\psi)_{\mathrm{av}}(\omega)$ stand for the unilateral Fourier (Laplace) transforms of the functions in (19). Hence, if we denote $\psi^{(l)}$, $l = 1,\ldots,S$ as the microscopic state vector determined by the time evolution of the initial state $\psi^{(l)}_{t=0} = \mathrm{i}/\hbar\,\mathrm{e}^{\mathrm{i}\mathbf{k}\cdot\mathbf{r}}\mathbf{u}_l$ (the proportionality constant was fixed as $\mathrm{i}/\hbar$ for convenience), it follows from the previous analysis that the effective Hamiltonian is given by:

$$\mathscr{H}_{\mathrm{ef}}(\mathbf{k},\omega) = \left[\left(\hat{H}\psi^{(1)}\right)_{\mathrm{av}}\ldots\left(\hat{H}\psi^{(S)}\right)_{\mathrm{av}}\right]\cdot\left[\psi^{(1)}_{\mathrm{av}}\ldots\psi^{(S)}_{\mathrm{av}}\right]^{-1}. \tag{21}$$

Here $\mathscr{H}_{\mathrm{ef}}$ and the two objects delimited by the square brackets are $S\times S$ matrices. Thus, $\mathscr{H}_{\mathrm{ef}}(\mathbf{k},\omega)$ can be written as the product of two matrices, whose columns are determined by the vectors $\psi^{(l)}_{\mathrm{av}}(\omega)$ and $(\hat{H}\psi^{(l)})_{\mathrm{av}}(\omega)$.

In summary, for an arbitrary $\mathbf{k} \in$ B.Z. the effective Hamiltonian can be found by solving S microscopic time evolution problems associated with initial states of the form $\psi^{(l)}_{t=0} = \mathrm{i}/\hbar\, \mathrm{e}^{i\mathbf{k}\cdot\mathbf{r}}\mathbf{u}_l$. The effective Hamiltonian is written in terms of the Fourier transforms in time of the functions (19).

2.3.2. *Calculation of $\mathscr{H}_{\mathrm{ef}}(\mathbf{k},\omega)$ with a frequency domain approach*

The effective Hamiltonian may also be determined based on frequency domain calculations. To prove this we note that $\psi_{\mathrm{av}}(\omega)$ and $(\hat{H}\psi)_{\mathrm{av}}(\omega)$ can be written explicitly as:

$$\psi_{\mathrm{av}}(\omega) = \frac{1}{V_{\mathrm{cell}}}\int_{\Omega} \mathrm{d}^N\mathbf{r}\, \psi(\mathbf{r},\omega)\mathrm{e}^{-\mathrm{i}\mathbf{k}\cdot\mathbf{r}}, \tag{22a}$$

$$\left(\hat{H}\psi\right)_{\mathrm{av}}(\omega) = \frac{1}{V_{\mathrm{cell}}}\int_{\Omega} \mathrm{d}^N\mathbf{r}\, \hat{H}\psi(\mathbf{r},\omega)\mathrm{e}^{-\mathrm{i}\mathbf{k}\cdot\mathbf{r}}, \tag{22b}$$

where $\psi(\mathbf{r},\omega)$ is the unilateral Fourier transform of $\psi(\mathbf{r},t)$. Applying the unilateral Fourier (Laplace) transform to both members of the microscopic Schrödinger equation (1) and using the property $\partial_t\psi(\mathbf{r},t) \leftrightarrow -\mathrm{i}\omega\psi(\mathbf{r},\omega) - \psi_{t=0}(\mathbf{r})$, it follows that:

$$\left[\hat{H} - \hbar\omega\right]\cdot\psi(\mathbf{r},\omega) = -\mathrm{i}\hbar\psi_{t=0}(\mathbf{r}). \tag{23}$$

Hence, $\psi^{(l)}(\mathbf{r},\omega)$ can be directly found by solving the above equation for $-\mathrm{i}\hbar\psi^{(l)}_{t=0} = \mathrm{e}^{\mathbf{i}\mathbf{k}\cdot\mathbf{r}}\mathbf{u}_l$, with $l = 1,\ldots,S$. Once $\psi^{(l)}(\mathbf{r},\omega)$ is known one can determine $\psi^{(l)}_{\mathrm{av}}$ and $(\hat{H}\psi^{(l)})_{\mathrm{av}}$ using (22), and finally obtain the effective Hamiltonian from (21).

It is interesting to note that for $-\mathrm{i}\hbar\psi^{(l)}_{t=0} = \mathrm{e}^{\mathbf{i}\mathbf{k}\cdot\mathbf{r}}\mathbf{u}_l$ equation (23) implies that $(\hat{H}\psi^{(l)})_{\mathrm{av}} - \hbar\omega\psi^{(l)}_{\mathrm{av}} = \mathbf{u}_l$. Substituting this result into (21) one may also write the effective Hamiltonian as:

$$\mathscr{H}_{\mathrm{ef}}(\mathbf{k},\omega) = \hbar\omega + \left[\psi^{(1)}_{\mathrm{av}}\ldots\psi^{(S)}_{\mathrm{av}}\right]^{-1}. \tag{24}$$

2.4. *Stationary states*

The spectrum of the effective Hamiltonian is exactly coincident with the spectrum of the microscopic Hamiltonian [35] (here, for simplicity it is assumed that there are no "dark states", for a discussion see [35]). The energy spectrum of the macroscopic Hamiltonian is determined by the nontrivial solutions of the stationary Schrödinger equation

$$\left[\mathscr{H}_{\mathrm{ef}}(\mathbf{k},\omega)|_{\omega=E/\hbar} - E\right]\cdot\Psi = 0, \tag{25}$$

where E stands for the energy of a certain stationary state. For example, in the electromagnetic case the photonic band structure calculated with the effective Hamiltonian is coincident with the exact band structure obtained using a microscopic theory [7]. The enunciated result follows from the fact that in a time evolution problem (with no source excitation) the state vector can be written as a superposition of eigenmodes. The eigenmodes have a time variation of the form $\mathrm{e}^{-\mathrm{i}\omega_n t}$, being $\omega_n = E_n/\hbar$ the relevant eigenfrequencies. Importantly, since the macroscopic and microscopic state vectors are related by the spatial-averaging operation ($\Psi = \{\psi\}_{\mathrm{av}}$), both Ψ and ψ have the same-type of time oscillations. In other words, the averaging affects only the space coordinates, while the time coordinate is not averaged in any manner. As a consequence, the spectrum of the microscopic and macroscopic Hamiltonians must be the same. For a detailed mathematical proof of this property the reader is referred to Appendix C of Ref. [35].

3. The electromagnetic case

The formalism of the previous section when applied to the electromagnetic case (2) yields a 6×6 effective Hamiltonian of the form [36]:

$$\mathscr{H}_{\mathrm{ef}}(\mathbf{k},\omega) = \hbar\begin{pmatrix} 0 & -\mathbf{k}\times\mathbf{1}_{3\times 3} \\ \mathbf{k}\times\mathbf{1}_{3\times 3} & 0 \end{pmatrix}\cdot\mathbf{M}^{-1}_{\mathrm{ef}}(\mathbf{k},\omega), \tag{26}$$

where $\mathbf{M}_{\text{ef}}(\mathbf{k},\omega)$ is the effective material matrix that links the averaged fields $\{\mathbf{f}\}_{\text{av}}$ and $\{\mathbf{g}\}_{\text{av}}$ of (2), [35,36]. For metamaterials made of non-magnetic particles the material matrix is of the form

$$\mathbf{M}_{\text{ef}}(\mathbf{k},\omega) = \begin{pmatrix} \overline{\overline{\varepsilon}}_{\text{ef}}(\mathbf{k},\omega) & 0 \\ 0 & \mu_0 \mathbf{1}_{3\times 3} \end{pmatrix}. \tag{27}$$

Thus, the homogenization problem reduces to the determination of the nonlocal effective permittivity $\overline{\overline{\varepsilon}}_{\text{ef}}(\mathbf{k},\omega)$. The permittivity can be found using the source-driven homogenization theory developed for electromagnetic metamaterials [7]. As shown in [36] the effective response obtained with this theory is exactly coincident with the one obtained with the general theory of previous section. Below, we quickly review the main ideas of the source-driven homogenization, highlighting that the homogenization problem can be reduced to an integral equation [7].

We consider a generic nonmagnetic periodic metamaterial described by the periodic permittivity $\varepsilon_r(\mathbf{r},\omega) = \varepsilon_r(\mathbf{r}+\mathbf{R},\omega)$ with $\mathbf{R}$ a vector of the Bravais lattice. Assuming a time variation of the form $\mathrm{e}^{-\mathrm{i}\omega t}$, the microscopic Maxwell equations in this system are

$$\nabla \times \mathbf{e} = \mathrm{i}\omega \mathbf{b} \tag{28a}$$

$$\nabla \times \frac{\mathbf{b}}{\mu_0} = \mathbf{j}_e - \varepsilon_0 \varepsilon_r \mathrm{i}\omega \mathbf{e} \tag{28b}$$

where $\mathbf{e},\mathbf{b}$ are the microscopic electric and magnetic field, respectively and $\mathbf{j}_e$ is an applied (macroscopic) electric current density that acts as a source of the electromagnetic fields. The applied current density is assumed to have the Bloch property and enforces a desired spatial variation within the unit cell. This means that the pair of parameters $(\omega,\mathbf{k})$ characterizing the time and space variations of the fields are independent of each other and do not need to be associated with an eigenmode. The applied current plays the same role as the initial state $\psi_{t=0}$ in the formulation of last section.

By applying the averaging operator (18a) to the microscopic Maxwell equations (28), one obtains the macroscopic Maxwell equations:

$$\mathbf{k} \times \mathbf{E}_{\text{av}} = \omega \mathbf{B}_{\text{av}}, \tag{29a}$$

$$\mathbf{k} \times \frac{\mathbf{B}_{\text{av}}}{\mu_0} = -\mathrm{i}\mathbf{J}_{e,\text{av}} - \omega \mathbf{P}_{\text{g}} - \varepsilon_0 \omega \mathbf{E}_{\text{av}}, \tag{29b}$$

where $\mathbf{E}_{\text{av}}, \mathbf{B}_{\text{av}}$ and $\mathbf{J}_{e,\text{av}}$ are the averaged $\mathbf{e},\mathbf{b}$ and $\mathbf{j}_e$, respectively, defined according to (22a). The averaged induced polarization $\mathbf{P}_{\text{g}}$ is given by

$$\frac{\mathbf{P}_{\text{g}}}{\varepsilon_0} = \frac{1}{V_{\text{cell}}} \int_{\Omega} \big(\varepsilon_r(\mathbf{r}) - 1\big)\mathbf{e}(\mathbf{r}) \mathrm{e}^{-\mathrm{i}\mathbf{k}\cdot\mathbf{r}} \, \mathrm{d}^3\mathbf{r}. \tag{30}$$

For system containing perfectly electric conducting (PEC) surfaces, the integration over the unit cell volume in the previous expression can be transformed into a surface integral, see [7, 10] for more details.

The nonlocal effective permittivity is defined through the relation between the averaged electric field and the averaged induced polarization:

$$\overline{\overline{\varepsilon}}_{\text{ef}}(\omega,\mathbf{k}) \cdot \mathbf{E}_{\text{av}} = \varepsilon_0 \mathbf{E}_{\text{av}} + \mathbf{P}_{\text{g}}. \tag{31}$$

As shown in [7], for every pair $(\omega,\mathbf{k})$ the homogenization problem can be reduced to an integral equation. The unknown of the integral equation is the microscopic vector field $\mathbf{p}_{\text{ind}}(\mathbf{r}) = (\varepsilon_r(\mathbf{r}) - 1)\mathbf{e}(\mathbf{r})$ and the excitation is the averaged electric field $\mathbf{E}_{\text{av}}$. A solution of the problem can be formally constructed using the Method of Moments (MoM). The unknown $\mathbf{p}_{\text{ind}}$ is expanded as

$$\mathbf{p}_{\text{ind}} = \sum_n c_n \mathbf{w}_{n,\mathbf{k}}, \tag{32}$$

where the set of expansion functions $\mathbf{w}_{n,\mathbf{k}}$ has the Bloch property and is assumed to be a complete set in $\{\mathbf{r} : \varepsilon_r(\mathbf{r}) - 1 \neq 0\}$.

For simplicity, next we focus on the case where the metamaterial inclusions can be modeled as impedance boundaries, characterized by some surface impedance Z_s [44]. The surface impedance links the tangential electric field $\mathbf{E}_{\tan}$ at the boundary surface (∂D) with the current surface density $\mathbf{J}_s = \hat{\boldsymbol{\nu}} \times \mathbf{H}$, as $\mathbf{E}_{\tan} = Z_s \mathbf{J}_s$ [45]. Here, $\hat{\boldsymbol{\nu}}$ is the unit normal vector oriented toward the exterior of the inclusion. A PEC inclusion is described by the surface impedance $Z_s = 0$. It can be shown that the effective permittivity is given by [7, 10]

$$\frac{\bar{\bar{\varepsilon}}_{\text{ef}}}{\varepsilon_0}(\omega, \mathbf{k}) = \bar{\bar{\mathbf{I}}} + \frac{1}{V_{\text{cell}}} \sum_{m,n} \chi^{m,n} \int_{\partial D} \mathbf{w}_{m,\mathbf{k}}(\mathbf{r}) \mathrm{e}^{-\mathrm{i}\mathbf{k}\cdot\mathbf{r}} \,\mathrm{d}s \otimes \int_{\partial D} \mathbf{w}_{n,-\mathbf{k}}(\mathbf{r}) \mathrm{e}^{\mathrm{i}\mathbf{k}\cdot\mathbf{r}} \,\mathrm{d}s \tag{33}$$

$$\begin{aligned} \chi_{m,n} = & \int_{\partial D} \int_{\partial D} [\nabla_s \cdot \mathbf{w}_{m,-\mathbf{k}}(\mathbf{r}) \nabla_{s'} \cdot \mathbf{w}_{n,\mathbf{k}}(\mathbf{r}') - (\omega/c)^2 \mathbf{w}_{m,-\mathbf{k}}(\mathbf{r}) \cdot \mathbf{w}_{n,\mathbf{k}}(\mathbf{r}')] \Phi_{p0}(\mathbf{r}|\mathbf{r}'; \omega, \mathbf{k}) \,\mathrm{d}s \,\mathrm{d}s' \\ & - \mathrm{i}\omega\varepsilon_0 Z_s \int_{\partial D} \mathbf{w}_{m,-\mathbf{k}}(\mathbf{r}) \cdot \mathbf{w}_{n,\mathbf{k}}(\mathbf{r}) \,\mathrm{d}s. \end{aligned} \tag{34}$$

In the above Φ_{p0} is the Green's function introduced in (35b) of [7], ∇_s stands for the surface divergence of a tangential vector field and the matrix $[\chi^{m,n}]$ is the inverse of $[\chi_{m,n}]$. In the next section, we illustrate the application of the above formulas to the case of wire metamaterials.

As shown in [7, 10], Equation (33) can be generalized to the case of volumetric dielectric inclusions. The MoM formulation is particularly well suited to characterize the effective response of metamaterials made of metallic structures. Due to this reason, for dielectrics it is typically more practical to solve the homogenization problem with finite differences methods in the frequency [11] or in the time domain [14].

4. Application to wire metamaterials

Next, we apply the homogenization method to periodic arrays of thin metallic wires. Wire metamaterials are generically characterized by a strong spatial dispersion in the long wavelength limit.

4.1. *Nonlocal effective models*

In the following subsections we obtain the effective medium responses of three different wire metamaterials: the uniaxial wire medium, the double wire medium and the 3D connected wire mesh. In all cases, it will be assumed that the metallic wires are thin, $R \ll a$, where R is the radius of the wires and a is the spatial period. The wires are modeled as impedance boundaries characterized by the surface impedance $Z_s = 2\mathrm{i}/(\omega\varepsilon_0(\varepsilon_m - 1)R)$ where ε_m is the metal relative permittivity. The wires are embedded in a host medium of permittivity ε_h.

4.1.1. *Uniaxial wire medium*

The simplest example of a wire metamaterial is the so-called uniaxial wire medium. It consists of a square lattice of parallel and infinitely long metallic wires oriented along a fixed direction, here taken as the $\hat{\mathbf{z}}$ direction as represented in Figure 2(a).

The study of such systems has a long history (dating back to the 1950s) that was renewed at the turn of this century after the discovery of negative index metamaterials [46–52].

As shown in [45], the application of the homogenization scheme of Section 3 to this wire metamaterial is particularly simple. Indeed, the current density induced on the metallic wires surface can be accurately modeled by a single expansion function:

$$\mathbf{w}_{1,\mathbf{k}}(\mathbf{r}) = \frac{\mathrm{e}^{\mathrm{i}\mathbf{k}\cdot\mathbf{r}}}{2\pi R} \hat{\mathbf{z}}. \tag{35}$$

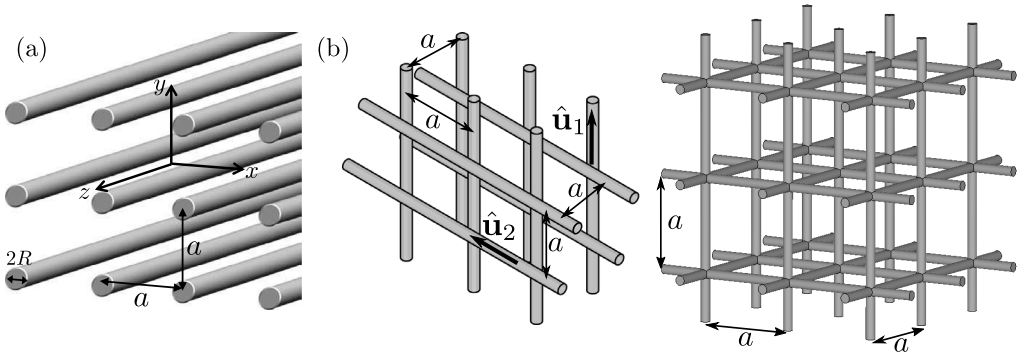

Figure 2. (a) Uniaxial wire medium formed by a square array (period a) of infinitely long metallic rods oriented along the $\hat{\mathbf{z}}$ direction. (b) Double wire medium formed by two non-connected arrays of parallel wires arranged in a cubic lattice with lattice constant a. The two arrays of wires are oriented along $\hat{\mathbf{u}}_1$ and $\hat{\mathbf{u}}_2$ and the distance between adjacent wires is $a/2$. (c) 3D wire mesh formed by a connected array of orthogonal metallic wires. In (a)–(c) the wires radius is R and the metal relative permittivity is ε_m.

Note that the electric current density is proportional to $\mathbf{p}_{\text{ind}}$. Using $\mathbf{w}_{1,\mathbf{k}}(\mathbf{r})$ in (33) and (34), it can be shown that the nonlocal effective permittivity reduces to [10, 45, 53]

$$\frac{\bar{\bar{\varepsilon}}_{\text{ef}}}{\varepsilon_0}(\omega,\mathbf{k}) = \bar{\bar{\mathbf{I}}} + \frac{1}{\frac{1}{f_V(\varepsilon_m-1)} + \frac{1}{\beta_p^2}\left(k_z^2 - \frac{\omega^2}{c^2}\right)}\hat{\mathbf{z}}\otimes\hat{\mathbf{z}}, \tag{36}$$

where $f_V = \pi R^2/a^2$ is the volume fraction of the wires and β_p is the plasma wavenumber for an array of parallel PEC wires. The parameter β_p depends solely on the system geometry (see the next subsection for the expression and Ref. [45] for further details).

As seen, the effective permittivity of the uniaxial wire medium depends on the z component of the wavevector along the wires (k_z), which leads to a pole of the material response at low frequencies (for good conductors $\varepsilon_m \to -\infty$ and the pole occurs for $k_z \approx \omega/c$). Thereby, the spatial dispersion effects are rather strong. This feature has several nontrivial consequences, e.g., it implies that the medium may support two modes with the same polarization [50, 53, 54]. For a full discussion about the uniaxial wire medium modes the reader is referred to [53]. The uniaxial wire medium has interesting applications in subwavelength imaging when operated in the canalization regime [31, 55–64].

4.1.2. *Double wire mesh*

A more complex situation from the homogenization perspective occurs when a second array of parallel wires with a different orientation is inserted in between the first set of wires (see Figure 2(b)). Such structures are usually referred to as double wire meshes, and can have several interesting applications and rather exotic physics [65–72]. While the expression of the nonlocal effective permittivity of this metamaterial is well known [66], its direct derivation using the homogenization formalism of Section 3 was not reported previously in the literature. Since we believe that the proof is pedagogical we do so in the following.

The wire arrays are oriented along the generic directions $\hat{\mathbf{u}}_1$ and $\hat{\mathbf{u}}_2$. For simplicity we restrict our analysis to PEC wires ($Z_s = 0$), orthogonal to each other $\hat{\mathbf{u}}_m \cdot \hat{\mathbf{u}}_n = \delta_{m,n}$, with $m, n = 1, 2$, and consider a cubic lattice with period a. Similar to the case of the uniaxial wire medium, one expansion function per wire (two in total) is sufficient to obtain an approximate analytical expression for the effective permittivity. The expansion function that models the density of

current induced in the nth wire oriented along $\hat{\mathbf{u}}_n$ (here assumed parallel to one of the coordinate axes) is taken as

$$\mathbf{w}_{n,\mathbf{k}}(\mathbf{r}) = \frac{\mathrm{e}^{\mathrm{i}\mathbf{k}\cdot\mathbf{r}}}{2\pi R}\hat{\mathbf{u}}_n, \quad n = 1,2. \tag{37}$$

Substituting the above formula into (33), one finds that the effective permittivity can be written as:

$$\frac{\bar{\bar{\varepsilon}}_{\mathrm{ef}}}{\varepsilon_0}(\omega,\mathbf{k}) = \bar{\bar{\mathbf{I}}} + \frac{1}{a}\sum_{m,n}\chi^{m,n}\hat{\mathbf{u}}_m \otimes \hat{\mathbf{u}}_n. \tag{38}$$

To obtain $\chi^{m,n}$, we substitute (37) into (34) and use the regularized lattice Green's function given by [7]

$$\Phi_{p0}(\mathbf{r}|\mathbf{r}';\omega,\mathbf{k}) = \frac{1}{V_{\mathrm{cell}}}\sum_{\mathbf{J}\neq 0}\frac{\mathrm{e}^{\mathrm{i}\mathbf{k}_\mathbf{J}\cdot(\mathbf{r}-\mathbf{r}')}}{\mathbf{k}_\mathbf{J}\cdot\mathbf{k}_\mathbf{J} - \frac{\omega^2}{c^2}} \approx \frac{1}{V_{\mathrm{cell}}}\sum_{\mathbf{J}\neq 0}\frac{\mathrm{e}^{\mathrm{i}\mathbf{k}_\mathbf{J}\cdot(\mathbf{r}-\mathbf{r}')}}{\mathbf{k}^0_\mathbf{J}\cdot\mathbf{k}^0_\mathbf{J}}, \tag{39}$$

where $\mathbf{k}_\mathbf{J} = \mathbf{k}+\mathbf{k}^0_\mathbf{J}$ with $\mathbf{k}^0_\mathbf{J} = j_1\mathbf{b}_1 + j_2\mathbf{b}_2 + j_3\mathbf{b}_3$ and the $\mathbf{b}_i$s are the reciprocal lattice primitive vectors. The second identity is valid in the long-wavelength limit, $\omega/c \ll \pi/a$ and $|\mathbf{k}| \ll \pi/a$ [45]. After straightforward calculations it is found that:

$$\chi_{m,n} = \frac{1}{a}\left[k_m k_n - \left(\frac{\omega}{c}\right)^2\delta_{m,n}\right]\frac{1}{\beta^2_{m,n}}, \tag{40}$$

where $k_i = \mathbf{k}\cdot\hat{\mathbf{u}}_i$ and $\beta_{m,n}$ is a quantity that depends only on the geometry of the system, and is given by

$$\frac{1}{\beta^2_{m,n}} = \sum_{\substack{j_n=0\\ j_m=0\\ \{j_1,j_2,j_3\}\neq\{0,0,0\}}} \frac{\left[J_0\left(|\mathbf{k}^0_\mathbf{J}|R\right)\right]^2}{|\mathbf{k}^0_\mathbf{J}|^2}\mathrm{e}^{\mathrm{i}\mathbf{k}^0_\mathbf{J}\cdot(\mathbf{r}_m-\mathbf{r}_n)}, \tag{41}$$

where $\mathbf{r}_n$ denotes the center of the nth wire in the unit cell (the nth wire translated by $-\mathbf{r}_n$ is centered at the origin) and J_0 is the Bessel function of 1st kind and 0th order. For $m = n$, $\beta_{m,m} = \beta_p$ is the plasma wavenumber for an array of parallel PEC wires mentioned in the last subsection [45].

For $m \neq n$ the parameter $\beta_{m,n}$ is given by a simple series with an oscillating generic term due to the nonzero complex exponential coefficient. In contrast, for $m = n$ the parameter $\beta_{m,n}$ is determined by a double series with the generic term of summation strictly positive. Due to this reason, one has $|1/\beta^2_{m,n}| \ll 1/\beta^2_p$ for $m \neq n$. The approximation is better for a larger physical distance between the two sub-lattices, as for a larger distance the complex exponential will oscillate faster. Thus, the off-diagonal terms of $[\chi_{m,n}]$ can be dropped, and with this approximation the inverse matrix elements are given by:

$$\chi^{m,n} \approx \begin{cases} \frac{1}{\chi_{n,n}} & m = n \\ 0 & m \neq n. \end{cases} \tag{42}$$

Substituting this expression into (38) it is found that the dielectric function of the double wire medium is

$$\frac{\bar{\bar{\varepsilon}}_{\mathrm{ef}}}{\varepsilon_0}(\omega,\mathbf{k}) = \bar{\bar{\mathbf{I}}} + \sum_i \frac{\beta^2_p}{\left[k^2_i - \left(\frac{\omega}{c}\right)^2\right]}\hat{\mathbf{u}}_i \otimes \hat{\mathbf{u}}_i. \tag{43}$$

This result agrees with the nonlocal effective permittivity for perfect electric conducting wires derived in [73] using a slightly different approach. Similar to the uniaxial wire medium, the effective

permittivity of the double wire mesh is strongly spatially dispersive. Remarkably, each wire array contributes independently to the permittivity function such that $\overline{\overline{\varepsilon}}_{\text{ef}}/\varepsilon_0 = \overline{\overline{\mathbf{I}}} + \sum_{n=1,2}\left(\overline{\overline{\varepsilon}}_n/\varepsilon_0 - \overline{\overline{\mathbf{I}}}\right)$, where $\overline{\overline{\varepsilon}}_n$ is the permittivity of the nth wire array alone.

The above derivation can be readily extended to plasmonic wires with a finite conductivity [66] and to triple non-connected wire arrays [73]. Furthermore, the proof can also be generalized to the case where the wire arrays are not perpendicular [70]. Also in this case, with similar approximations, one finds that each wire array contributes independently to the permittivity function.

4.1.3. *3D connected wire mesh*

The strong spatial dispersion characteristic of nonconnected wire arrays can be tamed by connecting the metallic wires, so that effectively the structure is formed by a single piece of conductor [73, 74]. Here, we illustrate this by considering a 3D connected wire mesh formed by three orthogonal and connected sets of wires as represented in Figure 2(c).

In this system, because of the discontinuity of the induced current at the wire junctions, a single expansion function per wire is not enough to correctly homogenize the electromagnetic response. Instead, it can be shown that five expansion functions $\mathbf{w}_{n,\mathbf{k}}$ are required to obtain an approximate analytic expression of the effective permittivity [45, 73]. Relying on an approach similar to that of the previous subsection (the details can be found in [45]), it can be shown that the effective permittivity of this metamaterial is

$$\frac{\overline{\overline{\varepsilon}}_{\text{ef}}}{\varepsilon_0}(\omega,\mathbf{k}) = \varepsilon_t(\omega)\left(\overline{\overline{\mathbf{I}}} - \frac{\mathbf{k}\otimes\mathbf{k}}{k^2}\right) + \varepsilon_l(\omega,k)\frac{\mathbf{k}\otimes\mathbf{k}}{k^2}, \tag{44}$$

where the transverse and longitudinal components are given respectively by

$$\varepsilon_t(\omega) = 1 + \frac{1}{\frac{1}{f_V(\varepsilon_m-1)} - \frac{\omega^2}{\beta_p^2 c^2}}, \tag{45}$$

$$\varepsilon_l(\omega,k) = 1 + \frac{1}{\frac{k^2}{l_0\beta_p^2} + \left(\frac{1}{f_V(\varepsilon_m-1)} - \frac{\omega^2}{\beta_p^2 c^2}\right)}. \tag{46}$$

In the above, $l_0 = 3/(1+2\beta_p^2/\beta_1^2)$ and β_1 is a constant (with unities of wave number) that depends solely on the geometry of the structured material (see [45] for more details).

Remarkably, the 3D connected wire medium has a homogenized response equivalent to that of a plasma described by the hydrodynamic model [75]. In particular, the response to transverse waves (with electric field perpendicular to the wave vector) is described by the **k**-independent transverse permittivity ε_t. However, the 3D connected wire medium remains spatially dispersive. The reason is that the response to longitudinal waves (with electric field parallel to the wave vector) is described by a **k**-dependent longitudinal permittivity ε_l. The effects of spatial dispersion are several orders of magnitude stronger than in metal nanostructures at optics because the parameter l_0 is relatively small ($l_0 \approx 2$). The effects of spatial dispersion can be further suppressed by loading the wires with metal plates, which leads to $l_0 \gg 1$ [74, 76].

In general, the 3D connected wire mesh supports 3 electromagnetic modes: a longitudinal and two transverse plane waves. Propagation is only feasible above the effective plasma frequency. Thus, for long wavelengths the 3D connected wire mesh is completely opaque to radiation. For further details about the electrodynamics of the connected wire medium, the reader is referred to [45].

4.2. *Quasi-static model*

The nonlocal response of wire metamaterials can be explained by a quasi-static model developed in [76]. In the quasi-static model the macroscopic electromagnetic fields are coupled to the currents in the wires and to an "additional potential". The additional potential may be understood as the average voltage drop from a given wire to the boundary of the cell wherein it is contained [76]. Both the additional potential (φ) and the current are interpolated as continuous functions defined in all space. As reported in [77,78], the quasi-static model is particularly useful in problems involving interfaces, e.g., to obtain "additional boundary conditions", and to derive conservation laws [78].

For the case of the uniaxial wire medium (with wires oriented along $\hat{\mathbf{z}}$) of Section 4.1.1 the quasi-static model is determined by:

$$\nabla \times \mathbf{E} = \mathrm{i}\omega\mu_0 \mathbf{H} \tag{47a}$$

$$\nabla \times \mathbf{H} = \frac{I_z}{a^2}\hat{\mathbf{z}} - \mathrm{i}\omega\varepsilon_h \mathbf{E} \tag{47b}$$

$$\frac{\partial I_z}{\partial z} = \mathrm{i}\omega C\varphi \tag{47c}$$

$$\frac{\partial \varphi}{\partial z} = E_z - \left(Z_w - \mathrm{i}\omega L\right) I_z \tag{47d}$$

where $\mathbf{E}$ and $\mathbf{H}$ are the macroscopic electromagnetic fields ($\mathbf{E} = \{\mathbf{e}(\mathbf{r})\}_{\mathrm{av}}$ and $\mathbf{H} = \{\mathbf{b}(\mathbf{r})\}_{\mathrm{av}}/\mu_0$), $E_z = \mathbf{E}\cdot\hat{\mathbf{z}}$, ε_h is the permittivity of the host medium and C, L and Z_w are the capacitance, inductance and self-impedance of a wire per unit of length, respectively, defined as in [76]. As seen, in this theory the macroscopic Maxwell equations are coupled to a set of differential equations governing the dynamics of the internal degrees of freedom of the medium (I_z and φ). The quasi-static model (47) fully describes the physical behavior of the uniaxial wire medium, as it can be transformed into the nonlocal model (36) by expressing I_z and φ in terms of the macroscopic fields [76].

Importantly, the quasi-static model is $local$ as it corresponds to a standard partial-differential system. The differential operators act on the 8-component state vector $(\mathbf{E},\mathbf{H},\varphi,I_z)$. The nonlocality of the electromagnetic response is a consequence of the fact that I_z and φ are coupled to each other through a space differential operator ($\partial/\partial z$), different from conventional local media where the internal degrees of freedom are coupled through time differential operators ($\partial/\partial t$).

Finally, it is worth mentioning that the quasi-static model is not restricted to the description of the uniaxial wire medium, as it can be extended to more complex connected and nonconnected wire medium topologies [76].

4.3. *Poynting vector*

In spatially-dispersive media, the energy density flux is not given by the standard textbook formula of the Poynting vector $\mathbf{E}\times\mathbf{H}$ [33,34,79,80]. For the case of lossless materials characterized by a nonlocal dielectric function the (time-averaged) Poynting vector must instead be calculated using:

$$\mathbf{S}_{\mathrm{av}}\cdot\hat{\mathbf{l}} = \frac{1}{2}\mathrm{Re}\left\{\left(\mathbf{E}\times\frac{\mathbf{B}^*}{\mu_0}\right)\cdot\hat{\mathbf{l}}\right\} - \frac{\omega}{4}\mathbf{E}^*\cdot\frac{\partial\overline{\overline{\varepsilon}}_{\mathrm{ef}}}{\partial k_l}(\omega,\mathbf{k})\cdot\mathbf{E}. \tag{48}$$

Here, $\hat{\mathbf{l}}$ is a generic (real-valued) unit vector. It is implicit that the spatial dependence is of the form $\mathrm{e}^{\mathrm{i}\mathbf{k}\cdot\mathbf{r}}$ with $\mathbf{k}$ real-valued and that the magnetic response is trivial. The formula can be generalized to a superposition of plane waves possibly associated with complex-valued wave vectors [79,81].

It was demonstrated in Refs. [79, 80] that for a generic dielectric metamaterial, Equation (48) agrees precisely with the cell-averaged microscopic Poynting vector,

$$\mathbf{S}_{\text{av}} = \frac{1}{V_{\text{cell}}} \int_{\Omega} \frac{1}{2} \text{Re}\left(\mathbf{e} \times \frac{\mathbf{b}^*}{\mu_0} \right) \text{d}^3\mathbf{r}, \tag{49}$$

provided the effective dielectric function is determined with the homogenization method of Section 3. Therefore, the macroscopic Poynting vector can be understood as a cell-averaged microscopic Poynting vector.

Evidently, in wire metamaterials the Poynting vector can be determined using (48), using the relevant expression of the nonlocal permittivity in the formula. However, as previously mentioned, such formalism is only applicable to plane waves. A more general and useful expression for the Poynting vector can be obtained using the quasi-static model of Section 4.2. Indeed, based on (47) it is possible to derive a generalized Poynting theorem, which for the particular case of the uniaxial wire medium yields the following expression for the Poynting vector [78]:

$$\mathbf{S}_{\text{av}} = \frac{1}{2} \text{Re}\left\{ \mathbf{E} \times \mathbf{H}^* + \frac{\varphi I_z^*}{a^2} \hat{\mathbf{z}} \right\}. \tag{50}$$

As seen, the Poynting vector is written in terms of the macroscopic electromagnetic fields and of the internal degrees of freedom (I_z and φ) of the metamaterial. It can be verified that in the lossless case and for a spatial dependence of the form $\text{e}^{\text{i}\mathbf{k}\cdot\mathbf{r}}$ with $\mathbf{k}$ real-valued the above expression reduces to (48). However, Equation (50) is more general than (48) as it can be applied to arbitrary electromagnetic field distributions. The stored energy in the wire metamaterial can also be expressed in terms of the state vector $(\mathbf{E}, \mathbf{H}, \varphi, I_z)$, and for more details the reader is referred to [78].

4.4. *Additional boundary conditions*

One important consequence of spatial dispersion is that the usual Maxwellian boundary conditions, i.e., the continuity of the tangential $\mathbf{E}$ and $\mathbf{H}$ fields, are insufficient to solve wave propagation problems in the presence of interfaces [34, 54, 81–86]. For example, consider a planar interface between two regions: a standard dielectric and a generic spatially dispersive material characterized by a nonlocal dielectric function. Suppose that a plane wave propagating in the dielectric illuminates the spatially-dispersive material half-space. The standard approach to find the scattered waves is to expand the electromagnetic fields into plane waves in the two regions and then to match the fields at the interfaces by imposing the standard Maxwellian boundary conditions. In standard dielectrics, there are exactly two plane-waves associated with an energy flow propagating away from the interface, i.e., there are only two polarization states per propagation direction. The potential problem is that in a nonlocal material the allowed number of polarization states per propagation direction may be greater than two, i.e., the medium may support "additional" waves. For example, a uniaxial wire medium typically supports three independent polarization states [85]. Consequently, it is generally impossible to solve a scattering problem relying only on the Maxwellian boundary conditions because the number of unknowns (number of waves that can be excited) is greater than the number of equations (number of boundary conditions). The problem is under-determined and additional boundary conditions (ABCs) are needed. The number of ABCs must be the same as the number of additional waves.

For wire metamaterials, the ABC requirement is particularly clear from the quasi-static formulation of Section 4.2 where it is evident that in a scattering problem the boundary conditions for the internal degrees of freedom φ and I_z must also be provided [77]. Thus, one needs to specify how the relevant internal variables behave at the interface. Unfortunately there is no systematic

theory to find the ABCs, and their derivation must be based on the specific microscopic properties of the system under consideration. In particular, it is underlined that the ABCs (which are interface dependent) cannot be directly obtained from the nonlocal dielectric function, i.e., from the bulk response.

Here, we restrict our attention to an interface between a wire metamaterial and a standard dielectric. This situation covers the important case of an interface between wire media and air, which is of particular interest for scattering or imaging applications. Evidently, the microscopic electric currents in the metal wires are interrupted at the interface. Hence, for a system with N independent wires in the unit cell, it follows that at the dielectric interface

$$\mathbf{J}_{\text{av}} \cdot \hat{\mathbf{u}}_n = 0, \quad n = 1, \ldots, N \tag{51}$$

where $\mathbf{J}_{\text{av}}$ is the cell-averaged microscopic conduction current and $\hat{\mathbf{u}}_n$ is the unit vector oriented along the direction of the nth wire array [81]. The vector $\mathbf{J}_{\text{av}}$ can typically be written in terms of the dielectric function of the medium [81].

In the particular case of a uniaxial wire medium, the ABC in the quasi-static model assumes the simple and intuitive form $I_z = 0$. This ABC (together with the standard Maxwellian boundary conditions) can be expressed in terms of the electromagnetic fields as [85]:

$$\varepsilon_h \, \hat{\mathbf{n}} \cdot \mathbf{E}|_{\text{WM}} = \varepsilon_d \, \hat{\mathbf{n}} \cdot \mathbf{E}|_{\text{diel.}}, \tag{52}$$

where $\hat{\mathbf{n}}$ is the unit vector normal to the interface, ε_h is the host medium permittivity and ε_d is the dielectric permittivity. Note that (52) is not equivalent to the continuity of the electric displacement vector, since the effective permittivity of the wire medium is different from ε_h. Similar ideas are used to obtain the ABCs for the case of connected wire arrays [45], interlaced wire meshes [87] and for wires terminated with lumped loads [77,81].

It should be noted that wire metamaterials are amongst the very few examples of structured media for which there is a clear understanding of how to model the nonlocal effects near interfaces [77,81,85,88]. Another example, less well-developed, is the case of quadrupolar metamaterials characterized by weak spatial dispersion [89,90]. The general problem of characterizing the interface response of a generic nonlocal metamaterial is unsolved.

5. Anomalous refraction and light tunneling with wire metamaterials

To illustrate some of the unusual opportunities created by the spatial dispersion in wire metamaterials, we review in the next subsections the effects of anomalous light refraction and anomalous light tunneling.

5.1. *Anomalous refraction in arrays of non-connected crossed metallic wires*

As noticed in [68], a remarkable consequence of spatial dispersion is the possibility to achieve a low-loss and broadband regime of anomalous light refraction such that, contrary to what happens in a standard glass prism, longer wavelengths are more refracted than shorter wavelengths. This effect is forbidden by Kramers–Kronig relations in transparent and local materials. It may however occur in a prism made of a double-wire medium formed by nonconnected wires [68,72], see Figure 3. To understand the physical origin of this effect, we consider the wave propagation in an unbounded double wire medium made of perfectly conducting wires lying in the xoz plane and tilted by $\pm 45^\circ$ with respect to the x-axis, as represented in Figure 3(b). For simplicity, we assume that the wave propagates along the z-direction ($\mathbf{k} = k_z \hat{\mathbf{z}}$). For fields polarized along the x-direction the characteristic equation is

$$\varepsilon_{xx}(\omega, k_z) \frac{\omega^2}{c^2} = k_z^2, \tag{53}$$

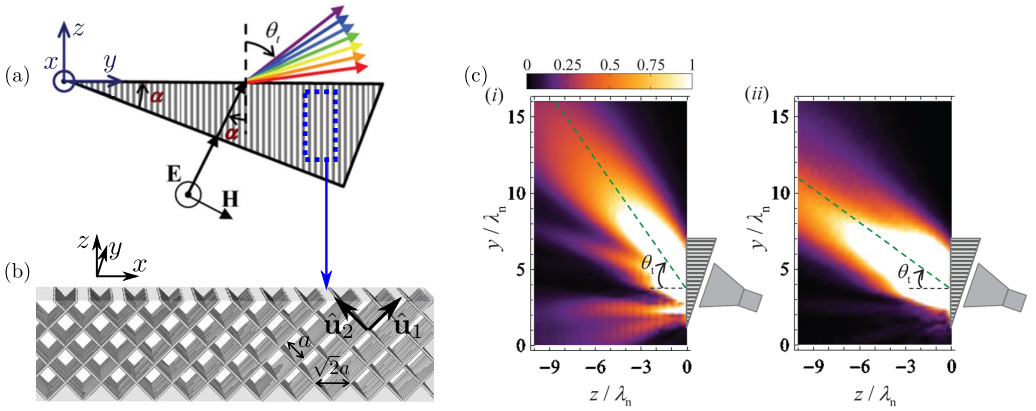

Figure 3. (a) Schematic of the anomalous light refraction in a prism made of non-connected arrays of parallel wires. (b) Each array of parallel wires is arranged in a square lattice with period a. The two arrays of wires are mutually orthogonal and lie in planes parallel to the x-axis. The distance between adjacent perpendicular wires is $a/2$. The metallic wires are tilted by $\pm 45°$ with respect to the xoy plane. (c) Normalized squared amplitude of the measured electric field for a prism made of a crossed array of metallic strips for a frequency of (i) 7.605 GHz (ii) 16.325 GHz. A schematic drawing of the metamaterial prism and horn antenna (at full scale) is shown. The propagation is towards the left-hand side region. The green dashed lines represent the refracted beam propagation direction, whereas the black dashed lines represent the direction normal to the interface. The spatial coordinates y and z are normalized to the reference wavelength $\lambda_n = 39.71$ mm [72].

where $\varepsilon_{xx} = \hat{\mathbf{x}} \cdot \overline{\overline{\varepsilon}}_{\text{ef}} \cdot \hat{\mathbf{x}}$ is the relevant component of the nonlocal effective permittivity for this polarization. According to the effective model (43), ε_{xx} is given by

$$\varepsilon_{xx}(\omega, k_z) = 1 + \frac{\beta_p^2}{\frac{k_z^2}{2} - \frac{\omega^2}{c^2}}. \tag{54}$$

Substituting ε_{xx} into (53) and solving for k_z, it is found that $k_z = (\omega/c)\, n_{\text{ef}}$, where n_{ef} is the effective refractive index of the double wire medium given by [68]

$$n_{\text{ef}} = \sqrt{\frac{3}{2} + \frac{1}{2}\sqrt{1 + 8\left(\frac{\beta_p c}{\omega}\right)^2}}. \tag{55}$$

Remarkably, even though the metamaterial is lossless, the refractive index is a strictly decreasing function of the frequency. This unique property is only possible due to the spatial dispersion which makes the permittivity seen by the transverse field (polarized along x) dependent on a perpendicular wave vector component (here k_z). The same effect occurs for other propagation directions in the yoz plane.

Due to the anomalous permittivity dispersion, a prism made of a crossed wire mesh can create a reverse rainbow as demonstrated theoretically in [68], and experimentally confirmed at microwave frequencies in [72]. In the experiment the prism is formed by a stack of dielectric slabs printed with the $\pm 45°$-oriented metallic strips. A sample of the experimental results is presented in Figure 3(c). As seen, unlike conventional prisms, in the metamaterial prism the refracted beam comes out closer to the normal of the output interface when the frequency is increased. Materials with anomalous light dispersion may be useful for many applications, e.g., for the compression of light pulses or for the correction of achromatic aberrations [71].

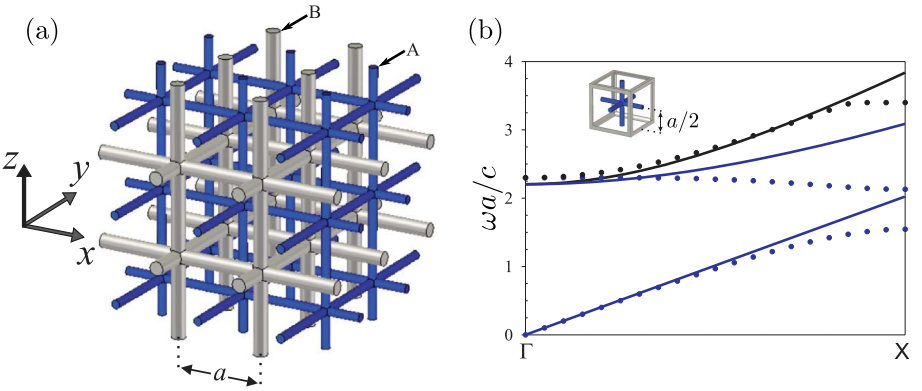

Figure 4. (a) Geometry of the interlaced wire mesh. The wire radii in mesh A and B are r_A and r_B, respectively. The wires of each network are spaced by a distance a along the coordinate axes. The distance between the two non-connected networks is $a/2$. (b) Band diagram of the electromagnetic modes along the direction ΓX. Solid lines: analytical model; discrete symbols: full wave simulations. The inset shows the cubic unit cell of the structure. The wires are PEC and are embedded in a dielectric with permittivity $\varepsilon_h = 1$; the radii of the wires are $r_A = 0.001a$ and $r_B = 0.05a$. Reprinted with permission [92].

5.2. *Anomalous light tunneling in interlaced wire meshes*

Here, we consider a metamaterial formed by two interlaced 3D connected wire meshes (mesh A and B) separated by half-lattice period, see Figure 4(a) [87, 91]. In what follows, we characterize the effective response of this "interlaced wire medium" and discuss a counter-intuitive tunneling effect rooted in the spatially dispersive response of the metamaterial.

Consider the general problem of homogenization of a metamaterial formed by two networks of inclusions A and B. In general, to find the effective response it is crucial to take into account the complex near-field interactions between the different types of scatterers. However, when the scatterers are physically distant in the unit cell it may be a good approximation to consider that each scatterer behaves as a "macroscopic source" from the point of view of the other scatterer. Essentially, this approximation is good when only the smooth (slowly varying) part of the fields radiated by one of the scatterers influences the currents on the other scatterer. It can be formally shown that in these conditions each component of the metamaterial contributes independently to the dielectric function such that [87, 93]:

$$\bar{\bar{\varepsilon}}_{\text{ef}} = \bar{\bar{\varepsilon}}^{A}_{\text{ef}} + \bar{\bar{\varepsilon}}^{B}_{\text{ef}} - \varepsilon_h \bar{\bar{\mathbf{I}}}, \tag{56}$$

where $\bar{\bar{\varepsilon}}^{i}_{\text{ef}}$ with $i = A, B$ is the nonlocal effective permittivity of the metamaterial formed only by the ith network of inclusions.

From the results of Section 4.1.2, it is readily recognized that a double-wired mesh of nonconnected wires provides a nontrivial example of a system in which the different types of scatterers interact with one another as "macroscopic sources". Interestingly, it turns out that the interlaced wire mesh of Figure 4(a) has the same property when the two 3D wire meshes are separated by the maximal possible distance ($a/2$) [87, 92]. For the interlaced wire mesh $\bar{\bar{\varepsilon}}^{i}_{\text{ef}}$ is the nonlocal effective permittivity of the (isolated) ith wire mesh given by (44).

Intuitively, the interlaced wire mesh should be opaque to radiation for frequencies below a certain effective plasma frequency. Surprisingly, that is not the case and it turns out that the metamaterial supports a longitudinal-type mode at arbitrary low-frequencies, as illustrated in

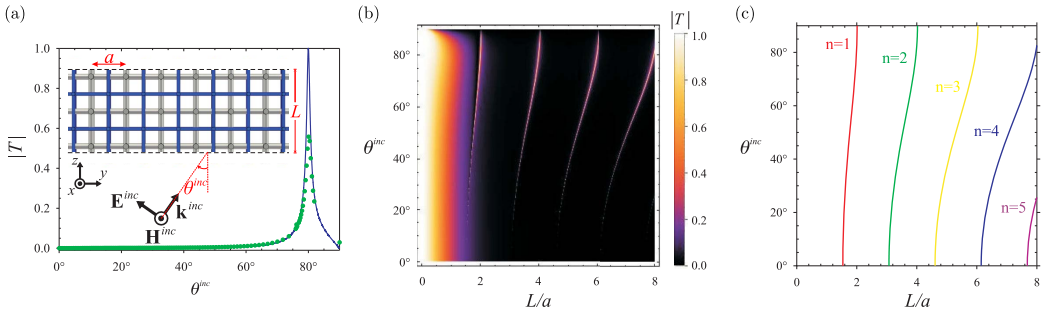

Figure 5. (a) Amplitude of the transmission coefficient as a function of the incidence angle θ^{inc} for the normalized frequency $\omega a/c = 1.32$ and normalized thickness $L/a \approx 6$. The remaining structural parameters are as in Figure 4. The inset shows the geometry of the problem. The solid lines represent the analytical results, and the discrete symbols represent the full wave simulations results. (b) Density plot of the transmission coefficient amplitude as a function of the normalized thickness L/a and of the incidence angle θ^{inc} at the fixed frequency of $\omega a/c = 1.32$. (c) Incidence angle θ^{inc} as a function of L/a for the nth ($n = 1, 2, \ldots$) Fabry–Pérot resonance of the propagating longitudinal mode at $\omega a/c = 1.32$.

the band diagram in Figure 4(b) [87, 91, 92]. This feature contrasts sharply with the properties of the individual 3D wire meshes, which do not support electromagnetic propagation for long wavelengths.

Remarkably, the low-frequency mode can originate a rather counter-intuitive tunneling effect. To illustrate this, we consider an interlaced wire mesh slab of finite length L (see the inset of Figure 5(a)). Using the effective permittivity model (56) and suitable ABCs, it is possible to find the transmission coefficient $|T|$ of the slab [92]. Strikingly, as shown in Figure 5(a), provided the wire radii are different ($r_A \neq r_B$) an incoming plane wave can tunnel through the metamaterial slab for large incidence angles. This transmission anomaly is due to a Fabry–Pérot resonance of the low-frequency longitudinal mode of the metamaterial. At the resonance the longitudinal wave vector satisfies the condition $k_z L = n\pi$, with $n = 1, 2, \ldots$ (see Figures 5(b) and (c)).

The physical origin of the tunneling anomaly is a Fano-type resonance [93] that occurs when $r_A \neq r_B$ and enables the cancellation due to destructive interference of the scattering by the two subcomponents of the interlaced wire mesh. This metamaterial structure may be useful for angle-dependent filtering and sensing. For a detailed discussion of the physical properties of the interlaced wire mesh, the reader is referred to [92].

6. Conclusions

We presented an overview of a first principles homogenization approach based on an effective Hamiltonian that describes exactly the time evolution of the wave packet envelope when the initial state is less localized than the lattice period. The effective Hamiltonian determines completely the band diagram of the time-stationary states of the periodic system. The homogenization formalism can be applied to a wide range of physical systems. Its specific implementation for the case of nonmagnetic periodic electromagnetic metamaterials was described.

In particular, we focused our attention in the homogenization of wire metamaterials with diverse topologies. These structures are typically characterized by a strong nonlocal response in the long wavelength limit. In wire metamaterials formed by two or more non-connected networks,

each metal network may contribute almost independently to the permittivity function. We underlined the nontrivial implications of the spatially dispersive response in different contexts, e.g., the emergence of additional waves, additional boundary conditions and a non-standard definition of the Poynting vector. Finally, we illustrated the richness of the physics of the wave propagation in wire medium, showing that it can lead to a counter-intuitive tunneling effect and anomalous frequency dispersion.

Acknowledgements

This work was partially funded by the Institute of Engineering and Technology (IET) under the A F Harvey Engineering Prize and by Fundação para a Ciência e a Tecnologia (FCT) under project UIDB/50008/2020. SL acknowledges FCT and IT-Coimbra for the research financial support with reference DL 57/2016/CP1353/CT000. TAM acknowledges FCT for the research financial support with reference CEECIND/04530/2017 under the CEEC Individual 2017, and IT-Coimbra for the contract as assistant researcher with reference CT/N°004/2019-F00069.

References

[1] A. Sihvola, "Mixing rules", in *Metamaterials Handbook: Applications of Metamaterials* (F. Capolino, ed.), CRC Press, 2009, p. 762.
[2] C. Kittel, *Introduction to Solid State Physics*, 8th ed., John Wiley & Sons, Hoboken, NJ, 2004.
[3] D. R. Smith, J. B. Pendry, "Homogenization of metamaterials by field averaging (invited paper)", *J. Opt. Soc. Am. B, JOSAB* **23** (2006), no. 3, p. 391-403.
[4] D. Sjöberg, "Dispersive effective material parameters", *Microwave Optical Technol. Lett.* **48** (2006), no. 12, p. 2629-2632.
[5] C. R. Simovski, "Bloch material parameters of magneto-dielectric metamaterials and the concept of Bloch lattices", *Metamaterials* **1** (2007), no. 2, p. 62-80.
[6] C. R. Simovski, S. A. Tretyakov, "Local constitutive parameters of metamaterials from an effective-medium perspective", *Phys. Rev. B* **75** (2007), no. 19, article ID 195111.
[7] M. G. Silveirinha, "Metamaterial homogenization approach with application to the characterization of microstructured composites with negative parameters", *Phys. Rev. B* **75** (2007), no. 11, article ID 115104.
[8] M. G. Silveirinha, "Generalized Lorentz–Lorenz formulas for microstructured materials", *Phys. Rev. B* **76** (2007), no. 24, article ID 245117.
[9] G. P. Ortiz, B. E. Martínez-Zérega, B. S. Mendoza, W. L. Mochán, "Effective optical response of metamaterials", *Phys. Rev. B* **79** (2009), no. 24, article ID 245132.
[10] M. G. Silveirinha, "Nonlocal homogenization theory of structured materials", in *Metamaterials Handbook: Applications of Metamaterials* (F. Capolino, ed.), CRC Press, 2009.
[11] J. T. Costa, M. G. Silveirinha, S. I. Maslovski, "Finite-difference frequency-domain method for the extraction of effective parameters of metamaterials", *Phys. Rev. B* **80** (2009), no. 23, article ID 235124.
[12] D. R. Smith, "Analytic expressions for the constitutive parameters of magnetoelectric metamaterials", *Phys. Rev. E* **81** (2010), no. 3, article ID 036605.
[13] C. R. Simovski, "On electromagnetic characterization and homogenization of nanostructured metamaterials", *J. Opt.* **13** (2010), no. 1, article ID 013001.
[14] M. G. Silveirinha, "Time domain homogenization of metamaterials", *Phys. Rev. B* **83** (2011), no. 16, article ID 165104.
[15] C. Fietz, G. Shvets, "Current-driven metamaterial homogenization", *Physica B: Condensed Matter* **405** (2010), no. 14, p. 2930-2934.
[16] A. V. Chebykin, A. A. Orlov, A. V. Vozianova, S. I. Maslovski, Y. S. Kivshar, P. A. Belov, "Nonlocal effective medium model for multilayered metal-dielectric metamaterials", *Phys. Rev. B* **84** (2011), no. 11, article ID 115438.
[17] A. V. Chebykin, A. A. Orlov, C. R. Simovski, Y. S. Kivshar, P. A. Belov, "Nonlocal effective parameters of multilayered metal-dielectric metamaterials", *Phys. Rev. B* **86** (2012), no. 11, article ID 115420.
[18] A. Alù, "First-principles homogenization theory for periodic metamaterials", *Phys. Rev. B* **84** (2011), no. 7, article ID 075153.
[19] A. D. Yaghjian, A. Alù, M. G. Silveirinha, "Homogenization of spatially dispersive metamaterial arrays in terms of generalized electric and magnetic polarizations", *Photonics Nanostructures - Fundam. Appl.* **11** (2013), no. 4, p. 374-396.

[20] A. D. Yaghjian, A. Alù, M. G. Silveirinha, "Anisotropic representation for spatially dispersive periodic metamaterial arrays", in *Transformation Electromagnetics and Metamaterials: Fundamental Principles and Applications* (D. H. Werner, D.-H. Kwon, eds.), Springer London, London, 2014, p. 395-457.
[21] V. Sozio, A. Vallecchi, M. Albani, F. Capolino, "Generalized Lorentz–Lorenz homogenization formulas for binary lattice metamaterials", *Phys. Rev. B* **91** (2015), no. 20, article ID 205127.
[22] C. Simovski, *Composite Media with Weak Spatial Dispersion*, 1st ed., Pan Stanford Publishing Pte Ltd, Singapur, 2018.
[23] D. Cioranescu, F. Murat, "A strange term coming from nowhere", in *Topics in the Mathematical Modelling of Composite Materials, Progress in Nonlinear Differential Equations and Their Applications* (A. Cherkaev, R. Kohn, eds.), Birkhäuser, Boston, MA, 1997, p. 45-93.
[24] D. Felbacq, G. Bouchitté, "Homogenization of a set of parallel fibres", *Waves Random Media* **7** (1997), no. 2, p. 245-256.
[25] C. G. Poulton, L. C. Botten, R. C. McPhedran, N. A. Nicorovici, A. B. Movchan, "Noncommuting limits in electromagnetic scattering: asymptotic analysis for an array of highly conducting inclusions", *SIAM J. Appl. Math.* **61** (2001), no. 5, p. 1706-1730.
[26] C. Poulton, S. Guenneau, A. B. Movchan, "Noncommuting limits and effective properties for oblique propagation of electromagnetic waves through an array of aligned fibres", *Phys. Rev. B* **69** (2004), no. 19, article ID 195112.
[27] V. Zhikov, "On gaps in the spectrum of some divergent elliptic operators with periodic coefficients", *St. Petersburg Math. J.* **16** (2005), no. 5, p. 773-790.
[28] A. Maurel, J.-J. Marigo, "Sensitivity of a dielectric layered structure on a scale below the periodicity: a fully local homogenized model", *Phys. Rev. B* **98** (2018), no. 2, article ID 024306.
[29] J. B. Pendry, "Negative refraction makes a perfect lens", *Phys. Rev. Lett.* **85** (2000), no. 18, p. 3966-3969.
[30] C. Luo, S. G. Johnson, J. D. Joannopoulos, J. B. Pendry, "Subwavelength imaging in photonic crystals", *Phys. Rev. B* **68** (2003), no. 4, article ID 045115.
[31] P. A. Belov, Y. Hao, S. Sudhakaran, "Subwavelength microwave imaging using an array of parallel conducting wires as a lens", *Phys. Rev. B* **73** (2006), no. 3, article ID 033108.
[32] F. Capolino, *Applications of Metamaterials*, 1st ed., CRC Press, Boca Raton, FL, 2009.
[33] L. D. Landau, L. P. Pitaevskii, E. M. Lifshitz, *Electrodynamics of Continuous Media: Volume 8*, 2nd ed., Butterworth-Heinemann, Amsterdam u.a., 1984.
[34] V. M. Agranovich, V. Ginzburg, *Crystal Optics with Spatial Dispersion, and Excitons*, 2nd ed., Springer Series in Solid-State Sciences, Springer-Verlag, Berlin Heidelberg, 1984.
[35] M. G. Silveirinha, N. Engheta, "Effective medium approach to electron waves: graphene superlattices", *Phys. Rev. B* **85** (2012), no. 19, article ID 195413.
[36] M. G. Silveirinha, "Effective medium theory of electromagnetic and quantum metamaterials", in *World Scientific Handbook of Metamaterials and Plasmonics* (E. Shamonina, S. A. Maier, eds.), World Scientific Series in Nanoscience and Nanotechnology, World Scientific, 2017, p. 37-86.
[37] M. G. Silveirinha, N. Engheta, "Metamaterial-inspired model for electron waves in bulk semiconductors", *Phys. Rev. B* **86** (2012), no. 24, article ID 245302.
[38] M. G. Silveirinha, N. Engheta, "Giant nonlinearity in zero-gap semiconductor superlattices", *Phys. Rev. B* **89** (2014), no. 8, article ID 085205.
[39] S. Lannebère, M. G. Silveirinha, "Effective Hamiltonian for electron waves in artificial graphene: a first-principles derivation", *Phys. Rev. B* **91** (2015), no. 4, article ID 045416.
[40] B. Gralak, A. Tip, "Macroscopic Maxwell's equations and negative index materials", *J. Math. Phys.* **51** (2010), no. 5, article ID 052902.
[41] M. G. Silveirinha, "Topological classification of Chern-type insulators by means of the photonic Green function", *Phys. Rev. B* **97** (2018), no. 11, article ID 115146.
[42] M. G. Silveirinha, "Modal expansions in dispersive material systems with application to quantum optics and topological photonics", in *Advances in Mathematical Methods for Electromagnetics* (K. Kobayashi, P. D. Smith, eds.), IET, 2019.
[43] G. Russakoff, "A derivation of the macroscopic Maxwell equations", *Amer. J. Phys.* **38** (1970), no. 10, p. 1188-1195.
[44] D. M. Pozar, *Microwave Engineering*, 4th ed., Wiley, Hoboken, NJ, 2011.
[45] M. G. Silveirinha, "Artificial plasma formed by connected metallic wires at infrared frequencies", *Phys. Rev. B* **79** (2009), no. 3, article ID 035118.
[46] W. Rotman, "Plasma simulation by artificial dielectrics and parallel-plate media", *IRE Trans. Antennas and Propagation* **10** (1962), no. 1, p. 82-95.
[47] J. B. Pendry, A. J. Holden, W. J. Stewart, I. Youngs, "Extremely low frequency plasmons in metallic mesostructures", *Phys. Rev. Lett.* **76** (1996), no. 25, p. 4773-4776.
[48] S. I. Maslovski, S. A. Tretyakov, P. A. Belov, "Wire media with negative effective permittivity: a quasi-static model", *Microw. Opt. Technol. Lett.* **35** (2002), no. 1, p. 47-51.

[49] P. A. Belov, S. A. Tretyakov, A. J. Viitanen, "Dispersion and reflection properties of artificial media formed by regular lattices of ideally conducting wires", *J. Electromagnetic Waves Appl.* **16** (2002), no. 8, p. 1153-1170.
[50] P. A. Belov, R. Marqués, S. I. Maslovski, I. S. Nefedov, M. Silveirinha, C. R. Simovski, S. A. Tretyakov, "Strong spatial dispersion in wire media in the very large wavelength limit", *Phys. Rev. B* **67** (2003), no. 11, article ID 113103.
[51] I. S. Nefedov, A. J. Viitanen, "Wire Media", in *Metamaterials Handbook: Applications of Metamaterials* (F. Capolino, ed.), CRC Press, 2009.
[52] C. R. Simovski, P. A. Belov, A. V. Atrashchenko, Y. S. Kivshar, "Wire metamaterials: physics and applications", *Adv. Mater.* **24** (2012), no. 31, p. 4229-4248.
[53] M. G. Silveirinha, "Nonlocal homogenization model for a periodic array of ε-negative rods", *Phys. Rev. E* **73** (2006), no. 4, article ID 046612.
[54] I. Nefedov, A. Viitanen, S. Tretyakov, "On reflection from interfaces with some spatially dispersive metamaterials", *J. Magnetism Magnetic Mater.* **300** (2006), no. 1, p. e107-e110.
[55] P. A. Belov, C. R. Simovski, P. Ikonen, "Canalization of subwavelength images by electromagnetic crystals", *Phys. Rev. B* **71** (2005), no. 19, article ID 193105.
[56] P. A. Belov, M. G. Silveirinha, "Resolution of subwavelength transmission devices formed by a wire medium", *Phys. Rev. E* **73** (2006), no. 5, article ID 056607.
[57] P. A. Belov, Y. Zhao, S. Sudhakaran, A. Alomainy, Y. Hao, "Experimental study of the subwavelength imaging by a wire medium slab", *Appl. Phys. Lett.* **89** (2006), no. 26, article ID 262109.
[58] P. A. Belov, Y. Zhao, S. Tse, P. Ikonen, M. G. Silveirinha, C. R. Simovski, S. Tretyakov, Y. Hao, C. Parini, "Transmission of images with subwavelength resolution to distances of several wavelengths in the microwave range", *Phys. Rev. B* **77** (2008), no. 19, article ID 193108.
[59] P. Ikonen, C. Simovski, S. Tretyakov, P. Belov, Y. Hao, "Magnification of subwavelength field distributions at microwave frequencies using a wire medium slab operating in the canalization regime", *Appl. Phys. Lett.* **91** (2007), no. 10, article ID 104102.
[60] G. Shvets, S. Trendafilov, J. B. Pendry, A. Sarychev, "Guiding, focusing, and sensing on the subwavelength scale using metallic wire arrays", *Phys. Rev. Lett.* **99** (2007), no. 5, article ID 053903.
[61] M. G. Silveirinha, P. A. Belov, C. R. Simovski, "Subwavelength imaging at infrared frequencies using an array of metallic nanorods", *Phys. Rev. B* **75** (2007), no. 3, article ID 035108.
[62] T. A. Morgado, M. G. Silveirinha, "Transport of an arbitrary near-field component with an array of tilted wires", *New J. Phys.* **11** (2009), no. 8, article ID 083023.
[63] T. A. Morgado, J. S. Marcos, M. G. Silveirinha, S. I. Maslovski, "Experimental verification of full reconstruction of the near-field with a metamaterial lens", *Appl. Phys. Lett.* **97** (2010), no. 14, article ID 144102.
[64] H. Latioui, M. G. Silveirinha, "Near-field transport by a bent multi-wire endoscope", *J. Appl. Phys.* **120** (2016), no. 6, article ID 063103.
[65] M. G. Silveirinha, C. A. Fernandes, "Homogenization of metamaterial surfaces and slabs: the crossed wire mesh canonical problem", *IEEE Trans. Antennas and Propagation* **53** (2005), no. 1, p. 59-69.
[66] M. G. Silveirinha, C. A. Fernandes, "Nonresonant structured material with extreme effective parameters", *Phys. Rev. B* **78** (2008), no. 3, article ID 033108.
[67] M. G. Silveirinha, "Broadband negative refraction with a crossed wire mesh", *Phys. Rev. B* **79** (2009), no. 15, article ID 153109.
[68] M. G. Silveirinha, "Anomalous refraction of light colors by a metamaterial prism", *Phys. Rev. Lett.* **102** (2009), no. 19, article ID 193903.
[69] T. A. Morgado, J. S. Marcos, M. G. Silveirinha, S. I. Maslovski, "Ultraconfined interlaced plasmons", *Phys. Rev. Lett.* **107** (2011), no. 6, article ID 063903.
[70] T. A. Morgado, J. S. Marcos, S. I. Maslovski, M. G. Silveirinha, "Negative refraction and partial focusing with a crossed wire mesh: physical insights and experimental verification", *Appl. Phys. Lett.* **101** (2012), no. 2, article ID 021104.
[71] J. T. Costa, M. G. Silveirinha, "Achromatic lens based on a nanowire material with anomalous dispersion", *Opt. Express, OE* **20** (2012), no. 13, p. 13915-13922.
[72] T. A. Morgado, J. S. Marcos, J. T. Costa, J. R. Costa, C. A. Fernandes, M. G. Silveirinha, "Reversed rainbow with a nonlocal metamaterial", *Appl. Phys. Lett.* **105** (2014), no. 26, article ID 264101.
[73] M. G. Silveirinha, C. A. Fernandes, "Homogenization of 3-D-connected and nonconnected wire metamaterials", *IEEE Trans. Microw. Theory Tech.* **53** (2005), no. 4, p. 1418-1430.
[74] A. Demetriadou, J. B. Pendry, "Taming spatial dispersion in wire metamaterial", *J. Phys.: Condens. Matter* **20** (2008), no. 29, article ID 295222.
[75] J. A. Bittencourt, *Fundamentals of Plasma Physics*, 3rd ed., Springer-Verlag, New York, 2004.
[76] S. I. Maslovski, M. G. Silveirinha, "Nonlocal permittivity from a quasistatic model for a class of wire media", *Phys. Rev. B* **80** (2009), no. 24, article ID 245101.
[77] S. I. Maslovski, T. A. Morgado, M. G. Silveirinha, C. S. R. Kaipa, A. B. Yakovlev, "Generalized additional boundary conditions for wire media", *New J. Phys.* **12** (2010), no. 11, article ID 113047.

[78] M. G. Silveirinha, S. I. Maslovski, "Radiation from elementary sources in a uniaxial wire medium", *Phys. Rev. B* **85** (2012), no. 15, article ID 155125.
[79] M. G. Silveirinha, "Poynting vector, heating rate, and stored energy in structured materials: a first-principles derivation", *Phys. Rev. B* **80** (2009), no. 23, article ID 235120.
[80] J. T. Costa, M. G. Silveirinha, A. Alù, "Poynting vector in negative-index metamaterials", *Phys. Rev. B* **83** (2011), no. 16, article ID 165120.
[81] M. G. Silveirinha, "Additional boundary conditions for nonconnected wire media", *New J. Phys.* **11** (2009), no. 11, article ID 113016.
[82] V. V. Yatsenko, S. A. Tretyakov, S. I. Maslovski, A. A. Sochava, "Higher order impedance boundary conditions for sparse wire grids", *IEEE Trans. Antennas and Propagation* **48** (2000), no. 5, p. 720-727.
[83] I. S. Nefedov, A. J. Viitanen, S. A. Tretyakov, "Electromagnetic wave refraction at an interface of a double wire medium", *Phys. Rev. B* **72** (2005), no. 24, article ID 245113.
[84] S. Pekar, "The theory of electromagnetic waves in a crystal in which excitons are produced", *Sov. Phys. JETP* **6** (1958), p. 785.
[85] M. G. Silveirinha, "Additional boundary condition for the wire medium", *IEEE Trans. Antennas and Propagation* **54** (2006), no. 6, p. 1766-1780.
[86] A. B. Yakovlev, Y. R. Padooru, G. W. Hanson, A. Mafi, S. Karbasi, "A generalized additional boundary condition for mushroom-type and bed-of-nails-type wire media", *IEEE Trans. Microw. Theory Tech.* **59** (2011), no. 3, p. 527-532.
[87] G. W. Hanson, E. Forati, M. G. Silveirinha, "Modeling of spatially-dispersive wire media: transport representation, comparison with natural materials, and additional boundary conditions", *IEEE Trans. Antennas and Propagation* **60** (2012), no. 9, p. 4219-4232.
[88] G. W. Hanson, M. G. Silveirinha, P. Burghignoli, A. B. Yakovlev, "Non-local susceptibility of the wire medium in the spatial domain considering material boundaries", *New J. Phys.* **15** (2013), no. 8, article ID 083018.
[89] M. G. Silveirinha, "Boundary conditions for quadrupolar metamaterials", *New J. Phys.* **16** (2014), no. 8, article ID 083042.
[90] A. D. Yaghjian, "Boundary conditions for electric quadrupolar continua", *Radio Sci.* **49** (2014), no. 12, p. 1289-1299.
[91] J. Shin, J.-T. Shen, S. Fan, "Three-dimensional electromagnetic metamaterials that homogenize to uniform non-Maxwellian media", *Phys. Rev. B* **76** (2007), no. 11, article ID 113101.
[92] H. Latioui, M. G. Silveirinha, "Light tunneling anomaly in interlaced metallic wire meshes", *Phys. Rev. B* **96** (2017), no. 19, article ID 195132.
[93] D. E. Fernandes, S. I. Maslovski, G. W. Hanson, M. G. Silveirinha, "Fano resonances in nested wire media", *Phys. Rev. B* **88** (2013), no. 4, article ID 045130.

Comptes Rendus
Physique
2020, 21, nº 4-5, p. 389-408
https://doi.org/10.5802/crphys.22

Metamaterials 1 / *Métamatériaux 1*

Transformation optics for plasmonics: from metasurfaces to excitonic strong coupling

Optique transformationnelle pour la plasmonique : des métasurfaces à l'excitonique en fort couplage

Paloma A. Huidobro[*, a] **and Antonio I. Fernández-Domínguez**[b]

[a] Instituto de Telecomunicações, Insituto Superior Teécnico-University of Lisbon, Avenida Rovisco Pais 1, 1049-001 Lisboa, Portugal

[b] Departamento de Física Teórica de la Materia Condensada and Condensed Matter Physics Center (IFIMAC), Universidad Autónoma de Madrid, E-28049 Madrid, Spain

E-mails: p.arroyo-huidobro@lx.it.pt (P. A. Huidobro), a.fernandez-dominguez@uam.es (A. I. Fernández-Domínguez)

Abstract. We review the latest theoretical advances in the application of the framework of Transformation Optics for the analytical description of deeply sub-wavelength electromagnetic phenomena. First, we present a general description of the technique, together with its usual exploitation for metamaterial conception and optimization in different areas of wave physics. Next, we discuss in detail the design of plasmonic metasurfaces, including the description of singular geometries which allow for broadband absorption in ultrathin platforms. Finally, we discuss the quasi-analytical treatment of plasmon–exciton strong coupling in nanocavities at the single emitter level.

Résumé. Nous passons en revue les dernières avancées dans l'application du cadre de l'optique transformationnelle pour la description analytique des phénomènes électromagnétiques en régime fortement sub-longueur d'onde. En premier lieu, nous présentons une description générale de la technique, ainsi que son exploitation usuelle dans la conception et l'optimisation des métamatériaux dans différentes disciplines de la physique des ondes. En second lieu, nous discutons en détail de la conception de métasurfaces plasmoniques, y compris la description de géométries singulières qui permettent une absorption sur une large plage de fréquences dans les plates-formes ultra-minces. Enfin, nous discutons du traitement quasi-analytique du couplage fort plasmon–exciton dans les nanocavités au niveau d'un seul émetteur.

Keywords. Transformation optics, Plasmonics, Metasurfaces, Excitonic strong coupling.

Mots-clés. Optique transformationnelle, Plasmonique, Métasurface, Excitonique en fort couplage.

* Corresponding author.

1. Introduction

The development of Transformation Optics [1, 2] (TO) has been instrumental in the fast growth that metamaterial science has experienced during the last years [3]. This theoretical tool exploits the invariance of macroscopic Maxwell's equations under coordinate transformations to establish a link between an electromagnetic (EM) phenomenon, described by the transformation, and the material response required for its realization. Thus, TO determines the way in which the EM constitutive relations, and therefore the permittivity and permeability tensors, must be tailored in space in order to obtain a desired effect.

TO theory states that, under a general spatial transformation, $\mathbf{r}' = \mathbf{r}'(\mathbf{r})$ like the one sketched in Figure 1(a), EM fields are modified exactly in the same way as they do for the following spatially-dependent electric permittivity and magnetic permittivity tensors

$$\boldsymbol{\epsilon}'(\mathbf{r}') = \frac{\boldsymbol{\Lambda}(\mathbf{r}')\boldsymbol{\epsilon}(\mathbf{r}(\mathbf{r}'))[\boldsymbol{\Lambda}(\mathbf{r}')]^{\mathrm{T}}}{\det[\boldsymbol{\Lambda}(\mathbf{r}')]}, \quad \boldsymbol{\mu}'(\mathbf{r}') = \frac{\boldsymbol{\Lambda}(\mathbf{r}')\boldsymbol{\mu}(\mathbf{r}(\mathbf{r}'))[\boldsymbol{\Lambda}(\mathbf{r}')]^{\mathrm{T}}}{\det[\boldsymbol{\Lambda}(\mathbf{r}')]} \tag{1}$$

where $\boldsymbol{\epsilon}(\mathbf{r})$ [$\boldsymbol{\mu}(\mathbf{r})$] and $\boldsymbol{\epsilon}'(\mathbf{r}')$ [$\boldsymbol{\mu}'(\mathbf{r}')$] are the permittivity [permeability] tensors in the original and final frames, respectively, and $\Lambda(\mathbf{r}') = \partial\mathbf{r}'/\partial\mathbf{r}$ is the Jacobian matrix for the transformation. Note that (x, y) and (u, v) denote original and transformed coordinates in Figure 1(a).

From a metamaterial perspective, Equations (1) establish the link between material characteristics and the EM effect resulting from the spatial operation. Thus, TO provides a recipe for the design of metamaterials with at-will functionalities. A recent review on the use of transformation optics for the design of cloaks, illusion devices and other elements such as rotators and concentrators can be found in Ref. [4]. In parallel to the development of optical metamaterials for such applications, there has been a wide variety of advances in different areas of wave physics. For instance, TO has been extended into the spatiotemporal domain to devise spacetime cloaks [5, 6] as well as analogues of other phenomena emerging from the link between electromagnetism in media and general relativity [7–10]. Another degree of design flexibility in the form of media with gain and loss can be obtained by analytic continuation of the mapping coordinates into the complex plane [11, 12]. This way, TO can be connected with PT symmetric media [13], and reflectionless devices can be designed [14]. TO has also been adapted for the control of surface waves [15], as well as guided waves on integrated optical circuits [16], and for antenna engineering [17].

Furthermore, it is possible to apply TO to other wave systems beyond electromagnetics. The cornerstone proposal of the invisibility cloak [18] has been reproduced in different fields, which initiated the expansion of metamaterials for different physical domains. Applications of TO include the cloaking of acoustic pressure waves [19–21], matter waves [22] or heat conduction [23]. Particularly interesting is the fact that while the elastodynamic equations are not form invariant under coordinate transformations [24], it has been shown that TO can still be a powerful tool in the design of mechanical metamaterials [25–27] and even of seismic cloaks [28, 29].

Much the development of transformation optics has gone hand in hand with that of plasmonics. In its most general form, TO accounts for the vectorial and undulatory nature of EM fields, which makes it exact at sub- and supra-wavelength scales. Taking advantage of this, TO has made possible the at-will moulding the flow of surface plasmons (SPs) that propagate along metal/dielectric interfaces with subwavelength confinement [30–34]. Although the SP field extends both into the dielectric and metallic sides of the interface, it has been shown that it is enough to act on the dielectric side by placing the metamaterial designed with (1) on top of the metal surface [35]. This way, plasmonic invisibility cloaks, such as shown in Figure 1 (b), beam benders and shifters operating at nearly subwavelength scales and in the visible regime have been devised. Experimental realizations of these ideas include a broadband carpet cloak which suppresses scattering from a bump on a metal surface [36], as well as Luneburg and Eaton lenses [37, 38].

From a purely computational electrodynamics perspective, Equations (1) provide the prescription to interchange geometric and material characteristics of an EM system. This was, in fact, the original motivation that led to the development of this theoretical framework. It was devised as a strategy to ease the numerical solution of Maxwell's Equations, using the TO mapping of complex and acute geometries into much simpler ones [1]. Frequently, this advantage comes at the expense of non-uniform and anisotropic permittivity and permeability distributions. Importantly, when the transformation chosen is conformal, the permittivity and permeability in the plane of the transformation are left unchanged, as well as the electrostatic potential. Conformal transformations are 2D analytical maps, $(x', y') = [x'(x, y), y'(x, y)]$, that conserve the angle between coordinate lines and leave $z' = z$. They satisfy the Cauchy–Riemann equations, $\partial x'/\partial x = \partial y'/\partial y$, $\partial x'/\partial y = -\partial y'/\partial x$, which directly imply that conformal transformations leave isotropic permittivities and permeabilities unchanged in the plane of the transformation, as we now show. Starting from a frame where $\boldsymbol{\epsilon}(\mathbf{r})$ is isotropic, we have from (1),

$$\boldsymbol{\epsilon}' = \epsilon \frac{\boldsymbol{\Lambda}\boldsymbol{\Lambda}^{\mathrm{T}}}{\det[\boldsymbol{\Lambda}]} = \frac{\epsilon}{\det[\boldsymbol{\Lambda}]} \begin{pmatrix} \frac{\partial x'}{\partial x} & \frac{\partial x'}{\partial y} & 0 \\ \frac{\partial y'}{\partial x} & \frac{\partial y'}{\partial y} & 0 \\ 0 & 0 & 1 \end{pmatrix} \begin{pmatrix} \frac{\partial x'}{\partial x} & \frac{\partial y'}{\partial x} & 0 \\ \frac{\partial x'}{\partial y} & \frac{\partial y'}{\partial y} & 0 \\ 0 & 0 & 1 \end{pmatrix} \tag{2}$$

$$= \begin{pmatrix} \epsilon & 0 & 0 \\ 0 & \epsilon & 0 \\ 0 & 0 & \dfrac{\epsilon}{\det[\boldsymbol{\Lambda}]} \end{pmatrix} \tag{3}$$

where the last step follows from straightforward application of the Cauchy–Riemann equations, which yield $\det[\boldsymbol{\Lambda}] = (\partial x'/\partial x)^2 + (\partial x'/\partial y)^2 = (\partial y'/\partial y)^2 + (\partial y'/\partial x)^2$. Doing the same derivation for the magnetic permeability, one has that conformal transformations preserve isotropic electromagnetic properties in the plane of the transformation. This has been used in recent years as a means to shed analytical, instead of numerical, insight into plasmonic phenomena taking place in deeply subwavelength metallic devices, thereby recovering the initial purpose of TO of aiding in solving Maxwell's equations. In an early work, conformal transformations were employed to transform the canonical perfect lens formed by a flat slab with negative refractive index into other two dimensional perfect lenses of various shapes [39].

Figure 1(c) shows an instance of two cascaded conformal transformation which first transform vertical (blue) and horizontal (orange) slabs into a concentric annulus and a knife edge, respectively, and next into an off-centered annulus and a lenticular shape. For instance, in the first step, the transformation is $z' = \exp(z)$. Writing it explicitly as $x' = \mathrm{e}^x \cos(y)$, $y' = \mathrm{e}^x \sin(y)$, it can be easily verified that it verifies the Cauchy–Riemann equations, and that its Jacobian matrix in the plane, $\boldsymbol{\Lambda} = [(\mathrm{e}^x \cos(y), -\mathrm{e}^x \sin(y)), (\mathrm{e}^x \sin(y), \mathrm{e}^x \cos(y))]$, satisfies $\boldsymbol{\Lambda}\boldsymbol{\Lambda}^{\mathrm{T}} \propto \mathbb{1}_{2\times 2}$. Hence it conserves the permittivity in the plane of the transformation. If we take the blue area in the left panel to represent a metal slab embedded in dielectric surroundings, then the annulus shaded in blue in the middle or right panel represent a cross-section of 2D core-shell nanoparticles, and similarly for the areas shaded in orange. Transformation optics relates the spectrum of all these structures, and allows us to derive analytically the optical response of a plasmonic nanostructure of complex shape in terms of the analytical solution of the more symmetric one.

At visible frequencies and (sub-)nanometric length scales, spatial derivatives in Maxwell's curl Equations are much larger than temporal ones. Therefore, the latter can be neglected, which translates into the decoupling of magnetic and electric fields. This is the so-called quasistatic

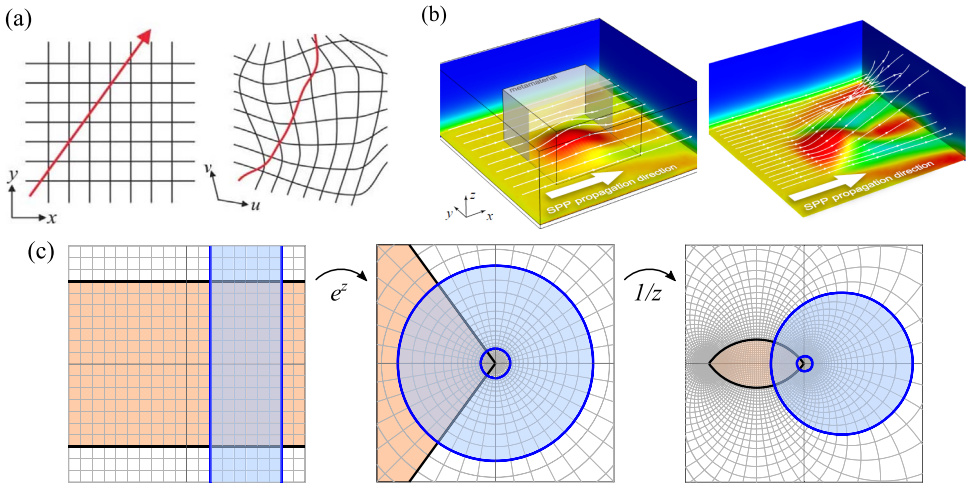

Figure 1. (a) EM fields propagation in free space (sketched as a single field line) with the background cartesian grid (left), and their distortion under an arbitrary geometric transformation, with the corresponding distorted coordinates in the background (right). Adapted with permission [2]. (b) A bump on a metal surface can be cloaked so that a SP propagating along the metal/dielectric interface propagates smoothly without being scattered as would occur without the cloak (right panel). Powerflow streamlines are depicted as with lines with arrows. Reproduced with permission from Ref. [30]. (c) Illustration of a cascade of two conformal transformations. An exponential map, e^z, transforms a blue slab (left panel) into a concentric annulus. Through an inversion, $1/z$, the annulus is off-centered (right panel). On the other hand, the orange slab transforms into a knife edge and subsequently into a lenticular shape.

approximation for metallic nanostructures [40], in which the spatial dependence of electric fields can be described in terms of an electrostatic potential, $\mathbf{E}(\mathbf{r}) = -\nabla\Phi(\mathbf{r})$, satisfying Gauss law

$$\nabla[\boldsymbol{\epsilon}(\mathbf{r})\nabla\Phi(\mathbf{r})] = 0, \tag{4}$$

where, in general, the permittivity is an inhomogeneous, anisotropic tensor. Importantly, although the quasistatic approximation only holds for sub-wavelength systems, the validity of (4) can be pushed to dimensions up to ~100 nm by introducing radiation losses through the so-called radiative reaction concept [40, 41]. Using these ideas [42–44], a set of analytical and quasi-analytical TO approaches have been devised to investigate the harvesting of light by a wide range of 2D and 3D geometries: touching nanoparticles [45, 46], nanocrescents [47, 48], nanorods [49], nanosphere dimers [50, 51]. Moreover, other EM phenomena have been explored theoretically using TO ideas, such as spatial nonlocality in metallic junctions [52, 53], electron energy loss in metal nanostructures [54], second harmonic generation in plasmonic dimers [55], near-field van der Waals interactions between nanoparticles [56, 57], or plasmon hybridization in collections of several touching nanoparticles [58].

In the following, we discuss the recent exploitation of TO framework in two areas of great interest in plasmonics in recent years. On the one hand, the design of conventional and singular plasmonic metasurfaces, which can be metallic or based on graphene. On the other hand, the description of strong-coupling phenomena between quantum emitters and the plasmonic spectrum supported by metallic nanocavities.

2. Plasmonic metasurfaces

Metasurfaces, the planar counterpart of bulk metamaterials, consist of resonant subwavelength units arranged in a two-dimensional (2D) array [59–64]. The geometry and materials of the subwavelength building blocks, as well as their arrangement, are appropriately designed and manufactured to provide an ultra-thin platform for manipulating EM waves. Metasurfaces have enabled effects such as broadband light bending and anomalous reflection and refraction in ultrathin platforms [65, 66]. While dielectric nanoantennas have been suggested for the design of metamaterials due to their lower loss compared to plasmonic nanoparticles [67], absorption losses are a less stringent constrain when considering metasurfaces. For that reason, plasmonic metasurfaces have been a particularly fruitful platform to control optical fields [68]. They are formed of subwavelength metallic elements with resonant electric or magnetic polarizabilities, enabling light confinement at the subwavelength scale, accompannied by large enhancements of the EM fields. On the other hand, the high electron mobility in graphene has also motivated the use of this 2D material for plasmonic metasurfaces at lower frequencies, making use of the unrivalled field enhancements provided by its THz plasmons [69–73].

The analytical power of TO has been instrumental in the design of plasmonic metasurfaces with unconventional properties, as we review in the following. In Section 2.1, we discuss in detail the TO insights into both subwavelength metallic gratings and graphene metasurfaces, as well as their applications. Next, in Section 2.2 we move on to present the so-called singular metasurfaces, their fundamental properties and their understanding in terms of hidden dimensions.

2.1. *Designing plasmonic gratings with transformation optics*

Here we review the theoretical framework for the design of metasurfaces by means of TO. While the use of coordinate transformations to facilitate diffraction calculations in gratings precedes the birth of transformation optics [74, 75], conformal transformations in particular have been recently used to design plasmonic metasurfaces. We concentrate on the most simple form of metasurface, that is, a thin film of a plasmonic material one of whose surfaces is periodically corrugated forming a subwavelength grating. Such plasmonic grating can be generated from a thin metallic slab (where analytical solutions of Laplace's equation are available) by means of a conformal transformation [76],

$$z = \frac{d'}{2\pi} \ln\left(\frac{1}{e^{w} - i w_0} + i y_0\right). \tag{5}$$

Here, $z = x + iy$ refers to the transformed coordinates in the frame of the grating, and $w = u + iv$ to the Cartesian coordinates in the frame of the slab. In addition, d' sets the length scale of the structure by determining the grating period, w_0 is a free parameter that sets the grating modulation strength, and y_0 is fixed by w_0, the slab thickness, δ, and its position, u_0, as $y_0 = w_0/(\exp[2(u_0 + \delta)] - w_0^2)$. A map of one period of the conformal transformation is shown in Figure 2(a). The space between the blue lines represents a silver slab with one periodically modulated surface, which maps through the transformation to a flat silver slab. The cascaded transformation first involves an exponential, which transforms the infinite slab into a closed annulus geometry, then an inversion that off-centers the annulus (see Figure 1(c)), and finally a logarithmic that restores the infinite length of the starting structure, but with periodic wiggles (Figure 2(a)).

As we have mentioned in Section 1, conformal transformations applied to Maxwell's equations conserve the electromagnetic parameres, and, furthermore, preserve the electrostatic potential. Hence, in the electrostatic limit (period $d' \ll \lambda$), the spectral properties of a subwavelength

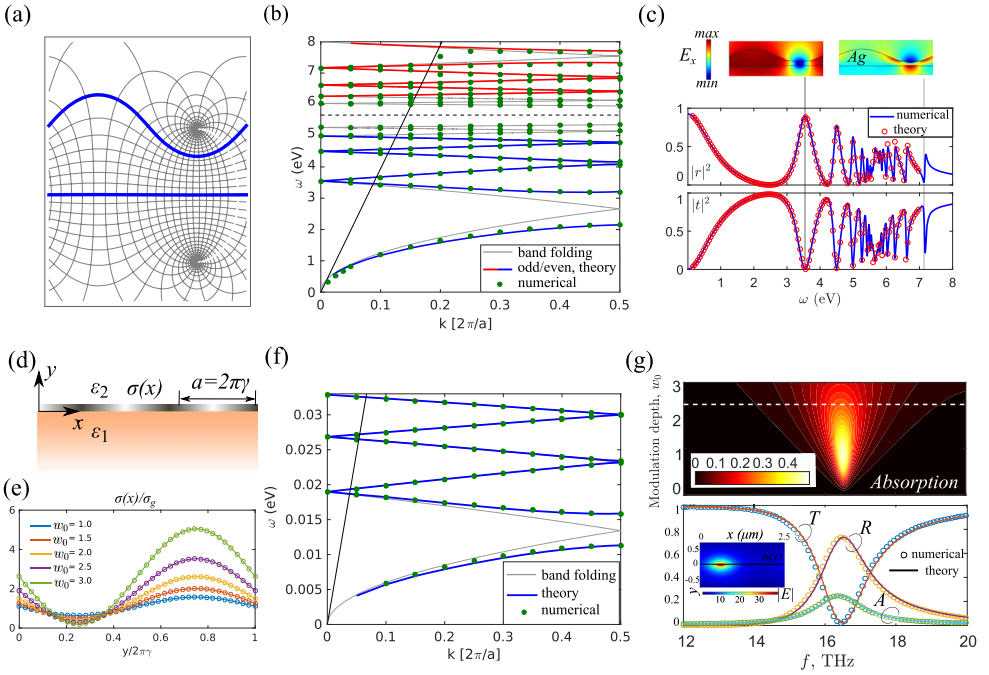

Figure 2. Realising plasmonic metasurfaces by means of conformal transformations. (a) One period of the conformal map used to generate gratings. (b) Dispersion relation of a silver grating modes above and below the SP frequency (dashed line). The grating inherits the mode spectrum of the flat slab (thin gray line). (c) Optical response of the subwavelength silver grating at normal incidence, and field distribution for the lowest and highest energy modes. (d) Graphene metasurfaces with spatially varying conductivity, $\sigma(x)$, and tunable modulation strength (e). (f) Dispersion relation of a graphene metasurface revealing the underlying homogeneous graphene layer (thin gray line). (g) Absorption can reach 50% at the dipolar SP resonance by tuning the modulation strenght (top). Absorption, reflection and transmission for $w_0 = 2.5$ (bottom). Panels (b,f) are adapted from Ref. [77], (c) from [76], (d,e) from [78].

plasmonic grating are equivalent to that of the thin plasmonic slab, whose dispersion relation is given by

$$\exp(|k|\delta) = \pm(\epsilon_m(\omega) - \epsilon_d)/(\epsilon_m(\omega) + \epsilon_d), \tag{6}$$

with $\epsilon_m = 1 - \omega_p^2/(\omega(\omega + i\gamma_D))$ being the metal permittivity (ω_p is the plasma frequency and γ_D is the Drude damping) and ϵ_d the one of the surrounding dielectric space. As a consequence, the dispersion relation of the grating can be accurately predicted from the simple analytical expression corresponding to the plasmonic slab.

Figure 2(b) shows the dispersion relation of a vacuum-embedded silver slab folded in the first Brillouin zone of the corresponding set of gratings (periodicity $2\pi \times 5$ nm), plotted as a thin gray line. The modes of a grating with modulation strength fixed by $w_0 = 1.5$ calculated from a numerical finite element solver [79] are plotted with dots, presenting an excellent agreement with the analytical prediction. The relationship between both systems ensures the quasi-degeneracies observed at the zone center, which are only slightly lifted due to magnetic effects (the magnetic field sees the periodicity of the grating through variations in the out-of-plane component of the permeability). On the other hand, band gaps open at the zone edge. This reflects the periodic

character of the grating structure, since the slab is translationally invariant and only the modes at $k = 0$ share exactly the same symmetry. Mathematically this is captured by the branch cuts of the transformation, which act as sinks and drains for the waves, effectively swapping them to opposite sides of the slab when incident and reflected waves on the grating are transformed. By taking this into account, band structures for the whole Brillouin zone, exact in the quasistatic limit, can be obtained [77] (plotted as thick red and blue lines). Furthermore, by going beyond the quasistatic approximation in a perturbative approach and including the radiative contribution of the grating, the optical spectrum at normal incidence can be obtained analytically (shown in Figure 2(c)). Finally, we remark that the general scope of TO has enabled to fully take into account retardation effects by transforming the full set of Maxwell's equations. This enables the semi-analytical calculation of optical spectra for gratings of periods not limited to the very subwavelength regime, for arbitrary polarization states, and is exact at the level of Maxwell's equations [80].

The conformal map shown in Figure 2(a) can also be used to devise graphene metasurfaces, see panel (d). We consider the limit of an infinitely thin plasmonic slab with conductivity $\sigma(\omega) = -\mathrm{i}(\epsilon(\omega) - 1)\omega\epsilon_0\delta$ and $\delta \to 0$. In the grating frame, the slab of modulated thickness equivalently represents an infinitely thin layer, i.e., graphene, with modulated conductivity [81]. Metasurfaces consisting of graphene with periodically modulated conductivity [82–84] can be designed this way [78], and a periodic doping modulation can be realized by optical [85] or electrostatic [86] means, or by patterning the graphene [87,88] or its environment [89,90].

The dispersion relation of a graphene metasurface is shown in panel (b), displaying the quasi-degeneracies at the zone center inherited from the dispersion relation of homogenously doped graphene (thin gray line). The modulation period is 2.5 μm, the modulation strength is given by $\omega_0 = 1.5$, see panel (e), and graphene's conductivity is taken from the random phase approximation with chemical potential $\mu = 0.1$ eV and scattering loss $\tau = 10$ ps. A close up of the absorption spectrum around the dipolar resonance, lower energy mode in panel (f), is presented in panel (g). Here the chemical potential was changed to $\mu = 0.65$ eV, which accounts for the frequency shift with respect to the resonance in panel (f) and a typical experimental mobility of 10^4 cm^2/(V·s) was used. The insensitivity of the absorption peak in the contour plot to the modulation strength, w_0, is due to the fact that gratings of different w_0 map into homogeneous graphene with the same conductivity, as this is a free parameter in the transformation. Hence, by tuning the modulation depth, absorption in the graphene metasurface can be switched, and, remarkably, up to 50% of the power of incident radiation can be absorbed by a single graphene layer owing to the excitation of deeply subwavelength SPs. While 50% absorption is the theoretical maximum for a thin layer of material, absorption can be further increased up to 100% by employing a Salisbury screen scheme and placing the metasurface close to a perfect reflector, such that a Fabry–Perot cavity is formed. Due to the strong EM confinement enabled by SPs, this idea allows for an ultrathin perfect absorber of deeply subwavelength thickness for THz frequencies [91].

2.2. *Singular plasmonic metasurfaces*

As discussed in Section 1, TO provided a successful understanding of the harvesting of light by plasmonic nanoparticles with singular geometries such as touching points [45,46]. In particular, TO highlighted the geometrical origin of the broadband absorption spectra characteristic of these systems by mapping them to infinitely extended geometries where the singularites map into points at infinity. The infinite extension in the transformed frame removes the quantization (discretization) condition and yields a broadband spectrum, while the large absorption efficiencies are caused by the SP fields travelling towards infinity with reducing group velocities. This

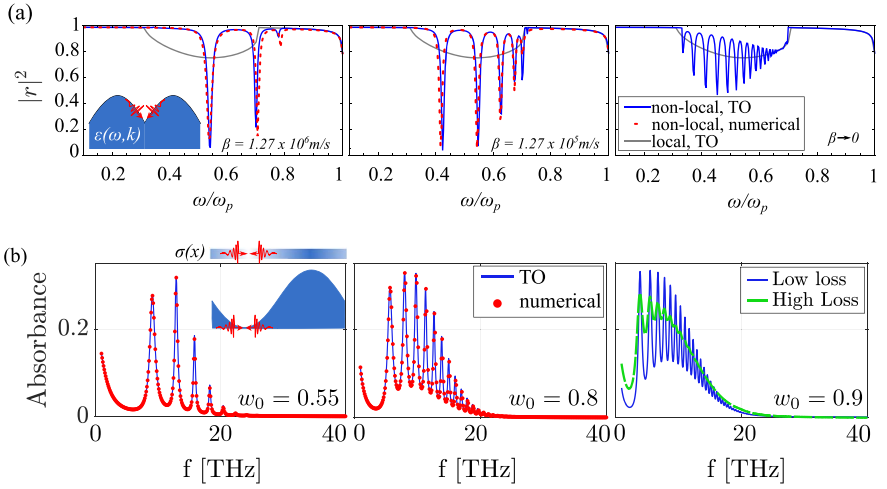

Figure 3. Optical response of singular metal (a) and graphene (b) metasurfaces. (a) Reflectivity spectrum of a silver surface with a periodic array of sharp grooves. As β is decreased from the realistic value towards zero (left to right), the spectrum approaches the continuum predicted by a local calculation. (b) Absorption spectrum for graphene metasurfaces as the singular case is approached by reducing $\sigma(\omega)$ at the grating valleys (w_0 increasing, left to right). In both panels TO analytical results are plotted as solid lines and EM simulations are plotted with dots. Adapted from Refs. [94] (a) and [95] (b).

effect has also been referred to as anomalous absorption as it is present even in the absence of material loss [92, 93].

The physics of SPs propagating towards geometrical singularities can also play a fundamental role in plasmonic metasurfaces. For instance, subwavelength arrays of ultra sharp grooves in a metal surface can turn good reflectors such as gold or silver into almost perfect broadband absorbers, usually referred to as plasmonic black metals [96]. These surfaces can be viewed as *singular plasmonic metasurfaces* [97] and here we review two instances of them, sheding light onto their continuous absorption spectra and highlighting how these can be interpreted by means of an extra compacted dimension. In the first case the singular metasurface consists of a periodic array of grooves with sharp edges carved on a metal surface [94, 98], see inset of Figure 3(a). In the second case, the singularities are achieved by strongly supressing the conductivity of graphene at the grating valleys [95, 99], see inset of Figure 3(b).

Plasmonic black metals [96] can be analytically modelled using TO by means of the periodic surface with sharp grooves shown in the inset of Figure 3(a) [97]. The sketch shows one period of the structure, which is generated by the same cascaded transformation as in (5), but by changing $\mathrm{i}w_0 \to -a$ and $\mathrm{i}y_0 \to -1/(2a)$, where a is a parameter that determines the inversion point. By now taking a periodically arranged set of slabs like the orange one shown in Figure 1(c), the transformation first maps the periodic array into a knife edge, compressing $-\infty$ to a point at the origin. Then $+\infty$ is compressed into another point, giving rise to a finite lenticular shape with two sharp edges as shown in Figure 1(c). Finally, a logarithmic transformation is used to generate a semi-infinite surface decorated with a periodic array of grooves (see Figure 3(a)), which inherit the sharp edges owing to the conformal character of the transformations. The final structure is thus a surface where SPs can be excited, and which are localized at the surface and decay evanescently away into the metal and dielectric half-spaces. Hence, it may seem at first sight that these modes are two-dimensional, that is, characterized by two wave-vectors parallel to the metal surface (one in the plane of the sketch in Figure 3(a), the other out of the page). However, due to

the conformal character of the transformations, the singular metasurface inherits the spectral properties of the slab array, which supports three-dimensional modes, characterized by the two wave-vectors in the planes where the slabs extend to infinity (one in the plane of the sketch in Figure 1(c, left), and one out of the page) and by a third one along the direction where they are periodic (the vertical direction in Figure 1(c, left)). As a consequence, the modes supported by the singular surface are also characterized by three wave-vectors, with the third one being inherited from the transformed structure and associated to an extra dimension that is compacted into the singularities [97]. This has remarkable consequences in the optical spectrum of the singular metasurface: the extra wave-vector is not subject to a selection rule, and therefore there is a mode available at every frequency, which results in a broadband absorption spectrum. In other words, these gratings are black (or gray) while conventional gratings, which have discrete absorption lines, are coloured.

The broadband spectral response of a singular silver metasurface of period 10 nm is shown in Figure 3(a), where the normal incidence reflectivity spectrum is plotted as a solid grey line. A continuous band of low reflectivity (high absorption) can be seen, which corresponds to the excitation of the antisymmetric mode between a cut-off frequency and the SP frequency ($\omega_{sp} = \omega_p/\sqrt{2}$). This is in striking difference with the results discussed in Section 2.1 for a non-singular plasmonic grating, which features a discrete series of resonant modes (see Figure 2 (c)). The optical response of the singular structure was calculated analytically by representing a plane wave incident on the metasurface as an array of magnetic line currents located at infinity [98]. These sources are mapped to a periodic array of sources in the slab array frame, where the power flow carried by the excited SPs as they travel towards $\pm\infty$ is calculated. Next, the singular periodic surface is represented by a flat surface with an effective conductivity, which can be determined through conservation of energy, and from which the reflectivity of the singular metasurface is calculated. We note that numerical calculations of this system are not possible due to the singular character of the geometry.

In practice, perfect singularities are not possible to realize. Even if recent advances in nanofabrication enable the experimental realization of plasmonic structures with high precision [100], achieving a perfectly singular point will always be limited by the discrete nature of the electron gas, which prevents the existence of a perfect singularity where the electron density would diverge. The finite screening length of metals (~0.1 nm in noble metals) limits the size where electrons can accumulate in the singularity, and prevents the density from blowing up. These *nonlocal effects* effectively blunt the singularities which has a strong impact on the optical response of singular metasurfaces [94, 101]. This can be seen in Figure 3 (a), which presents the reflectivity for the singular metasurface using a nonlocal dielectric permittivity as solid blue lines, with red dashed lines obtained from numerical simulations also shown for comparison. In the calculation, which makes use of the previously introduced coordinate transformation that defines the singular metasurface, the properties of the metal are taken from the hydrodynamic model. According to it, the metal hosts transverse modes described by the usual Drude permittivity, conserved under the conformal transformation, and longitudinal modes with a permittivity, $\epsilon_L(\omega, \vec{k}) = 1 - \omega_p^2/(\omega(\omega + i\gamma_D)) - \beta^2|\vec{k}|^2$, which changes under the mapping due to the $\vec{k}$-dependence. The value of β, the parameter that determines the screening length and hence the extent of the singularity, was tuned down artificially from a realistic value for silver (left panel) to a very low value (right panel). Nonlocality blunts the singularities, which map to slabs of finite length in the transformed frame (we refer the reader to Ref. [94] for more details on the calculations). These are cavities for the SPs, which discretizes the spectrum and a set of reflectivity dips are observed (left). As the local regime is approached, the singularity is effectively sharper and in the transformed frame the cavities are longer, such that the structure supports more and more resonances (middle), tending towards the continuum obtained in the local approximation when

nonlocality is very small (right). The remarkable influence of nonlocality in the optical spectrum of the singular metasurface indicates that they could be used as a platform to probe nonlocality in metals.

A second instance of singular metasurfaces that can be smoothly approached can be realized in graphene as proposed in Ref. [97], or in ultrathin metal slabs [101]. In this case, the conformal transformation introduced in Section 2.1 was adapted to generate a surface with singularities in the form of touching points rather than sharp edges. This is done by first renormalising the whole structure through the introduction of a new length scale in the slab frame, d (the period of slab that maps into the length between two branch points in the transformed geometry). With this, the transformation reads as,

$$z = \frac{d'}{2\pi} \ln\left(\frac{1}{e^{2\pi w/d} - i w_0} + i y_0 \right), \tag{7}$$

with y_0 now defined as $y_0 = w_0/(\exp[4\pi(u_0 + \delta)d])$. Then the origin of the inversion is taken at a point very close to one of the surfaces ($w_0 \to 1$), which generates a grating with vanishing thickness at the valley points (see inset of Figure 3(b)). Similar to the non-singular grating, the free parameter in the transformation, w_0, determines the shape of the grating, and the singular behaviour, with $w_0 \to 1$ representing the singularity where the two surfaces touch, or where the doping approaches zero in the case of graphene.

Figure 3(b) presents the absorption spectrum of singular metasurfaces realized on graphene. The singularity is approached by keeping the same maximum conductivity value while reducing the minimum value, which is suppressed from the left to the right panels. When the grating is far from singular, the spectrum shows a discrete set of peaks corresponding to plasmonic resonances of increasing order (left). As the singularity is approached, more and more resonances appear in the spectrum (medium), and when the system is very close to being singular, the spectrum tends to a broadband of continuous absorption. These results assume a realistic value of the loss (mobility $m = 10^4$ cm^2/(V·s)), and we stress that increasing the loss ($m = 3 \times 10^3$ cm^2/(V·s)) further merges the peaks into the broadband. This system has been suggested as a tunable ultra-thin broadband absorber for THz waves [95]. Similar to the singular silver surface, the broadband absorption spectrum can be explained by means of an extra dimension compacted in the singularity. This additional dimension is inherited from the periodicity introduced in the slab frame, which tends to infinity ($d \to \infty$), while the dimension of the slab along its length is itself infinite. This results in a hidden dimension in the singularity in the grating frame, where incident radiation can satisfy the dispersion relation over a continuous frequency band. In fact, as the period in the slab frame increases, the modes are discretized in a smaller Brillouin zone. As a consequence, SP modes at larger wavevectors are available at lower and lower frequencies. The large confinement characteristic of these modes is responsible for the large absorptions seen in the singular metasurfaces [99]. Finally, we remark that these singular graphene metasurfaces provide a platform for the study of nonlocality in graphene, which is stronger when the doping is lower. The SPs propagating towards the singularity are a sensitive probe of nonlocal effects in graphene, which would become observable in far field measurements [102].

In this Section we have reviewed the use of TO to design plasmonic metasurfaces, and the proposal of singular plasmonic metasurfaces which hide an extra dimension in the singularity and can be used as ultrathin broadband absorbers. In the following, we turn our attention into a different area of nanophotonics, that of exctiton–plasmon interactions in nanocavities.

3. Exciton–plasmon strong coupling

In recent years, much theoretical efforts have focused on developing a general methodology for the expansion of the Dyadic Green's functions in open, lossy and dispersive systems in terms of a discrete set of EM modes. However, although this is currently a topic of intense activity, there

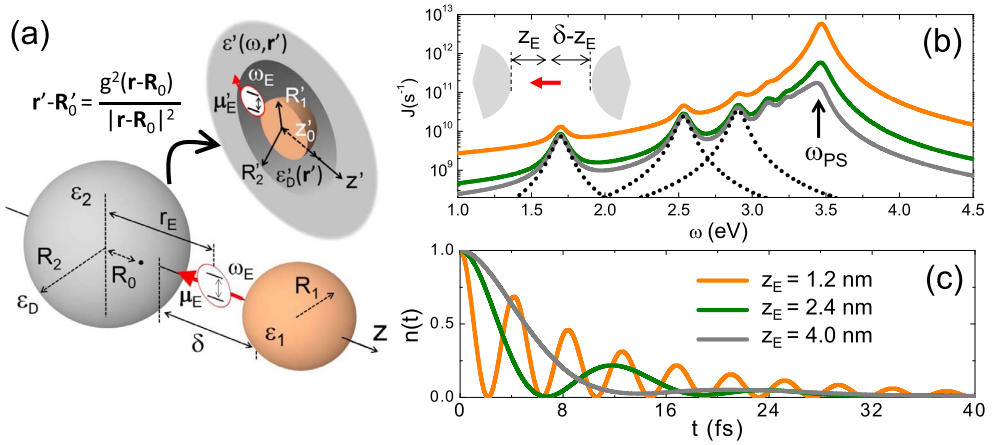

Figure 4. (a) Left: Sketch of a single QE with transition dipole moment $\boldsymbol{\mu}_{\mathrm{E}}$ and frequency ω_{E} placed within the gap between two nanospheres. Right: Spherically symmetric geometry obtained from the inversion of the original system. (b) Quasistatic spectral density at three different QE positions, see panel (c), along the z-axis and within the 8 nm gap between two Ag spheres ($R = 120$ nm). (c) Population dynamics, $n(t)$ ($n(0) = 1$), for a QE at resonance with the plasmonic pseudomode of the gap nanocavity, $\omega_{\mathrm{E}} = \omega_{\mathrm{PS}}$, for three z_{E} values. Adapted with permission [112, 113].

is not yet a consensus about the precise definition of these EM modes, their associated eigenfunctions and eigenvalues. As a consequence, various terms and definitions, such as resonant states [103], generalized normal [104] or quasinormal [105–107] modes, have been coined lately to refer to them. Indeed, the conception of a theoretical framework allowing for a general Green's function decomposition would mean a significant advance in multiple areas. The investigation of quantum optical phenomena in plasmonic [108, 109] and metallodielectric [110] nanocavities is among them. It would allow for a convenient quantization of subwavelength EM fields avoiding the enormous number of degrees of freedom inherent to macroscopic quantum electrodynamics calculations [111].

As discussed in Section 1, TO has been used in the past to obtain analytical descriptions of the light collection and concentration by a wide range of nanoparticle geometries. In this section, we discuss the application of similar methods to build 3D [112, 113] (Section 3.1) and 2D [114–117] (Section 3.2) models of the response of similar structures to point-like EM sources, such as quantum emitters (QEs), placed in their vicinity. This way, TO provides analytical insights into the Dyadic Green's function for these systems. Importantly, this approach also reveals its convenient decomposition and the proper definition of modal eigenvalues and eigenfunctions. Specifically, TO has been employed in the investigation of plasmon–exciton interactions in nanocavities, accounting for the full richness of the EM spectrum in these devices and revealing the conditions yielding strong coupling at the single QE level. Note that, contrary to nanoantennas, where the objective is enhancing the near- to far-field transfer of EM energy, this must be reduced in nanocavities for strong light-matter coupling. This means that the quasistatic approximation is an optimum starting point for the analysis of these phenomena.

3.1. *Three-dimensional model*

We consider first a nanocavity composed by two identical metallic spheres of radius $R_1 = R_2 = R$, with a Drude-like permittivity, separated by a nanometric gap, δ. As illustrated in Figure 4(a),

they can be transformed into a metal-dielectric-metal spherically-symmetric geometry under an inversion. This requires choosing judiciously the inversion point [112]

$$R_0 = \frac{L}{2} + \frac{R_2^2 - R_1^2 - \sqrt{\delta(\delta+2R_1)(\delta+2R_2)(2L-\delta)}}{2L}, \tag{8}$$

where $L = R_1 + R_2 + \delta$. As a result of the mapping, and differently from the 2D conformal transformations discussed in Section 2, the scalar permittivity in the transformed frame acquires a spatial dependence of the form $\epsilon'(\omega, \mathbf{r}') = g^2\epsilon(\omega, \mathbf{r}(\mathbf{r}'))/|\mathbf{r}' - \mathbf{R}_0'|^2$, where $\epsilon(\omega, \mathbf{r})$ is the original dielectric constant distribution. Note that the EM fields do not depend on the choice of g, a constant setting the length-scale of the mapping. It can be proven [46] that the quasistatic potential in the inverted system can be written as $\Phi'(\mathbf{r}') = |\mathbf{r}' - \mathbf{R}_0'|\phi'(\mathbf{r}')$ where $\phi'(\mathbf{r}')$ is a solution of Laplace's Equation in the primed frame. The potential in the transformed geometry can then be obtained by expanding $\Phi'(\mathbf{r}')$ in terms of spherical solutions of Laplace's Equation (labelled with degree l and order m of spherical harmonics) and imposing continuity conditions on the parallel component of the electric field and the normal component of the displacement field at the concentric spherical boundaries. Once this is known, the potential in the original frame is given by $\Phi(\mathbf{r}) = \Phi'(\mathbf{r}'(\mathbf{r}))$. In general, this procedure requires the numerical solution of the continuity equations, but in the limit $\delta \ll R$ analytical solutions can be obtained.

Using the TO approach briefly introduced above, the Dyadic Green's function for the system can be calculated by introducing a point-like dipole source, $\Phi_{\mathrm{E}}(\mathbf{r})$, modelling a QE as the EM excitation in the original frame [113]. By imposing $m = 0$ in the potential expansion, the calculations simplify significantly. With this restriction, only sources located along the z-direction (the nanocavity axis) and oriented parallel to it can be treated. Note that the interaction with the SPs supported by the spheres is maximum in these conditions. The component of the scattering Dyadic Green's function governing the QE–SP interaction is $G_{zz}^{\mathrm{sc}}(\omega, \mathbf{z}_{\mathrm{E}}, \mathbf{z}_{\mathrm{E}}) = (\epsilon_0/\mu_{\mathrm{E}})(c/\omega)^2|\partial_z\Phi_{\mathrm{sc}}(\omega, \mathbf{z}_{\mathrm{E}})|$, where μ_{E} is the QE dipole moment, z_{E} its position, and $\Phi_{\mathrm{sc}}(\omega, \mathbf{r}) = \Phi(\omega, \mathbf{r}) - \Phi_{\mathrm{E}}(\mathbf{r})$. Note that, for clarity, the spectral dependence of the scattered quasistatic potential is indicated, which originates from the presence of $\epsilon(\omega, \mathbf{r})$ in the continuity equations.

The spectral density [118], the physical magnitude that weights light-matter coupling in the nanocavity, can be expressed as [119, 120]

$$\begin{aligned} J(\omega) &= \frac{\gamma_{\mathrm{E}}(\omega)}{2\pi} P(\omega) = \frac{\mu_{\mathrm{E}}^2\omega^2}{\pi\epsilon_0\hbar c^2}\mathrm{Im}\{G_{zz}^{\mathrm{sc}}(\omega, \mathbf{r}_{\mathrm{E}}, \mathbf{r}_{\mathrm{E}})\} \\ &= \sum_{l=1}^{\infty}\sum_{\sigma=\pm1} \frac{g_{l,\sigma}^2}{\pi} \frac{\gamma_{\mathrm{D}}/2}{(\omega-\omega_{l,\sigma})^2 + (\gamma_{\mathrm{D}}/2)^2} \end{aligned} \tag{9}$$

where $\gamma_{\mathrm{E}}(\omega) = \omega^3\mu_{\mathrm{E}}^2/3\pi\epsilon_0\hbar c^3$ is the spontaneous decay rate of the QE ($\omega_{\mathrm{E}} = \omega$) in free space and $P(\omega)$ the Purcell enhancement induced by the nanocavity [40, 121]. Note that $J(\omega)$ is, except for a factor, the QE decay rate in the plasmonic environment. The right-hand side in (9) results from the Green's function decomposition given by the TO approach. In the limit of small gap sizes, $\rho = \delta/R \ll 1$, the SPs can be labelled in terms of their angular momentum l, and their even/odd parity across the gap, σ [112]. This way, analytical expressions for the SP frequencies, $\omega_{l,\sigma}$, and SP–QE coupling constants, $g_{l,\sigma}$, are obtained. Note that γ_{D} in (9) is the absorption rate in the metal Drude permittivity, the only damping mechanism in the quasistatic regime.

Figure 4(b) plots $J(\omega)$ at the 8 nm gap between two Ag spheres of radius 120 nm. Three different QE positions are considered, z_{E}: 4 nm (the gap center, in grey), 2.4 nm (green) and 1.2 nm (orange). The QE dipole moment is set to $\boldsymbol{\mu}_{\mathrm{E}} = 1.5\,\mathrm{e}{\cdot}\mathrm{nm}$. The first three even ($\sigma = 1$) Lorentzian terms in the expansion in (9) are plotted in blue dashed lines (they are the same for all z_{E}). These correspond to the lowest energy, most radiative SP modes which govern the absorption properties of the sphere dimer under plane wave illumination [51, 113]. The spectral density presents a much

stronger feature at higher frequencies, this is the plasmonic pseudomode, which emerges as a result of the spectral overlapping (within a frequency window γ_D) of SP modes with high angular momentum (large l) [120]. Note that ω_{PS} lies in the vicinity of the quasistatic SP frequency for the metal permittivity. Figure 4(b) shows that $J(\omega_{PS})$ increases as the QE is displaced away from the gap center and approaches one of the sphere surfaces (it couples more efficiently to SPs with shorter evanescent tails into the gap region), while the contribution due to low-frequency SPs do not vary with z_E.

Figure 4(c) renders the QE exciton population as a function of time, $n(t)$ in a spontaneous emission configuration ($n(0) = 1$) for the three positions in panel (b) and for $\omega_E = \omega_{PS}$. The popuplation dynamics are calculated using the Wigner–Weisskopf Equation [118],

$$\frac{\mathrm{d}}{\mathrm{d}t}c(t) = -\int_0^t \mathrm{d}\tau \int_0^\infty \mathrm{d}\omega\, J(\omega) \mathrm{e}^{\mathrm{i}(\omega_E-\omega)(t-\tau)} c(\tau) \tag{10}$$

where the exciton population is $n(t) = |c(t)|^2$. Equation (10) was fed with the TO-calculated spectral densities. The QE–SP interaction is in the weak-coupling regime at the gap center (grey) and $n(t)$ decays monotonically. However, for QEs away from the gap center, Rabi oscillations emerge in $n(t)$, and become stronger with smaller z_E. These are the fingerprint of the onset of strong coupling, and reveal that the population is transferred back and forth between the QE and the nanocavity (the pseudomode it supports) several times before its decay due to metal absorption. Figure 4(c) demonstrates that plasmon–exciton polaritons at the single QE level can be formed in nanocavities with large (4 nm) gaps by displacing the emitter position away from the gap center.

3.2. *Two-dimensional model*

The 3D model in the previous section presents several limitations. It yields analytical expressions only for dipolar sources located along, and oriented parallel to, the symmetry axis of cavities with small $\rho = \delta/R$. Moreover, the description of microscopic sources of higher order than dipolar ones cannot be handled analytically either. Finally, it is purely quasi-static and therefore does not provide any insight into far-field magnitudes, which are instrumental for the experimental probing of hybrid QE–SP systems. In the following, we show how these constraints can be overcome by considering a 2D model of the nanocavity, in which translational invariance along y-direction of the EM fields is assumed. Importantly, this approximation is justified by the remarkable similarity between plasmon–exciton strong-coupling phenomenology in 2D and 3D geometries [122].

Figure 5(a) shows how the 2D version of a nanoparticle-on-a-mirror (NPoM) geometry can be transformed into a metal-dielectric-metal waveguide under a logarithmic conformal map ($\varrho^{(\prime)} = x^{(\prime)} + \mathrm{i}z^{(\prime)}$) with $D = 2R$ and $s = \delta + D\sqrt{\rho}/(\sqrt{2+\rho} + \sqrt{\rho})$ [50]. The original EM point-like source transforms into an array of coherent identical sources, which makes the transformed system periodic. This periodicity provides again with appropriate indices for the SP modes: the Bloch band index, l, and, similarly to the 3D case, the parity with respect to the waveguide symmetry plane, σ [116]. The spectral densities can be calculated from the 2D model by using the first equality in (9), fed with 2D calculations of the Purcell enhancement $P(\omega) = (8\epsilon_0/\mu_E^2)(c/\omega)^2 \mathrm{Im}\{\boldsymbol{\mu}_E \nabla\, \Phi(\mathbf{r},\omega)|_{\mathbf{r}_E}\}$, where $\mathbf{r} = (x,z)$ and $\mathbf{r}_E$ is the position of the emitter in the xz-plane. This simplified model makes it possible treating quadrupolar exciton transitions in QEs in an analytical fashion as well [117]. Once 2D Purcell factors are known, they are combined with 3D free-space decay rates in (9).

Implementing radiation reaction corrections in the 2D model [41], the radiative decay rate for the even ($\sigma = +1$) SPs supported by NPoM cavities, $\gamma^{\mathrm{r}}_{l,+1}$, can be calculated [122] (note that,

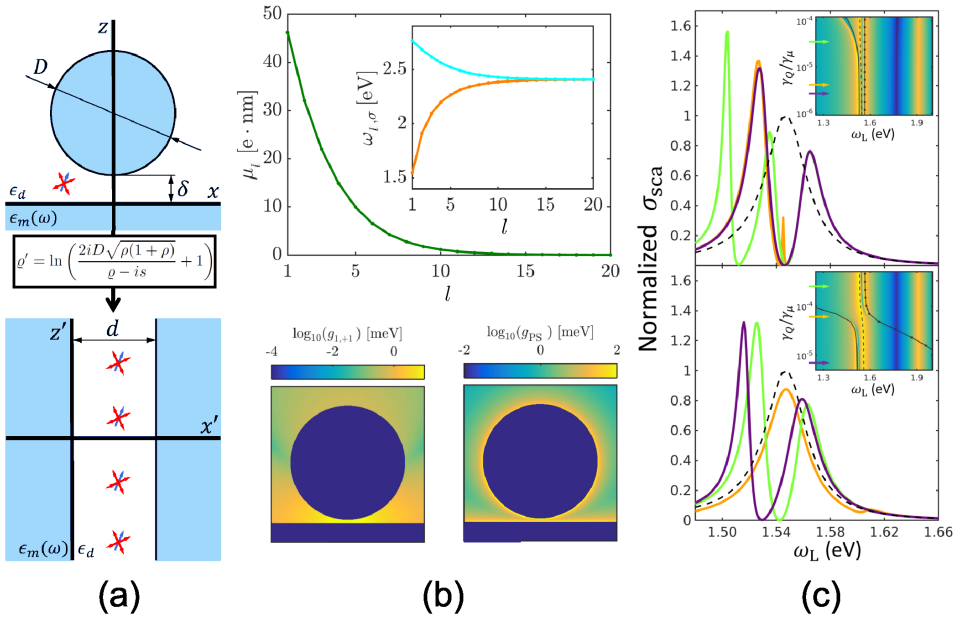

Figure 5. (a) 2D mapping between a Ag NPoM geometry and a silver-dielectric-silver waveguide. (b) Top: even SP dipole moment versus index l. Inset: even (orange) and odd (blue) SP frequencies ($D = 30$ nm, $\delta = 0.9$ nm). Bottom: coupling strength maps for vertically oriented QES and the lower-order dipolar SP mode (left) and the plasmonic pseudomode (right). (c) Scattering spectra around $\omega_{1+1} = \omega_\mu$ for three-level QEs (sustaining one dipolar and one quadrupolar transition) with $z_E = \delta/2$ and $\omega_Q = \omega_{1,+1}$ (top) and $z_E = 7\delta/8$ and $\omega_Q = \omega_{PS}$. Adapted with permission [116, 117].

by symmetry, $\gamma^r_{l,-1} = 0$). With this theory refinement, the spectral width of the Lorentzian terms in (9) acquire the form $\gamma_{l,\sigma} = \gamma_D + \gamma^r_{l,+1}\delta_{\sigma,+1}$. Moreover, using the method of images, the dipolar moment of even SPs can be extracted out of $\gamma^r_{l,+1}$ [117]. The top panel of Figure 5 renders the SP dipolar moment versus index l for the NPoM cavity in panel (a). As expected, they decrease as the mode order increases, and the SPs contributing to the plasmonic pseudomode are completely dark. The inset plots the SP frequencies for even (orange) and odd (blue) parity, showing that both branches overlap for large l. To illustrate the power of the TO approach, the bottom panels in Figure 5(b) display the coupling strength maps for vertically oriented QEs and for the lowest even SP mode ($g_{1,+1}$, left) and the plasmonic pseudomode (g_{PS}, right). The former is focused at the gap region, where it becomes rather uniform, and decays away from it. The latter is tightly confined to the metal boundaries, both at the particle and flat substrate, and presents little sensitivity to plasmon hybridization effects across the gap of the cavity.

Using the TO-calculated SP frequencies, $\omega_{l,\sigma}$, and the QE–SP coupling constants, $g_{l,\sigma}$, the Jaynes–Cummings Hamiltonian [118] describing plasmon–exciton interactions in the NPoM cavity can be parametrized

$$\hat{H} = \omega_E \hat{\sigma}^\dagger \hat{\sigma} + \sum_{l,\sigma} \omega_{l,\sigma} \hat{a}^\dagger_{l,\sigma} \hat{a}_{l,\sigma} + \sum_{l,\sigma} g_{l,\sigma} [\hat{\sigma}^\dagger \hat{a}_{l,\sigma} + \hat{\sigma} \hat{a}^\dagger_{l,\sigma}], \tag{11}$$

where $\hat{\sigma}$ and $\hat{a}_{l,\sigma}$ are the QE and SP annihilation operators. Equation (11) illustrates the exploitation of TO as a tool for the quantization of the complex plasmonic spectrum supported by the NPoM cavity. Moreover, through Lindblad terms weighted by the SP damping rates, $\gamma_{l,\sigma}$, we can account for plasmonic losses in a master equation description of the system [117].

Figure 5(c) shows scattering spectra for the cavity in panel (a) coupled to a QE modelled as a three-level system sustaining two, one dipolar and one quadrupolar, exciton transitions. Note that the latter is dark and could not be accessed by propagating EM fields. By adding a coherent driving term [123] to (11), we can describe the illumination of the system by a laser field of frequency ω_L around the lowest SP resonance, $\omega_{1,+1}$. The far-field scattering spectrum can be computed as the square of the steady-state expectation value of the total dipole moment operator, $\hat{M} = \sum_l \mu_l \hat{a}_{l+1} + \mu_E \hat{\sigma}_\mu$ [124]. The bare nanocavity is shown in dashed black lines. The QE is located at the center of the gap in the top panel and displaced along z-directon in the bottom one. In both cases, the dipolar transition is set at resonance with $\omega_{1,+1}$. In absence of the quadrupolar transition, a Rabi doublet [125] is apparent in the spectra of the hybrid system, the fingerprint of the onset of QE–SP strong coupling (see violet lines) [126]. These two scattering peaks emerge as a result of the formation of polaritons (hybrid plasmon–exciton states) in the system. They are displaced from the natural frequencies of their constituents, as a result of the coupling strength between them. Therefore, the upper (lower) polariton lies above (below) $\omega_\mu = \omega_{1,+1}$. By increasing the quadrupole moment of the dark QE transition (orange and green lines), this spectral profile is modified in opposite ways. In the top panel, a third peak emerges at the dip between the Rabi maxima, whereas a single peak (resembling the bare cavity) is observed in the bottom panel. These spectra show how TO allows exploring the remarkable effect that dark excitons can have in QE–SP interactions in the strong-coupling regime [116].

4. Conclusions

In this review we have discussed the theory of transformation optics and its applications. We have first reviewed its impact in metamaterial science for the design of electromagnetic devices and other aspects, such as the control of surface waves or its extension into other realms of wave physics. Next, we have revised how transformation optics has provided a set of analytical techniques for investigating complex problems in plasmonics. We have then focused on the application of this theoretical framework to the analytical treatment of two open problems of much relevance in current theoretical nanophotonics.

On the one hand, we have shown how transformation optics allows for the design of plasmonic metasurfaces with predictable optical responses inherited from a transformed structure with more symmetries. We have also reviewed the proposal of singular plasmonic metasurfaces in the form of subwavelength metal gratings with sharp edges or graphene metasurfaces with points of vanishing doping level. These singular structures are a realization of compacted dimensions, provide macroscopic signatures of nonlocality, and could be used as ultrathin broadband absorbers.

On the other hand, we have presented the description of plasmon–exciton coupling in nanocavities by means of transformation optics calculations. We have discussed the insights that this tool provides into both near- and far-field physical magnitudes, such as the exciton dynamics and the scattering spectrum. Finally, we have shown that this tool enables the analytical parametrization of the Jaynes–Cummings Hamiltonian describing light-matter interactions in these hybrid nanometric systems.

Acknowledgements

P.A.H. supported by the CEEC Individual program from Fundaçãao para a Ciência e a Tecnologia with reference CEECIND/03866/2017. She acknowledges funding from Fundaçãopara a Ciência e a Tecnologia and Instituto de Telecomunicações under project UID/50008/2020. A.I.F.-D. acknowledges funding from the Spanish MICINN under Contract RTI2018-099737-B-I00 and the

"María de Maeztu" programme for Units of Excellence in R&D (MDM-2014-0377). He was also supported by a 2019 Leonardo Grant for Researchers and Cultural Creators, BBVA Foundation.

References

[1] A. J. Ward, J. B. Pendry, "Refraction and geometry in Maxwell's equations", *J. Mod. Opt.* **43** (1996), no. 4, p. 773-793.
[2] J. B. Pendry, D. Schurig, D. R. Smith, "Controlling Electromagnetic Fields", *Science* **312** (2006), no. 5781, p. 1780-1782.
[3] H. Chen, C. T. Chan, P. Sheng, "Transformation optics and metamaterials", *Nat. Mater.* **9** (2010), no. 5, p. 387-396.
[4] F. Sun, B. Zheng, H. Chen, W. Jiang, S. Guo, Y. Liu, Y. Ma, S. He, "Transformation optics: from classic theory and applications to its new branches", *Laser Photon. Rev.* **11** (2017), no. 6, article ID 1700034.
[5] M. W. McCall, A. Favaro, P. Kinsler, A. Boardman, "A spacetime cloak, or a history editor", *J. Opt.* **13** (2010), no. 2, article ID 024003.
[6] M. Fridman, A. Farsi, Y. Okawachi, A. L. Gaeta, "Demonstration of temporal cloaking", *Nature* **481** (2012), no. 7379, p. 62.
[7] U. Leonhardt, T. G. Philbin, "General relativity in electrical engineering", *New J. Phys.* **8** (2006), no. 10, p. 247.
[8] A. Greenleaf, Y. Kurylev, M. Lassas, G. Uhlmann, "Electromagnetic wormholes and virtual magnetic monopoles from metamaterials", *Phys. Rev. Lett.* **99** (2007), no. 18, article ID 183901.
[9] I. I. Smolyaninov, E. E. Narimanov, "Metric signature transitions in optical metamaterials", *Phy. Rev. Lett.* **105** (2010), no. 6, article ID 067402.
[10] R. T. Thompson, S. A. Cummer, J. Frauendiener, "A completely covariant approach to transformation optics", *J. Opt.* **13** (2010), no. 2, article ID 024008.
[11] S. Horsley, C. King, T. Philbin, "Wave propagation in complex coordinates", *J. Opt.* **18** (2016), no. 4, article ID 044016.
[12] S. Horsley, M. Artoni, G. La Rocca, "Spatial kramers–kronig relations and the reflection of waves", *Nat. Photon.* **9** (2015), no. 7, p. 436.
[13] C. E. Rüter, K. G. Makris, R. El-Ganainy, D. N. Christodoulides, M. Segev, D. Kip, "Observation of parity–time symmetry in optics", *Nat. Phys.* **6** (2010), no. 3, p. 192.
[14] G. Castaldi, S. Savoia, V. Galdi, A. Alu, N. Engheta, "P t metamaterials via complex-coordinate transformation optics", *Phys. Rev. Lett.* **110** (2013), no. 17, article ID 173901.
[15] R. Mitchell-Thomas, T. McManus, O. Quevedo-Teruel, S. Horsley, Y. Hao, "Perfect surface wave cloaks", *Phys. Rev. Lett.* **111** (2013), no. 21, article ID 213901.
[16] S. Viaene, V. Ginis, J. Danckaert, P. Tassin, "Transforming two-dimensional guided light using nonmagnetic metamaterial waveguides", *Phys. Rev. B* **93** (2016), article ID 085429.
[17] O. Quevedo-Teruel, W. Tang, R. C. Mitchell-Thomas, A. Dyke, H. Dyke, L. Zhang, S. Haq, Y. Hao, "Transformation optics for antennas: why limit the bandwidth with metamaterials?", *Sci. Rep.* **3** (2013), p. 1903.
[18] D. Schurig, J. J. Mock, B. J. Justice, S. A. Cummer, J. B. Pendry, A. F. Starr, D. R. Smith, "Metamaterial electromagnetic cloak at microwave frequencies", *Science* **314** (2006), p. 977.
[19] S. A. Cummer, D. Schurig, "One path to acoustic cloaking", *New J. Phys.* **9** (2007), no. 3, p. 45.
[20] H. Chen, C. Chan, "Acoustic cloaking in three dimensions using acoustic metamaterials", *Appl. Phys. Lett.* **91** (2007), no. 18, article ID 183518.
[21] L. Zigoneanu, B.-I. Popa, S. A. Cummer, "Three-dimensional broadband omnidirectional acoustic ground cloak", *Nat. Mater.* **13** (2014), no. 4, p. 352-355.
[22] S. Zhang, D. A. Genov, C. Sun, X. Zhang, "Cloaking of matter waves", *Phys. Rev. Lett.* **100** (2008), no. 12, article ID 123002.
[23] S. Guenneau, C. Amra, D. Veynante, "Transformation thermodynamics: cloaking and concentrating heat flux", *Opt. Exp.* **20** (2012), no. 7, p. 8207-8218.
[24] G. W. Milton, M. Briane, J. R. Willis, "On cloaking for elasticity and physical equations with a transformation invariant form", *New J. Phys.* **8** (2006), no. 10, p. 248-248.
[25] N. Stenger, M. Wilhelm, M. Wegener, "Experiments on elastic cloaking in thin plates", *Phys. Rev. Lett.* **108** (2012), no. 1, article ID 014301.
[26] T. Bückmann, M. Thiel, M. Kadic, R. Schittny, M. Wegener, "An elasto-mechanical unfeelability cloak made of pentamode metamaterials", *Nat. Commun.* **5** (2014), p. 4130.
[27] T. Bückmann, M. Kadic, R. Schittny, M. Wegener, "Mechanical cloak design by direct lattice transformation", *Proc. Natl Acad. Sci. USA* **112** (2015), no. 16, p. 4930-4934.
[28] M. Brun, S. Guenneau, A. B. Movchan, "Achieving control of in-plane elastic waves", *Appl. Phys. Lett.* **94** (2009), no. 6, article ID 061903.
[29] S. Brûlé, E. H. Javelaud, S. Enoch, S. Guenneau, "Experiments on seismic metamaterials: molding surface waves", *Phys. Rev. Lett.* **112** (2014), article ID 133901.

[30] P. A. Huidobro, M. L. Nesterov, L. Martín-Moreno, F. J. García-Vidal, "Transformation optics for plasmonics", *Nano Lett.* **10** (2010), no. 6, p. 1985-1990.
[31] Y. Liu, T. Zentgraf, G. Bartal, X. Zhang, "Transformational plasmon optics", *Nano Lett.* **10** (2010), no. 6, p. 1991-1997.
[32] M. Kadic, G. Dupont, S. Guenneau, S. Enoch, "Controlling surface plasmon polaritons in transformed coordinates", *J. Mod. Opt.* **58** (2011), no. 12, p. 994-1003.
[33] M. Kadic, S. Guenneau, S. Enoch, S. A. Ramakrishna, "Plasmonic space folding: focusing surface plasmons via negative refraction in complementary media", *ACS Nano* **5** (2011), no. 9, p. 6819-6825.
[34] M. Kadic, S. Guenneau, S. Enoch, P. A. Huidobro, L. Martín-Moreno, F. J. García-Vidal, J. Renger, R. Quidant, "Transformation plasmonics", *Nanophotonics* **1** (2012), no. 1, p. 51-64.
[35] P. A. Huidobro, M. L. Nesterov, L. Martín-Moreno, F. J. García-Vidal, "Moulding the flow of surface plasmons using conformal and quasiconformal mappings", *New J. Phys.* **13** (2011), no. 3, article ID 033011.
[36] J. Renger, M. Kadic, G. Dupont, S. S. Aćimović, S. Guenneau, R. Quidant, S. Enoch, "Hidden progress: broadband plasmonic invisibility", *Opt. Express* **18** (2010), no. 15, p. 15757-15768.
[37] T. Zentgraf, Y. Liu, M. H. Mikkelsen, J. Valentine, X. Zhang, "Plasmonic luneburg and eaton lenses", *Nat. Nanotechnol.* **6** (2011), no. 3, p. 151.
[38] M. Alaoui, K. Rustomji, T. Chang, G. Tayeb, P. Sabouroux, R. Quidant, S. Enoch, S. Guenneau, R. Abdeddaim, "Cyclic concentrator, carpet cloaks and fisheye lens via transformation plasmonics", *J. Opt.* **18** (2016), no. 4, article ID 044023.
[39] J. Pendry, S. A. Ramakrishna, "Near-field lenses in two dimensions", *J. Phys.: Condens. Matter* **14** (2002), no. 36, p. 8463.
[40] L. Novotny, B. Hecht, *Principles of Nano-Optics*, Cambridge University Press, Cambridge, UK, 2012.
[41] A. Aubry, D. Y. Lei, S. A. Maier, J. Pendry, "Conformal transformation applied to plasmonics beyond the quasistatic limit", *Phys. Rev. B* **82** (2010), no. 20, article ID 205109.
[42] J. Pendry, A. Aubry, D. Smith, S. Maier, "Transformation optics and subwavelength control of light", *Science* **337** (2012), no. 6094, p. 549-552.
[43] Y. Luo, R. Zhao, A. I. Fernandez-Dominguez, S. A. Maier, J. B. Pendry, "Harvesting light with transformation optics", *Sci. China Information Sci.* **56** (2013), no. 12, p. 1-13.
[44] J. Pendry, Y. Luo, R. Zhao, "Transforming the optical landscape", *Science* **348** (2015), no. 6234, p. 521-524.
[45] A. Aubry, D. Y. Lei, A. I. Fernández-Domínguez, Y. Sonnefraud, S. A. Maier, J. B. Pendry, "Plasmonic light-harvesting devices over the whole visible spectrum", *Nano Lett.* **10** (2010), no. 7, p. 2574-2579.
[46] A. Fernández-Domínguez, S. Maier, J. Pendry, "Collection and concentration of light by touching spheres: a transformation optics approach", *Phys. Rev. Lett.* **105** (2010), no. 26, article ID 266807.
[47] A. Aubry, D. Y. Lei, S. A. Maier, J. Pendry, "Broadband plasmonic device concentrating the energy at the nanoscale: the crescent-shaped cylinder", *Phys. Rev. B* **82** (2010), no. 12, article ID 125430.
[48] A. I. Fernandez-Dominguez, Y. Luo, A. Wiener, J. Pendry, S. A. Maier, "Theory of three-dimensional nanocrescent light harvesters", *Nano Lett.* **12** (2012), no. 11, p. 5946-5953.
[49] M. Kraft, J. Pendry, S. Maier, Y. Luo, "Transformation optics and hidden symmetries", *Phys. Rev. B* **89** (2014), no. 24, article ID 245125.
[50] A. Aubry, D. Y. Lei, S. A. Maier, J. B. Pendry, "Plasmonic hybridization between nanowires and a metallic surface: a transformation optics approach", *ACS Nano* **5** (2011), no. 4, p. 3293-3308.
[51] J. Pendry, A. Fernández-Domínguez, Y. Luo, R. Zhao, "Capturing photons with transformation optics", *Nat. Phys.* **9** (2013), no. 8, p. 518.
[52] A. Fernández-Domínguez, A. Wiener, F. García-Vidal, S. Maier, J. Pendry, "Transformation-optics description of nonlocal effects in plasmonic nanostructures", *Phys. Rev. Lett.* **108** (2012), no. 10, article ID 106802.
[53] A. Fernández-Domínguez, P. Zhang, Y. Luo, S. Maier, F. García-Vidal, J. Pendry, "Transformation-optics insight into nonlocal effects in separated nanowires", *Phys. Rev. B* **86** (2012), no. 24, article ID 241110.
[54] M. Kraft, Y. Luo, J. Pendry, "Transformation optics: a time-and frequency-domain analysis of electron-energy loss spectroscopy", *Nano Lett.* **16** (2016), no. 8, p. 5156-5162.
[55] K. N. Reddy, P. Y. Chen, A. I. Fernández-Domínguez, Y. Sivan, "Surface second-harmonic generation from metallic-nanoparticle configurations: a transformation-optics approach", *Phys. Rev. B* **99** (2019), no. 23, article ID 235429.
[56] R. Zhao, Y. Luo, A. Fernández-Domínguez, J. B. Pendry, "Description of van der waals interactions using transformation optics", *Phys. Rev. Lett.* **111** (2013), no. 3, article ID 033602.
[57] Y. Luo, R. Zhao, J. B. Pendry, "van der Waals interactions at the nanoscale: the effects of nonlocality", *Proc. Natl Acad. Sci. USA* **111** (2014), no. 52, p. 18422-18427.
[58] S. Yu, H. Ammari, "Hybridization of singular plasmons via transformation optics", *Proc. Natl Acad. Sci. USA* **116** (2019), no. 28, p. 13785-13790, https://www.pnas.org/content/116/28/13785.full.pdf.
[59] C. L. Holloway, E. F. Kuester, J. A. Gordon, J. O'Hara, J. Booth, D. R. Smith, "An overview of the theory and applications of metasurfaces: the two-dimensional equivalents of metamaterials", *IEEE Antennas Propag. Mag.* **54** (2012), no. 2, p. 10-35.

[60] A. V. Kildishev, A. Boltasseva, V. M. Shalaev, "Planar photonics with metasurfaces", *Science* **339** (2013), no. 6125, article ID 1232009.
[61] A. E. Minovich, A. E. Miroshnichenko, A. Y. Bykov, T. V. Murzina, D. N. Neshev, Y. S. Kivshar, "Functional and nonlinear optical metasurfaces", *Laser Photonics Rev.* **9** (2015), no. 2, p. 195-213.
[62] S. B. Glybovski, S. A. Tretyakov, P. A. Belov, Y. S. Kivshar, C. R. Simovski, "Metasurfaces: from microwaves to visible", *Phys. Rep.* **634** (2016), p. 1-72.
[63] F. Monticone, A. Alù, "Metamaterial, plasmonic and nanophotonic devices", *Rep. Prog. Phys.* **80** (2017), no. 3, article ID 036401.
[64] P. A. Huidobro, A. I. Fernández-Domínguez, J. B. Pendry, L. Martin-Moreno, F. Garcia-Vidal, "Spoof surface plasmon metamaterials", in *Elements in Emerging Theories and Technologies in Metamaterials*, Cambridge University Press, Cambridge, UK, 2018.
[65] X. Ni, N. K. Emani, A. V. Kildishev, A. Boltasseva, V. M. Shalaev, "Broadband light bending with plasmonic nanoantennas", *Science* **335** (2012), no. 6067, p. 427-427.
[66] N. Yu, P. Genevet, M. A. Kats, F. Aieta, J.-P. Tetienne, F. Capasso, Z. Gaburro, "Light propagation with phase discontinuities: generalized laws of reflection and refraction", *Science (New York)* **334** (2011), no. 6054, p. 333-7.
[67] P. Genevet, F. Capasso, F. Aieta, M. Khorasaninejad, R. Devlin, "Recent advances in planar optics: from plasmonic to dielectric metasurfaces", *Optica* **4** (2017), no. 1, p. 139-152.
[68] N. Meinzer, W. L. Barnes, I. R. Hooper, "Plasmonic meta-atoms and metasurfaces", *Nat. Photon.* **8** (2014), no. 12, p. 889.
[69] F. H. L. Koppens, D. E. Chang, F. J. García de Abajo, "Graphene plasmonics: a platform for strong light-matter interaction", *Nano Lett.* **11** (2011), no. (8), p. 3370-3377.
[70] L. Ju, B. Geng, J. Horng, C. Girit, M. Martin, Z. Hao, H. A. Bechtel, X. Liang, A. Zettl, Y. R. Shen, F. Wang, "Graphene plasmonics for tunable terahertz metamaterials", *Nat. Nanotechnol.* **6** (2011), no. 10, p. 630-634.
[71] A. Y. Nikitin, F. Guinea, F. J. García-Vidal, L. Martín-Moreno, "Fields radiated by a nanoemitter in a graphene sheet", *Phys. Rev. B* **84** (2011), no. 19, article ID 195446.
[72] A. N. Grigorenko, M. Polini, K. S. Novoselov, "Graphene plasmonics", *Nat. Photon.* **6** (2012), no. 11, p. 749-758.
[73] T. Low, P. Avouris, "Graphene plasmonics for terahertz to mid-infrared applications", *ACS Nano* **8** (2014), no. 2, p. 1086-1101.
[74] J. Chandezon, G. Raoult, D. Maystre, "A new theoretical method for diffraction gratings and its numerical application", *J. Opt.* **11** (1980), no. 4, p. 235-241.
[75] W. L. Barnes, T. W. Preist, S. C. Kitson, J. R. Sambles, "Physical origin of photonic energy gaps in the propagation of surface plasmons on gratings", *Phys. Rev. B* **54** (1996), p. 6227-6244.
[76] M. Kraft, Y. Luo, S. A. Maier, J. B. Pendry, "Designing plasmonic gratings with transformation optics", *Phys. Rev. X* **5** (2015), no. 3, article ID 031029.
[77] P. A. Huidobro, Y. H. Chang, M. Kraft, J. B. Pendry, "Hidden symmetries in plasmonic gratings", *Phys. Rev. B* **95** (2017), no. 15, p. 1-8.
[78] P. A. Huidobro, M. Kraft, S. A. Maier, J. B. Pendry, "Graphene as a tunable anisotropic or isotropic plasmonic metasurface", *ACS Nano* **10** (2016), no. 5, p. 5499-5506.
[79] COMSOL, "Comsol multiphysics", 1998, published electronally at https://www.comsol.com/.
[80] J. B. Pendry, P. A. Huidobro, K. Ding, "Computing one-dimensional metasurfaces", *Phys. Rev. B* **99** (2019), article ID 085408.
[81] P. A. Huidobro, M. Kraft, R. Kun, S. A. Maier, J. B. Pendry, "Graphene, plasmons and transformation optics", *J. Opt.* **18** (2016), no. 4, article ID 044024.
[82] N. Peres, Y. V. Bludov, A. Ferreira, M. I. Vasilevskiy, "Exact solution for square-wave grating covered with graphene: surface plasmon-polaritons in the terahertz range", *J. Phys.: Condens. Matter* **25** (2013), no. 12, article ID 125303.
[83] T. M. Slipchenko, M. L. Nesterov, L. Martin-Moreno, a. Y. Nikitin, "Analytical solution for the diffraction of an electromagnetic wave by a graphene grating", *J. Opt. (Bristol, U. K.)* **15** (2013), no. 11, article ID 114008.
[84] P.-Y. Chen, C. Argyropoulos, M. Farhat, J. S. Gomez-Diaz, "Flatland plasmonics and nanophotonics based on graphene and beyond", *Nanophotonics* **6** (2017), no. 6, p. 1239-1262.
[85] M. Baudisch, A. Marini, J. D. Cox, T. Zhu, F. Silva, S. Teichmann, M. Massicotte, F. Koppens, L. S. Levitov, F. J. G. de Abajo *et al.*, "Ultrafast nonlinear optical response of dirac fermions in graphene", *Nat. Commun.* **9** (2018), no. 1, p. 1018.
[86] M. Bokdam, P. A. Khomyakov, G. Brocks, Z. Zhong, P. J. Kelly, "Electrostatic doping of graphene through ultrathin hexagonal boron nitride films", *Nano Lett.* **11** (2011), no. 11, p. 4631-4635.
[87] Y. Fan, N.-H. Shen, T. Koschny, C. M. Soukoulis, "Tunable terahertz meta-surface with graphene cut-wires", *ACS Photon.* **2** (2015), no. 1, p. 151-156.
[88] A. Y. Nikitin, F. Guinea, F. J. Garcia-Vidal, L. Martin-Moreno, "Surface plasmon enhanced absorption and suppressed transmission in periodic arrays of graphene ribbons", *Phys. Rev. B* **85** (2012), no. 8, article ID 081405(R).

[89] A. Vakil, N. Engheta, "Transformation optics using graphene", *Science (New York, N.Y.)* **332** (2011), no. 6035, p. 1291-1294.
[90] D. A. Iranzo, S. Nanot, E. J. Dias, I. Epstein, C. Peng, D. K. Efetov, M. B. Lundeberg, R. Parret, J. Osmond, J.-Y. Hong *et al.*, "Probing the ultimate plasmon confinement limits with a van der waals heterostructure", *Science* **360** (2018), no. 6386, p. 291-295.
[91] P. Huidobro, S. A. Maier, J. B. Pendry, "Tunable plasmonic metasurface for perfect absorption", *EPJ Appl. Metamat.* **4** (2017), p. 6.
[92] N. M. Estakhri, A. Alù, "Physics of unbounded, broadband absorption/gain efficiency in plasmonic nanoparticles", *Phys. Rev. B* **87** (2013), article ID 205418.
[93] H. Wallén, H. Kettunen, A. Sihvola, "Anomalous absorption, plasmonic resonances, and invisibility of radially anisotropic spheres", *Radio Sci.* **50** (2015), no. 1, p. 18-28.
[94] F. Yang, Y.-T. Wang, P. A. Huidobro, J. B. Pendry, "Nonlocal effects in singular plasmonic metasurfaces", *Phys. Rev. B* **99** (2019), article ID 165423.
[95] E. Galiffi, J. B. Pendry, P. A. Huidobro, "Broadband tunable THz absorption with singular graphene metasurfaces", *ACS Nano* **12** (2018), no. 2, p. 1006-1013.
[96] T. Søndergaard, S. M. Novikov, T. Holmgaard, R. L. Eriksen, J. Beermann, Z. Han, K. Pedersen, S. I. Bozhevolnyi, "Plasmonic black gold by adiabatic nanofocusing and absorption of light in ultra-sharp convex grooves", *Nat. Commun.* **3** (2012), p. 969.
[97] J. Pendry, P. A. Huidobro, Y. Luo, E. Galiffi, "Compacted dimensions and singular plasmonic surfaces", *Science* **358** (2017), no. 6365, p. 915-917.
[98] F. Yang, P. A. Huidobro, J. B. Pendry, "Transformation optics approach to singular metasurfaces", *Phys. Rev. B* **98** (2018), article ID 125409.
[99] E. Galiffi, J. B. Pendry, P. A. Huidobro, "Singular graphene metasurfaces", *EPJ Appl. Metamat.* **6** (2019), p. 10.
[100] F. Benz, M. K. Schmidt, A. Dreismann, R. Chikkaraddy, Y. Zhang, A. Demetriadou, C. Carnegie, H. Ohadi, B. de Nijs, R. Esteban, J. Aizpurua, J. J. Baumberg, "Single-molecule optomechanics in "picocavities"", *Science* **354** (2016), no. 6313, p. 726-729.
[101] F. Yang, E. Galiffi, P. A. Huidobro, J. Pendry, "Nonlocal effects in plasmonic metasurfaces with almost touching surfaces", *Phys. Rev. B* **101** (2020), no. 7, article ID 075434.
[102] E. Galiffi, P. A. Huidobro, P. A. D. Gonçalves, N. A. Mortensen, J. B. Pendry, "Probing graphene's nonlocality with singular metasurfaces", *Nanophotonics* **9** (2020), no. 2, p. 309-316.
[103] E. Muljarov, W. Langbein, "Resonant-state expansion of dispersive open optical systems: creating gold from sand", *Phys. Rev. B* **93** (2016), no. 7, article ID 075417.
[104] P. Y. Chen, D. J. Bergman, Y. Sivan, "Generalizing normal mode expansion of electromagnetic green's tensor to open systems", *Phys. Rev. Appl.* **11** (2019), no. 4, article ID 044018.
[105] C. Sauvan, J.-P. Hugonin, I. Maksymov, P. Lalanne, "Theory of the spontaneous optical emission of nanosize photonic and plasmon resonators", *Phys. Rev. Lett.* **110** (2013), no. 23, article ID 237401.
[106] P. T. Kristensen, S. Hughes, "Modes and mode volumes of leaky optical cavities and plasmonic nanoresonators", *ACS Photon.* **1** (2013), no. 1, p. 2-10.
[107] M. I. Abdelrahman, B. Gralak, "Completeness and divergence-free behavior of the quasi-normalmodes using causality principle", *OSA Contin.* **1** (2018), p. 340-348.
[108] J. Yang, M. Perrin, P. Lalanne, "Analytical formalism for the interaction of two-level quantum systems with metal nanoresonators", *Phys. Rev. X* **5** (2015), no. 2, article ID 021008.
[109] S. Hughes, M. Richter, A. Knorr, "Quantized pseudomodes for plasmonic cavity qed", *Opt. Lett.* **43** (2018), no. 8, p. 1834-1837.
[110] S. Franke, S. Hughes, M. K. Dezfouli, P. T. Kristensen, K. Busch, A. Knorr, M. Richter, "Quantization of quasinormal modes for open cavities and plasmonic cavity quantum electrodynamics", *Phys. Rev. Lett.* **122** (2019), no. 21, article ID 213901.
[111] H. T. Dung, L. Knöll, D.-G. Welsch, "Three-dimensional quantization of the electromagnetic field in dispersive and absorbing inhomogeneous dielectrics", *Phys. Rev. A* **57** (1998), no. 5, p. 3931.
[112] R.-Q. Li, D. Hernángomez-Pérez, F. García-Vidal, A. Fernández-Domínguez, "Transformation optics approach to plasmon-exciton strong coupling in nanocavities", *Phys. Rev. Lett.* **117** (2016), no. 10, article ID 107401.
[113] R.-Q. Li, F. García-Vidal, A. Fernandez-Dominguez, "Plasmon-exciton coupling in symmetry-broken nanocavities", *ACS Photon.* **5** (2018), no. 1, p. 177-185.
[114] V. Pacheco-Peña, M. Beruete, A. I. Fernández-Domínguez, Y. Luo, M. Navarro-Cía, "Description of bow-tie nanoantennas excited by localized emitters using conformal transformation", *Acs Photon.* **3** (2016), no. 7, p. 1223-1232.
[115] V. Pacheco-Peña, A. I. Fernández-Domínguez, Y. Luo, M. Beruete, M. Navarro-Cía, "Aluminum nanotripods for light-matter coupling robust to nanoemitter orientation", *Laser Photonics Rev.* **11** (2017), no. 5, article ID 1700051.
[116] A. Cuartero-González, A. Fernández-Domínguez, "Light-forbidden transitions in plasmon-emitter interactions beyond the weak coupling regime", *ACS Photon.* **5** (2018), no. 8, p. 3415-3420.

[117] A. Cuartero-González, A. Fernández-Domínguez, "Dipolar and quadrupolar excitons coupled to a nanoparticle-on-a-mirror cavity", *Phys. Rev. B* **101** (2020), article ID 035403.
[118] H.-P. Breuer, F. Petruccione *et al.*, *The Theory of Open Quantum Systems*, Oxford University Press on Demand, Oxford, UK, 2002.
[119] A. González-Tudela, P. Huidobro, L. Martín-Moreno, C. Tejedor, F. García-Vidal, "Reversible dynamics of single quantum emitters near metal-dielectric interfaces", *Phys. Rev. B* **89** (2014), no. 4, article ID 041402.
[120] A. Delga, J. Feist, J. Bravo-Abad, F. Garcia-Vidal, "Quantum emitters near a metal nanoparticle: strong coupling and quenching", *Phys. Rev. Lett.* **112** (2014), no. 25, article ID 253601.
[121] V. Giannini, A. I. Fernández-Domínguez, S. C. Heck, S. A. Maier, "Plasmonic nanoantennas: fundamentals and their use in controlling the radiative properties of nanoemitters", *Chem. Rev.* **111** (2011), no. 6, p. 3888-3912.
[122] A. Demetriadou, J. M. Hamm, Y. Luo, J. B. Pendry, J. J. Baumberg, O. Hess, "Spatiotemporal dynamics and control of strong coupling in plasmonic nanocavities", *ACS Photon.* **4** (2017), no. 10, p. 2410-2418.
[123] R. Esteban, J. Aizpurua, G. W. Bryant, "Strong coupling of single emitters interacting with phononic infrared antennae", *New J. Phys.* **16** (2014), no. 1, article ID 013052.
[124] R. Sáez-Blázquez, J. Feist, A. Fernández-Domínguez, F. García-Vidal, "Enhancing photon correlations through plasmonic strong coupling", *Optica* **4** (2017), no. 11, p. 1363-1367.
[125] F. P. Laussy, E. Del Valle, C. Tejedor, "Strong coupling of quantum dots in microcavities", *Phys. Rev. Lett.* **101** (2008), no. 8, article ID 083601.
[126] R. Sáez-Blázquez, J. Feist, F. García-Vidal, A. Fernández-Domínguez, "Photon statistics in collective strong coupling: nanocavities and microcavities", *Phys. Rev. A* **98** (2018), no. 1, article ID 013839.

Comptes Rendus
Physique
2020, 21, nº 4-5, p. 409-423
https://doi.org/10.5802/crphys.6

Metamaterials 1 / *Métamatériaux 1*

A review of anomalous resonance, its associated cloaking, and superlensing

Résonance anormale, invisibilité et super-resolution associée : état de l'art

Ross C. McPhedran[*, a] **and Graeme W. Milton**[b]

[a] School of Physics, The University of Sydney, Australia

[b] Department of Mathematics, University of Utah, USA

E-mails: ross.mcphedran@sydney.edu.au (R. C. McPhedran), milton@math.utah.edu (G. W. Milton)

Abstract. We review a selected history of anomalous resonance, cloaking due to anomalous resonance, cloaking due to complementary media, and superlensing.

Résumé. Nous passons en revue quelques faits saillant de l'historique de la résonance anormale, de l'invisibilité associée à la résonance anormale, et celle associée aux milieux complémentaires et de la super-résolution.

Keywords. Anomalous resonance, Cloaking, Superlensing.

Mots-clés. Résonance anormale, Invisibilité, Super-résolution.

1. Introduction

In usual resonance as the loss goes to zero, one is approaching a pole of the associated linear response function. By contrast, anomalous localized resonance (ALR) is associated with the approach to an essential singularity. The connection with essential singularities is evident in Figure 8 of [1] and shown explicitly in the analysis in [2], where the underlying theory was developed. Anomalous resonance has the following three defining features:

1. As the loss goes to zero, finer and finer scale oscillations develop as modes increasingly close to the essential singularity become excited.
2. As the loss goes to zero, the oscillations blow up to infinity in a region which is called the region of anomalous resonance, but outside of this region the fields converge to a smooth field.

* Corresponding author.

3. The boundary of the region of anomalous resonance depends on the source position.

It is to be emphasized that the approach to an essential singularity does not necessarily imply anomalous resonance. In particular, anomalous resonance does not occur for coated spheres, with the coating and the core each being isotropic and having constant complex dielectric constant [2]. (It can occur if one allows for an anisotropic coating [3]). Also anomalous resonance, defined in this way, should be distinguished from the unusual feature that, in the presence of materials with negative properties, corners or other singularities in the microstructure can behave like sinks of energy in the limit where the loss parameters of the materials tends to zero: see page 378 of [4, 5], Section 2 of [6] and [7, 8]. Such behavior is associated with branch cuts. For further mathematical development see [9–12].

Here we will review anomalous resonance and its associated cloaking. We will also review the closely related topic of superlensing which would not be possible without anomalous resonance: anomalous resonance provides the essential mechanism for a superlens producing an image of a point source beating the diffraction limit. At the same time it prevents the formation of a correct image when a dielectric object being imaged is too close to the superlens. This is contrary to what one would believe from reading most of the literature on superlenses, since this limitation is rarely pointed out both in published papers and in popular articles on the internet (such as in Wikipedia). It is unfortunate that wrong ideas may continue to propagate. This paper aims to contribute to correct the situation. At this stage the literature is so vast that we can only cover, or even reference, a selected subset of papers, partly chosen for their importance and partly chosen because we are familiar with them.

Our analysis and the analysis in the papers that we cite will mostly be for quasistatics. It is important to remember that quasistatics does not necessarily mean that the frequency of the applied field tends to zero. A better procedure is that, at any fixed frequency ω_0, the dimensions of the system should be shrunk to a size where they are much smaller than the free space wavelength for the quasistatic approximation to be valid.

2. The discovery of anomalous resonance and ghost sources

Back in 1993 we investigated with Nicolae Nicorovici the quasistatic effective properties of a square array of coated cylinders each having core dielectric constant ε_c and radius r_c, and with shell dielectric constant ε_s and outer radius r_s, and embedded in a matrix having dielectric constant 1 [1]. Surprisingly, we found that when $\varepsilon_s = -1$ the array had exactly the same effective dielectric constant as a square array of solid cylinders having core dielectric constant ε_c and radius $r_0 = r_s^2/r_c$ embedded in a matrix having dielectric constant 1. We subsequently looked at a single coated cylinder, with the z-axis as its cylinder axis, in an infinite medium of dielectric constant 1 subject to a non-uniform applied field at infinity independent of z [13]. Again, when $\varepsilon_s = -1$, it was found that the effect of the shell was to magnify the core by a factor of r_s^2/r_c^2 so its response was equivalent to a solid cylinder having core dielectric constant ε_c and radius $r_0 = r_s^2/r_c$. As the equivalent solid cylinder could have a very large radius when r_c is small, this marked the first discovery (in quasistatics) of what became known (for the full time-harmonic Maxwell's equations) as a superscatterer [14]. When $\varepsilon_c = 1$ we observed that the coated cylinder becomes invisible to any applied quasistatic field: in this sense, the shell cloaks the core. Inclusions that are invisible to any applied field at a prescribed frequency (not necessarily in the quasistatic regime) were also found by Dolin [15] as an example illustrating his discovery of what is now known as transformation optics. Later, Alu and Engheta [16] found that coated spheres, built from appropriate materials, could be invisible to incident plane waves at a prescribed frequency, thus extending the quasistatic results of Kerker [17]. To illuminate our discoveries further we investigated, in the same paper [13], the infinite body Green's function (fundamental solution)

for a single coated cylinder in a matrix having dielectric constant 1 with a line dipole source at a distance z_0 from the cylinder axis. If the equivalence held, then when $\varepsilon_c \neq 1$ by the method of images the exterior field should be the same as the field generated by the source line dipole and an image line dipole at the radius $r_0^2/z_0 = r_s^4/(z_0 r_c^2)$. This represents a paradox when $r_0^2/z_0 > r_s$, i.e. when $z_0 < r_s^3/r_c^2$ (the latter being greater than r_s), as then the image line dipole lies outside the coated cylinder, i.e. there is a source there but we have not physically introduced such a source. To resolve this paradox we recognized that any material with a negative dielectric constant should also have some imaginary part due to resistive losses, and therefore one should set $\varepsilon_s = -1 + \mathrm{i}\delta$ and take the limit $\delta \to 0$. Doing this we found that the field outside the radius r_0^2/z_0 converged to the field one expected, i.e that due to the source dipole and (a ghost source) image dipole at the radius r_0^2/z_0. Inside the radius r_0^2/z_0 (and outside the coated cylinder) the field exhibited large oscillations whose amplitude diverged and wavelength decreased as $\delta \to 0$. This marked the first discovery of ghost sources and anomalous resonance: see Figure 1. See also the unpublished introduction [18] written prior to 1996. Anomalous resonance occurs when as the loss goes to zero the field diverges in one region (the region of anomalous resonance) that is dependent on the position of the source, but converges to a smooth field outside this region. Insight into anomalous resonance can be obtained simply by considering the series expansion for a pole at the point $z = 1$ in the complex $z = x + \mathrm{i}y$-plane (not to be confused with the z-axis):

$$1/(1-z) = 1 + z + z^2 + z^3 \ldots \tag{2.1}$$

If we truncate at high order the function on the right we obtain a polynomial that inside the radius of convergence $|z| < 1$ almost looks like it has a singularity at $z = 1$ (corresponding to a ghost source) but outside the radius of convergence (corresponding to the region of anomalous resonance) exhibits enormous oscillations. The difficulty is finding systems where the series truncation is somehow correlated with the loss in the system, as in the anomalously resonant coated cylinder system.

3. Anomalous resonance and ghost sources in superlenses

Anomalous resonance and ghost sources were rediscovered, both in numerical simulations and in theoretical works [19–26], that analyzed and provided the first sound basis for Pendry's bold claim [27] that the Veselago lens [28] consisting of a slab of thickness d having dielectric constant -1 and relative magnetic permeability -1 would act as a superlens, capable of breaking Abbe's diffraction limit and focusing light to arbitrarily small length scales. In fact, anomalous resonance and ghost sources provide the necessary mechanism for superlensing. The papers [23, 29–31] show that there is an essential singularity associated with this problem too. With a point dipole source a distance $d_0 < d$ from the lens, and with a slab having a dielectric constant of $-1+\mathrm{i}\delta$ and a relative magnetic permeability $-1+\mathrm{i}\delta$, in the limit $\delta \to 0$ two (possibly overlapping) anomalously resonant regions of width $2(d-d_0)$ develop around the two slab interfaces, and a ghost dipole source appears at the position of the expected image, at a point a distance $d-d_0$ from the slab, on the opposite side of slab from the source. The wavelength of the oscillations in the anomalously resonant regions sets the length scale of resolution of the image ghost source. The connection with our earlier work on the coated cylinder becomes clearer once one realizes that a slab can be regarded as a coated cylinder of infinite radius keeping $d = r_s - r_c$ fixed as $r_c \to \infty$. In this limit our earlier analysis corresponds to a line dipole outside the Veselago lens in the quasistatic limit. This connection is made more explicit in the analysis of Section 4 of [32]. Moreover, even at high frequencies where the free-space wavelength is comparable or smaller than d, the fields in the anomalously resonant regions remain the same as in the quasistatic approximation because the field gradients are so large that the quasistatic approximation remains valid there (see (4.25)

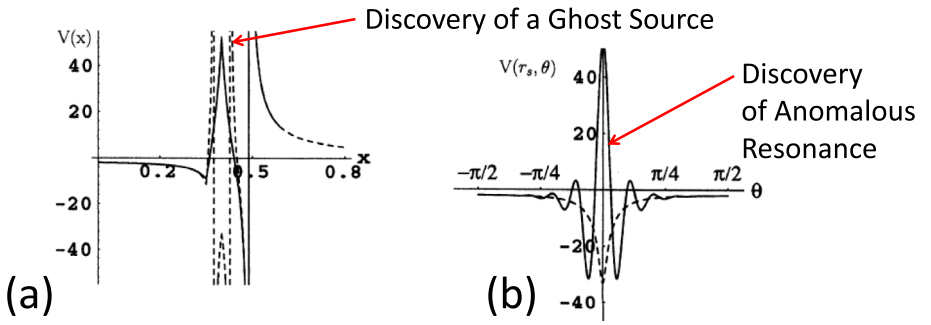

Figure 1. Reproduction, with permission, of Figure 2 of [13] highlighting our discoveries of ghost sources and anomalous resonance. The red arrows and accompanying text are new and are inserted to emphasize our findings. The solid curves show the actual potential, along the x-axis in (a) and around the outer surface of the coated cylinder, with parameters $\delta = 0.01$, $z_0 = 0.49$, $r_c = 0.35$, $r_s = 0.40$, $r_0 = 0.457$, and $r_0^2/z_0 = 0.426$. The latter radius, where the ghost source is located, is outside the coated cylinder. Outside this radius the solid curve in (a) slowly converges as $\delta \to 0$ to the dashed curve that has a singularity at this radius, representing the ghost source. The proof of convergence was established based on the ratio test for the series expansion for the actual potential. The large oscillations of the potential in (b) clearly show the anomalous resonance. There were some mistakes in our initial analysis, but everything was correct for the case considered here of a source on the real axis.

and (4.26) and the discussion below them in [33]). Our coated cylinder with $\varepsilon_s = -1$ and $\varepsilon_c = 1$ became known as the perfect cylindrical lens [34] or cylindrical superlens.

It is important to recognize that when $d_0 < d$ the anomalously resonant regions occur around both interfaces of the slab. Their presence is crucial to energy conservation as when $d_0 < d/2$ they interact with the source and provide the "radiation resistance" needed to account for the energy flowing towards the regions of anomalous resonance which is dissipated into heat there. When these anomalously resonant regions interact with the source they can destroy the claimed "perfect imaging" properties of the Veselago lens. On the other hand, when $d > d_0 > d/2$, then the image is in the region of anomalous resonance and it again can destroy the "perfect imaging" properties of the lens when the fields are measured at the plane through the ghost source [32]. In the presence of anomalously resonant fields acting on the source it is physically unlikely that the source will not react to these fields as otherwise the energy flowing to a source of fixed amplitude needs to be exactly tailored according to the magnitude of the anomalously resonant fields acting on the source.

With a line dipole source outside the slab lens the electrical potential in its near vicinity takes the form,

$$V = V_0 + \frac{k_e \cos\theta}{r} - \frac{k_o \sin\theta}{r} - E_x r\cos\theta - E_y r\sin\theta + O(r^2) \tag{3.1}$$

where V_0 is an additive constant, k_e and k_o are possibly complex constants governing the amplitude of the dipole line source, and E_x and E_y are the cartesian components of the field acting on the line source (defined by (3.1)), and (r,θ) are polar coordinates around the line source. Then the quasistatic formula for energy conservation takes the form (see [32]):

$$\begin{aligned}(\omega_0/2)\int_\Omega \varepsilon''\mathbf{E}\cdot\bar{\mathbf{E}} &= (\omega_0/2)\mathrm{Imag}\int_\Omega \mathbf{D}\cdot\bar{\mathbf{E}} = (\omega_0/2)\mathrm{Imag}\int_{\partial\Omega} -\varepsilon\frac{\partial V}{\partial \underline{r}}\bar{V} \\ &= \omega_0\pi\mathrm{Imag}[\bar{k}_e E_x - \bar{k}_o E_y]\end{aligned} \tag{3.2}$$

where the quantity on the left is the power generated per unit length of the line source, Ω is a two-dimensional domain consisting of a cross-sectional plane with an infinitesimal circle surrounding the source cut out from it, and the overline denotes complex conjugation. Notice that the energy flowing from (or to) the source (or sink) is dependent on the values of E_x and E_y. When the dipole source is in the region of anomalous resonance the fields E_x and E_y scale like $|\delta|^{2(d_0/d)-1}|\log\delta|$ which agrees with the scaling of the loss in the lens as demanded by (3.2). This blows up to infinity as $\delta \to 0$ when $d_0 < d/2$.

4. Cloaking due to anomalous resonance

In 2005 (private communication) Alexei Efros remarked that something was amiss in everyones understanding of the superlens. He had calculated the result just mentioned: that when $d_0 < d/2$ the electrical power consumed by the superlens (in the regions of anomalous resonance) with a constant amplitude source approaches infinity as $\delta \to 0$. He had thought that energy was not conserved and that therefore the concept of the superlens was flawed. In a closer analysis we found (at least in the quasistatic limit) that (3.2) shows energy is conserved. As δ is reduced, ever increasing amounts of power are drawn from the source due to its interaction with the anomalously resonant fields. The anomalously resonant fields provide a sort of "optical molasses" against which the source has to work – it is a type of radiation resistance. If one thinks of the source as being generated say by oscillating charges, then the forces generated by the anomalously resonant fields acting on these charges are directed in constant opposition to their movement.

Later we realized that since any realistic dipole source, such as a source providing constant power or a polarizable dipole (which becomes a source in the presence of an incident field) cannot provide ever increasing amounts of power, its amplitude must go to zero as $\delta \to 0$. In this limit it will become invisible outside the region of anomalous resonance – it should become cloaked. We then proved this for an arbitrary finite number of polarizable line dipoles, or constant power dipole sources, outside the quasistatic coated cylinder that lie within the cloaking region [33]. In particular, as proved in Section 3 of that paper, if the total power produced by the dipole sources remains bounded, then the amplitude of each and every dipole in the cloaking region must go to zero in the limit $\delta \to 0$. With polarizable dipoles inside the cloaking region, the field acting on each of them must tend to zero as $\delta \to 0$. Our paper was perhaps the first to introduce the word "cloaking" into the scientific literature, outside computer science. Shortly after the publication of our paper, the transformation based cloaking approaches of Pendry *et al.* [35] and Leonhardt [36] appeared, for the time harmonic Maxwell equation and for geometric optics respectively: the former can be regarded as a combination of the transformation optics ideas for electromagnetism, which date back to Dolin [15], and singular cloaking transformations, which date back to Greenleaf *et al.* [37]. One of the interesting features of cloaking due to anomalous resonance, as opposed to transformation based cloaking, is that the cloaking region lies outside the cloak. Rather than guiding fields around a collection of polarizable line dipoles in the cloaking region, the fields generated in the anomalously resonant regions are such as to almost cancel the fields acting on each polarizable line dipole. In the limit $\delta \to 0$, the nodal lines of the total field amazingly arrange themselves so as to almost intersect all polarizable line dipoles in the cloaking region. Numerical analysis [33, 38] confirmed these predictions, and moreover showed that a line quadrupole in the cloaking region outside would be cloaked as well. The original paper also established cloaking of a polarizable line dipole outside the slab lens at all frequencies (not just in the quasistatic limit) and for a point dipole outside the three-dimensional slab lens in the quasistatic limit. In that paper it was suggested that "it may be the case that any object of finite extent lying entirely within the cloaking region of the slab lens will

be cloaked" (in the limit as $\delta \to 0$). While, for the coated cylinder, initial calculations of Bruno and Lintner [39] suggested otherwise, a recent rigorous proof of Nguyen [40] has shown amazingly that cylindrical objects having a small but finite cross section that are near the coated cylinder are perfectly cloaked in the limit $\delta \to 0$. This extended earlier work of [41] that proved cloaking due to anomalous resonance of a cylinder with a radius going to zero as $\delta \to 0$. Even the paper of Bruno and Lintner established that small dielectric objects in the cloaking region can be partially cloaked in the limit as $\delta \to 0$. The important conclusion is that the cylindrical superlens (and presumably also the slab superlens) does not properly image dielectric objects close to the lens even in the limit $\delta \to 0$.

As recognized by Leonhardt and Philbin [42] the superlens can be obtained by using transformations to "unfold" a folded geometry having $\varepsilon' = \mu' = 1$ everywhere. In two-dimensions the unfolding transformation is simply the inverse of the folding transformation,

$$x' = x,\ y' = y \quad \text{for } x < 0; \quad x' = -x,\ y' = y \quad \text{for } 0 < x < d; \quad x' = x - 2d,\ y' = y \quad \text{for } x > d. \tag{4.1}$$

Using the rules of transformation optics this results in a material with

$$\varepsilon = \mu = 1 \quad \text{for } x < 0 \text{ and for } x > d; \quad \varepsilon = \mu = -1 \quad \text{for } 0 < x < d, \tag{4.2}$$

which is the superlens. This is consistent with the mirroring property of each interface in a superlens [43]. Anomalous resonance and cloaking also exist in other "folded" and equivalent "unfolded geometries" [3, 44]. In these folded geometries (unlike in the folded geometry of Leonhardt and Philbin) it is important to keep the fields on the different "sheets" separate to analyze the anomalous resonance and associated cloaking. In the unfolded geometries the material in the shell generally has a position dependent anisotropic dielectric tensor field.

Anomalous resonance due to cloaking with a continuous source in the cloaking region (rather than a discrete set of dipoles) was first investigated in [2]. The magnitude of the source is scaled so the net time averaged average power dissipation,

$$(\omega_0/2)\int_{\mathbb{R}^d} \varepsilon'' \mathbf{E}\cdot\bar{\mathbf{E}} = \delta(\omega_0/2)\int_{\text{lens}} \mathbf{E}\cdot\bar{\mathbf{E}} \tag{4.3}$$

remains constant as $\delta \to 0$. Then cloaking due to anomalous resonance is said to occur if the field becomes localized (in the region of anomalous resonance) and converges to zero outside of it. That paper also introduced the concept of weak cloaking due to anomalous resonance (weak CLAR). In that scenario cloaking due to anomalous resonance occurs for a sequence of values of δ tending to zero, but not necessarily for all sequences of values of δ tending to zero (which would imply strong CLAR).

One may ask if cloaking due to anomalous resonance applies to coated bodies of shapes that are not cylindrical. Then the separation of variables method in [2,32,33] is not appropriate. Using a variational approach Kohn, Lu, Schweizer and Weinstein [45] establish that quasistatic cloaking due to anomalous resonance occurs with a variety of cylindrical geometries that have a non-circular inner core, but a circular outer boundary. Kettunen, Lassas and Ola [46] went beyond the quasistatic limit and studied anomalous resonance and its absence in a variety of shaped bodies containing isotropic material in two and higher dimensions.

One may also ask if anomalous resonance and cloaking due to anomalous resonance occurs in other physical equations. Using a direct mathematical exact equivalence between the complex quasistatic equations and certain magnetoelectric or thermoelectric equations (see Section 6 in [32]) it follows that anomalous resonance and the associated cloaking occurs in these systems of equations as they loose ellipticity in an appropriate way. Also anomalous resonance and cloaking due to anomalous resonance has been shown to occur in the quasistatic elasticity equations [47–49]. In these papers they find that this occurs at the essential singularity of the

relevant Neumann–Poincaré operator. Assuming the Lame moduli of the two phases to be λ_1, μ_1 and $\lambda_2 = c\lambda_1$, $\mu_2 = c\mu_2$ they find this occurs in two-dimensions when

$$c = -\frac{\lambda_1 + 3\mu_1}{\lambda_1 + \mu_1} = -\frac{\kappa_1 + 2\mu_1}{\kappa_1}, \quad \text{or} \quad c = -\frac{\lambda_1 + \mu_1}{\lambda_1 + 3\mu_1} = -\frac{\kappa_1}{\kappa_1 + 2\mu_1}, \tag{4.4}$$

where $\kappa_1 = \lambda_1 + \mu_1$ is the bulk modulus of phase 1. Let $\kappa_2 = \lambda_2 + \mu_2 = c\kappa_1$ be the bulk modulus of phase 2. Now in any simply connected region that is devoid of a sources a stress field that solves the elasticity equations will also solve the elasticity equations if a constant is added to the inverse shear moduli, and the same constant subtracted from the inverse bulk moduli (see Section 4.5 of [4] and references therein). This strongly suggests that one can remove the constraint that the Lame moduli of phase 2 are a multiple c of the Lame moduli of phase 1, and that more generally anomalous resonance and cloaking will occur in these two-dimensional systems when

$$\nu_1 E_2 - \nu_2 E_1 = 3E_2 + E_1 \quad \text{or} \quad \nu_2 E_1 - \nu_1 E_2 = 3E_1 + E_2, \tag{4.5}$$

in which

$$\nu_1 = \frac{\kappa_1 - \mu_1}{\kappa_1 + \mu_1}, \quad \nu_2 = \frac{\kappa_2 - \mu_2}{\kappa_2 + \mu_2}, \quad E_1 = \frac{4\kappa_1\mu_1}{\kappa_1 + \mu_1}, \quad E_2 = \frac{4\kappa_2\mu_2}{\kappa_2 + \mu_2} \tag{4.6}$$

are the Poisson's ratios, and Young's moduli of the two phases. Anomalous resonance and cloaking have also been shown to occur for elastodynamics, without making a quasistatic approximation [50].

We remark that transformation based cloaking associated with many other physical equations has also been extensively studied and experimentally observed. The list is too long to include here, especially as transformation based cloaking is not the focus of this review.

5. A closer analysis of the lossless perfect lens and in the limit as the dispersion goes to zero

For a long while the hope persisted that the Veselago lens would be perfect if the lens was truly lossless. However, then there is no solution to the time harmonic equations with a dipole energy source a distance $d_0 < d$ from the lens unless one inserts a energy sink at the image point in the lens and an energy source at the image point outside the lens: each interface of the lens mirrors the field (or its extension) [43] and thus mirrors the field singularity. Each mirrored field singularity is interpreted as a sink or source depending on whether there is a net flow of energy towards it or away from it: see the numerical simulations in [51]. Physically inserting such sources or sinks assumes prior knowledge of the source and thus clearly diminishes the utility of the lens, so we disregard this possibility.

As discussed in [52] insight into the behavior of the lossless Veselago lens can be obtained by taking a source that is turned on at some time. From (62) in [53] it is seen that a source of constant strength E_0 switched on at $t = 0$ creates an electric field which near the back interface (and outside the lens) scales approximately as

$$E \sim E_0 t^{1-d_0/d}. \tag{5.7}$$

The stored electrical energy $S_E(t)$ will scale as the square of this, and consequently the time derivative of the stored electrical energy will scale approximately as

$$\frac{\mathrm{d}S_E}{\mathrm{d}t} \sim E_0^2 t^{1-2d_0/d}, \tag{5.8}$$

which blows up to infinity as $t \to \infty$ when $d_0 < d/2$. If the source produces a bounded amount of energy per unit time we have a contradiction. The conclusion is that if the energy production rate of the source is bounded then necessarily the amplitude E_0 must decrease to zero as $t \to \infty$.

More can be said [52] if we take a source that is turned on exponentially slowly, i.e. with a time dependence $e^{t/T}e^{-i\omega_0 t} = e^{-i\omega t}$ corresponding to a complex frequency $\omega = \omega_0 + i/T$ where T is a measure of the time the source has been "switched on" prior to time $t = 0$. (At times say before $t = -10T$ the source amplitude in negligibly small while for times between $t = -T/10$ and $t = 0$ is approximately constant). For simplicity we only analyze the quasistatic case, but similar conclusions should hold when one considers the full Maxwell equations.

Around the frequency ω_0 the dielectric constant in the shell has an expansion

$$\varepsilon_s = -1 + (\omega - \omega_0)a + O((\omega - \omega_0)^2) = -1 + ia/T + O(1/T^2), \quad \text{where } a = \left.\frac{d\varepsilon_s(\omega)}{d\omega}\right|_{\omega=\omega_0}, \tag{5.9}$$

and a is the dispersion at the frequency ω_0. Thus at long times T the mathematical analysis is the same as in the time harmonic case with the dielectric constant of the shell having a very small imaginary part $\delta \approx a/T$. A correspondence of this sort was noted before [53] but not fully exploited. Crucially, the anomalously resonant region in front of the lens still persists and again causes cloaking. After the source has been "switched on", say between times $t = -T/10$ and $t = 0$, the fields are very nearly time-harmonic. With $a > 0$ the electrical power produced by the source, say averaged over this time period, will be again given by the right hand side of (3.2) and for fixed source amplitudes k_e and k_o will scale like

$$|\delta|^{2(d_0/d)-1}|\log\delta| \approx |a/T|^{2(d_0/d)-1}|\log(a/T)| \tag{5.10}$$

and diverge as $T \to \infty$. If we want to avoid this power divergence then we need to rescale the source amplitudes k_e and k_o by the reciprocal of the quantity in (5.10). Then k_e and k_o will go to zero as $T \to \infty$, i.e. the source will be cloaked as $T \to \infty$. Thus we arrive at a scenario where the source fades from view, both when it is viewed from behind and in front of the lens, as the time "T" during which it is switched on is increased: essentially all of its energy is drawn to build up the fields in the regions of anomalous resonance [52]. (A somewhat analogous effect occurs with band-limited superresolution [54] where, as the width of the focal spot is decreased, increasingly more energy is necessarily diverted to the side lobes and, correspondingly, the relative amplitude at the image spot necessarily decreases [55].) With this scaling, the fields in the slab lens become localized to within the regions of anomalous resonance as $T \to \infty$. When $d > d_0 > d/2$, then the image is in the region of anomalous resonance and it again can destroy the "perfect imaging" properties of the lens. The interference of the surface waves associated with anomalous resonance and the image was also concluded by Collin [29] in a more complete analysis.

If we let $\mathbf{E}(\mathbf{x})$ denote the complex field that solves the time harmonic equations with $\varepsilon_s = -1 + ia/T$, then the physical electric field that solves the equations in the lossless perfect lens should at large times T be approximately

$$\widetilde{\mathbf{E}}(\mathbf{x}, t) = \mathrm{Re}[e^{i(\omega_0 + i/T)t}\mathbf{E}(\mathbf{x})] = e^{-t/T}\mathrm{Re}[e^{i\omega_0 t}\mathbf{E}(\mathbf{x})]. \tag{5.11}$$

We consider four cases:

(i) $a > 1/\omega_0$ so that the local electric field energy density in the slab is positive. At the frequency ω_0 this energy density is given by the Brillouin energy:

$$W_s(\mathbf{x}, t) \approx \frac{\mathrm{d}}{\mathrm{d}\omega}(\omega\varepsilon_s(\omega))|\widetilde{\mathbf{E}}(\mathbf{x}, t)|^2 \approx [-1 + a\omega_0]|\widetilde{\mathbf{E}}(\mathbf{x}, t)|^2 \approx \mathrm{e}^{2t/T}[-1 + a\omega_0]|\mathbf{E}(\mathbf{x})|^2 \tag{5.12}$$

In fact if the material in the slab is passive one has the tighter inequality that $a > 4/\omega_0$ [52,53,56]. Note that while there is no loss either in the slab or surrounding it, there is a buildup of the electrical energy density $W_s(\mathbf{x})$ given by the Brillouin formula. Thus it will appear that there is an absorption of energy given by

$$P_s(\mathbf{x}, t) = \frac{\mathrm{d}}{\mathrm{d}t} W_s(\mathbf{x}, t) = 2\mathrm{e}^{2t/T}[-1 + a\omega_0]|\mathbf{E}(\mathbf{x})|^2/T \tag{5.13}$$

(ii) $1/\omega_0 > a > 0$ so that the local electrical field energy density in the slab, given by the Brillouin formula, is negative, which requires the slab to be an active material

(iii) $a = 0$ so that there is absolutely no dispersion, which again requires an active material in the slab.

(iv) $a < 0$ so that the dispersion is negative and once again requires an active material in the slab.

The case (i) was studied in [52], and as discussed above the source becomes cloaked as $T \to \infty$. In case (ii) for a given T the imaginary part of $\varepsilon_s = -1 + \mathrm{i}a/T$ is lower than in case (i) which means that cloaking occurs quicker than in case (i): if we halve a and at the same time halve T then the solution remains unchanged. Now power from the source and power from the fields in the active material in the slab lens both flow towards the regions of anomalous resonance outside the slab, both in front and behind the slab. There should also be a flow of energy outwards along the slab interfaces carried by the surface plasmons associated with the anomalous resonance, but we have not investigated this. In case (iii) we would need to look at higher order terms in the expansion (5.9) in powers of $1/T$ to determine the asymptotic behavior as $T \to \infty$. In case (iv) $\varepsilon_s = -1 + \mathrm{i}a/T$ has a negative imaginary part and the solution is obtained by taking the complex conjugate of the solution with $a > 0$. In particular this means that the "so-called" dipole source that one puts in front of the lens needs to be a sink of energy, trapping the energy that is flowing from the slab of active material that forms the "lens".

Obviously these considerations show that the response of a lossless superlens is not at all quick, rather it takes a long while for the lens to achieve deep subwavelength resolution.

Since in the time domain, the time T the source has been "on" is mathematically equivalent to having a loss parameter $\delta = a/T$ a curious effect may happen if a source causes weak CALR and not strong CALR. Then one may expect the source (normalized so that it provides constant power) to flash on and off in brightness as time progresses as seen from either in front of the lens or behind the quasistatic slab lens.

More numerical work and rigorous theoretical work needs to be done in studying the quasistatic lens and the Veselago lens in the time domain, especially for sources that are turned on at a specific time and which supply a constant power (averaged over a cycle of oscillation) thereafter. Collin [29] studied the interesting case of what happens with a "Drude type metamaterial" when a time harmonic source is turned on and then turned off at a later time. Further studies were made in the papers [30, 31, 57] where the response due to a time harmonic point source turned on in front of a half-space again containing a "Drude type metamaterial" was investigated. Anomalous resonance does not occur with such a half space, rather the fields diverge linearly with time everywhere and consequently the image of a point source is not a point source even in the limit as $t \to \infty$ as shown by Gralak and Maystre [31]: the resonant fields shroud the image. All these analyses are for constant amplitude sources, rather than constant power sources.

6. Sensitivity of anomalous resonance, cloaking, and superlensing

As anomalous resonance is associated with essential singularities and as the behavior of analytic functions is quite wild around essential singularities it should come as no surprise that anomalous resonance, and hence cloaking due to anomalous resonance and superlensing, is quite sensitive to the material moduli. An indication of this sensitivity is that the cloaking region for the coated cylinder which has a radius $\sqrt{r_s^3/r_c}$ when $\varepsilon_c = 1$ changes dramatically to the radius r_s^3/r_c^2 when $\varepsilon_c \neq 1$ [33]. In fact, by considering the quasistatic slab superlens of thickness d with $\varepsilon_s = -1 + i\delta$ being the dielectric constant of the slab and with dielectric constants in front and behind the superlens of 1 and $\varepsilon_c = 1 + i(\delta + \lambda\delta^\beta)$, respectively, with λ and β being real constants satisfying $1 > \beta > 0$, one finds that the position of the cloaking region depends on the value of β [58]. Specifically, as follows from (4.11) in that paper, the cloaking region extends a distance $d/(\beta+1)$ in front of the slab. This varies continuously between d and $d/2$ as β varies between 0 and 1. Early studies of superlenses also show sensitivity to the material moduli of the lens: see, for example, the excellent paper of Merlin [23].

Interestingly, Xiao *et al.* [59] show that while a small dielectric cylinder near the slab lens can be cloaked due to anomalous resonance, at nearby frequencies the opposite can also occur: it can become more visible due to a cylinder-slab resonance.

The sensitivity to material moduli is reduced as the loss parameter δ is increased, but increasing δ greatly reduces the resolution of the superlens.

7. Cloaking due to complementary media

A different sort of superlens related cloaking, called cloaking due to complementary media, was proposed by Lai *et al.* [60]. The idea, which has its origin in work by Pendry and Ramakrishna (see Figure 2 in [61]), is that to cloak a given dielectric object close to the lens one should insert an appropriate cancelling "anti-object" in the lens. For the quasistatic slab lens if the front interface is at $x = 0$ and the object lying within a distance d has a dielectric constant $\varepsilon(x, y, z)$ then inside the lens one should modify the dielectric constant to $\varepsilon(x, y, z) = -\varepsilon(-x, y, z)$. If one takes the field for $x < -d$ without the object, antiobject and lens being present, and then analytically extends it to $x < 0$ in the presence of the object, then the mirroring property allows us to reconstruct the field everywhere without disturbing the field for $x < -d$. Cloaking due to complementary media also occurs with bianisotropic media [62].

Some caution is needed since in the numerical simulations in Figure 2 of [60] and Figures 8 and 10 of [62] it looks like regions of anomalous resonance are appearing, and anomalous resonance does not enter into the argument used to justify the cloaking. Also we know that the argument of complementary media is sometimes flawed. Specifically, the field generally will not have an analytic extension from $x < -d$ to $x = 0$ with the object being present. (The field outside the object generally will have singularities inside the object if one analytically extends it to the inside of the object while keeping $\varepsilon = 1$ everywhere. These singularities will not generally be in the extension of the field from $x < -d$ to $x < 0$, while keeping $\varepsilon = 1$ everywhere, as required by the principle of complementary media.) By the argument of complementary media the quasistatic slab lens is cancelled by a slab of material of moduli $\mu = 1$ directly behind it having thickness d. But this would imply the perfect imaging of polarizable dipoles, constant power sources, and dielectric objects close to the front of the lens, and we know that these are not perfectly imaged (even in the limit $\delta \to 0$). Thus it appeared that the foundations of cloaking due to complementary media were on rather shaky grounds. Fortunately, in major advances, Nguyen [63] and Nguyen and Nguyen [64] rigorously proved cloaking due to complementary media, subject to certain assumptions.

Associated with cloaking due to complementary media is illusion optics [65] and these simulations also appear to show anomalous resonance.

8. Classifying different types of cloaking

One way of classifying cloaking techniques is whether they satisfy the *ostrich effect* [66]. This term was designed to highlight whether the technique had the undesirable property wherein *the large object hides the small object, but the large object does not hide itself*. Cloaking by anomalous resonance passes this ostrich test when $\varepsilon_c = 1$, but not when $\varepsilon_c \neq 1$ as then the coated cylinder is visible as a larger cylinder of radius r_s^2/r_c and dielectric constant ε_c. Classical single frequency cloaking by transformation optics also passes it: the cloaking system as well as the object to be hidden are difficult or impossible to detect.

Another way of classifying cloaking techniques is whether the object to be cloaked is outside the cloaking device or not. This is a feature of cloaking due to anomalous resonance, and cloaking due to complementary media, and is called exterior cloaking as opposed to the interior cloaking associated with transformation based cloaks. When it boils down to it, the exterior cloaking of anomalous resonance is due to polarization charge sources at the surface of the lens. This then motivates one to investigate active exterior cloaks, where sources are chosen to achieve exterior cloaking. This was successfully done by choosing sources to create a *quiet zone*, where the fields are small and the object to be cloaked can be hidden, while only slightly disturbing the fields outside a certain radius [67–71]. Such active cloaks, including the active interior cloaks proposed earlier by Miller [72], and experimentally tested by Selvanayagam and Eleftheriades [73], have the advantage that they are broadband, but the disadvantage that the sources need to be tailored according to the incident field. For the plate equation realistic active cloaks have been proposed where the cloak is tailored both according to the incident field and according to the object one wants to cloak [74].

The question arises in cloaking due to anomalous resonance as to what happens when one has two or more cloaking devices (such two or more cylindrical superlenses) and their "cloaking regions" overlap. One might hope that one would get cloaking in the union of the two regions, and this may then help to design cloaks having cloaking regions of desired shapes. Unfortunately, our results in [66] indicate that cloaking is destroyed in the overlap region.

A challenge for cloaking by anomalous resonance is that it has yet to be experimentally demonstrated. It is hoped that such a demonstration will become available in the near future.

9. A possible future research direction

An interesting topic which may prove a fruitful research direction concerns density of states and related concepts in connection with anomalous resonance. Density of states functions have long been a central tool in solid state physics, and indeed were at the heart of the 1987 paper by Yablonovitch [75], which provided one of the two launching pads for the field of photonic crystals. Yablonovitch pointed out that if one could create a structure having band gaps for photons rather than electrons, one would then have in bandgap frequency ranges zero density of state for photons, and thus through Fermi's Golden Rule drastically inhibited spontaneous emission. The topic of density of states functions in photonic crystals was then much discussed, and various density of state functions were introduced- see for example [76].

The density of states function itself is only a function of frequency, but one may introduce a local density of states (LDOS) which depends both on frequency and position within a structured material. Note that the spatial integral of the LDOS is related to the classical density of states (DOS) – the spatial integral in the case of a periodic system is just that over the Wigner–Setiz cell.

Similarly, there exists a spectral density of states function (SDOS) which depends on frequency and direction of emission. For periodic systems, its integral over the Brillouin zone gives the DOS. All three of these functions may be constructed from the appropriate Green's function by taking its imaginary part at the source point, on, in the case of the SDOS, in the direction of source emission.

Related to these densities of state functions there are their Hilbert (or causal) transforms, which relate to the frequency shift between the source natural frequency and its emitted frequency in the structured material. This relates to the difference between the real part of the Green's function at the source point and its value in a homogeneous reference material, and is called the anomalous Lamb shift – see [77] and [78].

In the field of metamaterials, density of state concepts have chiefly been of interest in relation to hyperbolic metamaterials, where permittivities and/or permeabilities have different signs in different directions – see [79]. The result of this strong anisotropy is that the photonic density of states is no longer bounded, but may become very large for particular frequency ranges and directions. Systems exhibiting anomalous resonance offer similar possibilities and interest. Since the essential singularity at the heart of anomalous resonance is the limit point of a sequence of poles and zeros, this strongly suggests it is associated with an infinite density of states, but only at one frequency. The reasoning here refers immediately to the DOS, but given that the DOS is the spatial integral of the LDOS, flows on to the latter. In fact (2.6), (and to a lesser degree (2.25), (2.35), (2.44), (2.45), (4.27) and (5.23)) in the paper [33] shows that the imaginary part of the Green's function is infinite within the cloaking region. In fact it is infinite in two-dimensions simply for a dipole at any point outside a disk of dielectric constant $-1+\mathrm{i}\delta$ surrounded by a medium of dielectric constant 1, in the limit $\delta \to 0$. As is well known, this problem can be solved using the method of images and the magnitude of the image dipole blows up as $\delta \to 0$. Of course these two-dimensional geometries correspond to cylindrical geometries in three dimensions with a line dipole outside, and this is not the same as the point dipole required for the LDOS. For a point dipole within the cloaking region surrounding the slab lens the quasistatic LDOS is infinite, as can be seen from (5.14) and (5.23) in [33]. It is even infinite for a dipole at any point outside a sphere of dielectric constant $-1+\mathrm{i}\delta$ surrounded by a medium of dielectric constant 1, in the limit $\delta \to 0$. This can be seen from the expressions for the image dipole and accompanying image charge or charge distribution (see [80] and Table 4.2 on page 72 in [81]) which blow up in magnitude as $\delta \to 0$.

It would be of great interest to understand in more detail the various density of state functions and their behavior in systems undergoing anomalous resonance. It is tempting to speculate that the spontaneous emission would happen infinitely fast. But this would imply a mix of frequencies and the infinite LDOS only occurs at one frequency.

Certain other obvious questions spring to mind:

1. What are the effects of frequency, dispersion and loss on densities of state near anomalous resonances?
2. What happens to frequency Lamb shifts near anomalous resonances?

Those looking through the window offered by densities of states concepts will no doubt find other questions begging answers. However, perhaps the fundamental challenge remaining is to strengthen the bridge between static and dynamic formulations near an essential singularity of the former.

Acknowledgements

GWM thanks the National Science Foundation for support through grant DMS-1814854. The referees are thanked for their helpful comments and suggested references.

References

[1] N. A. Nicorovici, R. C. McPhedran, G. W. Milton, "Transport properties of a three-phase composite material: The square array of coated cylinders", *Proc. R. Soc. Lond. Ser. A* **442** (1993), no. 1916, p. 599-620.

[2] H. Ammari, G. Ciraolo, H. Kang, H. Lee, G. W. Milton, "Spectral theory of a Neumann–Poincaré-type operator and analysis of cloaking due to anomalous localized resonance", *Arch. Ration. Mech. Anal.* **208** (2013), no. 2, p. 667-692.

[3] H. Ammari, G. Ciraolo, H. Kang, H. Lee, G. W. Milton, "Anomalous localized resonance using a folded geometry in three dimensions", *Proc. R. Soc. A* **469** (2013), no. 2154, article ID 20130048.

[4] G. W. Milton, *The Theory of Composites*, Cambridge Monographs on Applied and Computational Mathematics, vol. 6, Cambridge University Press, Cambridge, UK, 2002.

[5] C.-W. Qiu, B. Luk'yanchuk, "Peculiarities in light scattering by spherical particles with radial anisotropy", *J. Opt. Soc. Amer. A* **25** (2008), no. 7, p. 1623-1628.

[6] J. Helsing, R. C. McPhedran, G. W. Milton, "Spectral super-resolution in metamaterial composites", *New J. Phys.* **13** (2011), no. 11, article ID 115005.

[7] A. Sihvola, H. Wallén, H. Kettunen, "Losses from lossless building blocks?", in *Metamaterials '2012: The 6th International Congress on Advanced Electromagnetic Materials in Microwaves and Optics*, 2012, p. 261-263.

[8] N. M. Estakhri, A. Alù, "Physics of unbounded, broadband absorption/gain efficiency in plasmonic nanoparticles", *Phys. Rev. B* **87** (2013), no. 20, article ID 205418.

[9] A. Bonnet-BenDhia, L. Chesnel, P. Ciarlet Jr., "T-coercivity for scalar interface problems between dielectrics and metamaterials", *Math. Model. Numer. Anal.* **46** (2012), p. 1363-1387.

[10] A.-S. Bonnet-Ben Dhia, L. Chesnel, X. Claeys, "Radiation condition for a non-smooth interface between a dielectric and a metamaterial", *Math. Models Methods Appl. Sci.* **23** (2013), no. 9, p. 1629-1662.

[11] A.-S. Bonnet-Ben Dhia, L. Chesnel, P. Ciarlet Jr., "Two-dimensional Maxwell's equations with sign-changing coefficients", *Appl. Numer. Math.* **79** (2014), p. 29-41, Workshop on Numerical Electromagnetics and Industrial Applications (NELIA 2011).

[12] A.-S. Bonnet-Ben Dhia, L. Chesnel, P. Ciarlet Jr., "T-coercivity for the Maxwell problem with sign-changing coefficients", *Comm. Partial Differential Equations* **39** (2014), no. 6, p. 1007-1031, Workshop on Numerical Electromagnetics and Industrial Applications (NELIA 2011).

[13] N. A. Nicorovici, R. C. McPhedran, G. W. Milton, "Optical and dielectric properties of partially resonant composites", *Phys. Rev. B* **49** (1994), no. 12, p. 8479-8482.

[14] T. Yang, H. Chen, X. Luo, H. Ma, "Superscatterer: enhancement of scattering with complementary media", *Opt. Express* **16** (2008), no. 22, p. 18545-18550.

[15] L. S. Dolin, "To the possibility of comparison of three-dimensional electromagnetic systems with nonuniform anisotropic filling", *Izv. Vyssh. Uchebn. Zaved.* **4** (1961), no. 5, p. 964-967, English translation available at http://www.math.utah.edu/ milton/DolinTrans2.pdf.

[16] A. Alú, N. Engheta, "Achieving transparency with plasmonic and metamaterial coatings", *Phys. Rev. E* **72** (2005), no. 1, article ID 0166623.

[17] M. Kerker, "Invisible bodies", *J. Opt. Soc. Amer.* **65** (1975), no. 4, p. 376-379.

[18] G. W. Milton, "Unusual resonant phenomena where ghost image charges appear in the matrix", Unpublished report, Courant Institute, New York, NY, USA, 1993–1996, Availble on ResearchGate. Timestamp: May 13th 1996.

[19] X. S. Rao, C. K. Ong, "Amplification of evanescent waves in a lossy left-handed material slab", *Phys. Rev. B* **68** (2003), no. 11, article ID 113103.

[20] G. Shvets, "Applications of surface plasmon and phonon polaritons to developing left-handed materials and nanolithography", in *Plasmonics: Metallic Nanostructures and their Optical Properties (Bellingham, WA)* (N. J. Halas, ed.), Proceedings of SPIE, vol. 5221, SPIE Publications, Bellingham, 2003, p. 124-132.

[21] G. Shvets, "Photonic approach to making a material with a negative index of refraction", *Phys. Rev. B* **67** (2003), no. 3, article ID 035109.

[22] S. A. Cummer, "Simulated causal subwavelength focusing by a negative refractive index slab", *Appl. Phys. Lett.* **82** (2003), no. 10, p. 1503-1505.

[23] R. Merlin, "Analytical solution of the almost-perfect-lens problem", *Appl. Phys. Lett.* **84** (2004), no. 8, p. 1290-1292.

[24] S. Guenneau, B. Gralak, J. B. Pendry, "Perfect corner reflector", *Opt. Lett.* **30** (2005), p. 1204-1206.

[25] V. A. Podolskiy, E. E. Narimanov, "Near-sighted superlens", *Opt. Lett.* **30** (2005), no. 1, p. 75-77.

[26] V. A. Podolskiy, N. A. Kuhta, G. W. Milton, "Optimizing the superlens: manipulating geometry to enhance the resolution", *Appl. Phys. Lett.* **87** (2005), no. 23, article ID 231113.

[27] J. B. Pendry, "Negative refraction makes a perfect lens", *Phys. Rev. Lett.* **85** (2000), no. 18, p. 3966-3969.

[28] V. G. Veselago, "The electrodynamics of substances with simultaneously negative values of ϵ and μ", *Uspekhi Fizicheskikh Nauk* **92** (1967), p. 517-526, English translation in *Sov. Phys. Uspekhi* **10** (1968), no. 4, 509–514.

[29] R. E. Collin, "Frequency dispersion limits resolution in Veselago lens", *Prog. Electromagn. Res. B* **19** (2010), p. 233-261.

[30] B. Gralak, A. Tip, "Macroscopic Maxwell's equations and negative index materials", *J. Math. Phys.* **51** (2010), no. 5, article ID 052902.
[31] B. Gralak, D. Maystre, "Negative index materials and time-harmonic electromagnetic field", *C. R. Phys.* **13** (2012), no. 8, p. 786-799.
[32] G. W. Milton, N.-A. P. Nicorovici, R. C. McPhedran, V. A. Podolskiy, "A proof of superlensing in the quasistatic regime, and limitations of superlenses in this regime due to anomalous localized resonance", *Proc. R. Soc. A* **461** (2005), no. 2064, p. 3999-4034.
[33] G. W. Milton, N.-A. P. Nicorovici, "On the cloaking effects associated with anomalous localized resonance", *Proc. R. Soc. A* **462** (2006), no. 2074, p. 3027-3059.
[34] J. B. Pendry, "Perfect cylindrical lenses", *Opt. Express* **11** (2003), no. 7, p. 755-760.
[35] J. B. Pendry, D. Schurig, D. R. Smith, "Controlling electromagnetic fields", *Science* **312** (2006), no. 5781, p. 1780-1782.
[36] U. Leonhardt, "Optical conformal mapping", *Science* **312** (2006), no. 5781, p. 1777-1780.
[37] A. Greenleaf, M. Lassas, G. Uhlmann, "Anisotropic conductivities that cannot be detected by EIT", *Physiol. Meas.* **24** (2003), no. 2, p. 413-419.
[38] N.-A. P. Nicorovici, G. W. Milton, R. C. McPhedran, L. C. Botten, "Quasistatic cloaking of two-dimensional polarizable discrete systems by anomalous resonance", *Opt. Express* **15** (2007), no. 10, p. 6314-6323.
[39] O. P. Bruno, S. Lintner, "Superlens-cloaking of small dielectric bodies in the quasistatic regime", *J. Appl. Phys.* **102** (2007), no. 12, article ID 124502.
[40] H.-M. Nguyên, "Cloaking an arbitrary object via anomalous localized resonance: the cloak is independent of the object", *SIAM J. Math. Anal.* **49** (2017), no. 4, p. 3208-3232.
[41] G. Bouchitté, B. Schweizer, "Cloaking of small objects by anomalous localized resonance", *Quart. J. Mech. Appl. Math.* **63** (2010), no. 4, p. 437-463.
[42] U. Leonhardt, T. G. Philbin, "General relativity in electrical engineering", *New J. Phys.* **8** (2006), no. 10, article ID 247.
[43] D. Maystre, S. Enoch, "Perfect lenses made with left-handed materials: Alice's mirror?", *J. Opt. Soc. Amer.* **21** (2004), no. 1, p. 122-131.
[44] G. W. Milton, N.-A. P. Nicorovici, R. C. McPhedran, K. Cherednichenko, Z. Jacob, "Solutions in folded geometries, and associated cloaking due to anomalous resonance", *New J. Phys.* **10** (2008), no. 11, article ID 115021.
[45] R. V. Kohn, J. Lu, B. Schweizer, M. I. Weinstein, "A variational perspective on cloaking by anomalous localized resonance", *Comm. Math. Phys.* **328** (2014), no. 1, p. 1-27 (English), Available as arXiv:1210.4823 [math.AP].
[46] H. Kettunen, M. Lassas, P. Ola, "On absence and existence of the anomalous localized resonance without the quasi-static approximation", *SIAM J. Appl. Math.* **78** (2018), no. 1, p. 609-628.
[47] H. Li, H. Liu, "On anomalous localized resonance for the elastostatic system", *SIAM J. Appl. Math.* **5** (2016), p. 3322-3344.
[48] K. Ando, H. Kang, K. Kim, S. Yu, "Spectrum of Neumann–Poincaré operator on annuli and cloaking by anomalous localized resonance for linear elasticity", *SIAM J. Appl. Math.* **49** (2017), no. 5, p. 4232-4250.
[49] K. Ando, Y.-G. Ji, H. Kang, K. Kim, S. Yu, "Spectral properties of the Neumann–Poincaré operator and cloaking by anomalous localized resonance for the elasto-static system", *Eur. J. Appl. Math.* **29** (2018), no. 2, p. 189-225.
[50] Y. Deng, H. Li, H. Liu, "Spectral properties of Neumann–Poincaré operator and anomalous localized resonance in elasticity beyond quasi-static limit", *J. Elast.* (2020), article ID Deng2020.
[51] G. Rosenblatt, M. Orenstein, "Power drainage and energy dissipation in lossy but perfect lenses", *Phys. Rev. A* **95** (2017), no. 5, article ID 053857.
[52] G. W. Milton, N.-A. P. Nicorovici, R. C. McPhedran, "Opaque perfect lenses", *Physica B* **394** (2007), no. 2, p. 171-175.
[53] A. D. Yaghjian, T. B. Hansen, "Plane-wave solutions to frequency-domain and time-domain scattering from magnetodielectric slabs", *Phys. Rev. E* **73** (2006), no. 4, article ID 046608.
[54] G. T. Di Francia, "Super-gain antennas and optical resolving power", *Il Nuovo Cimento* **9** (1952), p. 426-438.
[55] H. Shim, H. Chung, O. D. Miller, "Maximal free-space concentration of electromagnetic waves", *Phys. Rev. Appl.* **14** (2020), article ID 014007.
[56] A. D. Yaghjian, S. R. Best, "Impedance, bandwidth, and Q of antennas", *IEEE Trans. Antennas and Propagation* **53** (2005), no. 4, p. 1298-1324.
[57] M. Cassier, C. Hazard, P. Joly, "Spectral theory for maxwell's equations at the interface of a metamaterial. Part I: generalized Fourier transform", *Comm. Partial Differential Equations* **42** (2017), no. 11, p. 1707-1748.
[58] T. Meklachi, G. W. Milton, D. Onofrei, A. E. Thaler, G. Funchess, "Sensitivity of anomalous localized resonance phenomena with respect to dissipation", *Quart. Appl. Math.* **74** (2016), no. 2, p. 201-234.
[59] M. Xiao, X. Huang, H. Liu, C. T. Chan, "Enhancement of polarizabilities of cylinders with cylinder-slab resonances", *Sci. Rep.* **5** (2015), p. 8189.
[60] Y. Lai, H. Chen, Z.-Q. Zhang, C. T. Chan, "Complementary media invisibility cloak that cloaks objects at a distance outside the cloaking shell", *Phys. Rev. Lett.* **102** (2009), no. 9, article ID 093901.
[61] J. B. Pendry, S. A. Ramakrishna, "Focussing light using negative refraction", *J. Phys.: Condens. Matter* **15** (2003), no. 37, p. 6345-6364.

[62] Y. Liu, B. Gralak, R. C. McPhedran, S. Guenneau, "Finite frequency external cloaking with complementary bianisotropic media", *Opt. Express* **22** (2014), no. 14, p. 17387-17402.
[63] L. H. Nguyên, "Cloaking using complementary media in the quasistatic regime", *Ann. Inst. H. Poincaré Anal. Non Linéaire* **33** (2016), no. 6, p. 1509-1518.
[64] H.-M. Nguyên, L. H. Nguyên, "Cloaking using complementary media for the Helmholtz equation and a three spheres inequality for second order elliptic equations", *Trans. Amer. Math. Soc. B* **2** (2015), p. 93-112.
[65] Y. Lai, J. Ng, H. Chen, D. Han, J. Xiao, Z.-Q. Zhang, C. T. Chan, "Illusion optics: The optical transformation of an object into another object", *Phys. Rev. Lett.* **102** (2009), no. 25, article ID 253902.
[66] R. C. McPhedran, N.-A. P. Nicorovici, L. C. Botten, G. W. Milton, "Cloaking by plasmonic resonance among systems of particles: cooperation or combat?", *C. R. Phys.* **10** (2009), no. 5, p. 391-399.
[67] F. G. Vasquez, G. W. Milton, D. Onofrei, "Active exterior cloaking for the 2D Laplace and Helmholtz equations", *Phys. Rev. Lett.* **103** (2009), no. 7, article ID 073901.
[68] F. G. Vasquez, G. W. Milton, D. Onofrei, "Broadband exterior cloaking", *Opt. Express* **17** (2009), no. 17, p. 14800-14805.
[69] F. G. Vasquez, G. W. Milton, D. Onofrei, "Exterior cloaking with active sources in two dimensional acoustics", *Wave Motion* **48** (2011), no. 6, p. 515-524.
[70] F. G. Vasquez, G. W. Milton, D. Onofrei, "Mathematical analysis of the two dimensional active exterior cloaking in the quasistatic regime", *Anal. Math. Phys.* **2** (2012), no. 3, p. 231-246.
[71] A. N. Norris, F. A. Amirkulova, W. J. Parnell, "Active elastodynamic cloaking", *Math. Mech. Solids* **19** (2014), no. 6, p. 603-625.
[72] D. A. B. Miller, "On perfect cloaking", *Opt. Express* **14** (2006), no. 25, p. 12457-12466.
[73] M. Selvanayagam, G. V. Eleftheriades, "Experimental demonstration of active electromagnetic cloaking", *Phys. Rev. X* **3** (2013), no. 4, article ID 041011.
[74] J. O'Neill, Ö. Selsil, R. C. McPhedran, A. B. Movchan, N. V. Movchan, "Active cloaking of inclusions for flexural waves in thin elastic plates", *Quart. J. Mech. Appl. Math.* **68** (2015), no. 3, p. 263-288.
[75] E. Yablonovitch, "Inhibited spontaneous emission in solid-state physics and electronics", *Phys. Rev. Lett.* **58** (1987), no. 20, p. 2059-2062.
[76] R. C. McPhedran, L. C. Botten, J. McOrist, A. A. Asatryan, C. M. de Sterke, N. A. Nicorovici, "Density of states functions for photonic crystals", *Phys. Rev. E* **69** (2004), no. 1, article ID 016609.
[77] D. P. Fussell, R. C. McPhedran, C. M. de Sterke, "Decay rate and level shift in a circular dielectric waveguide", *Phys. Rev. A* **71** (2005), no. 1, article ID 013815.
[78] A. A. Asatryan, L. C. Botten, N. A. Nicorovici, R. C. McPhedran, C. M. de Sterke, "Frequency shift of sources embedded in finite two-dimensional photonic clusters", *Waves Random Complex Media* **16** (2006), no. 2, p. 151-165.
[79] Z. Jacob, J.-Y. Kim, G. V. Naik, A. Boltasseva, E. E. Narimanov, V. M. Shalaev, "Engineering photonic density of states using metamaterials", *Appl. Phys. B* **100** (2010), no. 1, p. 215-218.
[80] C. Neumann, *Hydrodynamische untersuchung: nebst einem anhange über die probleme der elektrostatik und der magnetischen induction*, Teubner, Leipzig, 1883, 271-282 pages.
[81] L. Poladian, "Effective transport and optical properties of composite materials", Ph.D. thesis, The University of Sydney, Sydney, Australia, Irvine, CA, USA, 1990, pp. xiii + 221.

Comptes Rendus
Physique
2020, 21, nº 4-5, p. 425-442
https://doi.org/10.5802/crphys.31

Metamaterials 1 / *Métamatériaux 1*

All-dielectric Mie-resonant metaphotonics

Méta-photonique diélectrique avec des résonateurs de Mie

Nicolas Bonod[*, a] **and Yuri Kivshar**[b, c]

[a] Aix Marseille Univ, CNRS, Centrale Marseille, Institut Fresnel, 13013 Marseille, France

[b] Nonlinear Physics Center, Research School of Physics, Australian National University, Canberra ACT 2601, Australia

[c] ITMO University, St. Petersburg 197101, Russia

E-mails: nicolas.bonod@fresnel.fr (N. Bonod), yuri.kivshar@anu.edu.au (Y. Kivshar)

Abstract. All-dielectric subwavelength structures made of high-refractive-index materials combine a unique set of advantages in comparison with their plasmonic counterparts. In particular, they can interact resonantly with light through the excitation of both electric and magnetic multipolar Mie-type resonances. This review discusses novel approaches to manipulate light with Mie-resonant dielectric subwavelength structures, spanning from individual nanoparticles to metasurfaces, and covering a broad range of effects, from near-field energy enhancement to far-field beam shaping.

Résumé. Les matériaux diélectriques à indice de réfraction élevé peuvent interagir de manière résonnante avec la lumière grâce à l'excitation de modes de Mie électriques et magnétiques. Cette revue présente un état de l'art du contrôle de la lumière par les résonances électriques et magnétiques de Mie dans les nanostructures diélectriques. Elle décrit tout d'abord la reproduction des conditions de Kerker pour un contrôle de la diffusion avant ou arrière de la lumière. Elle décrit ensuite l'intérêt des résonances de Mie pour (i) le contrôle de l'interaction entre la lumière et la matière dans les antennes optiques diélectriques (exaltation de champ proche, densité d'états et directivité d'émission), (ii) la génération d'états photoniques liés dans le continuum ou encore (iii) la génération de couleurs structurelles par des métasurfaces diélectriques.

Keywords. All-dielectric nanophotonics, Mie resonances, Kerker effect, Bound states in the continuum, Metaphotonics, Metasurfaces.

Mots-clés. Nanophotonique diélectrique, Résonances de Mie, Conditions de Kerker, Etats liés dans le continuum, Métaphotonique, Métasurfaces.

* Corresponding author.

1. Introduction

All-dielectric metamaterials were proposed in the 2000's to achieve an artificial optical magnetism without metals [1, 2]. They were based on materials with high values of dielectric permittivity, typically larger than 100. Composite materials with such high dielectric permittivities were proven to yield negative permeabilities when applying an effective medium theory [2]. Unfortunately, common materials studied in the visible and near infrared (near-IR) spectra feature much smaller values of dielectric permittivity, typically smaller than 20. This constraint limited the soar of all-dielectric metamaterials in the visible and near-IR spectra.

However, it was highlighted also in the 2010's that silicon (Si) nanoparticles feature low-order electric and magnetic Mie resonances [3–8] which can also be employed for the realization of optical magnetism, although Si exhibits much smaller dielectric permittivities (typically around 12). Soon after, in 2012 the first experimental observations with dark-field spectroscopy of a strong magnetic response of individual Si particles were reported by two experimental groups [9, 10]. The spectral response observed with dark-field spectroscopy in the visible and near-IR spectra evidenced several peaks associated with low-order electric and magnetic Mie resonances. In particular, the possibility to excite both electric or magnetic resonances, and to balance the weight between the electric and magnetic dipolar modes to tailor the scattering properties of the particles triggered a huge interest. The resonant interaction of electromagnetic waves with high-index nanostructures offers the possibility to engineer and control their phase and amplitude [11]. The possibility to combine electric and magnetic resonances inside the same dielectric nanostructure opened novel routes to develop planar metasurfaces able to tailor the phase of light as well as its transmittance and reflectance spectra.

Soon after, the field of "all-dielectric metamaterials", based on effective averaged parameters, has been replaced naturally by "metaphotonics" (or "meta-optics", also called "Mie-tronics") where not averaged parameters but individual resonances become important. This field is inspired by the physics of the magnetic dipole resonances and optical magnetism originating from the resonant dielectric nanostructures with high refractive index [12]. The concepts of meta-optics and all-dielectric resonant nanophotonics are driven by the idea to employ subwavelength dielectric Mie-resonant nanoparticles as "meta-atoms" for creating highly efficient optical metadevices, and the term "meta" is attributed to the importance of an optically-induced magnetic response.

Because of the unique optical resonances and their various combinations employed for realizing interference effects and strong localization of the electromagnetic fields, high-index nanoscale structures are expected to complement or even replace different plasmonic components in a range of potential applications. Moreover, many concepts developed for plasmonic structures, but fell short of their potential due to strong losses of metals at optical frequencies, can now be realized with Mie-resonant dielectric structures.

2. Mie resonances

Light scattering by small particles is a fundamental problem in optics and electromagnetism. It can be studied by solving Maxwell's equations in the spherical coordinates. This theory, called multipolar theory or Mie theory, was developed originally by Gustav Mie in 1908 [13] and improved by several contributors all over the XXth century [14, 15].

Spherical microstructures host high-order multipolar resonances associated with extremely high quality factors (Q factors) that are called whispering gallery modes. They are observed in almost lossless dielectrics such as silica or silicon nitride microstructured in microspheres or microdisks [16, 17]. When decreasing the size of the dielectric cavities from the micro to the sub-micrometer scale, the strength of the resonance weakens with refractive index typically

considered in whispering gallery modes (typically around $n \approx 1.3$ and $n \approx 1.9$). The order of the excited mode decreases with the size. The smallest size of an optical resonator is achieved when the lowest mode is excited. However, an efficient excitation of a low-order mode requires an increase of the refractive index, typically from 1.5 to values larger than 2.2 and ideally larger than 3. In the visible and near-IR spectra, semi-conductors such as silicon or germanium exhibit refractive index ranging between 3 and 4 while some oxides also feature nice optical properties such as titania.

Efficient resonant light-matter interactions at the nanoscale can be achieved for low-order resonances in sub-micrometer sized particles. Compared with high order multipolar whispering gallery modes, low-order resonances are characterized by smaller Q factors and a wider spectral response (see Figures 1(a–d)). The scattering cross section of a single dielectric particle is plotted in Figure 1(a), where R is the radius of a spherical particle. Several peaks can be observed over the visible spectrum. A multipolar decomposition of the scattered field (see Figure 1(b)) allows to identify the nature of the mode associated with each peak. When decreasing the wavelength, *i.e.* for the largest ratio between the wavelength and size of the scatterer, the first peak corresponds to the excitation of the magnetic dipolar mode, the second peak to the electric dipolar mode. The Mie resonances can also be obtained in non-spherical scatterers. This property results from the fact that the interest is brought in low-order resonances. Such resonances are less sensitive to high spatial frequencies than high-order multipolar resonances. That is the reason why a large set of geometries has been investigated to tailor low-order Mie resonances.

Spherical silicon particles can be fabricated with the laser ablation technique [19]. This technique is very convenient since it allows to disperse particles on glass cover-slips and to perform dark-field optical spectroscopy, see Figure 1(c). It is enlightening to observe such well defined electric and magnetic resonances that nicely match the numerical calculations. If the first interest of Mie resonances was brought in their far field response to retrieve for example the so-called Kerker conditions, one of the main interest of such resonances is to yield strong field intensities inside high-refractive-index materials.

It turns out that the terminology of "Mie resonance" is classically employed for describing resonances in dielectric particles. However, we stress that plasmonic and dielectric resonances can both be described by the Mie theory. In a sake of illustration, let us consider a silver particle at the frequency that maximizes its dipolar plasmonic resonances, *i.e.* at the frequency that maximizes its dipolar electric Mie coefficient a_1. It turns out that a dielectric scatterer can also maximize this Mie coefficient. An analytic expression between the two dielectric permittivities, of positive and negative real parts, derived in Ref. [18], permits to calculate the dielectric permittivity that maximizes the electric dipolar resonance, or in other words, the plasmonic resonance. The calculation of the scattering cross-section of the metallic and dielectric particles displayed in Figure 1(d) shows that the two particles can exhibit the same optical response. However, the magnetic response is almost negligible with spherical metallic particles and strong magnetic responses can be obtained only with more complex geometries.

The field of plasmonic metamaterials has investigated different geometries to overcome this limitation and to yield a strong magnetic response. Among a wide variety of plasmonic shapes, one can cite the U- and the Ω-shaped scatterers [20, 21]. Coupling a set of plasmonic scatterers that exhibit a resonant electric polarizability is also an efficient way to yield artificial magnetism [22]. The terminology employed to describe this effect is inspired by molecular chemistry where electronic orbitals of different atoms can couple. The coupling modifies the energy of the electronic orbitals and leads to the formation of bonding and anti-bonding chemical bonds [23]. The set of plasmonic scatterers is therefore called "plasmonic oligomers". This field of research aims at engineering the coupling between the different modes of the plasmonic scatterers to optimize either the electric or magnetic response of the plasmonic oligomers.

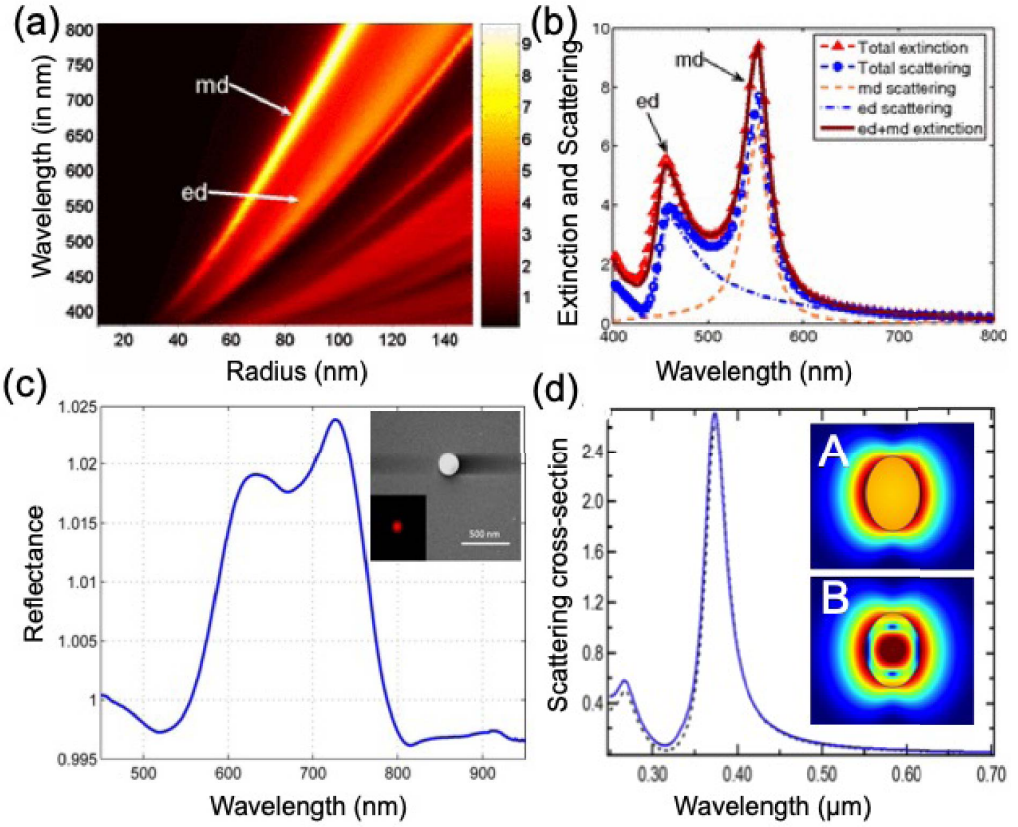

Figure 1. Scattering properties of subwavelength particles. (a) Scattering efficiency spectra of a spherical Si particle with the radius R in air. (b) Extinction and scattering spectra of a Si particle with $R = 65$ nm. The arrows indicate the electric dipole (ed) and magnetic dipole (md) contributions to the total efficiencies. Adapted with permission from [3]. (c) Experimental reflectance spectra of a 208 nm Si sphere on a glass substrate. Inset: Scanning Electron Microscopy (SEM) image of the corresponding Si nanoparticle and dark-field microscopic images. Adapted with permission from [10]. (d) Equivalence of Mie resonances in plasmonic and dielectric particles. Scattering cross-section with respect to the wavelength. Dotted line: silver particle A with $\epsilon = -2.5 + 0.5i$; Solid blue line: dielectric particle B with $\epsilon = 112 + 0.5i$. Both particles have the same diameter: 50 nm. Adapted with permission from [18].

The ability of spherical dielectric particles to yield a strong magnetic response is one of the main feature of Mie resonances. This property is at the core of many investigations with dielectric nanostructures to tailor the light scattering through the coherent excitation of electric and magnetic modes and also to enhance the magnetic interaction between matter and electromagnetic waves, *i.e.* the wave-matter interaction *via* the magnetic component of the field. The magnetic mode yields a strong magnetic response in the near field of the dielectric scatterer. The magnetic field distribution can be engineered and strong magnetic field intensities can be obtained. The strong magnetic response can also be used to engineer the magnetic local density of states and to promote magnetic spontaneous emission of quantum emitters. In the far field, the coherent excitation of both electric and magnetic dipoles leads to unique scattering properties.

3. Kerker effect and Kerker conditions

In 1983, Milton Kerker and co-authors [24] discovered an interesting effect in the scattering of electromagnetic waves by a spherical particle made of a magnetic material characterized by magnetic permeability μ and dielectric permittivity ϵ. This study revealed very unusual effect, nowadays called *Kerker effect*. More specifically, Kerker and his collaborators revealed the possibility to redirect the scattered radiation to either forward or backward direction, depending on the frequency. They discovered two conditions, known as *the first and second Kerker conditions*. The first Kerker condition corresponds to a cancellation of the backward scattering (with a maximum in the forward scattering), while the second Kerker condition corresponds to a deep minimum in the forward scattering direction. The backward and forward scattering are defined by the scattering along the axis of the incoming waves. The optical theorem states that the extinction cross-section of a scatterer can be cast with respect to its forward scattering, which means that the forward scattering cannot be canceled. Kerker and co-workers established that the first condition is obtained when $\epsilon = \mu$, and the second condition is satisfied when

$$\epsilon = -\frac{\mu - 4}{\mu + 1}.$$

Initially, this important study did not find a wide audience due to a lack of required magnetic materials, and also because the Kerker conditions require special values of the parameters.

Nevertheless, as was shown independently by two groups in 2011, the Kerker conditions can be extended to nonmagnetic dielectric spheres supporting both electric and magnetic Mie resonances [6, 25, 26]. This property of Mie scatterers to satisfy both Kerker conditions due to the electric and magnetic Mie resonances was actually one of the first unusual property investigated in this new field of all-dielectric metaphotonics. The artificial magnetism provided by the Mie resonances allows to mimic the anomalous scattering properties of magnetic spheres.

The Kerker conditions are predicted through the calculation of the electric and magnetic polarisabilities of the dielectric scatterer, α_e and α_h, respectively. It is convenient to derive the electric and magnetic polarisabilities from the elements of the $T_n^{(e,h)}$ matrix (e and h standing for electric and magnetic respectively), conventionally noticed a_n and b_n, with n standing for the multipolar orders:

$$\alpha_e = -T_n^{(e)} = \frac{3\mathrm{i}\epsilon a_1}{2k^3}, \quad \alpha_h = -T_n^{(h)} \frac{3\mathrm{i}b_1}{2\mu k^3}.$$

For a dipolar scatterer, *i.e.* a scatterer for which the multipolar Mie scattering coefficients a_n and b_n can be safely neglected for $n \geq 2$, the first Kerker condition is obtained when $a_1 = b_1$ while the second Kerker condition satisfies the relations: $\Re(\epsilon^{-1}\alpha_e) = -\Re(\mu\alpha_m)$ and $\Im(\epsilon^{-1}\alpha_e) = \Im(\mu\alpha_m)$ [25, 26]. These analytical derivations can be assessed by calculating and the scattering patterns of a single sphere at the first and second Kerker conditions [29] and first observed experimentally for microwaves [25, 30]. Experimental values of the scattered intensity of a sphere can be matched well with the theoretical results, as shown in Figures 2(a,b). Experimental observations of the Kerker conditions in the visible spectrum has been reported for Si and GaAs nanoparticles [27,31]. In Ref. [27], an AlGaAs particle was fabricated by reactive ion etching followed by a transfer on a transparent fused silica substrate. Bright field spectroscopy on a single particle allowed the measurement of the reflected spectrum and the observation of a cancellation of the reflected intensity in a short spectral range [27].

The first Kerker condition finds straightforward applications in the design of Huygens sources in planar metasurfaces [32]. This condition meets several conditions that make dipolar Mie scatterers ideal candidates to build metasurfaces: besides their weak losses, they can scatter light in the forward direction, with a maximum of forward light scattering when $a_1 = b_1$ while the phase of the polarisability of a dipolar scatterer experiences a phase shift of π at a resonance.

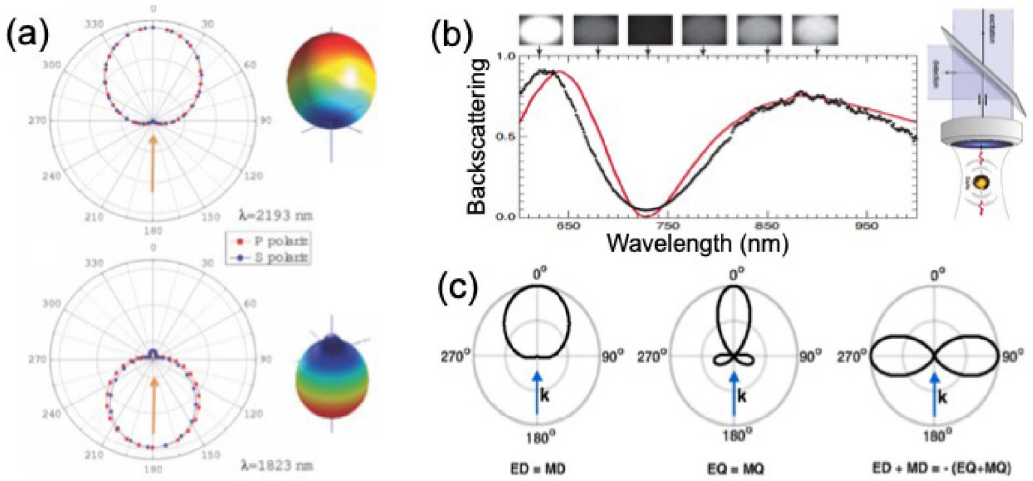

Figure 2. Kerker effects in dielectric nanoantennas. (a) Evidence of the Kerker effect in a germanium sphere. Scattering diagram plotted for the two polarization cases (TE (blue) and TM (red)) when illuminating a 140 nm Ge sphere at the wavelengths $\lambda = 2193$ nm (top; forward scattering) and $\lambda = 1823$ nm (bottom; backward scattering). Adapted with permission from [25]. (b) Observation of the Kerker effect in optics. Left: Spectrum of light intensity backscattered by an individual GaAs nanodisk of radius 90 nm. Black dotted curve: measurement; red curve: numerical spectrum. Right: sketch of the measurement: white light is weakly focused on a GaAs particle. Backscattered light is separated by a 50/50 beam-splitter and sent to a spectrometer. Adapted with permission from [27]. (c) Concept of the transverse Kerker effect. Electric dipole (ED) is in phase with a magnetic dipole (MD), and an electric quadrupole (EQ) is in phase with a magnetic quadrupole (MQ), whereas the dipoles are out of phase with the quadrupoles. Adapted with permission from [28].

When combining electric and magnetic resonances, the phase of the polarisability of a single Mie resonator can be tuned over 2π [32]. The forward light scattering being based on the excitation of both electric and magnetic dipolar resonances, this forward scattering can be associated with a strong modulation of the light phase. Efforts have been put to optimize the geometry of the scatterer to optimize the forward light scattering [33]. Regarding the second Kerker condition, we mention that besides the modulation of phase, it finds applications to develop highly refractive metasurfaces [34].

The extension of the Kerker effect to other multipoles has been discussed in a number of papers, and these studies have been summarized recently [35]. Here, we also mention a recently demonstrated novel effect of the so-called transverse scattering of light by Mie-resonant subwavelength particles with simultaneous suppression of both forward and backward scattering [28]. This generalized Kerker effect occurs when in-phase electric and magnetic dipoles become out of phase with the corresponding pairs of quadrupoles. Shamkhi *et al.* [28] obtained the general conditions for the simultaneous suppression of scattering in both forward and backward directions, and generalized these conditions to non-spherical particles, see Figure 2(c). They verified the concept in a proof-of-principle microwave experiment, with good agreement with analytical and numerical results, and also studied metasurfaces composed of the nanoparticles with the transverse scattering patterns. In a sharp contrast to Huygens' metasurfaces, these novel metasurfaces scatter neither forward nor backward, being almost invisible [36].

Subwavelength structures demonstrate many unusual optical properties which can be em-

ployed for a control of scattering of light and invisibility cloaking. Suppression of light scattering can be achieved for a uniform dielectric object with high refractive index, based on the novel physics of cascades of Fano resonances observed in the Mie scattering from a homogeneous dielectric rod [37]. Scattering cancellation and optical cloaking have been reported for a variety of systems based on dielectric metamaterials [38–40].

4. All-dielectric nanoantennas

Optical antennas are nanostructures aimed at manipulating spontaneous emission of solid-state emitters at room temperature [41]. Plasmonic antennas were proposed early in the 2000's, first to engineer the local density of states in the vicinity of metallic nanostructures [42–46], and second to control the direction of emission of quantum emitters [47]. This field of research has led to impressive results since metallic nanostructures can yield giant decay rates and can efficiently shape the emission pattern. Among the wide range of metallic antennas, Yagi–Uda antennas and corrugated antennas exhibit high gains in directivity [48, 49]. Self-assembled metallic particles were also proved to yield extremely high decay rates, either with DNA template nanoantennas in which is grafted a single fluorescent molecule [50, 51], or with gap plasmons obtained by depositing colloidal particles on metallic substrates and by inserting quantum emitters inside the extremely small nanogap separating a metallic film from a colloidal particle [52, 53].

Electromagnetic Mie resonances experienced in dielectrics with weak losses are very promising to develop highly radiative and directive optical antennas. The use of dielectric particles was first investigated with silica microspheres that host high multipolar orders [54]. The use of higher refractive index combined with a decrease of the size of dielectric particles was investigated numerically with a titania particle [55]. The titania particle was used to shape the emission pattern of an electric dipole located in the nanogap of a silver dimer of nanoparticles. The dimer was used to enhance the decay rates while the high refractive index was used to shape the emission direction into a narrow lobe [55]. A hybrid metal-dielectric antenna was experimentally developed in 2018 [56]. It was composed of a bow-tie gold nanoantenna coupled with 3 silicon nanorods. This antenna was fed by the photoluminescence of gold.

Silicon particles were numerically investigated in 2011 and 2012 to tailor the emission pattern of electric dipolar emitters. By studying the emission pattern of an electric dipole coupled with a silicon particle hosting electric and magnetic dipolar modes, it was showed as early as 2011 that the direction of emission can be optimized either in the backward or the forward direction [6]. The main interest of Mie resonant antennas comes from the possibility to couple the quantum emitter with both electric and magnetic modes [6–8]. The coherent excitation of electric and magnetic modes offers a higher degree of freedom to engineer the emission in a given direction through the phase and amplitude of electric and magnetic modes. The coherent excitation of electric and magnetic dipoles can be seen as an extension of the Kerker conditions in the near field, *i.e.* when the Mie resonator is excited from the near field. The emission of a quantum emitter coupled with a dielectric Mie resonator can therefore be maximized in either the forward or the backward directions. The gains in directivity that are obtained in these two conditions are higher than those that could be achieved with an antenna hosting a single mode resonance, *i.e.* an electric dipole resonance like in the case of spherical plasmonic nanoparticles.

Besides their strong interest to shape the emission pattern of solid-state emitters, dielectric Mie resonators are also very interesting to enhance the excitation strength of quantum emitters, to tailor their local density of states and to control their spontaneous emission rates. When compared with their plasmonic counterparts, the total decay rate enhancements yielded by dielectric antennas are smaller but the ratio between radiative and total decay rates can be larger thanks to smaller intrinsic losses. However, dielectric Mie resonators offer key properties

to manipulate spontaneous emission: (i) they can tailor decay rates of both electric and magnetic dipolar transitions, (ii) they exhibit weak intrinsic losses and can efficiently collect the emitted photons, (iii) semi-conductor based antennas can be easily integrated into photonic chips, (iv) internal fields can be engineered to boost the photoluminescence properties of emitters located inside the high refractive index material [57].

Controlling the electric or magnetic nature of the dipolar transition with Mie resonances, and more generally controlling higher order transition moments, is an inspiring way of investigation [58]. This field of research rapidly raised the interest since it coincided with the raise of interest in the higher order transition moments in rare earth ions [59–61]. Electric and magnetic resonances of Mie resonators were therefore investigated to promote either an electric or a magnetic transition of coupled rare-earth ions [62, 63]. However, from an experimental point of view, coupling rare earth ions with Mie resonators and more precisely locating the emitter at the position where the magnetic local density of states (LDOS) is maximum is very challenging. The main achievements in the control of magnetic spontaneous emission were reported only recently with either individual Si-based antennas [64] or Si-based metasurfaces [65].

If interest in Mie resonant antennas was initially driven by the original concept of magnetic spontaneous emission, they also offer a strong interest to enhance the electric LDOS that is suitable to enhance fluorescence of quantum dots or molecules (see Figure 3). Taking inspiration from plasmonic nanogap antennas [50, 51, 69, 70], dielectric dimer antennas were proposed to manipulate the spontaneous emission, as evidenced first numerically [62, 71] and in a second step experimentally [67, 68, 72]. The main challenge is to optimize the field outside the high refractive index and to yield strong electric field intensities with a strong contrast with the background in order to detect fluorescence signal of molecules located in the nanogap (see Figure 3). This method allows the enhancement of the electric field excitation on fluorescent molecules and to increase by several orders of magnitude their fluorescence signal [68, 72].

If dielectric gap antennas are based on the strong enhancement of the electric field intensity in the gap separating the two particles, a major interest of Mie resonant antennas lies in the fact that they can be fed directly inside the cavity where the Purcell factor is maximum [73]. The first result was reported in 2017 with quantum dots embedded in silicon nanodisks [74]. Let us notice that the concept of hybridization also applies to this case so that dimers and trimers of doped Si-nanodisks can be coupled to further boost the photoluminescence of quantum dots. The strong enhancement of the internal field intensity driven by Mie resonances can also be exploited to enhance the Raman signal of silicon particles [75, 76] and non linear signals. The richness of this field of research will undoubtedly lead to several outcomes in the upcoming years.

A very promising way of development is to consider active materials to design the photonic cavities (see Figure 4). For example, the high refractive index of diamond can be used to form a Mie resonant cavity around color centers [77, 78]. The resonant scattering of light on nanodiamonds due to the excitation of electric and magnetic dipolar modes has been evidenced (see Figure 4(a)). The photoluminescence of color centers can therefore benefit from Mie resonances. An enhancement of the photoluminescence of Nitrogen Vacancy (NV) color centers in nanodiamonds was reported recently: the fluorescence efficiency can be enhanced thanks to Mie resonances and the emission lifetime can be decreased [79] (see Figure 4(b)).

A very promising approach for developing active Mie resonators is to consider halide perovskites, a class of semi-conductor materials characterized by a high refractive index. The discovery of the exceptional excitonic properties almost 10 years ago triggered a huge interest to improve the efficiency of photovoltaics and light emitting devices [80]. Halide perovskites feature exceptional excitonic properties. Bridging the gap between this novel class of light emitting materials and Mie resonant cavities will lead to outcomes in integrated light sources [81]. Enhancement of the photoluminescence of halide perovskites was first reported in 2018 by considering par-

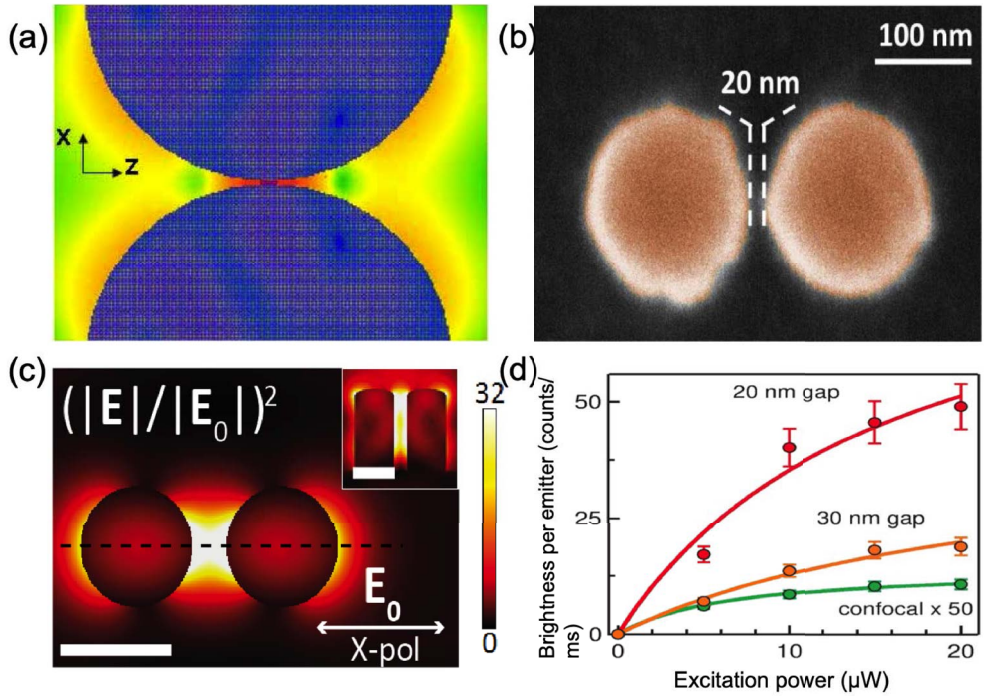

Figure 3. All-dielectric nanogap antennas. (a) Electric field distribution in the vicinity of a 20 nm nanogap separating two Si microdisks (diameter 2 μm, thickness of 200 nm) illuminated in normal incidence with an incident electric field linearly polarized along the x-axis at a wavelength of 2.437 μm. Adapted with permission from [66]. (b) SEM image of a silicon nanogap antenna fabricated with e-beam lithography. Diameter of 170 nm diameter, thickness of 60 nm and nanogap of 20 nm. (c) Enhancement of the electric field intensity yielded by a GaP dimer antenna composed of two GaP pillars, 100 nm in diameters, 200 nm in height and separated by a 35 nm nanogap. The field distribution is taken at mid-height (100 nm). Adapted with permission from [67]. (d) Brightness *per* emitter with respect to the emission power for two different nanogap lenghts, 20 nm and 30 nm, with the Si dimer nanogap antenna displayed in (b). Comparison with the brightness *per* emitter measured without antenna (measured signal × 50). Adapted with permission from [68].

ticles made of $MAPbI_3$ created by using a laser ablation technique on a perovskite thin film. A maximum of the photoluminescence signal was reported at the wavelength corresponding to the quadrupolar magnetic resonance [82]. The next challenge after performing Mie enhanced photoluminescence lies in the stimulated emission and the development of a novel class of laser cavities by forming Mie cavities in halide perovskites. The latest results were obtained with nanocubes made of $CsPbBr_3$ (see Figures 4(c–e)). High quality monocrystalline $CsPbBr_3$ nanocubes are first synthesized chemically on a sapphire substrate (see Figure 4(c)). Dark field spectrum performed on a single 420 nm nanocube displayed in Figure 4(d) clearly evidences the resonant light scattering due to the excitation of electric and magnetic multipoles. The photoluminescence spectrum of $CsPbBr_3$ is indicated by the green zone in Figure 4(d). A peak of the dark field spectrum can be observed in this spectral range. The resonant light scattering is assessed by observing a strong dependence of the scattering spectra on the size of the nanocubes. The photoluminescence spectra are recorded when exciting nanocubes with a 150 fs laser. Importantly, the spectra

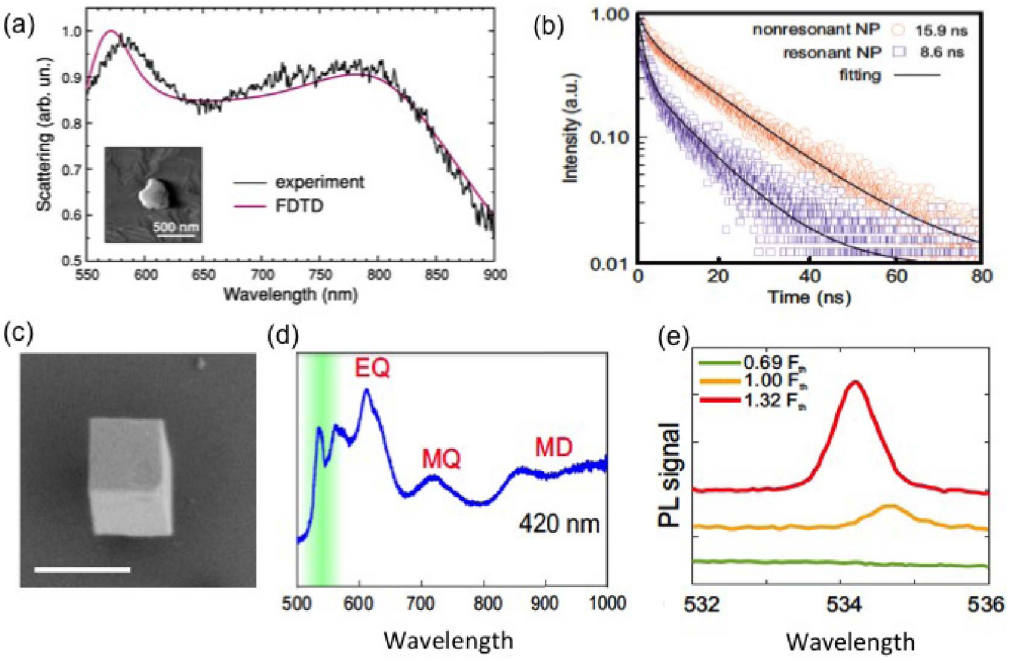

Figure 4. Mie resonances in excitonic materials: colored centers in nanodiamonds (top row) and perovskites (bottom row). (a) Unpolarized scattering spectrum of a single nanodiamond. Black line: experimental spectrum. Red line: numerical simulations implemented with FDTD (Finite Difference Time Domain) when considering a spherical nanodiamond with a diameter of 320 nm under the experimental conditions of the collection. Adapted with permission from [77]. (b) Time-resolved photoluminescence measurements for two sets of samples: NV centers in optically small (<100 nm) nanodiamonds (orange dots) and in large and optically resonant nanodiamonds (purple dots). Adapted with permission from [79]. (c) SEM images of $CsPbBr_3$ nanocubes placed on a sapphire substrate. Scale bar is 500 nm. (d) Dark-field spectra of the $CsPbBr_3$ nanocubes. The photoluminescence spectral range is indicated by the green zone. Pump intensity-dependent emission spectra for three different fluences compared with the lasing threshold: above (red), equal (orange) and below (green) the lasing threshold. (c–e) Adapted with permission from [83].

reveal a threshold-like appearance of a photoluminescence signal in the range $\lambda = (532; 538)$ nm, that corresponds to the red side of the emission line of the exciton (see Figure 4(e)).

5. Bound states in the continuum

Bound states in the continuum have attracted a lot of attention in photonics recently, and they originate from a coupling between the leaky modes in dielectric structures such as photonic crystals, metasurfaces, and isolated resonators [84]. These resonances provide an alternative mean to achieve very large Q factors for lasing [85] and also allow to tune a photonic system into the regime of the so-called *supercavity mode* [86]. A true bound state in the continuum (BIC) is a mathematical object with an infinite value of the Q factor and vanishing resonance width, and it can exist only in ideal loss-less infinite structures or for extreme values of parameters [87, 88]. In practice, BIC can be realized as a quasi-BIC mode, being directly associated with the supercavity

mode [86], when both the Q factor and resonance width become finite. However, the localization of light inspired by the BIC physics makes it possible to realize high-Q quasi-BIC modes in many optical structures such as cavities and coupled waveguides.

Importantly, there exists a direct link between quasi-BIC states and Fano resonances since these two phenomena are supported by the similar physics. More specifically, quasi-BIC resonance can be described explicitly by the classical Fano formula, and the observed peak positions and linewidths correspond exactly to the real and imaginary parts of the eigenmode frequencies. The Fano parameter becomes ill-defined at the BIC condition, which corresponds to a collapse of the Fano resonance. Importantly, every quasi-BIC modes can be linked with the Fano resonances, whereas the opposite is not always true: the Fano resonance may not converge to the BIC mode for any variation of the system parameters.

As an example, we consider all-dielectric metasurfaces with the in-plane symmetry breaking [89] that can support sharp high-Q resonances arising from a distortion of symmetry-protected BICs. We follow the recent paper [90], we consider a metasurface made of As_2S_3 and placed on a glass substrate consisting of a square lattice of meta-atoms with broken in-plane inversion symmetry, as illustrated in Figure 5(a). The meta-atom is constructed of a pair of rectangular bars which have lengths L and $L-\delta L$, respectively. The asymmetry of the unit cell is controlled by the difference in bar lengths, which is characterized by the asymmetry parameter $\alpha = \delta L/L$, see Figure 5(b).

Figure 5(c) demonstrates the dependence of the simulated transmission spectra on the wavelength of excitation and the asymmetry parameter α. The white dashed line illustrates the eigenmode dispersion. The eigenmode simulations show that the metasurface with a symmetric unit cell ($\alpha = 0$) supports a symmetry-protected BIC at 795 nm, which has infinite Q factor and is not manifested in the transmission spectrum. The BIC is unstable against perturbations that break the in-plane inversion symmetry, so for $\alpha > 0$ it transforms into a quasi-BIC with a finite Q factor [89]. The quasi-BIC is revealed in the transmission spectra as a sharp resonance with a Fano lineshape whose linewidth increases with the magnitude of asymmetry. The dependence of the radiative Q factor on α follows the inverse quadratic law for small values of the asymmetry parameter [89], as shown in Figure 5(d). Hence, the meta-atom asymmetry is necessary to obtain a sharp resonance whose position and width can be adjusted by the degree of asymmetry.

Thus, bound states in the continuum provide a new approach for engineering a resonant response of dielectric metasurfaces composed of meta-atoms with broken in-plane inversion symmetry. The similar approach can be applied to the case of nonlinear metasurfaces [91, 92] with broken-symmetry or nonlinear metasurfaces composed of arrays of chalcogenide nanoresonators designed for the nonlinear optical generation of higher harmonics.

6. Applications of Mie resonances: structural colors

Colors perceived by eyes result from the interaction between the incoming light and the three types of cone cells. A modification in the spectrum of the incoming light will result in a modification of the perceived color. When white light interacts with structured matter, its broad spectrum experiences a strong variation with peaks and dips which yield a color to the nanostructured matter. Colors resulting from the interaction between light and nano or microstructures are called structural colors. The terminology “structural” means that the color depends on the morphology of the structured matter. A modification of the morphology modifies the structural color. Structural colors can be found in a wide set of biological species, the most famous example being certainly the wings of the Morpho butterfly [93, 94]. Wings are structured at a sub-micrometer scale which provides photonic band gaps. In the case of the Morpho butterfly, the photonic band gap

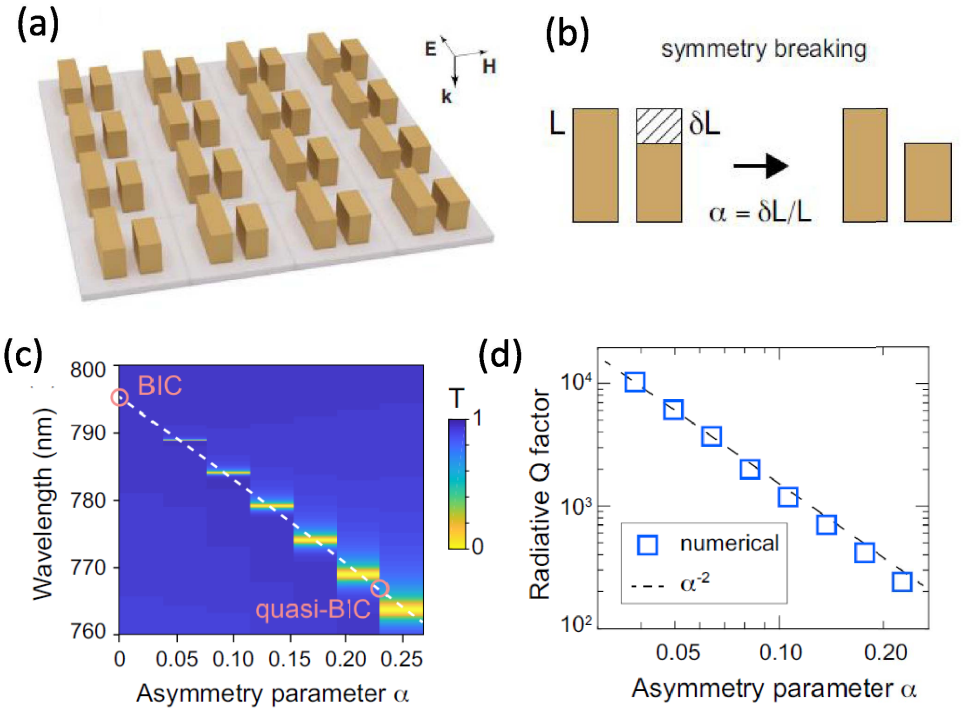

Figure 5. Metasurfaces with bound states in the continuum. (a) Design of a metasurface consisting of a square array of As_2S_3-bar pairs of different length placed on a glass substrate. The inset shows the orientation and polarization of the incident field. (b) Definition of the asymmetry parameter α. (c) Numerically simulated transmission spectra with respect to the excitation wavelength and the asymmetry parameter α. The white dashed line illustrates the quasi-BIC dispersion. (d) Dependence of the radiative Q factor on the parameter α. The dashed line shows an inverse quadratic fitting. Adapted with permission from [90].

is centered on the blue part of the spectrum. The blue part of the spectrum is therefore reflected which provides a vivid blue color to the wings.

Structural colors can also be found in plasmonics. When observing metallic particles of different sizes and shapes dispersed in a transparent substrate in dark field spectroscopy, a myriad of colors can be observed. It turns out that each particle yields its own color and behaves like a colored pixel. The pixel size stands under the diffraction limit and achieves the limit of resolution. This approach is very promising to create non fading colors with a high resolution. When assembling different scatterers on a surface, colored images can be finely designed which opens plenty of rooms to create images at high resolution [95]. Structural colors have benefited from intense developments to extend the gamut of colors, to decrease the cost of this technology and to extend its range of applications [96].

When observing silicon particles in dark-field spectroscopy, structural colors can also be observed (see Figure 1) [9, 10, 19, 97]. This result was expected since their resonant interaction with light strongly modulates the scattered spectrum. The coupling of light with electric and magnetic Mie resonant modes of high-index particles results in a perceived color that can be controlled through the shape and composition of the particles, and also through their mutual coupling. This result strengthens the field of resonant structural colors since cost effective and

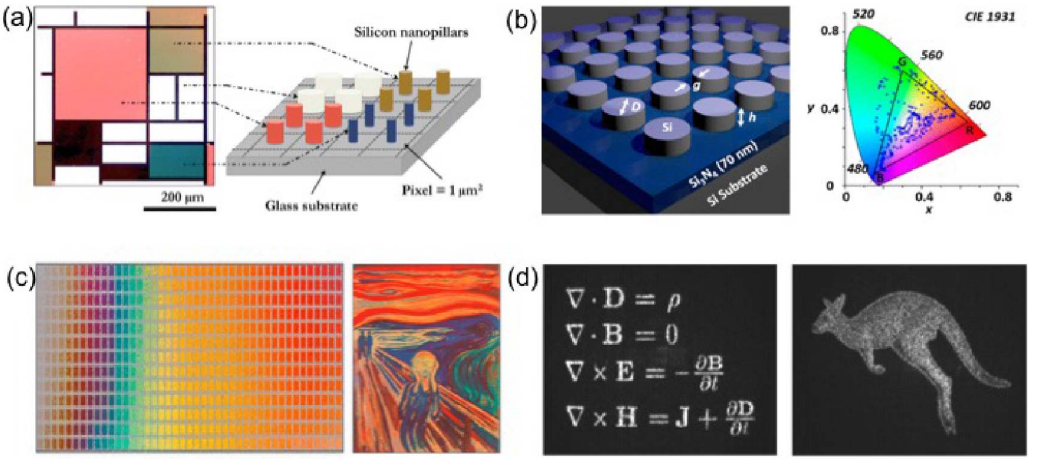

Figure 6. Silicon Mie-resonant metasurfaces for generating colors and holograms. (a) Mondrian's painting reproduced at a 1:1200 scale with silicon particles on a transparent substrate observed in dark-field imaging. Adapted with permission from [99]. (b) Extended gamut of colors obtained by coupling the nanostructured silicon layer with an unpatterned underlying high refractive index layer made of Si_3N_4. Adapted with permission from [100]. (c) Palette of colors obtained when varying the diameter of the silicon nanodisks and the period of the 2D array. Example of a painting reproduction. Here "The Scream" by the Norwegian painter Edvard Munch. Adapted with permission from [101]. (d) Experimental holographic images from two holograms at a 1600 nm wavelength. Adapted with permission from [106].

non toxic materials with high refractive index can be found. A strong interest has been brought to the case of silicon based nanostructures. One of the first examples of structural colours in silicon was presented in 2014 with periodical grooves patterned in silicon substrates [98]. When assembling silicon Mie resonators on a substrate and when controlling their size to tailor finely their spectral response, colored images can be obtained and painting can be reproduced. This was shown in 2016 in dark field spectroscopy with silicon particles of different diameters etched on a silicon film coated on a transparent substrate [99]. A palette of structural colors has been created when considering several arrays of similar Si nanodisks. In a second step, a Mondrian's painting was reproduced (Figure 6(a)). Mie resonant scatterers have been optimized to extend the gamut of colors, in particular through the control of their shape or through the coupling with an underlying layer [100] (see Figures 6(b,c)) or by adjusting the diameter of nanodisks and the period of the 2D array of nanodisks [101, 102]. This technique can also be employed to design spectral filters [102, 103]. Over the last two years, outstanding achievements have been reported in terms of designs and color rendering with different dielectric materials and fabrication methods [101, 104, 105]. The strong efforts devoted to the development of structural colors are motivated by numerous applications in anti-counterfeiting, spectral filtering, and color rendering of surfaces. The latest developments are focused on novel applications such as complex holograms [106, 107] (see Figure 6(d)).

7. Conclusion

The field of high-index dielectric metaphotonics has emerged recently as a new and rapidly developing direction of research in nanophotonics and metamaterials. The study of all-dielectric

resonant nanostructures is motivated by the rich physics of Mie resonances allowing to excite both electric and magnetic multipole modes in individual subwavelength particles. Metaphotonics has a broad range of applications, highlighting the importance of optically-induced magnetic response, and including structural coloring, optical sensing, spatial modulation of light, nonlinear and active media, as well as both integrated classical and quantum circuitry and topological photonics, underpinning a new generation of highly-efficient active metadevices. We anticipate further rapid development of these ideas into the field of *active metaphotonics* for creating new types of light sources, light-emitting metasurfaces, quantum signal processing, and efficient nanolasers.

References

[1] S. O'Brien, J. B. Pendry, "Photonic band-gap effects and magnetic activity in dielectric composites", *J. Phys.: Condens. Matter* **14** (2002), no. 15, p. 4035.
[2] J. A. Schuller, R. Zia, T. Taubner, M. L. Brongersma, "Dielectric metamaterials based on electric and magnetic resonances of silicon carbide particles", *Phys. Rev. Lett.* **99** (2007), article ID 107401.
[3] A. B. Evlyukhin, C. Reinhardt, A. Seidel, B. S. Luk'yanchuk, B. N. Chichkov, "Optical response features of si-nanoparticle arrays", *Phys. Rev. B* **82** (2010), article ID 045404.
[4] A. B. Evlyukhin, C. Reinhardt, B. N. Chichkov, "Multipole light scattering by nonspherical nanoparticles in the discrete dipole approximation", *Phys. Rev. B* **84** (2011), article ID 235429.
[5] A. García-Etxarri, R. Gómez-Medina, L. S. Froufe-Pérez, C. López, L. Chantada, F. Scheffold, J. Aizpurua, M. Nieto-Vesperinas, J. J. Sáenz, "Strong magnetic response of submicron silicon particles in the infrared", *Opt. Express* **19** (2011), no. 6, p. 4815-4826.
[6] A. Krasnok, A. Miroshnichenko, P. Belov, Y. Kivshar, "Huygens optical elements and Yagi–Uda nanoantennas based on dielectric nanoparticles", *JETP Lett.* **94** (2011), p. 593-598.
[7] B. Rolly, B. Stout, N. Bonod, "Boosting the directivity of optical antennas with magnetic and electric dipolar resonant particles", *Opt. Express* **20** (2012), no. 18, p. 20376-20386.
[8] A. E. Krasnok, A. E. Miroshnichenko, P. A. Belov, Y. S. Kivshar, "All-dielectric optical nanoantennas", *Opt. Express* **20** (2012), no. 18, p. 20599-20604.
[9] A. I. Kuznetsov, A. E. Miroshnichenko, Y. H. Fu, J. Zhang, B. Lukyanchuk, "Magnetic light", *Sci. Rep.* **2** (2012), p. 492.
[10] A. B. Evlyukhin, S. M. Novikov, U. Zywietz, R. L. Eriksen, C. Reinhardt, S. I. Bozhevolnyi, B. N. Chichkov, "Demonstration of magnetic dipole resonances of dielectric nanospheres in the visible region", *Nano Lett.* **12** (2012), no. 7, p. 3749-3755.
[11] A. I. Kuznetsov, A. E. Miroshnichenko, M. L. Brongersma, Y. S. Kivshar, B. Luk'yanchuk, "Optically resonant dielectric nanostructures", *Science* **354** (2016), no. 6314, article ID aag2472.
[12] S. Kruk, Y. Kivshar, "Functional meta-optics and nanophotonics governed by Mie resonances", *ACS Photon.* **4** (2017), p. 2638.
[13] G. Mie, "Beiträge zur optik trüber medien, speziell kolloidaler metallösungen", *Ann. Phys.* **330** (1908), no. 3, p. 377-445.
[14] H. Hulst, *Light scattering by small particles, Structure of matter series*, Wiley, 1957.
[15] A. Lagendijk, B. A. van Tiggelen, "Resonant multiple scattering of light", *Phys. Rep.* **270** (1996), no. 3, p. 143-215.
[16] A. B. Matsko, V. S. Ilchenko, "Optical resonators with whispering gallery modes i: basics", *IEEE J. Sel. Top. Quantum Electron.* **12** (2006), no. 3, p. 3.
[17] V. S. Ilchenko, A. B. Matsko, "Optical resonators with whispering-gallery modes-part ii: applications", *IEEE J. Sel. Top. Quantum Electron.* **12** (2006), no. 1, p. 15-32.
[18] A. Devilez, X. Zambrana-Puyalto, B. Stout, N. Bonod, "Mimicking localized surface plasmons with dielectric particles", *Phys. Rev. B* **92** (2015), no. 24, article ID 241412.
[19] U. Zywietz, A. B. Evlyukhin, C. Reinhardt, B. N. Chichkov, "Laser printing of silicon nanoparticles with resonant optical electric and magnetic responses", *Nat. Commun.* **5** (2014), p. 3402.
[20] F. B. Arango, A. F. Koenderink, "Polarizability tensor retrieval for magnetic and plasmonic antenna design", *New J. Phys.* **15** (2013), no. 7, article ID 073023.
[21] J. Proust, N. Bonod, J. Grand, B. Gallas, "Optical monitoring of the magnetoelectric coupling in individual plasmonic scatterers", *ACS Photon.* **3** (2016), no. 9, p. 1581-1588.
[22] M. Dubois, L. Leroi, Z. Raolison, R. Abdeddaim, T. Antonakakis, J. de Rosny, A. Vignaud, P. Sabouroux, E. Georget, B. Larrat *et al.*, "Kerker effect in ultrahigh-field magnetic resonance imaging", *Phys. Rev. X* **8** (2018), no. 3, article ID 031083.

[23] P. Nordlander, C. Oubre, E. Prodan, K. Li, M. Stockman, "Plasmon hybridizaton in nanoparticle dimers", *Nano Lett.* **4** (2004), no. 5, p. 899-903.
[24] M. Kerker, D.-S. Wang, C. L. Giles, "Electromagnetic scattering by magnetic spheres", *J. Opt. Soc. Am.* **73** (1983), no. 6, p. 765-767.
[25] R. Gomez-Medina, B. Garcia-Camara, I. Suarez-Lacalle, F. Gonzalez, F. Moreno, M. Nieto-Vesperinas, J. J. Saenz, "Electric and magnetic dipolar response of germanium nanospheres: interference effects, scattering anisotropy, and optical forces", *J. Nanophoton.* **5** (2011), article ID 053512.
[26] M. Nieto-Vesperinas, R. Gomez-Medina, J. J. Saenz, "Angle-suppressed scattering and optical forces on submicrometer dielectric particles", *J. Opt. Soc. Am. A* **28** (2011), no. 1, p. 54-60.
[27] S. Person, M. Jain, Z. Lapin, J. J. Saenz, G. Wicks, L. Novotny, "Demonstration of zero optical backscattering from single nanoparticles", *Nano Lett.* **13** (2013), no. 4, p. 1806-1809.
[28] H. Shamkhi, K. Baryshnikova, A. Sayanskiy, P. Kapitanova, P. Terekhov, P. Belov, A. Karabchevsky, A. Evlyukhin, Y. Kivshar, A. Shalin, "Transverse scattering and generalized Kerker effects in all-dielectric mie-resonant metaoptics", *Phys. Rev. Lett.* **122** (2019), article ID 193905.
[29] R. Paniagua-Domínguez, F. López-Tejeira, R. Marqués, J. A. Sánchez-Gil, "Metallo-dielectric core-shell nanospheres as building blocks for optical three-dimensional isotropic negative-index metamaterials", *New J. Phys.* **13** (2011), no. 12, article ID 123017.
[30] J. Geffrin, B. García-Cámara, R. Gómez-Medina, P. Albella, L. Froufe-Pérez, C. Eyraud, A. Litman, R. Vaillon, F. González, M. Nieto-Vesperinas *et al.*, "Magnetic and electric coherence in forward-and back-scattered electromagnetic waves by a single dielectric subwavelength sphere", *Nat. Commun.* **3** (2012), p. 1171.
[31] Y. H. Fu, A. I. Kuznetsov, A. E. Miroshnichenko, Y. F. Yu, B. Lukyanchuk, "Directional visible light scattering by silicon nanoparticles", *Nat. Commun.* **4** (2013), p. 1527.
[32] I. Staude, A. E. Miroshnichenko, M. Decker, N. T. Fofang, S. Liu, E. Gonzales, J. Dominguez, T. S. Luk, D. N. Neshev, I. Brener *et al.*, "Tailoring directional scattering through magnetic and electric resonances in subwavelength silicon nanodisks", *ACS Nano* **7** (2013), no. 9, p. 7824-7832.
[33] B. S. Luk'yanchuk, N. V. Voshchinnikov, R. Paniagua-Domínguez, A. I. Kuznetsov, "Optimum forward light scattering by spherical and spheroidal dielectric nanoparticles with high refractive index", *ACS Photon.* **2** (2015), no. 7, p. 993-999.
[34] P. Moitra, B. A. Slovick, W. Li, I. I. Kravchencko, D. P. Briggs, S. Krishnamurthy, J. Valentine, "Large-scale all-dielectric metamaterial perfect reflectors", *ACS Photon.* **2** (2015), no. 6, p. 692-698.
[35] W. Liu, Y. Kivshar, "Generalized kerker effects in nanophotonics and meta-optics", *Opt. Express* **26** (2018), p. 13085-13105.
[36] H. K. Shamkhi, A. Sayanskiy, A. C. Valero, A. S. Kupriianov, P. Kapitanova, Y. S. Kivshar, A. S. Shalin, V. R. Tuz, "Transparency and perfect absorption of all-dielectric resonant metasurfaces governed by the transverse kerker effect", *Phys. Rev. Mater.* **3** (2019), no. 8, article ID 085201.
[37] M. Rybin, D. Filonov, P. Belov, Y. Kivshar, M. Limonov, "Switching from visibility to invisibility via fano resonances: Theory and experiment", *Sci. Rep.* **5** (2015), p. 8774.
[38] Q. Zhao, J. Zhou, F. Zhang, D. Lippens, "Mie resonance-based dielectric metamaterials", *Mater. Today* **12** (2009), p. 60-69.
[39] J. Valentine, J. Li, T. Zentgraf, G. Bartal, X. Zhang, "An optical cloak made of dielectrics", *Nat. Mater.* **8** (2009), p. 568-571.
[40] M. M. Farhat, S. Muhlig, C. Rockstuhl, F. Lederer, "Scattering cancellation of the magnetic dipole field from macroscopic spheres", *Opt. Express* **20** (2012), p. 13896-13906.
[41] L. Novotny, N. van Hulst, "Antennas for light", *Nat. Photon.* **5** (2011), no. 2, p. 83-90.
[42] E. Dulkeith, A. Morteani, T. Niedereichholz, T. Klar, J. Feldmann, S. Levi, F. Van Veggel, D. Reinhoudt, M. Möller, D. Gittins, "Fluorescence quenching of dye molecules near gold nanoparticles: radiative and nonradiative effects", *Phys. Rev. Lett.* **89** (2002), no. 20, article ID 203002.
[43] P. Mühlschlegel, H. Eisler, O. Martin, B. Hecht, D. Pohl, "Resonant optical antennas", *Science* **308** (2005), no. 5728, p. 1607-1609.
[44] P. Anger, P. Bharadwaj, L. Novotny, "Enhancement and quenching of single-molecule fluorescence", *Phys. Rev. Lett.* **96** (2006), article ID 113002.
[45] P. Bharadwaj, L. Novotny, "Spectral dependence of single molecule fluorescence enhancement", *Opt. Express* **15** (2007), no. 21, p. 14266-14274.
[46] M. Ringler, A. Schwemer, M. Wunderlich, A. Nichtl, K. Kürzinger, T. Klar, J. Feldmann, "Shaping emission spectra of fluorescent molecules with single plasmonic nanoresonators", *Phys. Rev. Lett.* **100** (2008), no. 20, article ID 203002.
[47] J. Li, A. Salandrino, N. Engheta, "Shaping light beams in the nanometer scale: A Yagi–Uda nanoantenna in the optical domain", *Phys. Rev. B* **76** (2007), article ID 245403.
[48] A. G. Curto, G. Volpe, T. H. Taminiau, M. P. Kreuzer, R. Quidant, N. F. van Hulst, "Unidirectional emission of a quantum dot coupled to a nanoantenna", *Science* **329** (2010), no. 5994, p. 930-933.

[49] H. Aouani, O. Mahboub, N. Bonod, E. Devaux, E. Popov, H. Rigneault, T. W. Ebbesen, J. Wenger, "Bright unidirectional fluorescence emission of molecules in a nanoaperture with plasmonic corrugations", *Nano Lett.* **11** (2011), no. 2, p. 637-644.
[50] M. P. Busson, B. Rolly, B. Stout, N. Bonod, S. Bidault, "Accelerated single photon emission from dye molecule-driven nanoantennas assembled on DNA", *Nat. Commun.* **3** (2012), p. 962.
[51] G. Acuna, F. Möller, P. Holzmeister, S. Beater, B. Lalkens, P. Tinnefeld, "Fluorescence enhancement at docking sites of DNA-directed self-assembled nanoantennas", *Science* **338** (2012), no. 6106, p. 506-510.
[52] T. B. Hoang, G. M. Akselrod, M. H. Mikkelsen, "Ultrafast room-temperature single photon emission from quantum dots coupled to plasmonic nanocavities", *Nano Lett.* **16** (2015), no. 1, p. 270-275.
[53] J. J. Baumberg, J. Aizpurua, M. H. Mikkelsen, D. R. Smith, "Extreme nanophotonics from ultrathin metallic gaps", *Nat. Mater.* **18** (2019), p. 668-678.
[54] D. Gérard, A. Devilez, H. Aouani, B. Stout, N. Bonod, J. Wenger, E. Popov, H. Rigneault, "Efficient excitation and collection of single-molecule fluorescence close to a dielectric microsphere", *J. Opt. Soc. Am. B* **26** (2009), no. 7, p. 1473-1478.
[55] A. Devilez, B. Stout, N. Bonod, "Compact metallo-dielectric optical antenna for ultra directional and enhanced radiative emission", *ACS Nano* **4** (2010), no. 6, p. 3390-3396.
[56] J. Ho, Y. H. Fu, Z. Dong, R. Paniagua-Dominguez, E. H. Koay, Y. F. Yu, V. Valuckas, A. I. Kuznetsov, J. K. Yang, "Highly directive hybrid metal–dielectric Yagi–Uda nanoantennas", *ACS Nano* **12** (2018), no. 8, p. 8616-8624.
[57] S. Bidault, M. Mivelle, N. Bonod, "Dielectric nanoantennas to manipulate solid-state light emission", *J. Appl. Phys.* **126** (2019), no. 9, article ID 094104.
[58] D. G. Baranov, R. S. Savelev, S. V. Li, A. E. Krasnok, A. Alù, "Modifying magnetic dipole spontaneous emission with nanophotonic structures", *Laser Photon. Rev.* **11** (2017), no. 3, article ID 1600268.
[59] S. Karaveli, R. Zia, "Strong enhancement of magnetic dipole emission in a multilevel electronic system", *Opt. Lett.* **35** (2010), no. 20, p. 3318-3320.
[60] S. Karaveli, R. Zia, "Spectral tuning by selective enhancement of electric and magnetic dipole emission", *Phys. Rev. Lett.* **106** (2011), article ID 193004.
[61] C. M. Dodson, R. Zia, "Magnetic dipole and electric quadrupole transitions in the trivalent lanthanide series: Calculated emission rates and oscillator strengths", *Phys. Rev. B* **86** (2012), article ID 125102.
[62] B. Rolly, B. Bebey, S. Bidault, B. Stout, N. Bonod, "Promoting magnetic dipolar transition in trivalent lanthanide ions with lossless mie resonances", *Phys. Rev. B* **85** (2012), article ID 245432.
[63] M. K. Schmidt, R. Esteban, J. J. Sáenz, I. Suárez-Lacalle, S. Mackowski, J. Aizpurua, "Dielectric antennas - a suitable platform for controlling magnetic dipolar emission", *Opt. Express* **20** (2012), no. 13, p. 13636-13650.
[64] M. Sanz-Paz, C. Ernandes, J. U. Esparza, G. W. Burr, N. F. van Hulst, A. Maitre, L. Aigouy, T. Gacoin, N. Bonod, M. F. Garcia-Parajo *et al.*, "Enhancing magnetic light emission with all-dielectric optical nanoantennas", *Nano Lett.* **18** (2018), no. 6, p. 3481-3487.
[65] A. Vaskin, S. Mashhadi, M. Steinert, K. E. Chong, D. Keene, S. Nanz, A. Abass, E. Rusak, D.-Y. Choi, I. Fernandez-Corbaton, T. Pertsch, C. Rockstuhl, M. A. Noginov, Y. S. Kivshar, D. N. Neshev, N. Noginova, I. Staude, "Manipulation of magnetic dipole emission from eu3+ with mie-resonant dielectric metasurfaces", *Nano Lett.* **19** (2019), no. 2, p. 1015-1022.
[66] M. Sigalas, D. Fattal, R. Williams, S. Wang, R. Beausoleil, "Electric field enhancement between two si microdisks", *Opt. Express* **15** (2007), no. 22, p. 14711-14716.
[67] J. Cambiasso, G. Grinblat, Y. Li, A. Rakovich, E. Cortés, S. A. Maier, "Bridging the gap between dielectric nanophotonics and the visible regime with effectively lossless gallium phosphide antennas", *Nano Lett.* **17** (2017), no. 2, p. 1219-1225.
[68] R. Regmi, J. Berthelot, P. M. Winkler, M. Mivelle, J. Proust, F. Bedu, I. Ozerov, T. Begou, J. Lumeau, H. Rigneault *et al.*, "All-dielectric silicon nanogap antennas to enhance the fluorescence of single molecules", *Nano Lett.* **16** (2016), no. 8, p. 5143-5151.
[69] A. Kinkhabwala, Z. Yu, S. Fan, Y. Avlasevich, K. Mullen, W. E. Moerner, "Large single-molecule fluorescence enhancements produced by a bowtie nanoantenna", *Nat. Photon.* **3** (2009), no. 11, p. 654-657.
[70] D. Punj, M. Mivelle, S. B. Moparthi, T. S. Van Zanten, H. Rigneault, N. F. Van Hulst, M. F. García-Parajó, J. Wenger, "A plasmonic antenna-in-box platform for enhanced single-molecule analysis at micromolar concentrations", *Nat. Nanotechnol.* **8** (2013), no. 7, p. 512.
[71] P. Albella, M. A. Poyli, M. K. Schmidt, S. A. Maier, F. Moreno, J. J. Sáenz, J. Aizpurua, "Low-loss electric and magnetic field-enhanced spectroscopy with subwavelength silicon dimers", *J. Phys. Chem. C* **117** (2013), no. 26, p. 13573-13584.
[72] M. Caldarola, P. Albella, E. Cortés, M. Rahmani, T. Roschuk, G. Grinblat, R. F. Oulton, A. V. Bragas, S. A. Maier, "Non-plasmonic nanoantennas for surface enhanced spectroscopies with ultra-low heat conversion", *Nat. Commun.* **6** (2015), p. 7915.

[73] X. Zambrana-Puyalto, N. Bonod, "Purcell factor of spherical mie resonators", *Phys. Rev. B* **91** (2015), no. 19, article ID 195422.
[74] V. Rutckaia, F. Heyroth, A. Novikov, M. Shaleev, M. Petrov, J. Schilling, "Quantum dot emission driven by mie resonances in silicon nanostructures", *Nano Lett.* **17** (2017), no. 11, p. 6886-6892.
[75] K. Frizyuk, M. Hasan, A. Krasnok, A. Alú, M. Petrov, "Enhancement of Raman scattering in dielectric nanostructures with electric and magnetic mie resonances", *Phys. Rev. B* **97** (2018), no. 8, article ID 085414.
[76] D. G. Baranov, R. Verre, P. Karpinski, M. Kall, "Anapole-enhanced intrinsic Raman scattering from silicon nanodisks", *ACS Photon.* **5** (2018), no. 7, p. 2730-2736.
[77] D. A. Shilkin, M. R. Shcherbakov, E. V. Lyubin, K. G. Katamadze, O. S. Kudryavtsev, V. S. Sedov, I. I. Vlasov, A. A. Fedyanin, "Optical magnetism and fundamental modes of nanodiamonds", *ACS Photon.* **4** (2017), no. 5, p. 1153-1158.
[78] R. Savelev, A. Zalogina, S. Kudryashov, A. Ivanova, A. Levchenko, S. Makarov, D. Zuev, I. Shadrivov, "Control of spontaneous emission rate in luminescent resonant diamond particles", *J. Phys.: Conf. Ser.* **961** (2018), article ID 012007.
[79] A. Zalogina, R. Savelev, E. Ushakova, G. Zograf, F. Komissarenko, V. Milichko, S. Makarov, D. Zuev, I. Shadrivov, "Purcell effect in active diamond nanoantennas", *Nanoscale* **10** (2018), no. 18, p. 8721-8727.
[80] S. Makarov, A. Furasova, E. Tiguntseva, A. Hemmetter, A. Berestennikov, A. Pushkarev, A. Zakhidov, Y. Kivshar, "Halide-perovskite resonant nanophotonics", *Adv. Opt. Mater.* **7** (2019), no. 1, article ID 1800784.
[81] A. S. Berestennikov, P. M. Voroshilov, S. V. Makarov, Y. S. Kivshar, "Active meta-optics and nanophotonics with halide perovskites", *Appl. Phys. Rev.* **6** (2019), no. 3, article ID 031307.
[82] E. Y. Tiguntseva, G. P. Zograf, F. E. Komissarenko, D. A. Zuev, A. A. Zakhidov, S. V. Makarov, Y. S. Kivshar, "Light-emitting halide perovskite nanoantennas", *Nano Lett.* **18** (2018), no. 2, p. 1185-1190.
[83] E. Tiguntseva, K. Koshelev, A. Furasova, P. Tonkaev, V. Mikhailovskii, E. V. Ushakova, D. G. Baranov, T. Shegai, A. A. Zakhidov, Y. Kivshar *et al.*, "Room-temperature lasing from mie-resonant non-plasmonic nanoparticles", *ACS Nano* **14** (2020), no. 7, p. 8149-8156.
[84] C. Hsu, B. Zhen, A. Stone, J. Joannopoulos, M. Soljacić, "Bound states in the continuum", *Nat. Rev. Mater.* **1** (2016), article ID 16048.
[85] A. Kodigala, T. Lepetit, Q. Gu, B. Bahari, Y. Fainman, B. Kanté, "Lasing action from photonic bound states in continuum", *Nature* **541** (2017), p. 196-199.
[86] M. Rybin, Y. Kivshar, "Supercavity lasing", *Nature* **541** (2017), p. 165-166.
[87] C. Hsu, B. Zhen, J. Lee, S. Chua, S. Johnson, J. Joannopoulos, "Observation of trapped light within the radiation continuum", *Nature* **499** (2013), p. 188-191.
[88] F. Monticone, A. Alu, "Embedded photonic eigenvalues in 3d nanostructures", *Phys. Rev. Lett.* **112** (2014), article ID 213903.
[89] K. Koshelev, S. Lepeshov, M. Liu, A. Bogdanov, Y. Kivshar, "Asymmetric metasurfaces with high-Q resonances governed by bound states in the continuum", *Phys. Rev. Lett.* **121** (2018), no. 19, article ID 193903.
[90] E. Mikheeva, K. Koshelev, D.-Y. Choi, S. Kruk, J. Lumeau, R. Abdeddaim, I. Voznyuk, S. Enoch, Y. Kivshar, "Photosensitive chalcogenide metasurfaces supporting bound states in the continuum", *Opt. Express* **27** (2019), p. 33847-33853.
[91] L. Wang, S. Kruk, K. Koshelev, I. Kravchenko, B. Luther-Davies, Y. Kivshar, "Nonlinear wavefront control with all-dielectric metasurfaces", *Nano Lett.* **18** (2018), no. 6, p. 3978.
[92] K. Koshelev, Y. Tang, K. Li, D.-Y. Choi, G. Li, Y. Kivshar, "Nonlinear metasurfaces governed by bound states in the continuum", *ACS Photon.* **6** (2019), no. 7, p. 1639.
[93] B. Gralak, G. Tayeb, S. Enoch, "Morpho butterflies wings color modeled with lamellar grating theory", *Opt. Express* **9** (2001), no. 11, p. 567-578.
[94] P. Vukusic, J. R. Sambles, "Photonic structures in biology", *Nature* **424** (2003), no. 6950, p. 852.
[95] K. Kumar, H. Duan, R. S. Hegde, S. C. Koh, J. N. Wei, J. K. Yang, "Printing colour at the optical diffraction limit", *Nat. Nanotechnol.* **7** (2012), no. 9, p. 557.
[96] A. Kristensen, J. K. Yang, S. I. Bozhevolnyi, S. Link, P. Nordlander, N. J. Halas, N. A. Mortensen, "Plasmonic colour generation", *Nat. Rev. Mater.* **2** (2017), no. 1, article ID 16088.
[97] M. Abbarchi, M. Naffouti, B. Vial, A. Benkouider, L. Lermusiaux, L. Favre, A. Ronda, S. Bidault, I. Berbezier, N. Bonod, "Wafer scale formation of monocrystalline silicon-based mie resonators via silicon-on-insulator dewetting", *ACS Nano* **8** (2014), no. 11, p. 11181-11190.
[98] E. Højlund-Nielsen, J. Weirich, J. Nørregaard, J. Garnaes, N. A. Mortensen, A. Kristensen, "Angle-independent structural colors of silicon", *J. Nanophoton.* **8** (2014), no. 1, article ID 083988.
[99] J. Proust, F. Bedu, B. Gallas, I. Ozerov, N. Bonod, "All-dielectric colored metasurfaces with silicon mie resonators", *ACS Nano* **10** (2016), no. 8, p. 7761-7767.
[100] Z. Dong, J. Ho, Y. F. Yu, Y. H. Fu, R. Paniagua-Dominguez, S. Wang, A. I. Kuznetsov, J. K. Yang, "Printing beyond srgb color gamut by mimicking silicon nanostructures in free-space", *Nano Lett.* **17** (2017), no. 12, p. 7620-7628.

[101] V. Flauraud, M. Reyes, R. Paniagua-Dominguez, A. I. Kuznetsov, J. Brugger, "Silicon nanostructures for bright field full color prints", *ACS Photon.* **4** (2017), no. 8, p. 1913-1919.
[102] V. Vashistha, G. Vaidya, R. S. Hegde, A. E. Serebryannikov, N. Bonod, M. Krawczyk, "All-dielectric metasurfaces based on cross-shaped resonators for color pixels with extended gamut", *ACS Photon.* **4** (2017), no. 5, p. 1076-1082.
[103] T. Wood, M. Naffouti, J. Berthelot, T. David, J.-B. Claude, L. Métayer, A. Delobbe, L. Favre, A. Ronda, I. Berbezier *et al.*, "All-dielectric color filters using sige-based mie resonator arrays", *ACS Photon.* **4** (2017), no. 4, p. 873-883.
[104] X. Zhu, W. Yan, U. Levy, N. A. Mortensen, A. Kristensen, "Resonant laser printing of structural colors on high-index dielectric metasurfaces", *Sci. Adv.* **3** (2017), no. 5, article ID e1602487.
[105] S. Sun, Z. Zhou, C. Zhang, Y. Gao, Z. Duan, S. Xiao, Q. Song, "All-dielectric full-color printing with tio2 metasurfaces", *ACS Nano* **11** (2017), no. 5, p. 4445-4452.
[106] L. Wang, S. Kruk, H. Tang, T. Li, I. Kravchenko, D. N. Neshev, Y. S. Kivshar, "Grayscale transparent metasurface holograms", *Optica* **3** (2016), no. 12, p. 1504-1505.
[107] H. Ren, G. Briere, X. Fang, P. Ni, R. Sawant, S. Héron, S. Chenot, S. Vézian, B. Damilano, V. Brändli *et al.*, "Metasurface orbital angular momentum holography", *Nat. Commun.* **10** (2019), no. 1, p. 2986.

Comptes Rendus
Physique
2020, 21, nº 4-5, p. 443-465
https://doi.org/10.5802/crphys.21

Metamaterials 1 / *Métamatériaux 1*

Bottom-up nanocolloidal metamaterials and metasurfaces at optical frequencies

Nano métamateriaux auto-assemblés opérant en lumière visible

Alexandre Baron [a], Ashod Aradian [a], Virginie Ponsinet [a] and Philippe Barois*, [a]

[a] Univ. Bordeaux, CNRS, Centre de Recherche Paul Pascal, UMR 5031, 33600 Pessac, France

E-mails: alexandre.baron@crpp.cnrs.fr (A. Baron), ashod.aradian@crpp.cnrs.fr (A. Aradian), virginie.ponsinet@crpp.cnrs.fr (V. Ponsinet), philippe.barois@crpp.cnrs.fr (P. Barois)

Abstract. Metamaterials and metasurfaces are artificial composite media engineered to exhibit extraordinary properties of wave propagation. In bulk (3D) metamaterials, such extreme properties may result from non-conventional values of effective homogeneous optical parameters such as the electric permittivity and the magnetic permeability. These features generally originate in the collective response of the constitutive structural elements, which have to be of sub-wavelength dimensions to satisfy the requirement of optical homogeneity, and which have to be highly polarizable to provide efficient optical functions. For visible light applications, sub-wavelength dimensions imply structuration at the nanoscale whereas high polarizability can be achieved by optical resonators such as plasmonic or Mie resonators. Metasurfaces, on the other hand, are 2D equivalent of metamaterials, designed to control the phase, amplitude and possibly polarization of incident EM waves with subwavelength thickness, using interfacial discontinuities effects. This review shows how the bottom-up approach based on nano-chemistry and the self-assembly methods of colloidal physical-chemistry can be used to produce nano-sized tunable magneto-electric resonators which can subsequently be assembled in bulk nanostructured metamaterials as well as in optically thin metasurfaces. Focusing mainly on work carried out at the University of Bordeaux over the past decade, we review some of the optical properties observed in visible light from the fabricated systems. Specific optical experiments and numerical simulations are of crucial importance for the design of the most efficient structures and the extraction of the effective optical parameters.

Résumé. Les métamatériaux et les métasurfaces sont des milieux composites conçus pour posséder des propriétés optiques extraordinaires. Dans le cas des métamatériaux tridimensionnels, les propriétés nouvelles peuvent résulter de valeurs non conventionnelles des paramètres optiques effectifs tels que la permittivité diélectrique et la perméabilité magnétique. Elles proviennent en général de la réponse collective d'inclusions fortement polarisables de dimensions sub-longueur d'onde afin d'assurer une réponse optique homogène. Dans le spectre de la lumière visible, cette contrainte implique une structuration des matériaux à l'échelle nanométrique. Une forte polarisabilité peut être assurée par des résonances optiques plasmoniques ou de Mie.

* Corresponding author.

Les métasurfaces sont les équivalents bidimensionnels des métamatériaux conçus pour contrôler la phase, l'amplitude et si possible la polarisation des ondes transmises ou réfléchies. Cette revue, centrée essentiellement sur les travaux réalisés depuis une décennie à l'Université de Bordeaux, montre comment l'approche dite "bottom-up" fondée sur la nano-chimie et les méthodes d'auto-assemblage de la physico-chimie colloïdale permet de produire des résonateurs magnéto-électriques accordables de dimensions nanométriques et de les assembler pour former des métamatériaux ou des métasurfaces résonants. En parallèle, le développement de simulations numériques et leur association à des mesures optiques spécifiques sont des éléments cruciaux pour la conception des nanostructures les plus efficaces ainsi que l'extraction de leurs paramètres optiques effectifs.

Keywords. Metamaterials, Metasurfaces, Self-assembly, Colloids, Bottom-up, Optical resonances.

Mots-clés. Métamatériaux, Métasurfaces, Auto-assemblage, Colloïdes, Méthode ascendante, Résonances optiques.

1. Introduction

Conceptual notions, such as double-negative materials or artificial magnetic materials, form the backbone of the metamaterials research field. These notions have been available in the literature for decades and the seminal article of V. Veselago is one prominent early attempt [1–4]. However, to materialize, these ideas required modern fabrication techniques capable of effectively manufacturing the envisioned basic units—the so-called *meta-atoms*—and arranging them into a spatially organized ensemble (*metamaterials*).

Early realizations of metamaterials in the microwave range used classical radio-engineering manufacturing techniques, such as printed circuitry. However, for reaching higher operating frequencies, and the visible range, miniaturization to sizes a few tens of nanometers quickly became necessary as the metamaterials community moved toward the visible [5]. Initial designs resorted to *top-down* fabrication: in essence, top-down approaches start from raw pieces of materials that are carved (etched) into the basic units required to generate the desired properties. A classical example of a top-down fabricated meta-atom is the split-ring resonator, lying on a supporting substrate. Etching to the nanoscale with sufficient precision requires state-of-the-art fabrication facilities equipped with nanolithography devices such as electron beams, ion beams, extreme UV, etc. This top-down approach led to spectacular and well-known results [5].

In this review article, we will focus on a radically different range of fabrication methods, known as the *bottom-up* route [6–8]. This designates in reality a wide array of techniques, whereby meta-atoms are synthetized and assembled together from raw, primary materials, and subsequently, arranged spatially into the sought-after meta-structures. In this approach, and for the optical range, meta-atoms are *nanocolloids*, the complexity of which will depend on the desired properties. In physical chemistry, nanocolloids designate a category for microscopic objects with sizes broadly ranging from a few nanometers to a micrometer. They may be solid nanoparticles, aggregates, polymer coils, droplets or vesicles [9, 10]. In the case of metamaterials, the required nanocolloids are most often nanoparticles, or associations of nanoparticles and polymers.

Such a bottom-up approach has become viable only thanks to the extraordinary progress that was witnessed in nanocolloidal engineering and nanoparticle synthesis over the past three decades [6, 11, 12], where the variety of shapes, obtainable geometrical constructs, as well as the variety of usable primary materials (including noble metals and semiconductors) has immensely widened.

Nanocolloids are obtained, in most cases, in the form of a dispersion of a large number of nanoparticles in a liquid solvent; the task of collecting and distributing them into a more or

less dense, well-organized spatial arrangement cannot be done using any means of individual manipulation.[1]

Therefore, only massively *parallel* processes like self-assembly may produce large metamaterials. Self-assembly designates an ensemble of common and highly efficient processes well-known in chemical physics, soft condensed matter physics, and biology, leading to organized two-dimensional or three-dimensional structures of various symmetries. They can either be spontaneous, occurring under the effect of complex—pair or multi-object—interactions, until some free energy is minimized; or they can be directed, i.e. assisted by some external template such as a surface, a host matrix or else guided by external inputs of energy.

There are benefits and drawbacks in using the bottom-up approach compared to the top-down. On the one hand, top-down fabrication provides more precise and reproducible structures that are easily modelled in numerical simulations. This makes it straightforward to optimize and interpret the observed properties. However, samples in most cases are two- or quasi two-dimensional, with limited lateral sizes. Fabrication is time and energy-demanding and requires state-of-the-art, cost-intensive facilities.

On the other hand, the bottom-up approach is often less precise, as disorder is intrinsically introduced with respect to ideal designs, due to the role of thermal energy and entropy in both the synthesis and assembly stages. On the brighter side, chemistry and self-assembly are low-tech, table-top fabrication means, both energy-saving and cost-friendly. They are able to produce materials in greater quantities, making it easier to obtain 3D samples [7, 13, 14].

Globally speaking, it can be stated that the bottom-up routes introduce a trade-off between a lesser structural precision and a better energy footprint.

This review article is devoted to nanocolloidal metamaterials for optics obtained by the bottom-up approach. We will focus especially on the research efforts carried out at the University of Bordeaux over the past decade.

2. Nanocolloidal meta-atoms

As stated in Section 1, the expression *meta-atom* is often used to denote the basic functional element of a metamaterial. Some authors find it confusing since a meta-atom is not an atom (whereas a metamaterial *is* a material). The wording meta-atom nevertheless underlines its indivisible nature shared with true atoms ($\alpha\tau o\mu o\sigma$): the targeted optical function of this element is lost if its structure is broken into separate pieces. We define in the following the meta-atom as the smallest structural element that provides the wanted optical property. Once again, the *meta* prefix implies that the optical response of the meta-atom goes beyond the properties of natural materials. Moreover, anticipating that a metamaterial constructed as a collection of meta-atoms should exhibit homogeneous effective optical parameters, the size of the meta-atoms should be significantly smaller than the operating wavelength. Optical resonators constitute a major class of meta-atoms in which an optical response (e.g. the electric polarizability) exhibits a resonant behavior at some frequency ω_0 in the spectral range of interest. Indeed, the resonance may involve a considerable increase of the optical response upon approaching ω_0 hence leading to extreme values of the effective optical parameters. Moreover, the optical response exhibits a π phase shift upon crossing ω_0 which may lead to counter-intuitive "negative" optical behaviors. A wide set of multipolar electric and magnetic resonances can in principle be excited by the impinging electromagnetic wave. The price to pay is the presence of optical losses imposed by

[1] Indeed, for a volumic (3D) metamaterial operating in the visible, an average density of one to ten active units (nano-resonators) per wavelength will result in a collection of about 10^9 to 10^{12} nanocolloids for a sample with a volume on the order of a cubic millimeter.

causality through the Kramer–Kronig relations. This is a high price that is sometimes overlooked in yet exciting models.

The strategy of the bottom-up approaches to metamaterials reported in this review is to design, synthesize and assemble nanocolloidal meta-atoms exhibiting optical resonances in the visible or near infrared range. The requirement of sub-wavelength dimensions implies that the size of the meta-atoms should lie in the colloidal range from a few tens up to hundreds of nanometers. Two main classes of optical resonators have been proposed and extensively studied in the field of metamaterials, namely plasmonic and Mie resonators.

2.1. *Plasmonic resonators*

In metallic nanoparticles, free electrons oscillate harmonically driven by the electric field of the light wave. When the exciting frequency matches the natural frequency of the electrons in a metallic inclusion, the so-called localized surface plasmon resonance (LSPR) occurs. It is described in a simple way by considering a spherical particle of radius $a \ll \lambda$ and permittivity $\varepsilon_{\mathrm{NP}}$ immersed in a transparent medium of permittivity ε_m, the dipole moment $\mathbf{p}$ induced by the field $\mathbf{E}_0$ of the wave reads

$$\mathbf{p} = 4\pi a^3 \varepsilon_m \frac{\varepsilon_{\mathrm{NP}} - \varepsilon_m}{\varepsilon_{\mathrm{NP}} + 2\varepsilon_m} \mathbf{E}_0. \tag{1}$$

The resonance occurs when the real part of the denominator in (1) vanishes, which is made possible since the real part of the permittivity of the metal is negative below the plasma frequency. The strength of the induced dipole scales as the volume of the particle but the frequency of the LSPR in the dipolar approximation depends solely on the nature of the metal and of the host medium, regardless of the size as long as it satisfies $a \ll \lambda$. LSPR-based systems may indeed accommodate some degree of size-dispersion. For increasing sizes, higher order multipoles come into play and the LSPR red-shifts progressively [15]. Dense materials assembled from plasmonic nanospheres exhibit optical resonances reminiscent of the LSPR resonance of their meta-atoms, but which are generally affected by the electromagnetic coupling between them, as will be shown in Section 3 [16].

A major challenge of the field of metamaterials is the generation of artificial optical magnetism. Early models have suggested that controlling the magnetic response to light would give access to spectacular novel properties like super-lensing, cloaking or light steering by transformation optics [17–19]. The absence of magnetic polarizability in natural materials at visible light and near IR frequencies is well known [20]. Conventional optics indeed assigns the vacuum value μ_0 to the magnetic permeability μ. In 1999 however, Pendry *et al.* suggested that artificial magnetism could be produced by a resonant inductor-capacitor circuit of subwavelength dimension—split ring resonators (SRR)—in which the electromagnetic wave could induce a circular current, thus producing an effective magnetic response [21]. This concept was beautifully illustrated by the observation of negative refraction in microwaves [22]. It was subsequently extended to higher frequencies by reducing the size of the SRR [5], up to visible light frequencies, where the top-down techniques used to engrave SRRs on surfaces reach their limits. Alternative models were then proposed in which the resonant loop that generates the magnetic response is made of a nanoring of plasmonic nanoparticles [23–25]. We shall see in Section 2.2 that colloidal interactions can be used to synthesize 3-dimensional clusters of plasmonic nanoparticles along the models of Figure 1 and measurements of the magnetic response will be presented. The magnetic component of light can also come into play in chiral media. Chirality indeed enables the presence of a magneto-electric coupling within the constitutive relations of a material [26]. Several authors have shown that plasmonic resonances could be used to enhance the optical activity of chiral substances. We mention a few examples of this phenomenon observed in helical clusters of gold

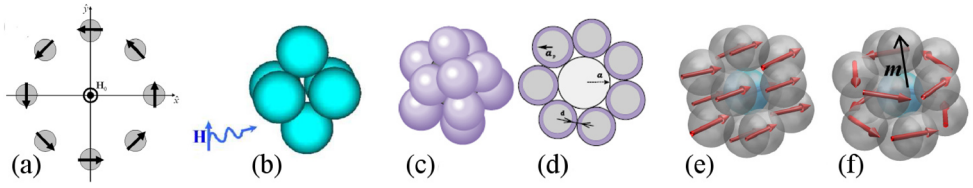

Figure 1. Models of magnetic meta-atoms. (a) Planar model of a ring of plasmonic nanoparticles [23]. (b) Octaedron 3D model [24]. (c, d) Simovski–Tretyakov model of isotropic magnetic nanoclusters [25]. (e, f) Sketch of the electric and magnetic modes in a plasmonic nanocluster [30].

nanoparticles driven by DNA origami, peptide fibrils templates or silica nanohelices obtained by mineralization of self-assembled helices of gemini surfactants [27–29].

2.2. *Mie resonators*

Most nano-antennas and metamaterials were initially designed with plasmonic meta-atoms [5, 31], but it was realized that dielectric meta-atoms could also be used to provide a lot of the functionalities already achieved with plasmonics. To do so, high-index dielectric nanostructures can be built to reach the Mie resonance regime, in which the resonance wavelength will typically be on the order of $n \times a$, where n is the index of refraction of the material and a the typical size of the resonator. As such, a large variety of all-dielectric metamaterials and metasurfaces have been proposed [32–34]. Crystalline silicon that exhibits a large refractive index with low losses for wavelengths above 600 nm is envisioned as a good candidate [35].

In the Mie regime, the scattering of dielectric nanoparticles exhibits electric and magnetic multipole resonances that are described by the coefficients of the vector spherical harmonic expansion of the scattered field under plane wave illumination. For a spherical particle, the electric (magnetic) Mie coefficients a_n (b_n) of order n are given by

$$\{a_n, b_n\} = \frac{\{m,\mu\}\psi_n(mx)\psi_n'(x) - \{\mu,m\}\psi_n(x)\psi_n'(mx)}{\{m,\mu\}\psi_n(mx)\xi_n'(x) - \{\mu,m\}\xi_n(x)\psi_n'(mx)} \tag{2}$$

where ψ_n and ξ_n are the nth order Ricatti–Bessel and Hankel functions of the first kind and are functions of the reduced frequency $x = n_\mathrm{h} kr$. μ is the magnetic permeability of the sphere material (assuming it is 1 for the host medium), n_S and n_h are the indices of refraction of the sphere and the host medium, $m = n_\mathrm{S}/n_\mathrm{h}$, r is the radius of the particle and k is the free-space wavector. The presence of magnetic Mie resonances in the visible spectrum opens the way to optical properties that are not observed in natural materials. A strong magnetic polarizability may indeed lead to yet unknown magnetic bulk materials or to the realization of Huygen's sources exhibiting zero backward scattering.

Nanocolloidal systems enable a tuning of the multipole resonances to achieve a desired optical response. For instance, by carefully tuning the size of a homogenous material with a moderate index of refraction—typically between 1.17 and 2.1—nanoparticles that scatter only in the forward direction can be achieved. This happens because the first order electric and magnetic dipoles resonate at similar wavelengths and with comparable amplitudes. When these resonances overlap perfectly in amplitude and in phase, a so-called Huygens dipole is produced, in reference to the Huygens–Fresnel principle. The concept is the same as the *first Kerker condition*, further detailed in Section 4.2 and occurs whenever $a_1 = b_1$. Zhang *et al.* have demonstrated experimentally direction forward-scattering using Cu_2O nanospheres that were synthesized by

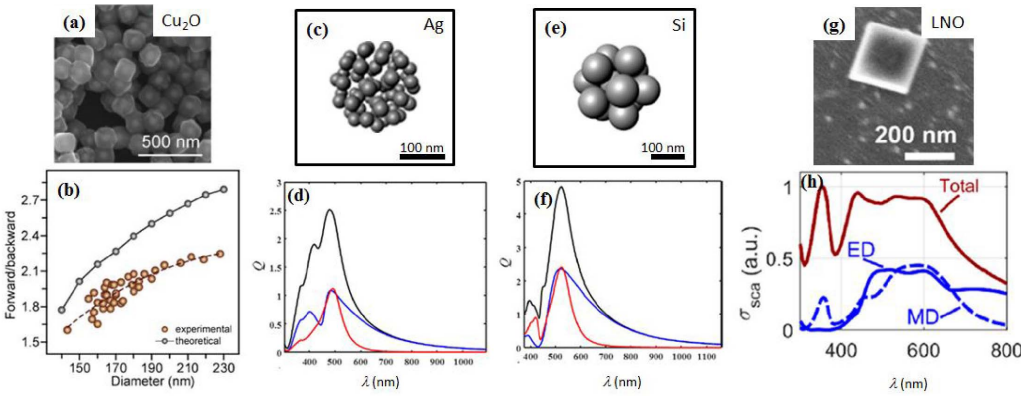

Figure 2. Examples of meta-atoms engineered as Mie resonators. (a) Scanning electron microscope (SEM) images of Copper oxide nanoparticles that exhibit a strong forward-scattering behavior due to their moderate refractive index. (b) Forward to backward scattering ratio as a function of nanoparticle diameter. (a) and (b) are adapted from [36]. (c) Illustration of a 200 nm cluster made of 60 silver nanospheres of diameter $(2r) = 30$ nm. (d) The black line is the total scattering efficiency of the silver cluster shown in (c)—defined as the ratio of the scattering cross-section efficiency to the geometrical cross-section (πr^2)—as a function the wavelength of the exciting field. The blue (red) line is the scattering efficiency due to the electric (magnetic) dipole resonance. (e) Illustration of a dense 13 nanoparticle cluster made of silicon inclusions with diameters of ~80 nm. (f) Same as (d) for the silicon cluster shown in (f). (c), (d), (e) and (f) are adapted from [37]. (g) SEM images of a lithium niobate nanocube for second harmonic generation in NUV. (h) Scattering cross-sections of the nanocube shown in (g) as a function of wavelength. The red line is the total scattering cross-section, the continuous (dashed) blue line is the scattering cross-section of the electric (magnetic) dipole moment. (g) and (h) are adapted from [38].

wet chemistry (see Figure 2 (a,b)) [36]. The concept is not limited to homogenous spheres. As a matter of fact, an effective meta-atom can be produced by clustering inclusions of small resonators that will exhibit a tailored Mie resonance. For instance in [37], Dezert *et al.* have shown theoretically that a cluster of 60 silver nanoparticles will act as a medium exhibiting an effective refractive index that is in the correct moderate range to act as a Huygens dipole (see Figure 2 (c,d)). Furthermore the same authors show that a dense meta-atom made of 13 silicon inclusions constitutes a very efficient Huygens dipole with scattering efficiencies much larger that anything achievable with a hypothetical homogeneous sphere [37] (see Figure 2 (e,f)). It should be noted that the Hugyens dipole concept can be generalized to multipolar systems as forward-scattering occurs whenever $a_n = b_n$ for any order n (see also Section 4.2).

Finally, Mie resonances hold great potential to act as meta-atoms for a variety of applications. A neat example is provided by Timpu *et al.*, who show that lithium niobate (LNO) nanocubes are excellent candidates for second-harmonic generation in the near ultraviolet (NUV) [38]. Indeed, since the energy band-gap is larger than 4 eV, it exhibits low losses in the visible and NUV. Furthermore, LNO has a strong second-order nonlinear susceptibility $\chi^{(2)}$ in those ranges. As a result, by selecting the size of LNO nanocubes fabricated by solvothermal synthesis in the (200 nm–300 nm) range, the authors were able to show SHG emission below 400 nm with giant enhancements compared to bulk LNO due to the Mie resonances of the nanocube (see Figure 2 (g,h)).

2.3. *Loss-compensated resonators and nanolasing*

Meta-atoms described above use resonant schemes in order to provide a significant electromagnetic response. Such schemes go along with resonant losses due to the Kramers–Kronig causality rule. This is even worsened in the often-encountered case of plasmonic resonators in the visible range, where intrinsic Ohmic losses in the metallic parts are already strong [39]. As a result, the obtained resonances are broader and weaker than expected ideally.

One of the strategies to mitigate the losses is to associate optical gain materials to the plasmonic parts in the resonators in what is sometimes called "active plasmonic" designs [40–42]. In the case of plasmonic nanoparticles, it has been shown that resonances can indeed be sharpened, and the associated light emission enhanced, as gain levels are increased [43–45]. Moreover, when gain in the system is increased enough that it exceeds losses, new regimes of spasing and nanolasing are observed; this has been evidenced both in top-down-fabricated structures [41,46] and bottom-up-fabricated ones [46–49].

While experimental realizations for nanoparticle-based nanolasers are still scarce, and investigation mostly relies on full-wave numerical simulations [47], work initiated at the University of Bordeaux was based essentially on theoretical analysis. The studied geometries were either spherical plasmonic nanoparticles immersed in gain, core-shells (with a metal core and active shell), or conversely, nanoshells (with a metal shell and a gain core).

The polarisability α of the particle can be calculated from (1) as $\alpha = p/E_0 = 4\pi a^3 \varepsilon_m (\varepsilon_{\mathrm{NP}} - \varepsilon_m)/(\varepsilon_{\mathrm{NP}} + 2\varepsilon_m)$. When the gain level $\mathrm{Im}(\varepsilon_m)$ is negative (representing a gain material with negative losses) and increased in absolute value (increasing gain), the plasmon resonance is amplified and gradually sharpened [50], or in other terms, the losses in the nanoresonator are compensated. When gain reaches a value such that the imaginary part of the denominator at the plasmon frequency cancels, a singularity of the polarizability appears as the complete denominator vanishes. This was conjectured to be the signature of the onset of spasing/nanolasing [50].

To further investigate the situation theoretically, a detailed electromagnetic description was set up [51]: using an exact Green function formalism, involving individual active emitters randomly aggregated around a metal nanosphere, the equivalent polarizability of the metal-and-emitters system was calculated, composed of the direct response from the metal sphere as well as the contribution arising from the cooperative coupling between emitters and surface plasmons. The analysis was based on an eigenvalue decomposition, where the eigenmodes are coupled, hybrid exciton (from the emitters)-plasmon modes. The calculated optical response of the aggregate indeed showed amplified, loss-compensated plasmon responses as gain was increased. Moreover, when gain levels becomes high enough, sharp peaks corresponding to coherent light emission akin to the Dicke effect were found [51], thereby providing some insight into the physical nature of nanolasing.

In these works, however, as well as in almost all simulation studies on nanoparticle-based nanolasing available in the literature [47], it is implicitly or explicitly assumed that the energy provided by the gain is both stationary in time and independent of the intensity of the nanolasing emission. It is well-known from laser physics that none of these are true in general, as time-dependent regimes may appear (e.g., oscillations) and non-linear effects such as gain depletion occur at high intensity.

A more complete theoretical approach was therefore introduced [52] where the plasmonic response of a homogeneous metal nanoparticle immersed in a sea of surrounding gain elements (dipole emitters) was studied in a space and time-dependent description. The model integrates a quantum formalism (optical Bloch equations) to describe the gain and a classical, fully multipolar treatment for the metal particle. The presence of a lasing threshold was then demonstrated. For gain levels below the lasing threshold, loss compensation takes place and the nanoparticle

plasmon is amplified as usual. For gain above the threshold, a lasing instability sets in: an exponential growth of the emission is initially observed, followed by an energy cascade where all multipolar modes activate. The intricate nonlinear couplings between these modes control the state of emission in the long term.

Recently, the nature of the long-term nanolasing state could be calculated in exact form within the same type of theoretical model, but for a nanoshell geometry, where the core is made of an active material and the shell is a plasmonic metal [53]. For various aspect ratios of the nanoshell, steady-state regimes for nanolasing were demonstrated, with remarkably sharp emission lines with widths as little as 1 nm (and possibly even less with optimization).

In conclusion of this section, situations involving meta-atoms (plasmonic nanoresonators) coupled to optical gain were studied using increasingly elaborate theoretical models. In all cases, a gain level threshold was evidenced, above which lasing in the form of sharp emission lines was found. Below the threshold, plasmon amplification regimes are always found, where the losses of the "natural" resonance of the meta-atom are gradually compensated as the gain level is raised.

3. Metamaterials

In the preceding section, we described several types of nano-resonators which can serve as meta-atoms in the optical wavelength range. In this section, we discuss metamaterials, i.e., materials obtained by assembling such meta-atoms together. We shall present materials made of meta-atoms contained into a host-matrix, as well as materials made of dense packings of only meta-atoms.

Bottom-up techniques can fabricate samples with chemically large numbers of meta-atoms, meaning that they are not restricted to quasi-surfaces, so that 3D bulk materials can be produced. Depending on the specific approach, the actual thickness of the samples can be adjusted from one or a few layers of meta-units up to macroscopic thickness. Therefore, in this section, we will use the formalism of optically-thick materials, such as the optical index, the electrical permittivity and the magnetic permeability. Also, effective-medium approaches will be used to transfer individual meta-atom properties into global, macroscopic ones. This is in contrast with metasurfaces, which will be discussed in the next section, where the optical thickness is small compared to the wavelength.

3.1. *Tunable index of refraction*

Assembling nanocolloidal meta-atoms into 3D (or quasi-3D) materials allows monitoring the optical index. As mentioned before, self-assembly processes intrinsically introduce some degree of disorder or defects, hindering the numerical rendering of the assembled materials. Optical properties are then either fully determined experimentally, or modelled and predicted using somewhat phenomenological effective medium laws.

A very simple situation [54] is a set of spherical plasmonic resonators (14 nm gold nanoparticles), randomly dispersed into a 3D host matrix (a transparent polymer film), see Figure 3 (a). Films of thicknesses ranging from about 40 to 150 nm were obtained by spin-coating aqueous dispersions of gold nanoparticles and polymer onto a silicon wafer, and their optical properties were analyzed using spectroscopic ellipsometry. Due to the plasmonic resonance, the introduction of increasing amounts of gold nanoparticles generates increasing variations in the optical indices of the film. For example, at 6% gold volume fraction, the extracted optical index shows a wide resonance in the visible range, with the refraction index n displaying variations $n = 1.66 \pm 0.13$, see Figures 3(b) and (c).

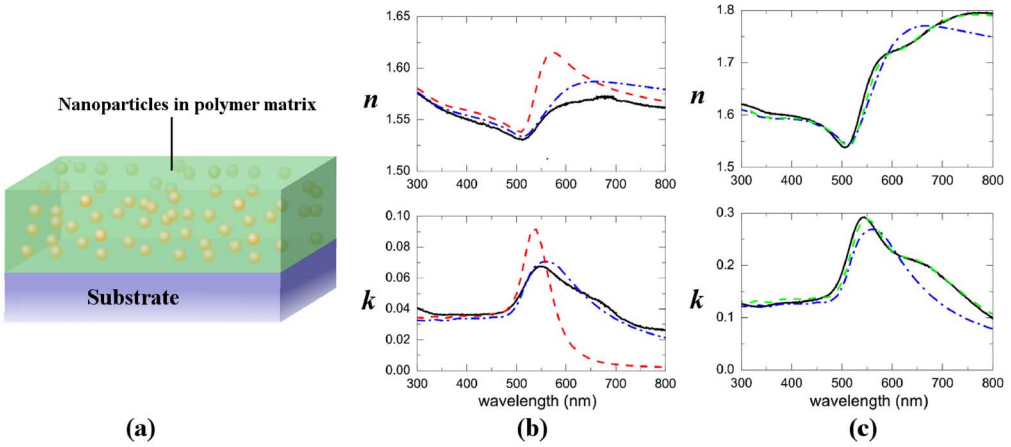

Figure 3. (a) Polymer film with gold nanoparticles [54]. (b, c) Films with 1.6% (b) and 5.7% (c) gold volume fraction. Experimental index of refraction n and extinction coefficient k extracted from ellipsometry (black continuous line). Fits by the classical Maxwell Garnett EMA (red dashed line), by a unimodal ellipsoidal Maxwell Garnett EMA (blue dashed line) or by a bimodal ellipsoidal EMA (green dashed line).

More surprisingly, it was found that even for a low volume fraction of gold nanoparticles ($f \sim 1\%$–5%), the observed plasmonic resonance was affected by electromagnetic coupling between particles, due to disorder and inevitable local inhomogeneities in particle density, which bring some particles close together. As a consequence, even for such dilute systems, the classical Maxwell Garnett Effective Medium Approximation (EMA) failed to predict the measured indices (Figure 3 (b)). Such couplings could be taken into account phenomenologically, using a modified Maxwell Garnett EMA based on a random distribution of ellipsoidal polarizabilities, since couplings can in effect be represented as deformations of the polarizability tensor of individual particles [54], while the nanoparticles actually are and remain spherical. This simple effective model for interparticle couplings proved successful: in simple cases, a unimodal distribution of ellipsoidal polarizabilities was enough to provide reasonably good fits of the experimental data with only two free parameters (Figure 3 (b)). Using bimodal distributions (Figure 3 (c)) made it even possible to reproduce more complex cases where the resonance presented a shoulder in the red; the bimodal population suggested that particles could be categorized into weakly vs. strongly coupled resonators. Such modified Maxwell Garnett EMAs present the advantage of relying on physically meaningful parameters and provide a general tool for the phenomenological description of plasmonic couplings in various disordered nanocomposites, without resorting to advanced (and often impractical) effective-medium theories.

Inhomogeneity in the inter-particle distance can be drastically reduced by encapsulating the plasmonic particles in a unalterable dielectric shell of well-defined thickness. Dense thin films of such core(silver)-shell(silica) nanoparticles were fabricated by several successive Langmuir–Schaefer transfers of a monolayer of nanoparticles at the water–air interface onto a silicon substrate. Their refractive index exhibits a sharp resonant behavior which is nicely reproduced by a single Lorentz oscillator (Figure 4) [55]. Thicker 3D materials can be made by controlled evaporation of a dispersion of plasmonic meta-atoms in microfluidic devices, and the effective refractive index of the final bulk metamaterials can be tuned by controlling the shape, the size and the density of the resonators (Figure 5) [13].

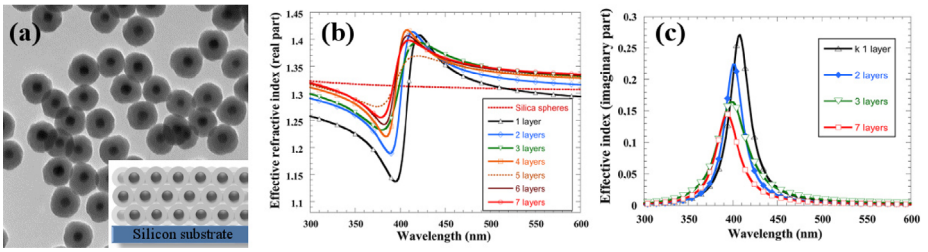

Figure 4. (a) TEM view of core-shell nanoparticles. The diameters of the particle and of the $Ag@SiO_2$ core are 83±4 nm and 27±3 nm respectively. Inset is a sketch of the structure of a 3-layer film deposited on a silicon substrate by the Langmuir–Shaefer technique. (b, c) Plots of the real (b) and imaginary (c) part of the refractive index of metamaterial films as a function of the number of layers (adapted from [55]).

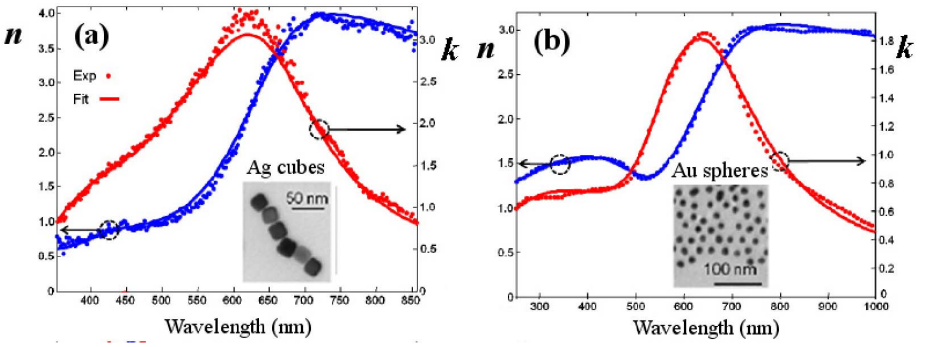

Figure 5. Examples of effective refractive index of 3D composite plasmonic materials made of dense assemblies of silver cubes in (a) and gold spheres in (b). The dots are obtained by direct retrieval from the ellipsometric data, while the continuous lines are a fit to a Tauc–Lorentz model [13].

Although the high volume fraction of metal in self-assembled 3D systems precludes the use of simple mixing rules for the calculation of the effective refractive index, the ellipsometric studies show that the materials behave as homogeneous resonant metamaterials [13].

3.2. *Topological darkness*

The cancellation of the TM reflection from a transparent medium at Brewster's angle is well-known. If losses are introduced via an imaginary part of the optical index, the exact Brewster's extinction disappears. Nevertheless, an exact cancellation of the TM or TE reflection can be reached in thin absorbing films deposited on an absorbing substrate as will be shown below.

For a homogeneous film on a flat surface, the amplitude reflection coefficient of the TM wave is given in standard textbooks

$$r_{\mathrm{TM}} = \frac{r_{\mathrm{TM},1} + r_{\mathrm{TM},2}\mathrm{e}^{2\mathrm{i}\beta}}{1 + r_{\mathrm{TM},1}r_{\mathrm{TM},2}\mathrm{e}^{2\mathrm{i}\beta}} \tag{3}$$

where $\beta = (2\pi/\lambda)N_1 d\cos\phi_1$ is the propagation constant inside the medium, $r_{\mathrm{TM},1(2)}$ is the reflection coefficient from the top (1) and bottom (2) interface, $N_1 = n+\mathrm{i}k$ is the refractive index of the film, d its thickness, λ the wavelength in vacuum and ϕ_1 denotes the direction of the refracted beam within the film. The solutions of the extinction condition display multiple branches shown

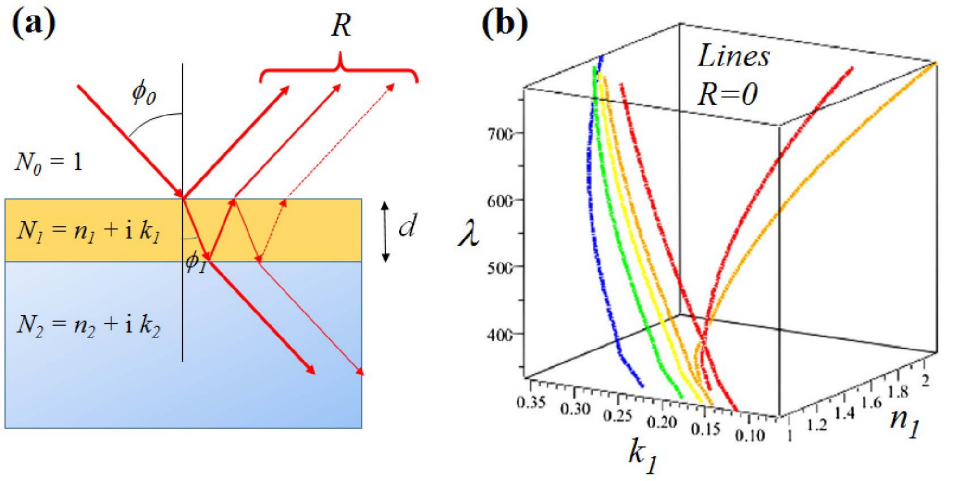

Figure 6. (a) Sketch of the optical geometry. The dark point corresponds to $R = 0$ (destructive interference). (b) Theoretical extinction lines computed numerically for a homogeneous film of index $N_1 = n + ik$ deposited on a silicon substrate at constant angle of incidence $\phi_0 = 50°$ and TM polarization. Colors red, orange, yellow, green and blue correspond, respectively, to thicknesses d of 350, 300, 280, 250 and 200 nm. Note that more than one extinction branch may exist for each thickness (only shown for thicknesses 350 and 300 nm for sake of clarity). Different angles of incidence result in different sets of lines. Similar sets of extinction lines are found for TE polarization (adapted from [56]).

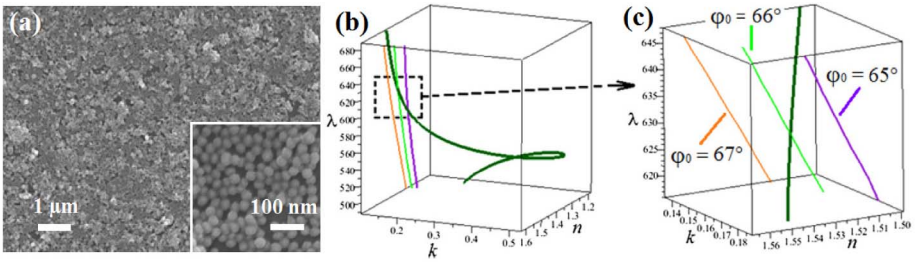

Figure 7. (a) SEM micrographs of a monolayer of core-shell nanoparticles Au(14 nm)@SiO_2(11 nm) transferred on a silicon substrate by the Langmuir–Blodgett technique. (b) 3D views showing the dispersion curve of a 2-layer film of core-shell particles Au(48 nm)@SiO_2(18 nm) (dark green) and the theoretical extinction curves computed for three angles of incidence (AOI). (c) details of the crossing region showing the strong dependence on the AOI. The figure is adapted from [57].

in Figure 6 in (n, k, λ) axes for a particular value of the angle of incidence (AOI = 50°) and for different thicknesses.

A dark point arises when the dispersion curve of a film $(n(\lambda), k(\lambda))$ crosses a line $r_{TM} = 0$. For a film of given thickness on a given substrate, the only experimental parameter is the angle of incidence which must be adjusted to reach the dark point. The existence of the intersection is guaranteed by the Jordan theorem [56]. We illustrate this effect in Figure 7 with experiments carried out on a thin film of core-shell nanoparticles made of a gold core (diameter 14 nm) surrounded by a silica shell (thickness 11 nm) deposited by successive Langmuir–Schaefer transfers onto a

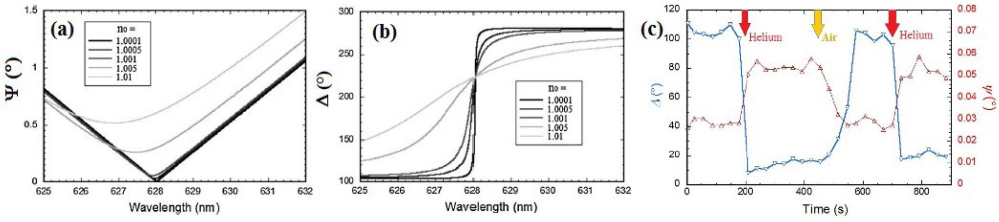

Figure 8. Illustration of the high sensitivity of a plasmonic sensor based on the dark point. The ellipsometric angles Ψ (a) and Δ (right) are computed and plotted for increasing but weak variations of the refractive index of the ambient medium. Note the strong effect on the phase Ψ which provides much higher sensitivity than Δ. (c) Variations of the ellipsometric angles Δ (blue line, left scale) and Ψ (red line, right scale) in the vicinity of the dark point. Helium is injected above the film at $t = 200$ s and $t = 700$ s, air is injected at $t = 450$ s. Note the large variation of $\Delta \sim 100°$ for a change of 2.4×10^{-4} in the refractive index N_0 of the gas. The film is a transparent polymer loaded with 10% vol. gold nanoparticles spin coated on a silicon wafer. The thickness is 179 nm, the dark point is found at AOI = 69.6° and λ = 616 nm.

silicon wafer [57]. A resonant dispersion produces a large exploration of the (n, k) space, which favors the occurrence of the dark condition (see Figure 7), but the presence of a plasmonic resonance is in fact not required to observe a dark point, and it may actually occur either near [58] or away [59] from the resonance, providing in the later case a low-loss phase jump effect.

The dark phenomenon is easily detected by spectroscopic ellipsometry measuring the ratio of the TM to TE reflection coefficients $\rho = r_{\mathrm{TM}}/r_{\mathrm{TE}} = \tan\Psi \mathrm{e}^{-\mathrm{i}\Delta}$. At the dark point, Ψ vanishes and the phase Δ undergoes a sharp jump equal to π. The steep variation of the phase can be exploited for ultra-sensitive sensing [56, 60].

Figure 8 (a,b) illustrates the variation of Ψ and Δ for weak variations of the refractive index of the ambient medium. Figure 8 (c) shows an application to the detection of weak variations of the refractive index of a gas. A phase shift of 100° is observed when air is replaced by helium in the ambient medium above the film. The change in refractive index is 2.4×10^{-4} which yields a sensitivity of the phase on the order of 4×10^5 deg/RIU. Figure 8 (c) shows that a detection accuracy better than 10^{-5} RIU is easily achieved, which is comparable to SPR instruments based on photodiode arrays for instance [61].

This example shows that the total extinction of the reflection due to destructive interferences in a thin absorbing film (topological darkness), similar to the Brewster's extinction on a transparent medium, can be used for sensing with a high sensitivity.

3.3. *3D isotropic optical magnetism*

The magnetism of matter is vanishingly small in natural materials at high frequencies. Paramagnetism and ferromagnetism are slow process that are usually extremely inefficient at frequencies larger than the GHz and diamagnetism typically exhibits magnetic susceptibilities χ_m on the order of 10^{-4} at best. As a consequence, the relative magnetic permeability μ is equal to one for all optical materials in optics and electromagnetism at such frequencies. Natural diamagnetism occurs—in a semi-classical description—because impinging electromagnetic fields induce local polarization currents in atoms or molecules due to circulating charges such as an electron, resulting in an angular momentum that itself produces a magnetic dipole moment **m**. However, these dipole moments are very weak at optical frequencies [20].

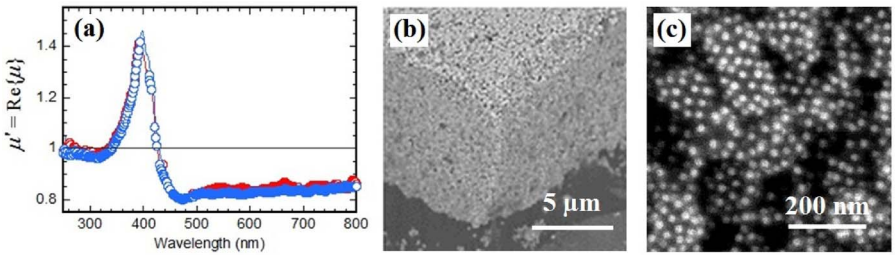

Figure 9. Three-dimensional magnetic metamaterial at optical frequencies. (a) Spectral variations of the retrieved magnetic permeability μ of the metamaterial. (b, c) Scanning electron micrographs of the self-assembled metamaterial at two different scales. Figure adpated from [14].

Plasmonic raspberry systems such as those presented in Section 2.1 (see Figure 1(c–f)) conceptually play the same diamagnetic role as the atom, because circulating plasmonic currents are created that produce an effective magnetic dipole moment near the plasmon resonance wavelength. This resonance wavelength is large compared to the size of the nanosystem [62]. Furthermore, they have pseudo-spherical symmetry, which means that their behavior does not depend on the directions of the electric and magnetic fields incident on the material. As a result, they are ideal to serve as the building blocks of a *three-dimensional isotropic* metamaterial that will exhibit a resonance in the magnetic permeability μ. This contrasts with most realizations of magnetic metamaterials that have been proposed thus far by the *top-down* approach that were mainly two-dimensional and composed of anisotropic meta-atoms [5].

Using a microfluidic evaporation technique aiming at (meta)materials fabrication [13, 63, 64], a three-dimensional metamaterial composed of these raspberries is produced by flowing the solvent containing the colloids through a micro-channel. The solvent eventually evaporates through a semi-permeable membrane and a dense three-dimensional ensemble is molded into the channel. The final metamaterial is truly bulk and constitutes a chunk 100 µm wide, 5 µm deep and several mm long.

For all practical purposes, this means that at optical frequencies the metamaterial may be considered as semi-infinite, and a variable angle spectroscopic ellipsometric analytical retrieval procedure enables the unambiguous determination of the spectral variations of $\varepsilon(\lambda)$ and $\mu(\lambda)$ [14]. The obtained metamaterial reveals a resonant behavior of the magnetic permeability μ with a real part ranging from 0.8 to 1.45 as shown on Figure 9 (a). This corresponds to a magnetic susceptibility comprised between −0.2 and 0.45, three orders of magnitude higher than the highest natural—static—diamagnetic susceptibility. As far as the authors know, this is the first realization of a bulk magnetic metamaterial exhibiting reflexion properties in visible light which are correctly described by an effective isotropic permeability parameter. A tutorial on the direct experimental retrieval procedure is given by Flamant *et al.* [65].

3.4. *Hyperbolic dispersion*

Another type of nanostructures referred to as hyperbolic metamaterials has been proven very promising, as it exploits anisotropy effects to monitor the propagative modes via engineering of the dispersion relation. Indeed, hyperbolic metamaterials present, in some spectral range, two components of the dielectric permittivity tensor ε with opposite signs, as if the material behaved like a metal ($\varepsilon_i < 0$) along at least one direction and like a dielectric ($\varepsilon_j > 0$) along at least another. Because of this extraordinary anisotropy, the isofrequency surfaces open up into

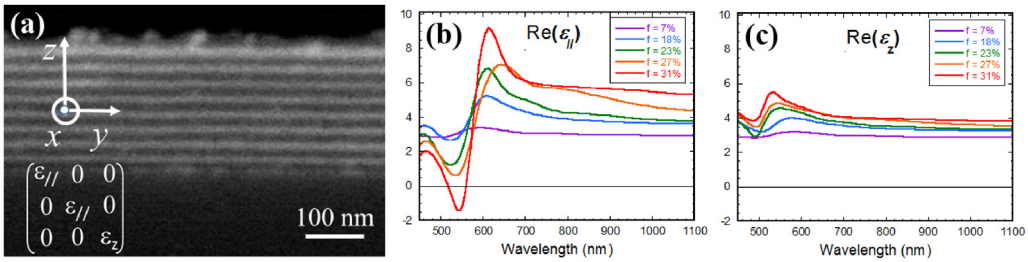

Figure 10. Block copolymer based lamellar metamaterial. (a) Scanning electron micrograph evidencing the regular uniaxial nanostructure. (b, c) Real part of the ordinary and extraordinary permittivities as a function of wavelength for increasing volume fraction f of gold NPs in the lamellae. Figure adapted from [66].

hyperboloids, instead of ellipsoids in a natural material. The extended shape of the isofrequency surfaces allows for propagating waves with large wavevectors, which would be evanescent waves in a natural material. This unique property of propagating high-k waves opens possibilities for imaging with subwavelength resolution. In addition, the phase space volume between two hyperboloids for two values of frequency is infinite, which corresponds to an infinite density of photonic states. Finally, the peculiar dispersion relation gives rise to a number of specific properties, from subwavelength modes to emission engineering, as reviewed in a number of past reports [67–70].

Anisotropic metal-dielectric nanostructures with a hyperbolic dispersion law in the visible wavelength range have been produced with either lamellar stack or cylinder array geometries. Metal-dielectric multilayers are often grown by physical vapor deposition, using either sputtering or evaporation, while cylinder arrays are often produced via the growth of aligned nanowires within porous templating matrices [71] as well as electron beam lithography [72]. As a matter of fact, nanostructuration and anisotropy, along with some degree of long-range order, are spontaneously arising in several self-assembled "soft matter" systems as surfactant organized phases [73], liquid crystals [74], organized nanoparticles, and block copolymers [75]. 3D self-assembly in the form of magnetic NPs chains, induced by the application of an external magnetic field to a ferrofluid, creates a sufficient anisotropy to achieve hyperbolic dispersion laws [76, 77]. Carbon nanotubes packed and aligned by filtration can also constitute hyperbolic metamaterials [78]. Block copolymers present many advantages for the design of anisotropic nanocomposites. They are the result of covalently linking two or more long polymer chains, each called a block, with a chemical nature that can be chosen within a very wide range of chemical functions. Most polymers are incompatible with one another and phase separate in a blend, but because they are covalently linked, distinct blocks of a block copolymer can segregate only as far as the size of the macromolecule, which results in the formation of nanodomains of each block in the solid material. The morphology and degree of order of these nanodomains are fully controlled by the number and relative length of the blocks, while their size directly depends on the whole macromolecule molar mass [79]. By hybridizing an aligned block copolymer nanostructure with gold precursors, Wang *et al.* have produced periodic lamellar stacks of period 28 nm, of alternating layers of pure polymer (dielectric) and layers of composite of polymer loaded with a variable density of 7 nm gold nanoparticles [66]. For large gold loading and close to the plasmon resonance of the nanoparticles, the lamellar stack presents ordinary and extraordinary components of the dielectric function of opposite signs, as evidenced by spectroscopic ellipsometry and shown on Figure 10, demonstrating the potential of this fabrication route for self-assembled bulk hyperbolic metamaterials.

4. Metasurfaces

Metasurfaces are 2D equivalent of metamaterials, designed to control the phase, amplitude and possibly polarization of incident EM waves with subwavelength thickness, using interfacial discontinuities effects (see for instance [80]). Metasurfaces rely on the tailored light scattering of sub-wavelength resonators organized in thin films.

4.1. *Large surfaces*

Just as for 3D assemblies, bottom-up routes for the organization of nano-objects on surfaces rely on constrained hydrodynamics or templating by patterned substrates in order to direct and benefit from self-assembly phenomena, with the major advantage of providing low-cost, large-scale fabrication routes. For instance, dewetting phenomena on topographically patterned substrates have led to silver NPs arrays presenting surface lattice resonance modes [81]. While the size, shape or complex geometry of nanoresonators can tailor their responses, in terms of light absorption and scattering, the relation between these responses and the properties of a metasurface made of the assembled resonators will be computable only if the assembly process results in a surface of good homogeneity. Templating may be a good process to target such homogeneity. A combination of lithography-based topographically patterned substrates and confined drying conditions of a colloidal suspension can lead to well-controlled 2D assembly [82] as demonstrated for instance by an anisotropic appearance in the far-field in the case of aligned nanorods [83]. Templating can also be performed using low-tech wafer-wide spin-coated block copolymer thin films (<50 nm). They constitute chemically patterned substrates, on which metal or dielectric nano-objects can be attached [84] or grown [85–88]. They can also be used as nanometric masks for lithography-like fabrication methods [89, 90]. At the University of Bordeaux, such large scale block copolymer thin films have been used to produce tunable gold nanoresonators in fingerprint-like structures illustrated in the Figure 11, insuring a global azimuthal isotropy together with inter-particle distance homogeneity [86]. The tunable aspect ratio of the resonators strongly affects the optical response of the surface nanostructure on a silicon substrate. Indeed, a description of the optical properties of the samples was derived from ellipsometry data in reflection in terms of an effective optical index, even though the index of so thin films may not be defined independently of the measurement conditions [91,92]. In Ref. [86], increasing the in-plane aspect ratio of the nanoresonators to 2, while keeping the nanostructure thickness constant, was achieved by tuning a simple fabrication process parameter and led to an increase of the index up to 3.2, against ∼1.6 for a nanostructure with same gold density and resonators of aspect ratio 1.

4.2. *Flat optics*

The recent surge in metasurfaces has shown that it is possible to conceive a wide variety of flat optical components that operate thanks to the careful engineering of the amplitudes and phases of the fields scattered by individual resonant objects [34,93]. Bottom-up nanocolloidal routes can play a role here notably thanks to the large amounts of nanoresonators they can produce and the vast surfaces that can be coated by various self-assembly techniques. The variety of meta-atoms that can be synthesized makes it possible to tailor the resonances of the electric dipole moment ($\mathbf{p}$) as well as the magnetic dipole moment ($\mathbf{m}$) both in amplitude and in resonance wavelength.

For instance, when a particle has the property that $|\mathbf{p}| = |\mathbf{m}|$, the so-called *first Kerker condition* is reached and a Huygens dipole is produced [94]. The Huygens dipoles emit spherical waves solely in a direction $\mathbf{u}$ such that $(\mathbf{u}, \mathbf{p}, \mathbf{m})$ forms a direct trihedron. This dipole is named after

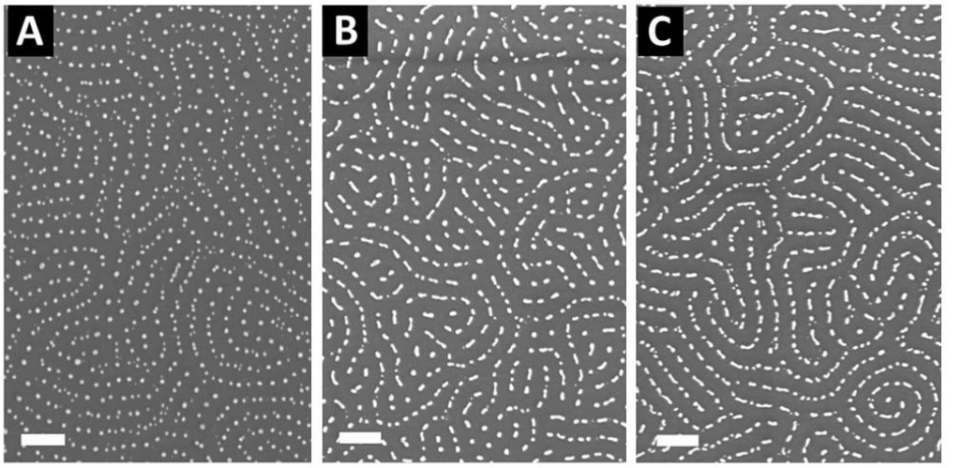

Figure 11. SEM images of gold nanoparticle arrays formed on a silicon wafer using a PS-b-P2VP block copolymer template by immersion in a 1 wt% aqueous gold precursor solution for (A) 1 h, (B) 48 h and (C) 120 h [86]. Scale bars = 100 nm.

Christiaan Huygens as it corresponds to the fictitious point sources of secondary spherical wavelets from the Huygens–Fresnel principle [95]. As a result, when the meta-atom is excited by an impinging plane wave, scattering only occurs in the direction of the exciting wave. This means that a surface composed of these meta-atoms are reflection-less and exhibit a transmission close to unity, these are Huygens metasurfaces [96]. Furthermore the fact that both dipolar resonances are super-imposed means that a full range of dephasing is accessible on the $[0, 2\pi]$ interval and virtually any wavefront may be shaped and flat optical components may be produced, such as prisms or lenses. Huygens sources can be obtained with several systems such as those described in Section 2.2, by exploiting the Mie resonances of homogenous nanoparticles that have the right dispersion and size to reach the Huygens regime, or else by using the clusters system proposed by Dezert *et al.* [37]. It was demonstrated that clusters of plasmonic or dielectric inclusions were good candidates to produce flat lenses and prisms [97]. This 2π phase-shift occurs over narrow-spectral ranges and as a result group-velocity dispersion may be large. This potentially means that metasurfaces composed of isotropic Huygens sources could be used for temporal pulse shaping as was proposed by Decker *et al.* [96] in the case of a periodic metasurface. But since ordering does not play a role, disordered metasurfaces could be used and this is adapted to the bottom-up platform.

Additional types of flat optical components such as filters may be produced. The cases of resonant perfect absorbers is discussed below.

4.3. *Perfect absorbers*

In many circumstances, it may be useful to have a material that absorbs all of the incoming radiation. This concept is certainly applicable to photovoltaics or even some classes of sensors for instance. Furthermore, Kirschoff's law of thermal radiation roughly states that the emissivity of a body is equal to its absorptivity at a given temperature [98]. This means that a perfectly absorbing metamaterial or metasurface may act as a great thermal emitter, or else, due to its thermal activity, it may act as an insulator or bolometer.

Bottom-up colloidal metasurfaces may also play a role in this field, since the metasurface inherits its property from the properties of meta-atoms. Film-coupled metasurfaces acting as

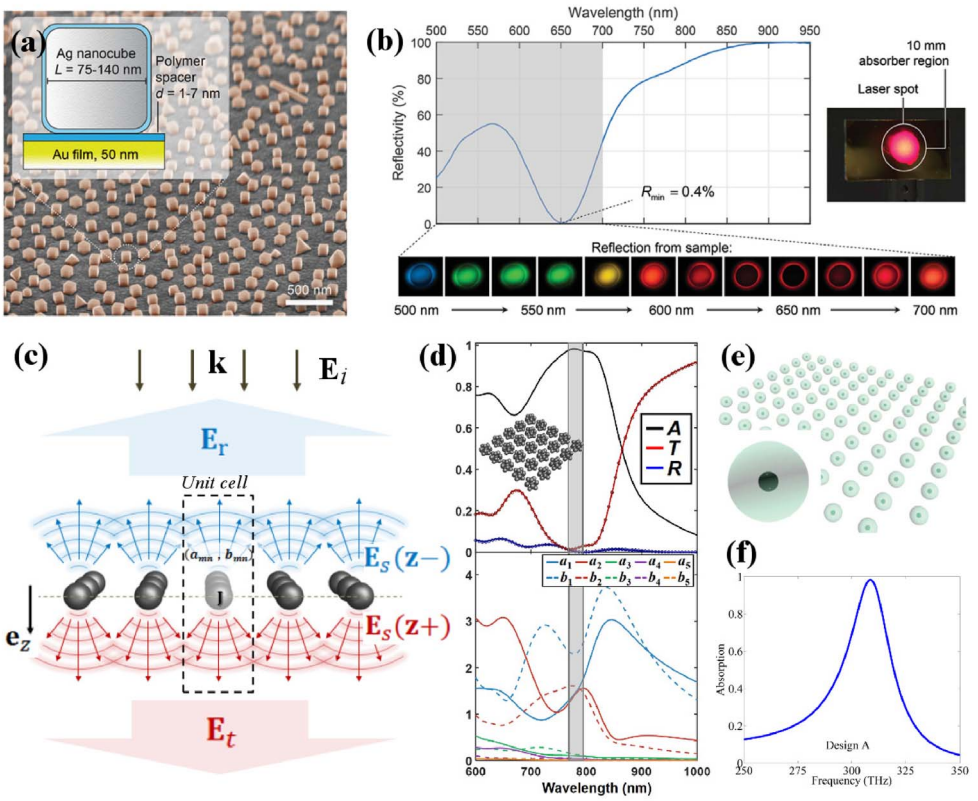

Figure 12. Nanocolloidal Perfect Absorbers. (a) Perfect absorbing metasurface composed of film coupled silver nanocubes ranging from 75 to 140 nm in size deposited on a gold evaporated film and spaced a few nanometers above the gold film. (b) Wavelength-dependence of the reflectivity exhibiting a resonant dip at $\lambda \approx 650$ nm. The photograph on the right-hand side of the graph show that large areas can be covered. (c) Illustration of a canonical metasurface composed of nanocolloids. The metasurface inherits its radiation properties from the scattering properties of the multipoles of the colloids. (d) Top graph: absorption (black), transmisttance (blue) and reflectance (red) spectrum of a perfect absorber composed of a periodic array of germanium nanoclusters. Bottom-graph: multipolar decomposition of the nanocluster in the array. (e) Metasurface composed of core-shell nanocolloids containing a silver core and a n-doped silicon shell. (f) Absorption spectrum of the core-shell metasurface. (a) and (b) are adapted from [102]. (c) and (d) are adapted from [103]. (e) and (f) are adapted from [104].

perfect absorbers have been demonstrated by Moreau *et al.* [99]. They are composed of silver nanocubes deposited on gold films with a separating dielectric gap layer of a couple of nanometers typically. The gap layer is composed of alternating positively and negatively charged polyelectrolytes deposited on the gold surface by dip-coating. The surfaces operate in reflectance and exhibit a resonance dip in the reflectance at a wavelength that is determined by the nanocube size and gap thickness. The amplitude of the resonance is governed by the surface fill fraction [100, 101]. Akselrod *et al.* have shown that such perfect absorbers could cover and conform to large areas (see Figure 12 (a,b)) [102].

Alternatively, it is also possible to produce perfect absorbers, that operate as transmissive monolayers of nanocolloids resonantly absorbing all the impinging light. For instance, a design was proposed by Radi *et al.* consisting in a periodic square array composed of core-shell nanocolloids containing a silver core and a n-doped silicon shell [104] (see Figure 12 (e)). These systems may resonantly act as Huygens dipoles (see Section 4.2), which ensures that no reflection from the metasurface occurs. Furthermore, they show that the perfect absorption condition is reached when both the electric and magnetic polarizabilities (α_e and α_m respectively) of the core-shell in the metasurface satisfies the following relation

$$\frac{\mu_0}{\varepsilon_0}\alpha_e = \frac{\varepsilon_0}{\mu_0}\alpha_m = \mathrm{i}\frac{S}{\omega} \tag{4}$$

where S is the area of the unit cell of the periodic array and μ_0 is the free-space magnetic permittivity. Figure 12 (f) shows that unity absorption is achieved for this system near a frequency equal to 300 THz.

It was shown recently by Dezert *et al.* that the nanocolloids do not have to be dipolar and that multipolar systems can be used in a periodic array to achieve perfect absorbtion (see Figure 12 (c)) [103]. Indeed, what is required is (i) that the sum of odd multipole modes be equal to the sum of even multipole modes, which is a generalization of the famous first Kerker condition (see Section 4.2) and produces Huygens multipoles (i.e. no back-scattering) and (ii) that they both be real and equal to a specific value such that zero-transmission occurs. The condition is summarized by the following relation

$$\sum_{n=1}^{\infty} \mathscr{O}_n = \sum_{n=1}^{\infty} \mathscr{E}_n = \frac{k^2 S}{\pi} \tag{5}$$

where $\mathscr{O}_n$ ($\mathscr{E}_n$) is the nth order odd (even) multipole and k is the free-space wavevector. This property, will ensure that the field radiated by all mutipoles will interfere destructively in the backward direction and reflectance will be cancelled. As a result of this generalization, several designs of perfect absorbing metasurfaces can be proposed. Figure 12 (d) provides an example where near unity absorption is achieved at optical wavelengths, with an array composed of germanium nanoclusters, which operate in a severely multipolar regime.

These designs have great potential for bottom-up nanocolloidal metasurfaces operating at optical frequencies.

5. Conclusion

The examples given in this review illustrate some advantages of the bottom-up approach over top-down fabrication routes for the realization of metamaterials operating in visible light. The extreme versatility of nanochemistry enables the large-scale synthesis of finely engineered meta-atoms. Moreover, self-assembly, relying solely on colloidal interactions, or directed-assembly, benefiting from external guiding constraints, enable the fabrication of bulk materials at little energy cost. In this way, assembling more than 10^9 meta-atoms in a volume of 10^6 μm^3 is routinely achieved. The successful observation of an isotropic effective magnetic permeability different from the vacuum value μ_0 in an optically thick metamaterial follows from this ability to produce and assemble a large number of resonators.

Bottom-up metamaterials nevertheless face many difficult challenges. Nanochemistry and self-assembly result in statistical distributions of the shape, size and ordering of the meta-atoms. For optical functions requiring a high precision in the response and the location of each meta-atom, like planar lenses, some top-down fabrication processes seem inescapable. On the other hand, if homogeneous effective optical properties are sought for, some degree of structural disorder at scales shorter than the wavelength has little impact. The random packing

of the magnetic meta-atoms is even necessary to enable the validity of an effective magnetic permeability parameter [14].

Increasing the optical response of the meta-atoms is another important challenge. In particular, higher values of their magnetic polarizability are needed for the production of Huygens metasurfaces or mu-near-zero (MNZ) materials. Silver has proved to be more efficient than gold in the raspberry model [14,62]. Mie-resonators made of high-index dielectric seem particularly promising for future materials [32, 105]. Increasing the magnetic response of the meta-atoms may however affect the validity of the permeability parameter μ and stimulate more theoretical work. Indeed, artificial magnetism is an effect of spatial dispersion of the permittivity that cannot in principle be reduced to a second-rank tensor μ_{ij} [106].

Optical losses constitute a major limitation for most applications of metamaterials in optics. Compensation of losses by addition of a gain medium excited by optical pumping is a complex and costly process that may be reserved for research studies or specific applications. The impact of losses can nevertheless be limited by using dielectric instead of plasmonic resonators or by reducing the optical thickness in metasurfaces. On the other hand, the Ohmic losses of plasmonic resonators are welcome for applications requiring a local source of heat like heat therapy.

Acknowledgements

The authors acknowledge support from the LabEx AMADEus (ANR-10-LABX-42) in the framework of IdExBordeaux (ANR-10-IDEX-03-02).

References

[1] V. Veselago, "Electrodynamics of substances with simultaneously negative electrical and magnetic permeabilities", *Phys.-Usp.* **10** (1968), no. 4, p. 504-509.
[2] C. R. Simovski, S. A. Tretyakov, "Historical notes on metamaterials", in *Theory and Phenomena of Metamaterials* (F. Capolino, ed.), vol. 1, CRC Press, 2009.
[3] N. Engheta, R. W. Ziolkowski, "Introduction, history, and selected topics in fundamental theories of metamaterials", in *Metamaterials* (N. Engheta, R. Ziolkowski, eds.), IEEE Press, 2006.
[4] A. I. Iyer, G. V. Eleftheriades, "Negative-refractive-index transmission-line metamaterials", in *Negative-Refracton Metamaterials* (G. V. Eleftheriades, K. G. Balmain, eds.), Wiley and Sons, 2005.
[5] C. M. Soukoulis, M. Wegener, "Past achievements and future challenges in the development of three-dimensional photonic metamaterials", *Nat. Photon.* **5** (2011), no. 9, p. 523.
[6] V. Ponsinet, A. Aradian, P. Barois, S. Ravaine, "Self-assembly and nanochemistry techniques for the fabrication of metamaterials", in *Theory and Phenomena of Metamaterials* (F. Capolino, ed.), vol. 2, CRC Press, 2009.
[7] A. Baron, A. Aradian, V. Ponsinet, P. Barois, "Self-assembled optical metamaterials", *Opt. Laser Technol.* **82** (2016), p. 94-100.
[8] V. Ponsinet, A. Baron, E. Pouget, Y. Okazaki, R. Oda, P. Barois, "Self-assembled nanostructured metamaterials", *Europhys. Lett.* **119** (2017), no. 1, article ID 14004.
[9] J. C. Berg, *An Introduction to Interfaces and Colloids: The Bridge to Nanoscience*, World Scientific, 2010.
[10] T. Cosgrove, *Colloid Science: Principles, Methods and Applications*, Wiley and Sons, 2010.
[11] M. Lahmani, C. Bréchignac, P. Houdy, "Les nanosciences", in *Nanomateriaux et nanochimie*, vol. 2, Belin, 2006.
[12] C. Bréchignac, P. Houdy, M. Lahmani, *Nanomaterials and Nanochemistry*, Springer, 2007.
[13] A. Baron, A. Iazzolino, K. Ehrhardt, J.-B. Salmon, A. Aradian, V. Kravets, A. N. Grigorenko, J. Leng, A. Le Beulze, M. Tréguer-Delapierre *et al.*, "Bulk optical metamaterials assembled by microfluidic evaporation", *Opt. Mater. Express* **3** (2013), no. 11, p. 1792-1797.
[14] S. Gomez-Graña, A. Le Beulze, M. Treguer-Delapierre, S. Mornet, E. Duguet, E. Grana, E. Cloutet, G. Hadziioannou, J. Leng, J.-B. Salmon *et al.*, "Hierarchical self-assembly of a bulk metamaterial enables isotropic magnetic permeability at optical frequencies", *Mater. Horiz.* **3** (2016), no. 6, p. 596-601.
[15] X. Fan, W. Zheng, D. J. Singh, "Light scattering and surface plasmons on small spherical particles", *Light: Sci. Appl.* **3** (2014), no. 6, article ID e179–e179.
[16] S. Gwo, H.-Y. Chen, M.-H. Lin, L. Sun, X. Li, "Nanomanipulation and controlled self-assembly of metal nanoparticles and nanocrystals for plasmonics", *Chem. Soc. Rev.* **45** (2016), no. 20, p. 5672-5716.

[17] J. B. Pendry, "Negative refraction makes a perfect lens", *Phys. Rev. Lett.* **85** (2000), no. 18, p. 3966.
[18] J. B. Pendry, D. Schurig, D. R. Smith, "Controlling electromagnetic fields", *Science* **312** (2006), no. 5781, p. 1780-1782.
[19] V. M. Shalaev, "Transforming light", *Science* **322** (2008), no. 5900, p. 384-386.
[20] L. D. Landau, J. Bell, M. Kearsley, L. Pitaevskii, E. Lifshitz, J. Sykes, *Electrodynamics of Continuous Media, Vol. 8*, Elsevier, 2013.
[21] J. B. Pendry, A. J. Holden, D. J. Robbins, W. Stewart *et al.*, "Magnetism from conductors and enhanced nonlinear phenomena", *IEEE Trans. Microw. Theory Tech.* **47** (1999), no. 11, p. 2075-2084.
[22] R. A. Shelby, D. R. Smith, S. Schultz, "Experimental verification of a negative index of refraction", *Science* **292** (2001), no. 5514, p. 77-79.
[23] A. Alù, A. Salandrino, N. Engheta, "Negative effective permeability and left-handed materials at optical frequencies", *Opt. Express* **14** (2006), no. 4, p. 1557-1567.
[24] A. Alu, N. Engheta, "The quest for magnetic plasmons at optical frequencies", *Opt. Express* **17** (2009), no. 7, p. 5723-5730.
[25] C. Simovski, S. Tretyakov, "Model of isotropic resonant magnetism in the visible range based on core-shell clusters", *Phys. Rev. B* **79** (2009), no. 4, article ID 045111.
[26] J. Lekner, "Optical properties of isotropic chiral media", *Pure Appl. Opt.: J. Eur. Opt. Soc. A* **5** (1996), no. 4, p. 417.
[27] A. Kuzyk, R. Schreiber, Z. Fan, G. Pardatscher, E.-M. Roller, A. Högele, F. C. Simmel, A. O. Govorov, T. Liedl, "DNA-based self-assembly of chiral plasmonic nanostructures with tailored optical response", *Nature* **483** (2012), no. 7389, p. 311.
[28] X. Fu, Y. Wang, L. Huang, Y. Sha, L. Gui, L. Lai, Y. Tang, "Assemblies of metal nanoparticles and self-assembled peptide fibrils—formation of double helical and single-chain arrays of metal nanoparticles", *Adv. Mater.* **15** (2003), no. 11, p. 902-906.
[29] J. Cheng, G. Le Saux, J. Gao, T. Buffeteau, Y. Battie, P. Barois, V. Ponsinet, M.-H. Delville, O. Ersen, E. Pouget *et al.*, "Goldhelix: gold nanoparticles forming 3d helical superstructures with controlled morphology and strong chiroptical property", *ACS Nano* **11** (2017), no. 4, p. 3806-3818.
[30] A. Vallecchi, M. Albani, F. Capolino, "Collective electric and magnetic plasmonic resonances in spherical nanoclusters", *Opt. Express* **19** (2011), no. 3, p. 2754-2772.
[31] V. Giannini, A. I. Fernández-Domínguez, S. C. Heck, S. A. Maier, "Plasmonic nanoantennas: fundamentals and their use in controlling the radiative properties of nanoemitters", *Chem. Rev.* **111** (2011), no. 6, p. 3888-3912.
[32] S. Jahani, Z. Jacob, "All-dielectric metamaterials", *Nat. Nanotechnol.* **11** (2016), no. 1, p. 23.
[33] J. Valentine, J. Li, T. Zentgraf, G. Bartal, X. Zhang, "An optical cloak made of dielectrics", *Nat. Mater.* **8** (2009), no. 7, p. 568.
[34] M. Khorasaninejad, W. T. Chen, R. C. Devlin, J. Oh, A. Y. Zhu, F. Capasso, "Metalenses at visible wavelengths: diffraction-limited focusing and subwavelength resolution imaging", *Science* **352** (2016), no. 6290, p. 1190-1194.
[35] A. B. Evlyukhin, S. M. Novikov, U. Zywietz, R. L. Eriksen, C. Reinhardt, S. I. Bozhevolnyi, B. N. Chichkov, "Demonstration of magnetic dipole resonances of dielectric nanospheres in the visible region", *Nano Lett.* **12** (2012), no. 7, p. 3749-3755.
[36] S. Zhang, R. Jiang, Y.-M. Xie, Q. Ruan, B. Yang, J. Wang, H.-Q. Lin, "Colloidal moderate-refractive-index Cu_2O nanospheres as visible-region nanoantennas with electromagnetic resonance and directional light-scattering properties", *Adv. Mater.* **27** (2015), no. 45, p. 7432-7439.
[37] R. Dezert, P. Richetti, A. Baron, "Isotropic Huygens dipoles and multipoles with colloidal particles", *Phys. Rev. B* **96** (2017), no. 18, article ID 180201.
[38] F. Timpu, A. Sergeyev, N. R. Hendricks, R. Grange, "Second-harmonic enhancement with Mie resonances in perovskite nanoparticles", *ACS Photon.* **4** (2016), no. 1, p. 76-84.
[39] A. L. Lereu, R. Farahi, L. Tetard, S. Enoch, T. Thundat, A. Passian, "Plasmon assisted thermal modulation in nanoparticles", *Opt. Express* **21** (2013), no. 10, p. 12145-12158.
[40] P. Berini, I. De Leon, "Surface plasmon-polariton amplifiers and lasers", *Nat. Photon.* **6** (2011), p. 16-24.
[41] O. Hess, J. B. Pendry, S. Maier, R. Oulton, J. Hamm, K. Tsakmakidis, "Active nanoplasmonic metamaterials", *Nat. Mater.* **11** (2012), p. 573-584.
[42] K. F. MacDonald, N. I. Zheludev, "Active plasmonics: current status", *Laser Photon. Rev.* **4** (2010), no. 4, p. 562-567.
[43] M. Noginov, G. Zhu, M. Bahoura, J. Adegoke, C. Small, B. Ritzo, V. Drachev, V. Shalaev, "The effect of gain and absorption on surface plasmons in metal nanoparticles", *Appl. Phys. B* **86** (2007), no. 3, p. 455-460.
[44] A. De Luca, M. P. Grzelczak, I. Pastoriza-Santos, L. M. Liz-Marzán, M. La Deda, M. Striccoli, G. Strangi, "Dispersed and encapsulated gain medium in plasmonic nanoparticles: a multipronged approach to mitigate optical losses", *ACS Nano* **5** (2011), no. 7, p. 5823-5829.
[45] A. De Luca, M. Ferrie, S. Ravaine, M. La Deda, M. Infusino, A. R. Rashed, A. Veltri, A. Aradian, N. Scaramuzza, G. Strangi, "Gain functionalized core–shell nanoparticles: the way to selectively compensate absorptive losses", *J. Mater. Chem.* **2** (2012), p. 8846-8852.
[46] R.-M. Ma, R. F. Oulton, "Applications of nanolasers", *Nat. Nanotechnol.* **14** (2019), p. 12-22.

[47] Z. Wang, X. Meng, A. V. Kildishev, A. Boltasseva, V. M. Shalaev, "Nanolasers enabled by metallic nanoparticles: from spasers to random lasers", *Laser Photon. Rev.* **11** (2017), no. 6, article ID 1700212.
[48] M. Noginov, G. Zhu, A. Belgrave, R. Bakker, V. M. Shalaev, E. Narimanov, S. Stout, E. Herz, T. Suteewong, U. Wiesner, "Demonstration of a spaser-based nanolaser", *Nature* **460** (2009), p. 1110-1112.
[49] X. Meng, A. V. Kildishev, K. Fujita, K. Tanaka, V. M. Shalaev, "Wavelength-tunable spasing in the visible", *Nano Lett.* **13** (2013), no. 9, p. 4106-4112.
[50] A. Veltri, A. Aradian, "Optical response of a metallic nanoparticle immersed in a medium with optical gain", *Phys. Rev. B* **85** (2012), no. 11, article ID 115429.
[51] V. Pustovit, F. Capolino, A. Aradian, "Cooperative plasmon-mediated effects and loss compensation by gain dyes near a metal nanoparticle", *J. Opt. Soc. Am. B* **32** (2015), no. 02, p. 188-193.
[52] A. Veltri, A. Chipouline, A. Aradian, "Multipolar, time-dynamical model for the loss compensation and lasing of a spherical plasmonic nanoparticle spaser immersed in an active gain medium", *Sci. Rep.* **6** (2016), p. 33018.
[53] A. Veltri, K. Caicedo, A. Cathey, A. Aradian, to be published (2019).
[54] J. Vieaud, O. Merchiers, M. Rajaoarivelo, M. Warenghem, Y. Borensztein, V. Ponsinet, A. Aradian, "Effective medium description of plasmonic couplings in disordered polymer and gold nanoparticle composites", *Thin Solid Films* **603** (2016), p. 452-464.
[55] L. Malassis, P. Massé, M. Tréguer-Delapierre, S. Mornet, P. Weisbecker, V. Kravets, A. Grigorenko, P. Barois, "Bottom-up fabrication and optical characterization of dense films of meta-atoms made of core–shell plasmonic nanoparticles", *Langmuir* **29** (2013), no. 5, p. 1551-1561.
[56] V. Kravets, F. Schedin, R. Jalil, L. Britnell, R. Gorbachev, D. Ansell, B. Thackray, K. Novoselov, A. Geim, A. V. Kabashin *et al.*, "Singular phase nano-optics in plasmonic metamaterials for label-free single-molecule detection", *Nat. Mater.* **12** (2013), no. 4, p. 304.
[57] C. Coutant, S. Ravaine, X. Wang, J. Toudert, V. Ponsinet, P. Barois, "Plasmonic metamaterials for ultra-sensitive sensing: topological darkness", *Rend. Lincei* **26** (2015), no. 2, p. 175-182.
[58] F. Aubrit, F. Testard, A. Paquirissamy, F. Gobeaux, X. Wang, F. Nallet, P. Fontaine, V. Ponsinet, P. Guenoun, "Ligand-free synthesis of gold nanoparticles incorporated within cylindrical block copolymer films", *J. Mater. Chem. C* **6** (2018), no. 30, p. 8194-8204.
[59] J. Toudert, X. Wang, C. Tallet, P. Barois, A. Aradian, V. Ponsinet, "Plasmonic optical interferences for phase-monitored nanoscale sensing in low-loss three-dimensional metamaterials", *ACS Photon.* **2** (2015), no. 10, p. 1443-1450.
[60] A. Grigorenko, P. Nikitin, A. Kabashin, "Phase jumps and interferometric surface plasmon resonance imaging", *Appl. Phys. Lett.* **75** (1999), no. 25, p. 3917-3919.
[61] K. Johansen, R. Stålberg, I. Lundström, B. Liedberg, "Surface plasmon resonance: instrumental resolution using photo diode arrays", *Meas. Sci. Technol.* **11** (2000), no. 11, p. 1630.
[62] V. Ponsinet, P. Barois, S. M. Gali, P. Richetti, J.-B. Salmon, A. Vallecchi, M. Albani, A. Le Beulze, S. Gomez-Grana, E. Duguet *et al.*, "Resonant isotropic optical magnetism of plasmonic nanoclusters in visible light", *Phys. Rev. B* **92** (2015), no. 22, article ID 220414.
[63] J. Angly, A. Iazzolino, J.-B. Salmon, J. Leng, S. P. Chandran, V. Ponsinet, A. Désert, A. Le Beulze, S. Mornet, M. Tréguer-Delapierre *et al.*, "Microfluidic-induced growth and shape-up of three-dimensional extended arrays of densely packed nanoparticles", *ACS Nano* **7** (2013), no. 8, p. 6465-6477.
[64] V. Kravets, O. Marshall, R. Nair, B. Thackray, A. Zhukov, J. Leng, A. Grigorenko, "Engineering optical properties of a graphene oxide metamaterial assembled in microfluidic channels", *Opt. Express* **23** (2015), no. 2, p. 1265-1275.
[65] Q. Flamant, D. Torrent, S. Gomez-Graña, A. N. Grigorenko, V. G. Kravets, P. Barois, V. Ponsinet, A. Baron, "Direct retrieval method of the effective permittivity and permeability of bulk semi-infinite metamaterials by variable-angle spectroscopic ellipsometry", *OSA Contin.* **2** (2019), no. 5, p. 1762-1772.
[66] X. Wang, K. Ehrhardt, C. Tallet, M. Warenghem, A. Baron, A. Aradian, M. Kildemo, V. Ponsinet, "Hyperbolic-by-design self-assembled metamaterial based on block copolymers lamellar phases", *Opt. Laser Technol.* **88** (2017), p. 85-95.
[67] L. Ferrari, C. Wu, D. Lepage, X. Zhang, Z. Liu, "Hyperbolic metamaterials and their applications", *Prog. Quantum Electron.* **40** (2015), p. 1-40.
[68] A. Poddubny, I. Iorsh, P. Belov, Y. Kivshar, "Hyperbolic metamaterials", *Nat. Photon.* **7** (2013), no. 12, p. 948.
[69] Y. Guo, W. Newman, C. L. Cortes, Z. Jacob, "Applications of hyperbolic metamaterial substrates", *Adv. OptoElectron.* **2012** (2012), article ID 452502.
[70] I. I. Smolyaninov, V. N. Smolyaninova, "Hyperbolic metamaterials: novel physics and applications", *Solid-State Electron.* **136** (2017), p. 102-112.
[71] J. Yao, Z. Liu, Y. Liu, Y. Wang, C. Sun, G. Bartal, A. M. Stacy, X. Zhang, "Optical negative refraction in bulk metamaterials of nanowires", *Science* **321** (2008), no. 5891, p. 930-930.
[72] N. A. Melosh, A. Boukai, F. Diana, B. Gerardot, A. Badolato, P. M. Petroff, J. R. Heath, "Ultrahigh-density nanowire lattices and circuits", *Science* **300** (2003), no. 5616, p. 112-115.

[73] W. M. Gelbart, A. Ben-Shaul, D. Roux, *Micelles, Membranes, Microemulsions, and Monolayers*, Springer Science & Business Media, 2012.
[74] P.-G. De Gennes, J. Prost, *The Physics of Liquid Crystals, Vol. 83*, Oxford University Press, 1995.
[75] T. P. Lodge, "Block copolymers: past successes and future challenges", *Macromol. Chem. Phys.* **204** (2003), no. 2, p. 265-273.
[76] Y. Gao, J. Huang, Y. Liu, L. Gao, K. Yu, X. Zhang, "Optical negative refraction in ferrofluids with magnetocontrollability", *Phys. Rev. Lett.* **104** (2010), no. 3, article ID 034501.
[77] V. N. Smolyaninova, B. Yost, D. Lahneman, E. E. Narimanov, I. I. Smolyaninov, "Self-assembled tunable photonic hyper-crystals", *Sci. Rep.* **4** (2014), p. 5706.
[78] J. A. Roberts, S.-J. Yu, P.-H. Ho, S. Schoeche, A. L. Falk, J. A. Fan, "Tunable hyperbolic metamaterials based on self-assembled carbon nanotubes", *Nano Lett.* **19** (2019), no. 5, p. 3131-3137.
[79] I. W. Hamley, *The Physics of Block Copolymers, Vol. 19*, Oxford University Press, Oxford, 1998.
[80] S. B. Glybovski, S. A. Tretyakov, P. A. Belov, Y. S. Kivshar, C. R. Simovski, "Metasurfaces: from microwaves to visible", *Phys. Rep.* **634** (2016), p. 1-72.
[81] P. Jacquet, B. Bouteille, R. Dezert, J. Lautru, R. Podor, A. Baron, J. Teisseire, J. Jupille, R. Lazzari, I. Gozhyk, "Periodic arrays of diamond-shaped silver nanoparticles: from scalable fabrication by template-assisted solid-state dewetting to tunable optical properties", *Adv. Funct. Mater.* (2019), article ID 1901119.
[82] Y. Cui, M. T. Björk, J. A. Liddle, C. Sönnichsen, B. Boussert, A. P. Alivisatos, "Integration of colloidal nanocrystals into lithographically patterned devices", *Nano Lett.* **4** (2004), no. 6, p. 1093-1098.
[83] C. Kuemin, L. Nowack, L. Bozano, N. D. Spencer, H. Wolf, "Oriented assembly of gold nanorods on the single-particle level", *Adv. Funct. Mater.* **22** (2012), no. 4, p. 702-708.
[84] Z. Liu, T. Chang, H. Huang, T. He, "Gold nanoparticle arrays assembled on the reconstructed surface of block copolymer thin films", *RSC Adv.* **3** (2013), no. 43, p. 20464-20470.
[85] K. Aissou, M. Mumtaz, A. Alvarez-Fernandez, J. Mercat, S. Antoine, G. Pécastaings, V. Ponsinet, C. Dobrzynski, G. Fleury, G. Hadziioannou, "Metallic nanodot patterns with unique symmetries templated from ABC triblock terpolymer networks", *Macromol. Rapid Commun.* **39** (2018), no. 7, article ID 1700754.
[86] A. Alvarez-Fernandez, K. Aissou, G. Pécastaings, G. Hadziioannou, G. Fleury, V. Ponsinet, "High refractive index in low metal content nanoplasmonic surfaces from self-assembled block copolymer thin films", *Nanoscale Adv.* **1** (2019), no. 2, p. 849-857.
[87] J. Chai, D. Wang, X. Fan, J. M. Buriak, "Assembly of aligned linear metallic patterns on silicon", *Nat. Nanotechnol.* **2** (2007), no. 8, p. 500.
[88] Q. Peng, Y.-C. Tseng, S. B. Darling, J. W. Elam, "Nanoscopic patterned materials with tunable dimensions via atomic layer deposition on block copolymers", *Adv. Mater.* **22** (2010), no. 45, p. 5129-5133.
[89] R. Ruiz, H. Kang, F. A. Detcheverry, E. Dobisz, D. S. Kercher, T. R. Albrecht, J. J. de Pablo, P. F. Nealey, "Density multiplication and improved lithography by directed block copolymer assembly", *Science* **321** (2008), no. 5891, p. 936-939.
[90] C. Cummins, T. Ghoshal, J. D. Holmes, M. A. Morris, "Strategies for inorganic incorporation using neat block copolymer thin films for etch mask function and nanotechnological application", *Adv. Mater.* **28** (2016), no. 27, p. 5586-5618.
[91] M. Haarmans, D. Bedeaux, "Optical properties of thin films up to second order in the thickness", *Thin Solid Films* **258** (1995), no. 1–2, p. 213-223.
[92] A. Alvarez-Fernandez, G. Fleury, V. Ponsinet, P. M. Walmsness, M. Kildemo, "Formation and optical response of self-assembled gold nanoparticle lattices on oxidized silicon synthesized using block copolymers", *J. Vac. Sci. Technol. B* **38** (2020), no. 1, article ID 013601.
[93] A. Arbabi, Y. Horie, M. Bagheri, A. Faraon, "Dielectric metasurfaces for complete control of phase and polarization with subwavelength spatial resolution and high transmission", *Nat. Nanotechnol.* **10** (2015), no. 11, p. 937.
[94] M. Kerker, D.-S. Wang, C. Giles, "Electromagnetic scattering by magnetic spheres", *JOSA* **73** (1983), no. 6, p. 765-767.
[95] C. Huygens, *Traité de la lumière*, Gauthier-Villars, 1920, 174 pages.
[96] M. Decker, I. Staude, M. Falkner, J. Dominguez, D. N. Neshev, I. Brener, T. Pertsch, Y. S. Kivshar, "High-efficiency dielectric Huygens' surfaces", *Adv. Opt. Mater.* **3** (2015), no. 6, p. 813-820.
[97] R. Dezert, P. Richetti, A. Baron, "Isotropic Huygens sources made of clusters of nanoparticles for metasurfaces applications", *J. Phys.: Conf. Ser.* **1092** (2018), article ID 012022.
[98] G. Kirchhoff, "Ueber das verhältniss zwischen dem emissionsvermögen und dem absorptionsvermögen der körper für wärme und licht", *Ann. Phys.* **185** (1860), no. 2, p. 275-301.
[99] A. Moreau, C. Ciracì, J. J. Mock, R. T. Hill, Q. Wang, B. J. Wiley, A. Chilkoti, D. R. Smith, "Controlled-reflectance surfaces with film-coupled colloidal nanoantennas", *Nature* **492** (2012), no. 7427, p. 86.
[100] P. T. Bowen, A. Baron, D. R. Smith, "Theory of patch-antenna metamaterial perfect absorbers", *Phys. Rev. A* **93** (2016), no. 6, article ID 063849.

[101] P. Bowen, A. Baron, D. Smith, "Effective-medium description of a metasurface composed of a periodic array of nanoantennas coupled to a metallic film", *Phys. Rev. A* **95** (2017), no. 3, article ID 033822.
[102] G. M. Akselrod, J. Huang, T. B. Hoang, P. T. Bowen, L. Su, D. R. Smith, M. H. Mikkelsen, "Large-area metasurface perfect absorbers from visible to near-infrared", *Adv. Mater.* **27** (2015), no. 48, p. 8028-8034.
[103] R. Dezert, P. Richetti, A. Baron, "Complete multipolar description of reflection and transmission across a metasurface for perfect absorption of light", *Opt. Exp.* **27** (2019), p. 26317-26330.
[104] Y. Ra'di, V. S. Asadchy, S. U. Kosulnikov, M. M. Omelyanovich, D. Morits, A. V. Osipov, C. R. Simovski, S. A. Tretyakov, "Full light absorption in single arrays of spherical nanoparticles", *ACS Photon.* **2** (2015), no. 5, p. 653-660.
[105] M. L. De Marco, S. Semlali, B. A. Korgel, P. Barois, G. L. Drisko, C. Aymonier, "Silicon-based dielectric metamaterials: focus on the current synthetic challenges", *Angew. Chem.* **57** (2018), p. 4478-4498.
[106] V. M. Agranovich, V. Ginzburg, *Crystal Optics with Spatial Dispersion, and Excitons*, Springer-Verlag, Berlin, Heidelberg GmbH, 1984.

Comptes Rendus
Physique
2020, 21, nº 4-5, p. 467-499
https://doi.org/10.5802/crphys.3

Metamaterials 1 / *Métamatériaux 1*

Topological wave insulators: a review

Isolants topologiques pour les ondes: un état de l'art

Farzad Zangeneh-Nejad [a], Andrea Alù [b] and Romain Fleury*, [a]

[a] Laboratory of Wave Engineering, School of Electrical Engineering, EPFL, Station 11, 1015 Lausanne, Switzerland

[b] Photonics Initiative, Advanced Science Research Center, City University of New York, New York, NY 10031, USA

E-mails: farzad.zangenehnejad@epfl.ch (F. Zangeneh-Nejad), aalu@gc.cuny.edu (A. Alu), romain.fleury@epfl.ch (R. Fleury)

Abstract. Originally discovered in condensed matter systems, topological insulators (TIs) have been ubiquitously extended to various fields of classical wave physics including photonics, phononics, acoustics, mechanics, and microwaves. In the bulk, like any other insulator, electronic TIs exhibit an excessively high resistance to the flow of mobile charges, prohibiting metallic conduction. On their surface, however, they support one-way conductive states with inherent protection against certain types of disorder and defects, defying the common physical wisdom of electronic transport in presence of impurities. When transposed to classical waves, TIs open a wealth of exciting engineering-oriented applications, such as robust routing, lasing, signal processing, switching, etc., with unprecedented robustness against various classes of defects. In this article, we first review the basic concept of topological order applied to classical waves, starting from the simple one-dimensional example of the Su–Schrieffer–Heeger (SSH) model. We then move on to two-dimensional wave TIs, discussing classical wave analogues of Chern, quantum Hall, spin-Hall, Valley-Hall, and Floquet TIs. Finally, we review the most recent developments in the field, including Weyl and nodal semimetals, higher-order topological insulators, and self-induced non-linear topological states.

Résumé. Découverte à l'origine en matière condensée, la notion d'isolant topologique (IT) a été étendue à divers domaines de la physique des ondes classiques, notamment la photonique, la phononique, l'acoustique, la mécanique et les micro-ondes. Dans leur volume, comme tout autre isolant, les IT électroniques présentent une résistance excessivement élevée à l'écoulement des charges, interdisant la conduction métallique. Sur leur surface, cependant, ils présentent des états conducteurs unidirectionnels avec une protection inhérente contre certains types de défauts, au-delà de ce que pouvait laisser présager la physique du transport électronique en présence d'impuretés. Transposés aux ondes classiques, les IT ouvrent une multitude d'applications passionnantes en ingénierie, comme le routage, les lasers, le traitement du signal, les commutations, etc. avec une robustesse sans précédent face à différentes classes de défauts. Dans cet article, nous passons d'abord en revue le concept de base des IT appliqué aux ondes classiques, à partir de l'exemple simple et monodimensionnel du modèle Su–Schrieffer–Heeger (SSH). Nous passons ensuite aux IT à ondes bidimensionnelles, en discutant des analogues pour les ondes classiques des IT de Chern, d'effet Hall quantique, de spin-Hall, de Valley-Hall, et de Floquet. Enfin, nous passons en revue les développements les plus récents dans le domaine, y compris les semi-métaux de Weyl et nodaux, les isolants topologiques d'ordre supérieur et les états topologiques non linéaires auto-induits.

* Corresponding author.

Keywords. Condensed matter, Photonics, Phononics, Acoustics, Mechanics, Microwaves.
Mots-clés. Matière condensée, Photonique, Phononique, Acoustique, Mécanique, Micro-ondes.

1. Introduction

Phases of matter are conventionally characterized using the so-called Landau's approach [1], classifying them in terms of the symmetries that break spontaneously at phase transitions. In the 1980's, however, the discovery of the so-called quantum Hall effect, the quantum mechanical version of the classical Hall effect, suggested a fresh view on how to distinguish insulating phases [2]. More specifically, this phenomenon, observed in a 2D electron gas subject to an out-of-plane magnetic field, indicated a completely different classification paradigm based on the abstract concept of topology [3], a branch of mathematics concerned with the study of quantities that are preserved under continuous transformations.

Over the past few years, the topological classification of phases of matter has been extensively developed in order to understand the pivotal differences in the physical properties of electronic insulators, allowing for the distinction between ordinary and topological insulators (TIs) [4–6]. In the bulk, like any other ordinary insulator, a TI exhibits an energy band gap separating the valance and conduction bands. However, contrary to normal insulators, TIs support conductive gapless states flowing along their edges. These edge states are characterized by a special non-local integer number, known as a topological invariant or Chern number [7], which guarantees their presence and cannot change unless the insulating phase undergoes a discontinuous transformation that closes the band gap.

The edge modes of topological insulators can exhibit various interesting properties, the most important ones being the robustness of their existence, as well as their resilience to disorder-induced backscattering. Indeed, in order to destroy the presence of the edge states, topology requires that the bandgap is first closed, implying a stringent modification of the bulk properties, impossible with localized edge imperfections or weak disorder. In addition, fermionic topological edge propagation is typically unidirectional or spin-locked, due to symmetry properties that are not broken by most impurity types. In electronics, these features have been established as a cornerstone for the realization of novel devices with a strong immunity against imperfections [8–11]. For instance, new types of spin-resolved electronic devices have recently been proposed that, by taking the advantage of the robustness of TIs, perfectly separate the "read" current path from the "write" one [12, 13]. This leads to not only a better output signal but also an improved reliability of spintronic systems.

Although discovered in quantum condensed matter systems, topological insulators are not intrinsically based on quantum phenomena and, as such, can be also obtained in classical systems. Indeed, the topological properties of insulators boil down to geometrical phase effects [14] that are, in principle, not related to the spatial scale or the physical nature of the system. In a pioneering paper [15], Haldane and Raghu proposed to extend the notion of Chern topological insulators to electromagnetic waves propagating in periodic media comprising magnetically biased ferrites. This sparked a search for classical applications of topological physics, in particular in wave phenomena of various kinds, from electromagnetics and photonics [16–68], to acoustics and phononics [69–100], as well as mechanics [101–122]. Classical wave systems can therefore benefit from a new kind of topologically inherited robustness to defects and disorder. In comparison with their fermionic counterparts, classical topological systems offer a larger control over

their space and time properties, representing a particularly relevant platform to design, fabricate and detect all kinds of topological effects that may not be straightforwardly observed in condensed matter systems.

In this paper, we provide a comprehensive overview of recent advances of wave-based classical topological insulators, with an emphasis on the multidisciplinary aspect of this research field, and the important underlying physical concepts. The review is organized as follows: we first discuss the basic consequences of topological order when applied to classical waves, starting from the one-dimensional scenario, which includes the realization of the so-called Su–Schrieffer–Heeger (SSH) model in various wave physical platforms. We then move to two-dimensions, reviewing wave analogues of the quantum Hall and quantum spin Hall phases, as well as other related ideas such as valley-selective waveguiding, and Floquet topological insulators. We next move on to more recent developments of the field including higher-order topological insulators, three-dimensional topological phases in semi-metals, and nonlinear self-induced topological insulators. Finally, the last section reviews some of the most important technology-oriented applications that are actively being pursued for wave-based topological insulators, providing a clear overview of the future directions in this field.

2. Ordinary topological phases

2.1. *One-dimensional wave topological insulators*

One of the simplest forms of topological insulating phase is found in a periodic one-dimensional discrete chain, known as the Su–Schrieffer–Heeger (SSH) chain [123–135], consisting of identical evanescently coupled resonators with alternating coupling coefficients. The unit cell of the SSH tight-binding chain includes two resonators with identical resonance frequency coupled to each other with an intra-cell coupling coefficient K, whereas an extra-cell coupling coefficient J couples adjacent unit cells. When $K = J$, the two dispersion bands of this one-dimensional crystal touch each other at the edge of the Brillouin zone, as a result of band folding. For $K \neq J$, on the other hand, the band structure is gapped, leading to an insulating phase. Depending on whether $K > J$ or $K < J$, this insulating phase can be of trivial or topological nature. In particular, it has been shown that when the value of the extra-cell coupling coefficient is larger than the intra-cell one (i.e. $K < J$), the corresponding insulating phase is of topological nature, supporting mid-gap edge modes at the interface with any trivial insulator. On the contrary, $K > J$ leads to a trivial insulating phase without any edge mode [123]. While both cases ($K > J$ or $K < J$) look similar when only considering the band structure, i.e. the eigenvalues of the tight-bighting Hamiltonian, the topological difference resides in the associated eigenmodes, which shows a band inversion as one goes from the center to the edge of the Brillouin zone. In this one-dimensional case, the topology is defined from the mapping between the Brillouin circle to the space of 2×2 Hermitian Hamiltonian with chiral symmetry (also known as the equator of the Bloch sphere), and is characterized by a winding number [123]. Importantly, this topological invariant is only well defined for chiral symmetric systems, meaning that all of the resonators should have the same resonance frequency. As a consequence, edge modes are robust to any disorder that preserves this symmetry and is not strong enough to close the band gap, which happens at the onset of Anderson localization. Note also that there exist different types of topological phases in one-dimension, which are all symmetry protected, and summarized in the Altland-Zirnbauer classification table for topological phases [136].

Considering the simplicity of the SSH model, this topological system has been implemented in a large variety of classical wave platforms. For instance, in [137] Parto, *et al.*, realized the optical version of the SSH structure making use of 16 identical coupled micro ring resonators

fabricated on InGaAsP quantum wells (Figure 1a). By changing the successive distances between the adjacent rings, the strengths of intra-cell and extra-cell coupling coefficients were engineered such that they give rise to a non-trivial topological phase. The inset of Figure 1b illustrates the profile of the corresponding topological mid-gap state, which is pinned to the edge of the array, and exploited for lasing.

The SSH model has also been implemented in acoustics. In [138], Xiao, *et al.* demonstrated the model in a one-dimensional sonic crystal consisting of cylindrical pipes with alternating cross-sectional areas, thereby mimicking the SSH scheme. Figure 1c shows a photograph of the fabricated SSH structure, which consists of two one-dimensional arrays with different topological properties (different winding numbers), connected to each other to form a mid-gap edge state at the phase transition interface. The inset of Figure 1d shows the profile of the edge mode.

The strong localization of the edge mode of the SSH array has been of particular interest for applications such as lasing [137,139], and sensing [140]. Yet, these kinds of edge modes cannot be used for waveguiding, as they are confined in zero dimensions. In the next part of this section, we move to two dimensions and describe 2D topological insulators whose edge modes are confined in one dimension and can therefore be leveraged for waveguiding and energy transport.

2.2. *Chern wave insulators*

The integer quantum Hall effect (IQHE) provides the first example of a two-dimensional (2D) electronic topological insulator, in which the electrons flow unidirectionally along the edge of a 2D system subject to an out-of-plane external magnetic field [141]. Under these conditions, the Hall conductance takes the quantized values $\sigma_{\mathrm{H}} = Ce^2/h$, in which h is the Plank constant, e is the electron charge, and C is an integer, corresponding to the topological invariant of the system. This quantity, also known as Chern number, is defined as a surface integral over the entire Brillouin zone (BZ), which is a torus in the three dimensional momentum space. The integral is expressed as

$$C = \frac{1}{2\pi} \oint_{\mathrm{BZ}} A(k)\, \mathrm{d}k. \tag{1}$$

The parameter $A(k)$ in (1) is the so-called Berry curvature defined as $A(k) = \nabla_k \times [\langle \psi_n(k) | i\partial_k | \psi_n(k) \rangle]$, in which $\psi_n(k)$ represents the corresponding Bloch state on the nth band, k is the Bloch wave number, and ∂_k and $\nabla_k \times$ are the derivative and curl operators with respect to k, respectively. Since $A(k)$ is an odd function for time-reversal symmetric systems, the Chern number C is zero in the absence of an external magnetic field. Applying a bias odd under time reversal is therefore essential to achieve a non-zero Chern number. Insulating phases with non-trivial topological order exhibit intriguing unidirectional charge transport along their edges. Note that in two dimensions the topology is defined by mapping the Brillouin torus to the entire Bloch sphere. In this picture, a twisted topology corresponds to an obstruction to define the Bloch wave functions over the entire Brillouin zone using a single phase convention [123].

Motivated by the developments of quantum Hall phases in electronic and quantum systems, the classical analogues of such phases were realized shortly thereafter. As mentioned earlier, Chern insulating phases are associated with a broken time reversal symmetry, which can be achieved in the context of microwave engineering using ferromagnetic materials. In [142], Wang *et al.* realized the electromagnetic version of quantum Hall phases based on gyromagnetic microwave materials. This achievement was obtained in a two-dimensional square lattice of ferrite rods, implemented inside a microwave waveguide and biased with an external uniform magnetic field (see Figure 1e). The one-way character of the topological edge mode was studied and demonstrated both in numerical simulations and experiments, as illustrated in Figure 1f.

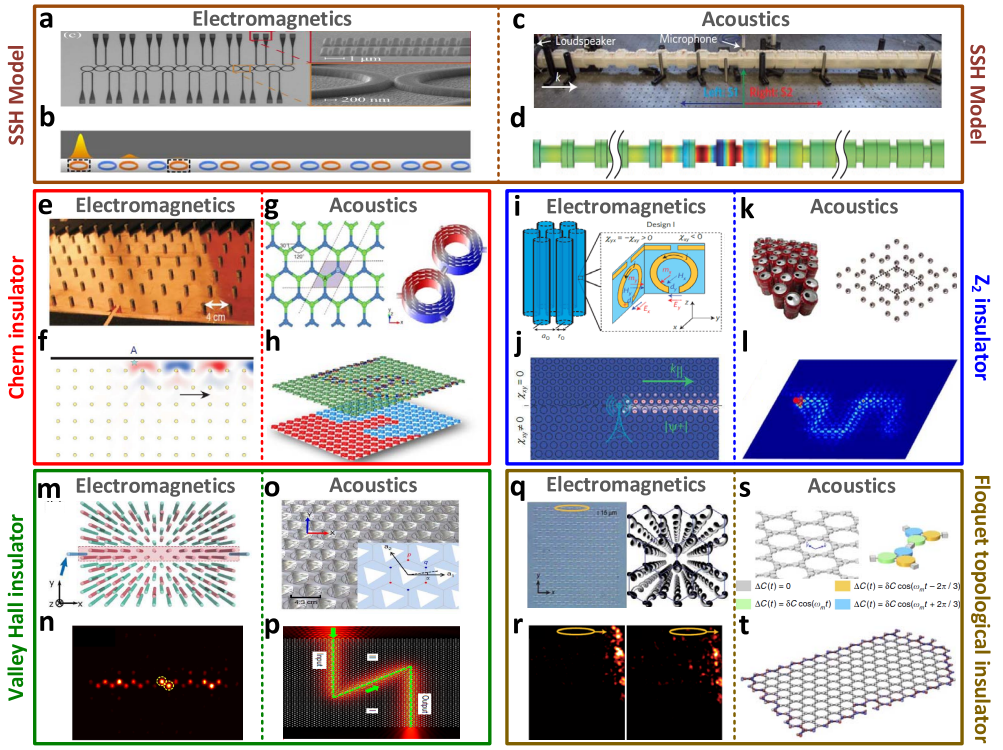

Figure 1. Topological wave insulators. a, b, Realization of a one-dimensional electromagnetic topological insulator (based on the SSH scheme) in an array of coupled micro ring resonators fabricated on InGaAsP quantum wells. c, d, Realization of the SSH model in acoustics based on cylindrical waveguides with alternating cross-sectional areas, tuning the strengths of the coupling coefficients. e, f, Two-dimensional Chern wave insulators were firstly realized in electromagnetics based on a square lattice of magnetically-biased gyromagnetic ferrite rods, implemented inside a microwave waveguide. g, h, Realization of a Chern insulator in acoustics by constructing a hexagonal lattice of sonic ring cavities filled with rotationally biased moving fluids. i, j, Photonic realization of $\mathbb{Z}_2$ wave insulating phases based on a metamaterial with strong bi-anisotropic behavior, providing TE and TM polarized modes with opposite spin-orbit forces. k, l, A strategy to achieve acoustic versions of $\mathbb{Z}_2$ insulators is to expand the primitive unit-cell of a hexagonal lattice to a larger one, and use the corresponding folded degenerate Bloch states as pseudo-spins. m, n, Photonic realization of Valley Hall insulators based on a zigzag edge domain wall of two crystals with opposite on-site potential organizations. o, p, Realization of Valley Hall insulators in a sonic crystal consisting of triangular polymethyl methacrylate rods positioned in a triangular-lattice with opposite rotation angles. q, r, Photonic analogue of Floquet topological insulator, based on a graphene-like lattice of helical waveguides evanescently coupled to each other. The helicity of the waveguides breaks z-reversal symmetry. s, t, Realization of Floquet topological insulator based on a hexagonal lattice of acoustic trimers, with capacitances modulated in time in a rotating fashion.

Just a few years after this work, researchers extended such extraordinary phases to another field of classical wave physics, namely acoustics. This extension, however, required a different

trick [143]. In particular, since sound waves do not interact efficiently with magnetic fields, a different strategy was employed to break time-reversal symmetry, namely the use of fluid motion [144]. In 2015, two independent works proposed the use of rotating fluids to realize acoustic analogues of quantum Hall phases [145,146]. Fleury *et al.* proposed an acoustic analogue of magnetically-biased graphene (Figure 1g), based on a honeycomb network of ring cavities filled with rotationally moving fluids [145]. Yang, *et al.* [146] suggested a different approach employing a triangular array of rotating cylinders in a viscous fluid. The corresponding edge modes of such topological phases provide the unique opportunity of reflection-less routing of sound along irregularly shaped pathways, as seen in Figure 1h. Such backscattering-immune classical wave transport has been confirmed in a series of related proposals [147, 148], as well as experimental investigations [149, 150].

2.3. $\mathbb{Z}_2$ *wave insulators*

While Chern insulators require breaking of time-reversal symmetry, there exists another type of topological insulators in two-dimensions that, on the contrary, *preserve* time-reversal symmetry. In electronic condensed matter systems, these insulators are referred to as $\mathbb{Z}_2$ topological insulators, and typically emerge in the presence of spin-orbit coupling, as in the quantum spin-Hall effect [151, 152]. Such phases can be pictured as systems in which two time-reversed copies of a quantum Hall phase with opposite Chern numbers coexist without coupling. One of the copies corresponds to electrons with positive spins, and its time-reversed version to electrons with negative spins. As a consequence, two topological edge modes exist that propagate in opposite directions, carrying electrons with different spins. In presence of time-reversal symmetry, Kramers theorem prevents any interaction between the two spin species, which cannot backscatter at non-magnetic defects. Since they do not require time-reversal symmetry breaking, $\mathbb{Z}_2$ topological insulators may appear easier to realize than the Chern class in electronic systems. Yet, realization of these phases in classical systems is not quite straightforward for two principal reasons. First, photons (and also phonons), associated with electromagnetic (or sound) waves, are spin-less particles. Second, they are bosons, for which the time-reversal operator $\mathcal{T}_b$ squares to +1, and not to −1, as for electrons, which are fermions ($\mathcal{T}_f^2 = -1$). Interestingly, the relation $\mathcal{T}_f^2 = -1$ is essential for Kramers theorem to hold, guaranteeing truly independent spin subspaces. In order to solve these issues, one must construct a pseudo-spin degree of freedom and "augment" bosonic time-reversal with another symmetry operation $\mathscr{C}$ such that $(\mathscr{C}\mathcal{T}_b)^2 = -1$, enforcing Kramers degeneracy when both $\mathscr{C}$ and $\mathcal{T}_b$ are preserved [153–186]. Note that this procedure potentially makes the classical version of a $\mathbb{Z}_2$ topological phase less robust than its electronic counterpart, since not only $\mathcal{T}_b$ breaking defects induces backscattering for the topological edge modes, but also defects that break $\mathscr{C}$.

For electromagnetic waves, described by Maxwell equations, spin can be emulated by leveraging electromagnetic duality as an additional symmetry $\mathscr{C}$, by enforcing $\varepsilon = \mu$. This assumption indeed restores the duality of Maxwell's equations, creating two degenerate, time-reversed (pseudo)spins. By properly introducing some bi-anisotropy (coupling the TE and TM components of the field), the two spins of such a system can undergo opposite interaction terms emulating spin-orbit coupling. This leads to the realization of an electromagnetic analogue of the quantum spin Hall effect, based on the combination of duality and time-reversal symmetry. Employing this scheme, in [187] Khanikaev *et al.* proposed the photonic analogue of the quantum spin Hall effect in a hexagonal lattice of a spin-degenerate dual metamaterial, composed of split ring resonators with strong bianisotropic behavior (Figure 1i). The inset of Figure 1j represents the profile of one (spin up) of the corresponding edge modes. Defects in the form of sharp turns that do not couple the two polarizations do not break duality nor time-reversal symmetry, hence they do not

reflect the spin-locked topological edge modes that can seamlessly be routed along an irregularly shaped topological interface. Note that the duality condition $\varepsilon = \mu$ is hard to achieve as dispersive effects might make it difficult to guarantee this condition over a broad frequency range. Nevertheless, it can be enforced with very good approximation over a couple of crystal bands, which is more than sufficient for observing exceptionally robust edge wave transport along bent paths. A similar idea has been implemented for Lamb waves over a structured plate based on accidental degeneracy between two Lamb modes with distinct polarizations [188]. Finally, the extension of these concepts to continuous electromagnetic media satisfying a generalized form of symmetry, $\mathscr{PTD}$ symmetry, has been successfully conducted by a series of paper by Silveirinha [189, 190]. These photonic systems have similar properties as those based on duality.

In fluid acoustics, the explained strategy to achieve quantum spin Hall phases is not readily functional due to the absence of a polarization degree of freedom. An alternative strategy to emulate acoustic pseudospin is to exploit the symmetry of a crystal lattice, in which case $\mathscr{C}$ is some sort of crystalline symmetry operation. Such a scheme, based on six-fold rotational symmetry, was initially proposed by Wu and Hu in 2015 in a triangular lattice of hexagonal resonators [191], and implemented in a variety of platforms including microwaves [192], photonics [193–197], elastic [198–201] and acoustics [202–205]. Figure 1k and 1l show an example [205] that employed this strategy to induce a deeply subwavelength acoustic topological edge mode in a subwavelength sonic crystal made of Helmholtz resonators (simple soda cans) arranged in a modified hexagonal-like lattice. The unit cell of the crystal is shown in the inset of Figure 1k. Figure 1l illustrates how the edge mode of such a crystal propagates with good transmission along a path involving sharp turns. Note that all symmetry-based strategies for emulating pseudo-spins only allow for an approximate realization of Kramers degeneracy, which only holds at the high-symmetry points of the Brillouin zone (Γ point in the case of six-fold rotational symmetry). Thus, the quantum spin-Hall Hamiltonian can only be emulated "locally" around this degenerate point, as may be proven by performing a first order $k \cdot p$ approximation of the Hamiltonian around the point [191]. However, pushing the $k \cdot p$ analysis beyond first order reveals that Kramers degeneracy is quickly broken away from the high symmetry point, on the same band. Direct use of topological quantum chemistry concepts [206] has confirmed the impossibility of rigorously defining a global $\mathbb{Z}_2$ topological invariant on the entire band structure of these systems. Rigorous quantitative statistical analysis of the edge mode robustness against different kinds of defects [207] is also consistent with an incomplete, or approximate, level of topological protection. Nevertheless, designs based on exploiting crystalline symmetries work very well in practice, and they allow easy and direct exploitation of topological ideas based on lattice symmetries regardless of the physical platform, still leading to relatively large robustness to backscattering.

2.4. *Valley Hall wave insulators*

In a hexagonal lattice in which the Dirac degeneracy has been lifted by breaking inversion symmetry, modes belonging to the K and K' valleys, which are obviously time-reversed images of each other, also carry some form of chirality or pseudospin [208–245]. Locally, these time reversed pairs, which correspond to valleys created by opening time-reversed Dirac cones, carry an opposite Berry flux. Since inversion also changes the K valley into the K' one, one can construct two crystals, inversion images of each other, with valleys having opposite Berry fluxes oriented along a given direction. Then, interfacing these two crystals along this direction amounts to requiring an abrupt sign change of the Berry flux, which requires the band gap to close at the interface, supporting the necessary presence of an edge mode. Similar to the schemes based on six-fold rotational symmetries, it is not possible to define a global topological invariant over the full Brillouin zone, and this type of edge modes is not globally topological. However, it

remains exceptionally robust to Valley-preserving defects, like Z shaped turns. In [246], Noh, *et al.* leveraged the valley degree of freedom to realize photonic analogues of the Valley Hall effect in a two-dimensional honeycomb lattice of optical waveguides, shown in Figure 1m. The red and green waveguides in the figure possess different refractive indices, corresponding to two different on-site potentials that allow inversion symmetry breaking. The valley edge modes were obtained along a zigzag edge domain between two crystals with opposite on-site potential configurations (referred to as AB and BA). Under this condition, the edge modes cross the band gaps formed at the proximity of high-symmetric corners of the Brillouin zone. The inset of Figure 1n illustrates the profile of one of the corresponding edge modes.

Interestingly, the valley Hall waveguiding scheme also works in other types of lattices, when some form of operation that flips the sign of the Berry curvature is used. For instance, topological valley Hall phases were realized in acoustic systems based on symmetry-breaking rotations of the crystal constituents. In [247], Lu *et al.* built a sonic valley Hall waveguide with a sonic crystal consisting of triangular polymethyl methacrylate rods (Figure 1o) positioned in a triangular lattice with a rotation angle α with respect to the vector $\boldsymbol{a_1}$. When $\alpha = n\pi/3$, the crystal supports two-folded Dirac cones at the edge of the Brillouin zone. These degeneracies are lifted for other rotation angles, opening a frequency band gap. By connecting two different domain walls with opposite rotation angles of $\alpha = 10^\circ$ and $\alpha = -10^\circ$ corresponding to opposite Berry fluxes, a pair of valley chiral edge states, counterpropagating at the interface, can be realized. Such edge modes can be utilized for guiding of sound along an irregularly shaped zigzag path (Figure 1p). This method is transposable to other wave platforms, including highly dispersive ones, such as gravity-capillary waves at the surface of liquids [248].

2.5. *Floquet topological insulators*

Another conceptually distinct route to achieve electronic topological phases without the need for an external magnetic field is to apply a time-periodic modulation in the electron potential energy or hopping rate [249–251]. In the field of semiconductor physics, it was firstly shown [252] that, by irradiating a trivial semiconductor quantum Well with a time periodic microwave wave, a new kind of topological phase transition can be achieved. Such topological phases, dubbed as Floquet topological insulators, support helical edge modes in their quasi-energy spectral gaps.

Parallel to the developments of Floquet topological insulators in condensed matter systems, these concepts were extended to classical systems [253–267]. In [268], Rechtsman, *et al.*, demonstrated the photonic analogue of a Floquet topological insulator, based on a graphene-like lattice of helical waveguides evanescently coupled to each other, as seen in Figure 1q. The dynamics of beam diffraction through such a lattice is described by the Schrödinger equation, where the distance of propagation takes the role of time. The helicity of the waveguides breaks z-reversal symmetry, effectively emulating time-Floquet modulation, in which the coordinate space z takes the role of time. Within the framework of this mapping, the quasi-band structure of the crystal becomes identical to the one of a Floquet topological insulator, supporting one-way edge states that are protected from scattering at the lattice corners. Shown in Figure 1r is the profile of such edge modes when a beam excites the array from its top edge.

Time-Floquet topological insulators have also been proposed in acoustics. In [269], Fleury *et al.* demonstrated a time-Floquet topological insulator based on a hexagonal lattice of acoustic trimers, whose acoustic properties were periodically modulated in time in a rotating fashion, with uniform handedness throughout the lattice (Figure 1s). Figure 1t shows the profile of one of the corresponding edge states, flowing across the boundary of a finite piece of such a crystal. Compared to acoustic quantum Hall phases discussed in Figure 1g and h, such kinds of topological states are potentially more practical as they do not rely on moving background fluids.

It is also worth mentioning at this point that a one-to-one correspondence between time-Floquet systems and unitary scattering networks can be made, where the unitary network scattering matrix takes the role of the Floquet time-evolution operator over a period [270, 271]. This has allowed an easier experimental exploration of different Floquet topological phases (Chern or anomalous [272]), in both photonics and acoustics [273–275].

3. Topological semimetals

In 2D periodic systems, the topological phases usually stem from point degeneracies in the band structure, which are known as Dirac cones. By properly tuning the system parameters, the degenerate points can be lifted, and bandgaps can be opened, leading to different topologies. In three dimensions, possible band degeneracies are line nodes [276–282], Weyl points [283–303], or 3D Dirac points [304–311]. Weyl points are particularly interesting as they behave as sources of Berry flux, carrying a Chern number of ± 1, which manifests itself as topological surface states along any surface interface enclosing a non-vanishing number of Weyl charges [16].

Following the discovery of Weyl and nodal semimetals in the field of semiconductor physics [284], Lu *et al.* theoretically realized both line nodes and Weyl points in a gyroid photonic crystal made from germanium high-index glasses [312]. Shown in Figure 2a is the real space unit cell of the 3D periodic structure. By applying proper symmetry-breaking perturbations to the unit-cell of such structure, a nodal line degeneracy was realized. This is accomplished by replacing part of the gyroids with air spheres, as seen in the inset of Figure 2a. Figure 2b represents the 3D band structure of the crystal cut at (101) plane. A closed line degeneracy around the Γ point is observed in the band structure of the crystal. Note that the area enclosed by this line degeneracy can be controlled by the strength of the applied perturbation, that is, the radius of the air-sphere.

The unit cell of the crystal in Figure 2a respects parity-time (PT) symmetry. A possible approach to achieve Weyl point degeneracies is to break the PT symmetry of the unit cell. In fact, it is known that a line node degeneracy creates either a frequency band gap or a set of paired Weyl points upon breaking PT symmetry. The PT symmetry of the double gyroid crystal can be broken by, for example, removing one of the air spheres of the two gyroids. By doing so, the line node degeneracy splits into four Weyl degenerate points along ΓN and ΓH directions, as observed in the band structure of Figure 2c.

Weyl and nodal semimetals have also been realized in acoustic systems. In [313], Xiao, *et al.* theoretically discussed the possibility to achieve Weyl and nodal semimetals in a lattice made of coupled sonic resonators and waveguides, described by a tight-binding model involving chiral interlayer couplings. A few years later, phononic Weyl phases were experimentally demonstrated [314] in a chiral phononic crystal, fabricated using layer-stacking technique. The insets of Figure 1d represent the corresponding 3D structure, consisting of stacked layers of air-filled hollow waveguides, connected to each other via spiral hollow channels. Such a structure supports two pairs of Weyl points at $k_z = 0$ and $k_z = \pi/a$. Shown in Figure 2d is the measured band structure of the crystal for $k_z = 0$, from which the existence of Weyl points at the high-symmetry point K is apparent. The inset of Figure 2e shows the Fermi arcs of the corresponding surface states.

Despite the fact that topological semi-metallic phases have successfully been demonstrated in photonic and phononic systems, the realization of such phases is often challenging due to their 3D structure. Based on the notion of synthetic dimension, in [315] Lin, *et al.* explored Weyl physics in a planar 2D geometry, consisting of on-chip ring resonators with dynamic modulation of the refractive index, as sketched in Figure 2g. Each resonator supports a set of discrete modes, whose resonance frequencies are equally spaced. These discrete resonance modes can therefore be pictured as a periodic lattice in the synthetic frequency dimension. Together with the real dimensionality of the crystal, this third, synthetic frequency dimension

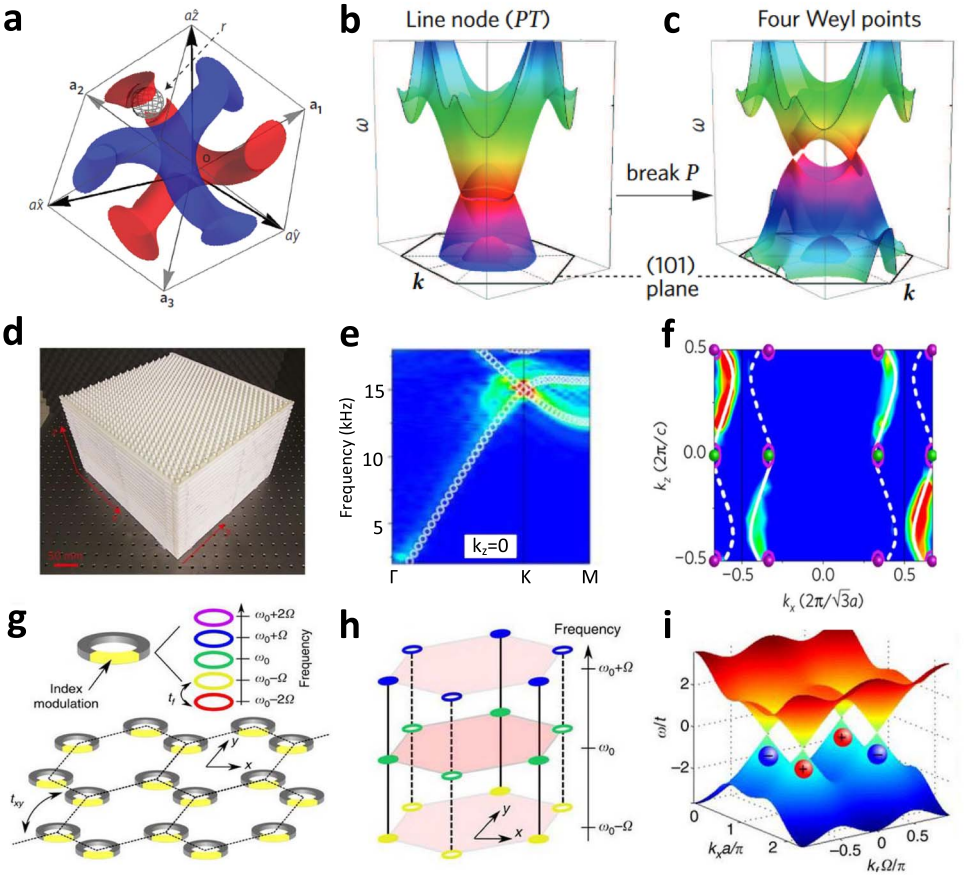

Figure 2. Classical wave Weyl semimetals. a, Realization of electromagnetic analogues of topological semimetals based on a crystal with the real-space unit cell shown in the panel, consisting of two inversion-symmetric gyroids made of germanium high-index glasses. b, Band structure of the corresponding nodal semi metallic phase. c, By breaking the spatial inversion symmetry of the unit cell, the line node degeneracy splits into four distinct Weyl points. d, Realization of acoustic topological semimetals in a chiral phononic crystal fabricated using a layer-stacking strategy. The structure consists of stacked layers of air-filled hollow waveguides, connected to each other via spiral hollow channels. e, Band structure of the crystal shown in panel f, exhibiting Weyl degeneracy at K point. f, Fermi arc surface of the corresponding topological states. g, Exploring Weyl physics in a planar 2D geometry, consisting of on-chip ring resonators with dynamic modulation of refractive indices. h, The discrete resonance modes can be pictured as a periodic lattice in the synthetic frequency dimension. i, Band structure of the crystal in the 3D synthetic dimension, exhibiting four Weyl points.

forms a three-dimensional space (Figure 2h). By modulating the refractive indices of the ring resonators properly, one can then appropriately couple these modes to each other so as to achieve Weyl point degeneracies in the 3D synthetic space formed by the two spatial dimensions and the frequency axis. The inset of Figure 2i shows the corresponding Weyl points and their charges.

4. Higher-order topological insulators

All the topological phases discussed thus far obey the so-called bulk boundary correspondence principle [316, 317] in codimension 1, stating that a d-dimensional topological insulator with Chern number C, hosts a number C of $d-1$ dimensional boundary states, when interfaced with a trivial insulator. Recently, a new class of topological phases has been proposed, which obeys another form of bulk-boundary correspondence. These topological phases of matter, called higher-order topological insulators, exhibit gapped boundaries that are themselves topological phases in a lower dimension. A d-dimensional higher order topological insulator (of order n) supports $d-n$ dimensional gapless boundary states. For instance, a two-dimensional second order topological insulator supports zero dimensional (0D) topological corner states that, as their name suggests, are localized not only at the edges, but also at the "edges of edges", i.e., at the corners of the insulator [318–325].

In [326], Benalcazar, *et al.* theoretically introduced the concept of higher-order topological insulators, based on a C_4 symmetric square lattice crystal with detuned hopping terms and two non-commuting reflection symmetries, leading to an insulating phase with quantized Wannier centers and a quadrupole bulk polarization. Both ordinary 1D edge states and higher-order 0D corner states were simultaneously realized in this lattice. Following this theoretical proposal, higher-order topological states were experimentally observed in various fields. For instance, in electronics a topological circuit was introduced in [327], realizing 0D corner modes. The circuit, shown in Figure 3a, consists of LC tanks coupled to each other via coupling capacitances. The connectivity of the circuit elements guarantees the required C_4 rotational symmetry of the Hamiltonian, as well as the two non-commuting reflection symmetries with respect to x and y directions. Hence, the circuit can indeed be pictured as a second-order topological phase supporting gap-less corner states. The corner mode of the circuit shows itself as a topological boundary resonance in the corner impedance profile of the circuit, as seen in Figure 3c.

At microwaves, higher-order topological insulators have been implemented [328] in a square lattice with unit cell composed of four identical resonators, implemented using H-shaped microstrip transmission lines (Figure 3d). Adjacent cells were connected to each other via transmission lines with proper lengths. Figure 3e shows the measured spectrum of the absorption coefficient, exhibiting in-gap resonances corresponding to the corner state. The inset of Figure 3f shows the spatial distribution of absorptance, summed over the shaded bands. It is observed that the corner states are indeed localized at the four corners of the crystal.

Higher-order topological insulators have also been transferred to the realm of acoustics. In [329, 330], Xue *et al.*, and Ni *et al.*, independently demonstrated a second-order topological insulator in an acoustic metamaterial, based on a breathing Kagome lattice with non-trivial bulk polarization. The corresponding Kagome lattice is shown in Figure 3g, consisting of coupled acoustic air-filled cylindrical resonators with metal walls. When the extra-cell couplings become higher than the intra-cell ones, the lattice crystal under study becomes topological (of second-order character). Figure 3h represents the spectrum of normalized density of states obtained from the measurements of acoustic energy stored in the bulk (yellow), at the edges (red) and corners (blue) of the crystal. Figure 3i shows the profile of the corresponding corner state integrated over the corresponding frequency region. Such 0D states hold great promise for controlling and trapping waves at specific points in a robust fashion, which is relevant in a variety of applications such as energy harvesting, lasing, sensing, and enhanced wave-matter interactions.

In the context of mechanical topological insulators, the in-gap corner states have also been realized and experimentally observed on a structured elastic plate [331]. The realization is based on a perturbative mechanical metamaterial shown in Figure 3j, consisting of coupled plates of single-crystal silicon. The thin beams between the nearest neighboring plates controls the sign

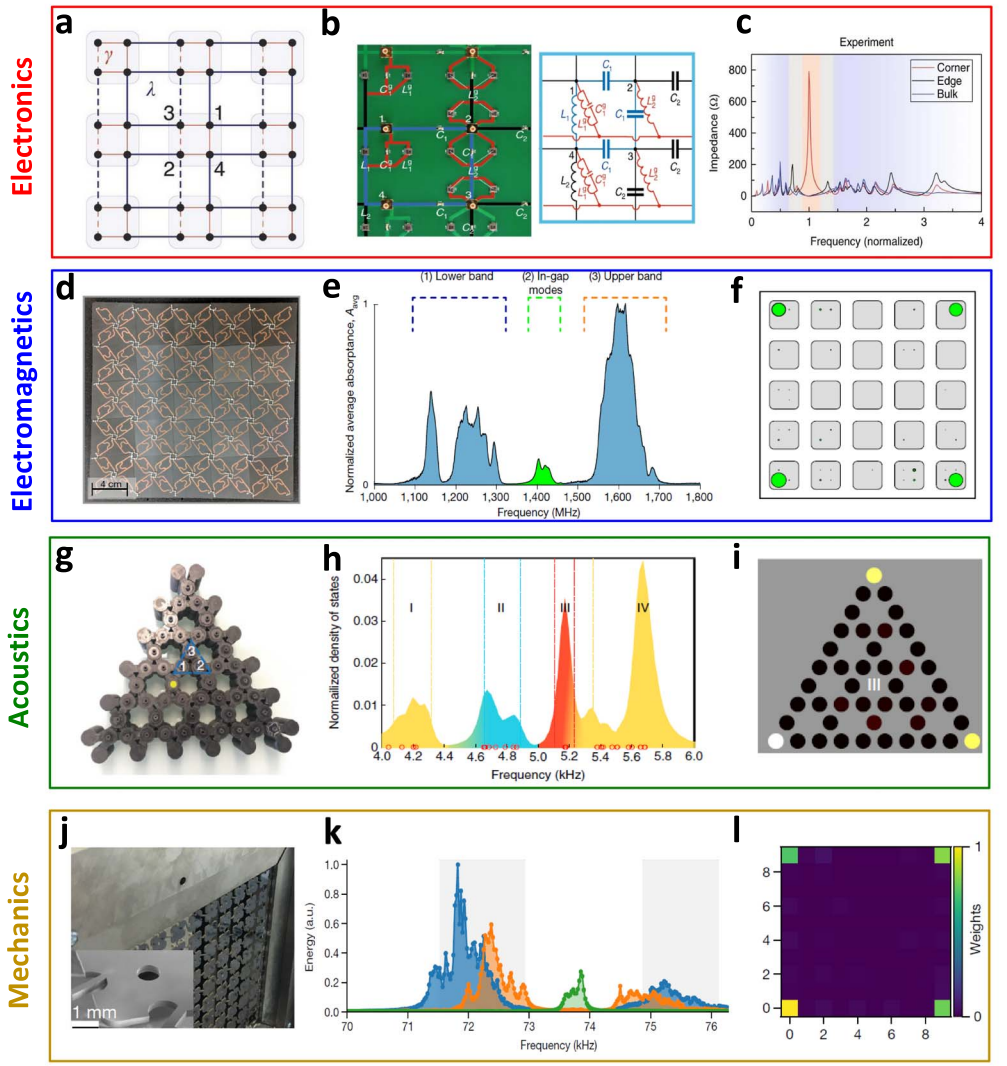

Figure 3. Higher-order classical topological insulators. a, Tight binding lattice realizing topological corner modes. b, A circuit design realizing corner modes circuit, consisting of *LC* tanks coupled to each other via some coupling capacitances. c, Corner impedance profile of the circuit, exhibiting a dominant resonance peak associated with the topological corner mode. d, Realization of higher order topological states in microwaves, based on a square crystal of four identical resonators implemented using H-shaped micro strip transmission lines. e, The measured spectrum of the absorption coefficient, exhibiting in-gap resonances corresponding to the corner state. f, Spatial distribution of absorptance, summed over the shaded bands. g, Acoustic higher order topological insulators based on a Kagome lattice with a non-trivial bulk polarization. The structure consists of coupled acoustic air-filled cylindrical resonators with metal walls. h, Spectrum of normalized density of states obtained from measuring acoustic power at the bulk (yellow), edge (red) and corner (blue) of the crystal. i, Profile of the corresponding corner state. j, Realization of an elastic second order mechanical topological insulator based on a perturbative mechanical metamaterials consisting coupled plates of single-crystal silicon. k, Spectrum of the bulk (blue), edge (orange) and corner (green) modes. l, Profile of the corner mode of the structure at its resonance frequency.

and amplitude of the corresponding coupling coefficients. Figure 3k shows the spectrum of bulk (blue), edge (orange), and corner (green) states, when the structure is excited with an ultrasound air-transducer. Figure 3l depicts the profile of corner states, demonstrating their confinement to the corners of the crystal. Other realizations of higher-order TIs have been reported in [332–346].

5. Nonlinear topological insulators

All topological phases discussed thus far are based on linear structures. The presumption of linearity, albeit crucial to define a band structure, can however imply stringent geometrical conditions. For instance, in order to realize spin Hall phases in the acoustic lattice crystal discussed in Figure 1g and h, the extra cell coupling between resonators are necessarily required to be larger than the intra-cell ones. Amplitude-dependent nonlinear phenomena [347–352], however, can be utilized to achieve the same kind of topological phases without this special condition. In [353], Hadad *et al.* investigated a one-dimensional nonlinear topological system based on a SSH toy model with nonlinear staggered potentials (Figure 4a). Each unit cell of the SSH array consisted of two atoms with the same on-site potentials. These atoms were connected to each other via linear intra-cell coupling κ_0. The nearest-neighboring cells were connected to each other with amplitude-dependent nonlinear extra-cell coupling coefficients of the form $\vartheta_n = \vartheta_0 + \alpha(|a_n^{(1)}|^2 + |a_n^{(2)}|^2)$, in which $\vartheta_0 < \kappa_0$ is a constant, and α is a Kerr coefficient. Under these assumptions, and assuming weak nonlinearity, the dynamics of the system can be expressed with a tight-binding Hamiltonian of the form $H = \cos(k_B a)[\kappa_0 - (\vartheta_0 + \alpha I(|a_0^{(1)}|^2 + |a_0^{(2)}|^2))]\sigma_x + \sin(k_B a)[(\vartheta_0 + \alpha I(|a_0^{(1)}|^2 + |a_0^{(2)}|^2))]\sigma_y$, in which σ_x are σ_y are Pauli matrices. Note that, in contrast to the linear case, the Hamiltonian H depends on the eigenstates of the system. Hence, in principle, its eigenvalues should be calculated in an iterative manner. Since $\vartheta_0 < \kappa_0$, the Hamiltonian H corresponds to a trivial insulator at low excitation intensities ($I \to 0$), exhibiting a frequency band gap that is topologically trivial. The enhancement of the field amplitude, however, effectively increases the extracell couplings. At some threshold intensity I_{th}, the strengths of ϑ_n and κ_0 become equal, which closes the band gap and results in a topological phases transition. By increasing the excitation intensity further, the strength of extra-cell couplings becomes larger than that of the intra-cell ones, opening a band gap in the band structure of the crystal with a nontrivial topological order (Figure 4b). Interestingly, these predictions based on assumptions of periodicity for the infinite non-linear lattice correctly predict the behavior of edge modes when the non-linear system is truncated to a finite size. Figure 4c shows the evolution of the mode profile of the mid-gap state versus intensity, illustrating the transition from bulk to exponentially decaying edge modes. Note that, as opposed to their linear counterparts, these nonlinear topological edge states decay to a plateau of non-zero amplitude, highlighting the local nature of the associated band gaps [353]. Essentially, as the intensity of the mode decays away from the edge, locally the gap becomes narrower, and asymptotically tends to close, yielding the plateau profile that extends into the lattice.

Such kinds of topological phases with nonlinear staggered potentials have been implemented in a circuit [354], composed of *LC* tanks connected to each other with linear capacitances (intra-cell dynamics) and nonlinear varactor diodes (extra-cell dynamics), as seen in Figure 4d. Shown in Figure 4e is the spectrum of the input admittance of the circuit at high power intensity, corresponding to a non-trivial topological phase. As observed, the spectrum exhibits a dominant resonance peak, which corresponds to the self-induced topological corner state. Figure 4f exhibits the voltage distribution of the circuit at the resonance frequency of the corner mode.

Not only does the nonlinear phenomenon allow one to achieve self-induced topological phases, but it also establishes an ideal platform for dynamically tuning the spectral and localization characteristics of the edge modes. In [355], Dobrykh, *et al.* demonstrated such a striking

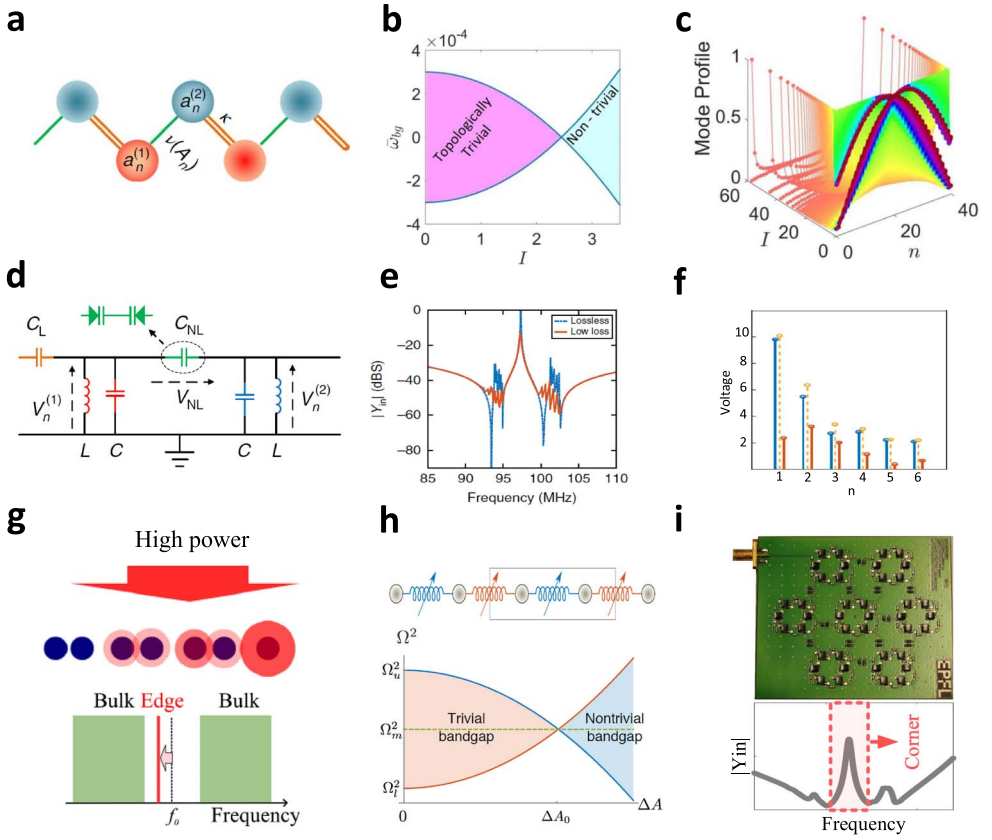

Figure 4. Nonlinear self-induced classical topological insulators. a, A one-dimensional nonlinear topological system, based on a SSH toy model with alternating linear and nonlinear staggered potentials. b, Evolution of the band gap of the SSH array versus the excitation intensity. At low excitation intensities, the SSH array is topologically trivial, with its extra-cell couplings being smaller than the intra-cell ones. Enhancing the excitation intensity, however, closes the band gap of the crystal and re-opens it as topological. c, Evolution of the mode profile of the mid-gap state versus intensity. d, Implementation of the nonlinear topological insulator discussed in Figure 4a, based on a circuit lattice composed of *LC* tanks connected to each other via linear capacitances (intra-cell dynamics) and nonlinear varactor diodes (extra-cell dynamics). e, Spectrum of the input admittance of the circuit at high power intensity. The spectrum exhibits a dominant resonance peak, which corresponds to the self-induced topological corner state. f, Voltage distribution of the circuit at the resonance frequency of the corner mode. g, Enhancing the excitation intensity allows one to tune the spectral characteristics of the topological edge mode of a one-dimensional photonic crystal. h, Self-induced topological phase transition in a SSH array consisting of masses connected to each other with two types of alternating nonlinear springs, dubbed as “stiffening” (orange) and “softening” (blue). i, Self-induced second order topological insulator, based on a circuit lattice of *LC* tanks, connected to each other with alternating linear and nonlinear capacitors. The circuit supports zero-dimensional topological corner modes, manifesting themselves as a dominant resonance peak in the corner input admittance spectrum of the circuit (bottom panel).

possibility for a one-dimensional SSH array of coupled nonlinear photonic resonators. The array is designed to be of topological nature in the linear regime, corresponding to low excitation intensity. Hence it supports an edge mode, protected by chiral symmetry, at its boundary. When the excitation intensity is enhanced, the spectral line shape of the edge modes shifts towards the bulk modes as observed in Figure 4g, top. This shift reduces the localization of the edge modes as seen in the bottom panel of the figure. These observations demonstrate how the nonlinear phenomenon enables dynamic reconfiguration of the spectral characteristics of the supported topological edge modes.

The nonlinear phenomenon has also been studied in phononic systems to achieve self-induced topological transitions. In [356], Chaunsali and Theocharis demonstrated such kind of transitions in a SSH array consisting of masses connected to each other with two types of alternating nonlinear springs (Figure 4h), namely "stiffening" and "softening" types. As mentioned earlier, such system can go through a topological phase transition by enhancing the excitation intensity and invoking the nonlinear dynamics. The bottom panel of Figure 4h illustrates the evolution of the band gap of the SSH structure versus the excitation intensity, indicating the topological phase transition induced by nonlinearity.

Finally, we remark that nonlinear phenomena have also been applied to realize self-assembled higher-order topological insulators. In [357], it was shown how the nonlinear phenomenon can be leveraged to achieve self-induced topological corner states. Unlike the linear case, the spectral properties of such 0D topological modes can be tuned by changing the excitation intensity, enabling dynamic reconfigurability. The inset of Figure 4i (top) shows the realization of such topological phases in a modified hexagonal lattice of *LC* tanks, connected to each other via alternating linear and nonlinear coupling capacitors. The circuit is designed to be in the trivial phase when it is excited at a low excitation intensity. Upon enhancing the excitation power, however, the circuit becomes topological (of second-order character), supporting zero-dimensional corner states. Such topological states manifest themselves as a resonance peak in the corner admittance spectrum of the circuit, as seen in Figure 4i (bottom panel).

6. Applications

In the previous sections we have discussed how the field of topological insulators has provided a rich platform to manipulate waves in a variety of platforms, and to implement topological phases of matter in classical wave physics. However, the impact of this area of research has been rapidly expanding in the realm of practical applications of these concepts, as we detail in this section, in which we discuss the most important recently proposed technology-oriented applications of topological wave insulators.

6.1. *Robust waveguiding*

An important application of classical topological insulators is robust guiding of energy over arbitrary paths [357–380]. An ordinary waveguide exhibits a bi-directional type of dispersion. On the contrary, the gapless edge states of Chern wave insulators possess a frequency dispersion with only positive (or negative) slope (or group velocity). Consequently, waves (light or sound) cannot couple to any backward state when it reaches an imperfection, and does not backscatter. Suppose that a perfectly conducting obstacle is placed on the way of the electromagnetic wave propagating along the edge of the topological system discussed in Figure 1e. While this normally induces strong reflection in any ordinary waveguide, the topological insulator lets the electromagnetic energy flow around the PEC with perfect transmission (Figure 5a). Such fascinating property has also been proposed in acoustics for reflection-less guiding of sound waves. Figure 5b shows how

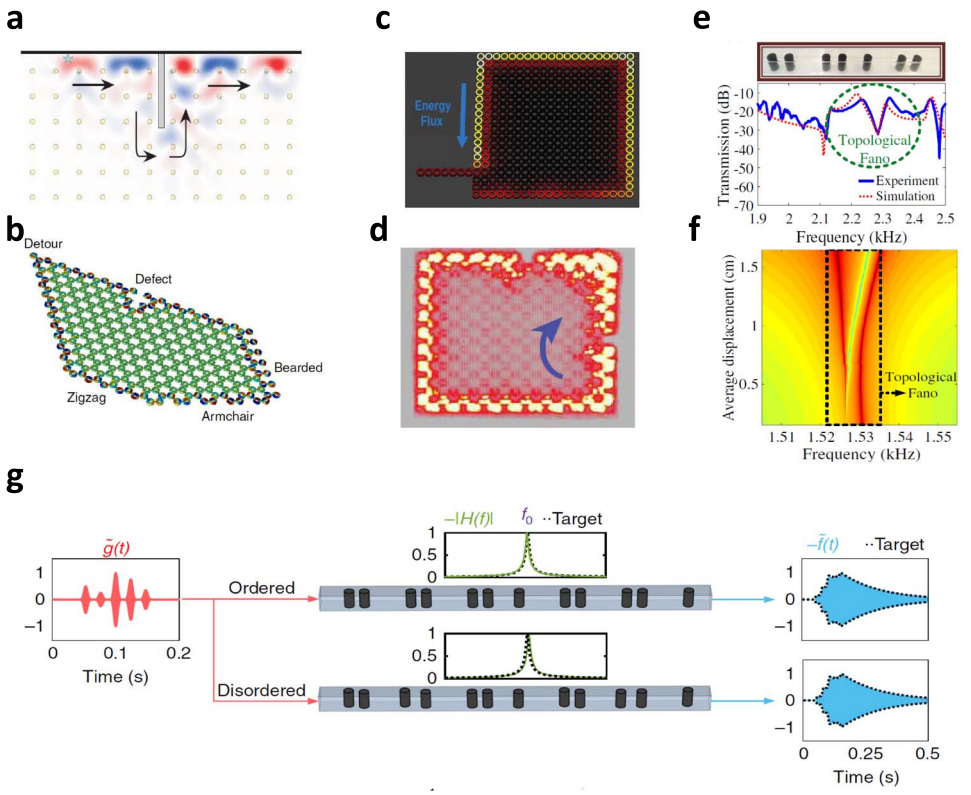

Figure 5. Applications of classical wave topological insulators. a, In contrast to any ordinary type of waveguide, the edge mode of the topological insulator discussed in Figure 1a smoothly flows around a PEC obstacle without backscattering, enabling robust guiding of electromagnetic energy. b, Reflection-less guiding of sound waves using the topological insulator discussed in Figure 1c. Despite the presence of several types of defects on the way of the edge mode, it flows along the perimeter of the crystal with almost perfect transmission. c, Theoretical realization of the lasing action from the edge mode of a topological insulator, based on an aperiodic topological array of micro ring resonators. d, Experimental demonstration of the lasing action. The lasing mode shows strong robustness to disorder. e, By inducing two topological subspaces of even and odd modes in a SSH array of cylinders arranged inside a monomode acoustic waveguide (top panel), a new class of Fano resonances, namely topological Fano resonances, is obtained (bottom panel). f, Evolution of the spectral line shape of the topological Fano resonance versus disorder strength. g, Topological analog signal processing based on the mid-gap state of a SSH array, built from cylindrical rods arranged inside an acoustic waveguide. Upon exciting the mid-gap state, such a system performs time domain differential equation solving (top signal path), with a strong immunity against imperfection (bottom signal path).

the edge mode of the acoustic topological insulator discussed in Figure 1g ideally travels along an interface involving various types of defects and detours. This is in stark contrast to ordinary acoustic waveguides in which two subsequent defects always create Fabry–Pérot interferences and, more generally, impedance matching issues. These unusual properties have been proposed to realize compact delay lines [381].

6.2. *Lasing*

Another promising application of topological insulators is single-mode robust lasing [382–389]. In [389], Harari, *et al.*, theoretically proposed to achieve the lasing action from the edge modes of a topological insulator. The realization was based on an aperiodic topological array of micro-ring resonators, which was one of the basic platforms explored for achieving photonic topological insulators [390, 391]. The aperiodic nature of such structure creates an artificial gauge field, allowing one to have edge states analogues to quantum Hall phases without the presence of any external magnetic field. By providing gain to the resonator cavities located on the perimeter of the crystal, the lasing action from such a configuration was demonstrated, as seen in Figure 5b, and demonstrated to be robust to spin-preserving defects.

Based on these theoretical findings, in [392], Bandres *et al.* experimentally verified the lasing action from such kind of a system. Figure 5c represents the lasing from such a topological system. Remarkably and consistent with the topological nature of the structure, the lasing mode and its slope efficiency shows a strong immunity against disorder. We note that the edge modes of this topological lasing systems are time-reversal symmetry preserved and, as such, are not truly unidirectional. Yet, there are proposals [383] on the realization of topological lasers with a broken time-reversal symmetry, enabling truly unidirectional and non-reciprocal lasing action at telecommunication wavelength.

6.3. *Fano resonances*

Fano resonances are caused by the interference between a sharp resonance state (the dark state) with a wider-band one (bright state). Such exotic kind of resonances, which are characterized by an asymmetric and ultra-sharp spectral line shape, have found a large variety of applications in sensing, due to their extremely high sensitivity to perturbations. However, this sensitivity is not desirable in other applications such as switching, filtering, and lasing. In [393], a new class of Fano resonances was introduced, whose ultrasharp line shapes is guaranteed and protected by topology. This was achieved by inducing two topological subspaces of even and odd modes in a SSH array of cylinders arranged inside a mono-modal acoustic waveguide. The corresponding even edge mode, originating from multiple scattering of sound, takes the role of the bright state. On the other hand, the odd edge mode, stemming from so-called bound states in the continuum, served as the dark state. By slightly breaking the reflection mirror symmetry of the system, these two topological states were then allowed to couple to each other, creating a Fano line shape (Figure 1e). Thanks to the topological nature of the bright and dark states, such resonance was found to be robust to high levels of disorder. Figure 1f plots the evolution of the Fano line shape versus disorder strength, constituting a direct evidence of its robustness. These Fano resonances are immune to fabrication imperfections and weak disorder, and can be envisioned in other physical platforms, such as optics and microwaves [393].

6.4. *Analog signal processing*

Wave-based analog computing systems have recently been attracted considerable amount of attention for carrying out specialized computational tasks such as differentiation, integration and convolution at extremely fast speeds and low power requirements [394–399]. These advantages are due to the fact that these systems perform the computation at the speed of the wave in the analog domain, without having to digitize the signals, giving rise to real-time and high-throughput computation. Yet, like any other analog system, they suffer from their relatively high sensitivity to perturbations. In [400], the relevance of topological insulators for performing robust

signal processing tasks was demonstrated, based on mid-gap one-dimensional topological states. The array was made of cylindrical rods arranged inside an acoustic waveguide. The topological state of such an array induces a Lorentzian transmission spectrum, corresponding to a first-order transfer function. Hence, upon exciting its mid-gap state, the topological system performs time-domain differential equation solving (see Figure 5d, top signal path). Such analog signal processing system is expected to be robust to disorder by virtue of its topological nature. This salient feature is demonstrated in the bottom signal path of Figure 5d, in which the cylinders are randomly shifted away from their original positions. It is observed that the topological analog computing system interestingly maintains its original functionality in the presence of disorder.

7. Discussion and conclusion

In this paper, we reviewed recent findings in the field of classical-wave-based topological insulators. While we discussed a few important technology-oriented applications of topological wave insulators in the previous section, there exists a large variety of reports on other relevant applications, including switching [401–407], modulation [408–410], lensing [411], negative refraction [412], sensing [413], beam splitting [414–418], mode locked fiber lasers [419–424], delay lines [425–427], integrated photonic and phononic devices [428, 429], frequency filters [430], frequency converters [431–433], interferometers [434], and amplifiers [435,436]. It is important to realize that the advantageous properties of topological wave systems, especially in acoustics, are often mitigated by the presence of dissipation losses, imposing certain restrictions on the available bandwidth of operation or propagation length of the topological edge modes. Studying the effect of losses on the topological phases of matter is therefore an emerging direction of research, which has recently inspired the new field of non-Hermitian topological insulators [437–453]. By exploiting the interplay between gain, loss and coupling strengths, such types of insulating phases allow one to go beyond the restrictions of Hermitian topological insulators, especially their sensitivity to absorption losses.

Apart from the Chern insulating phases that are protected by time-reversal symmetry, the remaining topological phases discussed in this review are protected by special symmetries that can be easily broken (like rotational symmetry of the underlying crystal). Enhancing the robustness of topological insulators to disorders that break these symmetries is therefore another important direction, which needs to be pursued. In order to develop defect-immunity engineering at optical frequencies, it may be possible to exploit metatronic techniques [454], so as to optimize the system parameters in a way that it not only benefits from topological protection but it also minimizes its sensitivity to the types of disorder that break the topology of the system.

Exploring topological phases of matter in dimensions higher than what is physically accessible is another promising direction of research [455–458]. In particular, while here we restricted our discussion to two-dimensional and three-dimensional topological phases, there have been several recent reports on topological phases in four dimensions and above, based on the notion of synthetic dimensions [459–473]. Despite the fact that such states have not found specific engineering-oriented applications up to date, they have established an elegant experimental platform, stimulating the deep connection between condensed-matter and elementary particle physics. In general, the idea of exploiting temporal modulations in this context appears to be very rich and not yet fully exploited.

Overall, while to date many of the ideas explored in the context of wave topological insulators have been motivated by physics-driven explorations, the field has a bright future not only in emerging theoretically-driven directions (non-linear, non-Hermitian, etc), but also in the plethora of practical applications of topology in wave engineering (disorder immunity, signal processing, sensing, lasing, etc).

References

[1] L. D. Landau, "On the theory of phase transitions", *Ukr. J. Phys.* **11** (1937), p. 19-32.
[2] F. D. M. Haldane, "Model for a quantum Hall effect without Landau levels: condensed-matter realization of the "parity anomaly"", *Phys. Rev. Lett.* **61** (1988), no. 18, p. 2015.
[3] X.-G. Wen, "Topological orders in rigid states", *Intl J. Modern Phys. B* **4** (1990), no. 02, p. 239-271.
[4] M. Z. Hasan, C. L. Kane, "Colloquium: topological insulators", *Rev. Mod. Phys.* **82** (2010), no. 4, p. 3045.
[5] X.-L. Qi, S.-C. Zhang, "Topological insulators and superconductors", *Rev. Mod. Phys.* **83** (2011), no. 4, p. 1057.
[6] B. A. Bernevig, T. L. Hughes, *Topological Insulators and Topological Superconductors*, Princeton University Press, 2013.
[7] Y. Hatsugai, "Chern number and edge states in the integer quantum Hall effect", *Phys. Rev. Lett.* **71** (1993), no. 22, p. 3697.
[8] C. Wang, A. C. Potter, T. Senthil, "Classification of interacting electronic topological insulators in three dimensions", *Science* **343** (2014), no. 6171, p. 629-631.
[9] C. Nayak *et al.*, "Non-Abelian anyons and topological quantum computation", *Rev. Mod. Phys.* **80** (2008), no. 3, p. 1083.
[10] J. D. Sau *et al.*, "Generic new platform for topological quantum computation using semiconductor heterostructures", *Phys. Rev. Lett.* **104** (2010), no. 4, article ID 040502.
[11] M. Freedman *et al.*, "Topological quantum computation", *Bull. Am. Math. Soc.* **40** (2003), no. 1, p. 31-38.
[12] D. Pesin, A. H. MacDonald, "Spintronics and pseudospintronics in graphene and topological insulators", *Nat. Mater.* **11** (2012), no. 5, p. 409.
[13] L. Šmejkal *et al.*, "Topological antiferromagnetic spintronics", *Nat. Phys.* (2018), p. 1.
[14] M. V. Berry, "Quantal phase factors accompanying adiabatic changes", *Proc. R. Soc. Lond. A. Math. Phys. Sci.* **392** (1984), no. 1802, p. 45-57.
[15] F. D. M. Haldane, S. Raghu, "Possible realization of directional optical waveguides in photonic crystals with broken time-reversal symmetry", *Phys. Rev. Lett.* **100** (2008), no. 1, article ID 013904.
[16] L. Lu, J. D. Joannopoulos, M. Soljačić, "Topological photonics", *Nat. Photonics* **8** (2014), no. 11, p. 821.
[17] A. B. Khanikaev, G. Shvets, "Two-dimensional topological photonics", *Nat. Photonics* **11** (2017), no. 12, p. 763.
[18] T. Ozawa *et al.*, "Topological photonics", *Rev. Mod. Phys.* **91** (2019), no. 1, article ID 015006.
[19] C. Liu *et al.*, "Disorder-induced topological state transition in photonic metamaterials", *Phys. Rev. Lett.* **119** (2017), no. 18, article ID 183901.
[20] S. Barik *et al.*, "A topological quantum optics interface", *Science* **359** (2018), no. 6376, p. 666-668.
[21] W. Gao *et al.*, "Topological photonic phase in chiral hyperbolic metamaterials", *Phys. Rev. Lett.* **114** (2015), no. 3, article ID 037402.
[22] S. Kruk *et al.*, "Edge states and topological phase transitions in chains of dielectric nanoparticles", *Small* **13** (2017), no. 11, article ID 1603190.
[23] C. Yin *et al.*, "Realizing topological edge states in a silicon nitride microring-based photonic integrated circuit", *Opt. Lett.* **41** (2016), no. 20, p. 4791-4794.
[24] J. Noh *et al.*, "Topological protection of photonic mid-gap defect modes", *Nat. Photonics* **12** (2018), no. 7, p. 408.
[25] S. R. Pocock *et al.*, "Topological plasmonic chain with retardation and radiative effects", *Acs Photonics* **5** (2018), no. 6, p. 2271-2279.
[26] A. V. Poshakinskiy, A. N. Poddubny, "Optomechanical Kerker effect", *Phys. Rev. X* **9** (2019), no. 1, article ID 011008.
[27] J. Perczel *et al.*, "Topological quantum optics in two-dimensional atomic arrays", *Phys. Rev. Lett.* **119** (2017), no. 2, article ID 023603.
[28] B. Yang *et al.*, "Direct observation of topological surface-state arcs in photonic metamaterials", *Nat. Commun.* **8** (2017), no. 1, p. 97.
[29] W. Tan *et al.*, "Photonic simulation of topological excitations in metamaterials", *Sci. Rep.* **4** (2014), p. 3842.
[30] X.-D. Chen, X.-T. He, J.-W. Dong, "All-dielectric layered photonic topological insulators", *Laser Photonics Rev.* **13** (2019), no. 8, article ID 1900091.
[31] J. Yuen-Zhou *et al.*, "Topologically protected excitons in porphyrin thin films", *Nat. Mater.* **13** (2014), no. 11, p. 1026.
[32] T. Ma, G. Shvets, "Scattering-free edge states between heterogeneous photonic topological insulators", *Phys. Rev. B* **95** (2017), no. 16, article ID 165102.
[33] D. A. Jacobs *et al.*, "Photonic topological Chern insulators based on Tellegen metacrystals", *New J. Phys.* **17** (2015), no. 12, article ID 125015.
[34] R. E. Christiansen, F. Wang, O. Sigmund, "Topological insulators by topology optimization", *Phys. Rev. Lett.* **122** (2019), no. 23, article ID 234502.
[35] F.-F. Li *et al.*, "Topological light-trapping on a dislocation", *Nat. Commun.* **9** (2018), no. 1, p. 2462.
[36] T. Karzig *et al.*, "Topological polaritons", *Phys. Rev. X* **5** (2015), no. 3, article ID 031001.

[37] M. C. Rechtsman *et al.*, "Topological creation and destruction of edge states in photonic graphene", *Phys. Rev. Lett.* **111** (2013), no. 10, article ID 103901.
[38] Q. Huang *et al.*, "Observation of a topological edge state in the X-ray band", *Laser Photonics Rev.* **13** (2019), no. 6, article ID 1800339.
[39] F. Liu, H.-Y. Deng, K. Wakabayashi, "Topological photonic crystals with zero Berry curvature", *Phys. Rev. B* **97** (2018), no. 3, article ID 035442.
[40] J. Han, C. Gneiting, D. Leykam, "Helical transport in coupled resonator waveguides", *Phys. Rev. B* **99** (2019), no. 22, article ID 224201.
[41] F. Lindel *et al.*, "Inducing and controlling rotation on small objects using photonic topological materials", *Phys. Rev. B* **98** (2018), no. 14, article ID 144101.
[42] L. Xu *et al.*, "Accidental degeneracy in photonic bands and topological phase transitions in two-dimensional core-shell dielectric photonic crystals", *Opt. Express* **24** (2016), no. 16, p. 18059-18071.
[43] B.-Y. Xie *et al.*, "Photonics meets topology", *Opt. Express* **26** (2018), no. 19, p. 24531-24550.
[44] M. Bello *et al.*, "Unconventional quantum optics in topological waveguide QED", *Sci. Adv.* **5** (2019), no. 7, article ID eaaw0297.
[45] Y. Wang *et al.*, "Topological protection of two-photon quantum correlation on a photonic chip", *Optica* **6** (2019), no. 8, p. 955-960.
[46] T. Dubček *et al.*, "The Harper–Hofstadter Hamiltonian and conical diffraction in photonic lattices with grating assisted tunneling", *New J. Phys.* **17** (2015), no. 12, article ID 125002.
[47] Z. A. Kudyshev *et al.*, "Photonic topological phase transition on demand", *Nanophotonics* **8** (2019), p. 1349-1356.
[48] S. A. Sato *et al.*, "Microscopic theory for the light-induced anomalous Hall effect in graphene", *Phys. Rev. B* **99** (2019), no. 21, article ID 214302.
[49] Y. Li, J. Mei, "Double Dirac cones in two-dimensional dielectric photonic crystals", *Opt. Express* **23** (2015), no. 9, p. 12089-12099.
[50] X.-C. Sun *et al.*, "Two-dimensional topological photonic systems", *Prog. Quantum Electron.* **55** (2017), p. 52-73.
[51] L. Wang *et al.*, "Subwavelength topological edge states based on localized spoof surface plasmonic metaparticle arrays", *Opt. Express* **27** (2019), no. 10, p. 14407-14422.
[52] J. W. McIver *et al.*, "Control over topological insulator photocurrents with light polarization", *Nat. Nanotechnol.* **7** (2012), no. 2, p. 96.
[53] Y. Long *et al.*, "Inverse design of photonic topological state via machine learning", *Appl. Phys. Lett.* **114** (2019), no. 18, article ID 181105.
[54] P. Di Pietro *et al.*, "Observation of Dirac plasmons in a topological insulator", *Nat. Nanotechnol.* **8** (2013), no. 8, p. 556.
[55] F. Gao *et al.*, "Probing topological protection using a designer surface plasmon structure", *Nat. Commun.* **7** (2016), article ID 11619.
[56] Y. Ke *et al.*, "Topological phase transitions and thouless pumping of light in photonic waveguide arrays", *Laser Photonics Rev.* **10** (2016), no. 6, p. 995-1001.
[57] M. S. Rider *et al.*, "A perspective on topological nanophotonics: current status and future challenges", *J. Appl. Phys.* **125** (2019), no. 12, article ID 120901.
[58] M. I. Shalaev, W. Walasik, N. M. Litchinitser, "Optically tunable topological photonic crystal", *Optica* **6** (2019), no. 7, p. 839-844.
[59] S. Klembt *et al.*, "Exciton-polariton topological insulator", *Nature* **562** (2018), no. 7728, p. 552.
[60] X. Yao, M. Tokman, A. Belyanin, "Efficient nonlinear generation of THz plasmons in graphene and topological insulators", *Phys. Rev. Lett.* **112** (2014), no. 5, article ID 055501.
[61] F. Cardano *et al.*, "Detection of Zak phases and topological invariants in a chiral quantum walk of twisted photons", *Nat. Commun.* **8** (2017), article ID 15516.
[62] T. Kitagawa *et al.*, "Observation of topologically protected bound states in photonic quantum walks", *Nat. Commun.* **3** (2012), p. 882.
[63] N. P. Mitchell *et al.*, "Amorphous topological insulators constructed from random point sets", *Nat. Phys.* **14** (2018), no. 4, p. 380.
[64] E. Lustig *et al.*, "Curved-space topological phases in photonic lattices", *Phys. Rev. A* **96** (2017), no. 4, article ID 041804.
[65] P. N. Dyachenko *et al.*, "Controlling thermal emission with refractory epsilon-near-zero metamaterials via topological transitions", *Nat. Commun.* **7** (2016), article ID 11809.
[66] T. Ma, G. Shvets, "All-Si valley-Hall photonic topological insulator", *New J. Phys.* **18** (2016), no. 2, article ID 025012.
[67] B. Yang *et al.*, "Topological states in amorphous magnetic photonic lattices", *Phys. Rev. B* **99** (2019), no. 4, article ID 045307.
[68] A. Girschik, F. Libisch, S. Rotter, "Percolating states in the topological Anderson insulator", *Phys. Rev. B* **91** (2015), no. 21, article ID 214204.

[69] J.-P. Xia *et al.*, "Programmable coding acoustic topological insulator", *Adv. Mater.* **30** (2018), no. 46, article ID 1805002.
[70] C. Brendel *et al.*, "Snowflake phononic topological insulator at the nanoscale", *Phys. Rev. B* **97** (2018), no. 2, article ID 020102.
[71] Z. Yang *et al.*, "Strain-induced gauge field and Landau levels in acoustic structures", *Phys. Rev. Lett.* **118** (2017), no. 19, article ID 194301.
[72] Y. Meng *et al.*, "Designing topological interface states in phononic crystals based on the full phase diagrams", *New J. Phys.* **20** (2018), no. 7, article ID 073032.
[73] J. Chen *et al.*, "Self-ordering induces multiple topological transitions for in-plane bulk waves in solid phononic crystals", *Phys. Rev. B* **98** (2018), no. 1, article ID 014302.
[74] F. Zangeneh-Nejad, R. Fleury, "Active times for acoustic metamaterials", *Rev. Phys.* (2019), article ID 100031.
[75] X. Ni *et al.*, "Topologically protected one-way edge mode in networks of acoustic resonators with circulating air flow", *New J. Phys.* **17** (2015), no. 5, article ID 053016.
[76] X. Wen *et al.*, "Acoustic Landau quantization and quantum-Hall-like edge states", *Nat. Phys.* **15** (2019), p. 352-356.
[77] D. Zhao *et al.*, "Topological interface modes in local resonant acoustic systems", *Phys. Rev. B* **98** (2018), no. 1, article ID 014110.
[78] M.-J. Tuo *et al.*, "Twist-projected two-dimensional acoustic topological insulators", *Phys. Rev. B* **99** (2019), no. 20, article ID 205432.
[79] L.-Y. Zheng *et al.*, "Observation of edge waves in a two-dimensional Su–Schrieffer–Heeger acoustic network", *Phys. Rev. Appl.* **12** (2019), no. 3, article ID 034014.
[80] G. Arregui *et al.*, "Coherent generation and detection of acoustic phonons in topological nanocavities", *APL Photonics* **4** (2019), no. 3, article ID 030805.
[81] G. Baardink *et al.*, "Localizing softness and stress along loops in 3D topological metamaterials", *Proc. Natl Acad. Sci. USA* **115** (2018), no. 3, p. 489-494.
[82] J. Ma *et al.*, "Optically Controlled Topologically Protected Acoustic Wave Amplification", *IEEE J. Selected Topics Quantum Electron.* **26** (2019), p. 1-10.
[83] X. Zhang *et al.*, "Topological sound", *Commun. Phys.* **1** (2018), no. 1, p. 97.
[84] J. Yin *et al.*, "Band transition and topological interface modes in 1D elastic phononic crystals", *Sci. Rep.* **8** (2018), no. 1, p. 6806.
[85] V. Peano *et al.*, "Topological phases of sound and light", *Phys. Rev. X* **5** (2015), no. 3, article ID 031011.
[86] S. Shankar, M. J. Bowick, M. C. Marchetti, "Topological sound and flocking on curved surfaces", *Phys. Rev. X* **7** (2017), no. 3, article ID 031039.
[87] B. Xie *et al.*, "Acoustic topological transport and refraction in a Kekulé lattice", *Phys. Rev. Appl.* **11** (2019), no. 4, article ID 044086.
[88] Y. Liu *et al.*, "Pseudospins and topological effects of phonons in a Kekulé lattice", *Phys. Rev. Lett.* **119** (2017), no. 25, article ID 255901.
[89] H. Abbaszadeh *et al.*, "Sonic Landau levels and synthetic gauge fields in mechanical metamaterials", *Phys. Rev. Lett.* **119** (2017), no. 19, article ID 195502.
[90] Z.-G. Chen, Y. Wu, "Tunable topological phononic crystals", *Phys. Rev. Appl.* **5** (2016), no. 5, article ID 054021.
[91] A. Darabi, M. J. Leamy, "Reconfigurable topological insulator for elastic waves", *J. Acoust. Soc. Am.* **146** (2019), no. 1, p. 773-781.
[92] Z.-Y. Ong, C. H. Lee, "Transport and localization in a topological phononic lattice with correlated disorder", *Phys. Rev. B* **94** (2016), no. 13, article ID 134203.
[93] G. Gupta *et al.*, "Role of acoustic phonons in Bi_2Se_3 topological insulator slabs: a quantum transport investigation", *Phys. Rev. B* **89** (2014), no. 24, article ID 245419.
[94] Z. Yang, F. Gao, B. Zhang, "Topological water wave states in a one-dimensional structure", *Sci. Rep.* **6** (2016), article ID 29202.
[95] S.-Y. Huo, J.-J. Chen, H.-B. Huang, "Topologically protected edge states for out-of-plane and in-plane bulk elastic waves", *J. Phys.: Condens. Matter* **30** (2018), no. 14, article ID 145403.
[96] G. Ma, M. Xiao, C. T. Chan, "Topological phases in acoustic and mechanical systems", *Nat. Rev. Phys.* **1** (2019), p. 281-294.
[97] K. Saha, I. Garate, "Phonon-induced topological insulation", *Phys. Rev. B* **89** (2014), no. 20, article ID 205103.
[98] T. Lee, H. Iizuka, "Bragg scattering based acoustic topological transition controlled by local resonance", *Phys. Rev. B* **99** (2019), no. 6, article ID 064305.
[99] Y. Liu *et al.*, "Model for topological phononics and phonon diode", *Phys. Rev. B* **96** (2017), no. 6, article ID 064106.
[100] Z. Yu, Z. Ren, J. Lee, "Phononic topological insulators based on six-petal holey silicon structures", *Sci. Rep.* **9** (2019), no. 1, p. 1805.
[101] R. Süsstrunk, S. D. Huber, "Observation of phononic helical edge states in a mechanical topological insulator", *Science* **349** (2015), no. 6243, p. 47-50.

[102] S. D. Huber, "Topological mechanics", *Nat. Phys.* **12** (2016), no. 7, p. 621.
[103] H. Chen, H. Nassar, G. Huang, "Topological mechanics of edge waves in Kagome lattices", *preprint*, arXiv:1802.04404 (2018).
[104] B. Liu *et al.*, "Topological kinematics of origami metamaterials", *Nat. Phys.* **14** (2018), no. 8, p. 811.
[105] A. S. Meeussen, J. Paulose, V. Vitelli, "Geared topological metamaterials with tunable mechanical stability", *Phys. Rev. X* **6** (2016), no. 4, article ID 041029.
[106] T. Tian *et al.*, "Observation of dynamical phase transitions in a topological nanomechanical system", *Phys. Rev. B* **100** (2019), no. 2, article ID 024310.
[107] J. Cha, K. W. Kim, C. Daraio, "Experimental realization of on-chip topological nanoelectromechanical metamaterials", *Nature* **564** (2018), no. 7735, p. 229.
[108] Y.-W. Tsai *et al.*, "Topological phase transition in a one-dimensional elastic string system", *Crystals* **9** (2019), no. 6, p. 313.
[109] Y. Zhou *et al.*, "Kink-antikink asymmetry and impurity interactions in topological mechanical chains", *Phys. Rev. E* **95** (2017), no. 2, article ID 022202.
[110] E. Prodan *et al.*, "Dynamical Majorana edge modes in a broad class of topological mechanical systems", *Nat. Commun.* **8** (2017), article ID 14587.
[111] J. Paulose, B. G.-g. Chen, V. Vitelli, "Topological modes bound to dislocations in mechanical metamaterials", *Nat. Phys.* **11** (2015), no. 2, p. 153.
[112] J. Köpfler *et al.*, "Topologically protected twist edge states for a resonant mechanical laser-beam scanner", *Phys. Rev. Appl.* **11** (2019), no. 3, article ID 034059.
[113] P. Deymier, K. Runge, "One-dimensional mass-spring chains supporting elastic waves with non-conventional topology", *Crystals* **6** (2016), no. 4, p. 44.
[114] R. Chaunsali, F. Li, J. Yang, "Stress wave isolation by purely mechanical topological phononic crystals", *Sci. Rep.* **6** (2016), article ID 30662.
[115] M. Brandenbourger *et al.*, "Non-reciprocal robotic metamaterials", *Nat. Commun.* **10** (2019), no. 1, p. 1-8.
[116] S. M. Young *et al.*, "Theoretical investigation of the evolution of the topological phase of Bi_2Se_3 under mechanical strain", *Phys. Rev. B* **84** (2011), no. 8, article ID 085106.
[117] Y.-T. Wang, P.-G. Luan, S. Zhang, "Coriolis force induced topological order for classical mechanical vibrations", *New J. Phys.* **17** (2015), no. 7, article ID 073031.
[118] D. Z. Rocklin *et al.*, "Transformable topological mechanical metamaterials", *Nat. Commun.* **8** (2017), article ID 14201.
[119] G. Wang, H. Xu, Y.-C. Lai, "Mechanical topological semimetals with massless quasiparticles and a finite Berry curvature", *Phys. Rev. B* **95** (2017), no. 23, article ID 235159.
[120] J. Attig *et al.*, "Topological mechanics from supersymmetry", *Phys. Rev. Res.* **1** (2019), no. 3, article ID 032047.
[121] Z. Xiong *et al.*, "Topological node lines in mechanical metacrystals", *Phys. Rev. B* **97** (2018), no. 18, article ID 180101.
[122] H. Chen, H. Nassar, G. L. Huang, "A study of topological effects in 1D and 2D mechanical lattices", *J. Mech. Phys. Solids* **117** (2018), p. 22-36.
[123] M. Fruchart, D. Carpentier, "An introduction to topological insulators", *C. R. Phys.* **14** (2013), no. 9–10, p. 779-815.
[124] J. K. Asbóth, L. Oroszlány, A. Pályi, "A short course on topological insulators", *Lecture Notes in Physics* **919** (2016), p. 166.
[125] P. A. Kalozoumis *et al.*, "Finite-size effects on topological interface states in one-dimensional scattering systems", *Phys. Rev. A* **98** (2018), no. 2, article ID 023838.
[126] C. E. Whittaker *et al.*, "Effect of photonic spin-orbit coupling on the topological edge modes of a Su–Schrieffer–Heeger chain", *Phys. Rev. B* **99** (2019), no. 8, article ID 081402.
[127] L. Ge *et al.*, "Topological phase transition and interface states in hybrid plasmonic-photonic systems", *J. Opt.* **19** (2017), no. 6, p. 06LT02.
[128] C. L. Kane, T. C. Lubensky, "Topological boundary modes in isostatic lattices", *Nat. Phys.* **10** (2014), no. 1, p. 39.
[129] Y. Hadad, V. Vitelli, A. Alu, "Solitons and propagating domain walls in topological resonator arrays", *ACS Photonics* **4** (2017), no. 8, p. 1974-1979.
[130] B. Midya, L. Feng, "Topological multiband photonic superlattices", *Phys. Rev. A* **98** (2018), no. 4, article ID 043838.
[131] Q. Cheng *et al.*, "Topologically protected interface mode in plasmonic waveguide arrays", *Laser Photonics Rev.* **9** (2015), no. 4, p. 392-398.
[132] C. W. Ling *et al.*, "Topological edge plasmon modes between diatomic chains of plasmonic nanoparticles", *Opt. Express* **23** (2015), no. 3, p. 2021-2031.
[133] F. Bleckmann *et al.*, "Spectral imaging of topological edge states in plasmonic waveguide arrays", *Phys. Rev. B* **96** (2017), no. 4, article ID 045417.
[134] Z. Zhang *et al.*, "Experimental realization of multiple topological edge states in a 1D photonic lattice", *Laser Photonics Rev.* **13** (2019), no. 2, article ID 1800202.

[135] R. K. Pal, J. Vila, M. Ruzzene, "Topologically protected edge states in mechanical metamaterials", *Adv. Crystals Elastic Metamaterials* **52** (2019), p. 147.
[136] A. Altland, M. R. Zirnbauer, "Nonstandard symmetry classes in mesoscopic normal-superconducting hybrid structures", *Phys. Rev. B* **55** (1997), no. 2, p. 1142.
[137] P. St-Jean *et al.*, "Lasing in topological edge states of a one-dimensional lattice", *Nat. Photonics* **11** (2017), no. 10, p. 651.
[138] M. Xiao *et al.*, "Geometric phase and band inversion in periodic acoustic systems", *Nat. Phys.* **11** (2015), no. 3, p. 240.
[139] M. Parto *et al.*, "Edge-mode lasing in 1D topological active arrays", *Phys. Rev. Lett.* **120** (2018), no. 11, article ID 113901.
[140] D. Woolard, J. L. Jensen, *Spectral Sensing Research for Water Monitoring Applications and Frontier Science and Technology for Chemical, Biological and Radiological Defense, Volume 48*, World Scientific, 2008.
[141] Y. Zhang *et al.*, "Experimental observation of the quantum Hall effect and Berry's phase in graphene", *Nature* **438** (2005), no. 7065, p. 201.
[142] Z. Wang *et al.*, "Observation of unidirectional backscattering-immune topological electromagnetic states", *Nature* **461** (2009), no. 7265, p. 772.
[143] W. Śmigaj *et al.*, "Magneto-optical circulator designed for operation in a uniform external magnetic field", *Opt. Lett.* **35** (2010), no. 4, p. 568-570.
[144] R. Fleury *et al.*, "Sound isolation and giant linear nonreciprocity in a compact acoustic circulator", *Science* **343** (2014), no. 6170, p. 516-519.
[145] A. B. Khanikaev *et al.*, "Topologically robust sound propagation in an angular-momentum-biased graphene-like resonator lattice", *Nat. Commun.* **6** (2015), p. 8260.
[146] Z. Yang *et al.*, "Topological acoustics", *Phys. Rev. Lett.* **114** (2015), no. 11, article ID 114301.
[147] A. Souslov *et al.*, "Topological waves in fluids with odd viscosity", *Phys. Rev. Lett.* **122** (2019), no. 12, article ID 128001.
[148] A. Souslov *et al.*, "Topological sound in active-liquid metamaterials", *Nat. Phys.* **13** (2017), no. 11, p. 1091.
[149] Y. Ding *et al.*, "Experimental demonstration of acoustic Chern insulators", *Phys. Rev. Lett.* **122** (2019), no. 1, article ID 014302.
[150] L. M. Nash *et al.*, "Topological mechanics of gyroscopic metamaterials", *Proc. Natl Acad. Sci. USA* **112** (2015), no. 47, p. 14495-14500.
[151] C. L. Kane, E. J. Mele, "Quantum spin Hall effect in graphene", *Phys. Rev. Lett.* **95** (2005), no. 22, article ID 226801.
[152] B. A. Bernevig, T. L. Hughes, S.-C. Zhang, "Quantum spin Hall effect and topological phase transition in HgTe quantum wells", *Science* **314** (2006), no. 5806, p. 1757-1761.
[153] R. K. Pal, M. Schaeffer, M. Ruzzene, "Helical edge states and topological phase transitions in phononic systems using bi-layered lattices", *J. Appl. Phys.* **119** (2016), no. 8, article ID 084305.
[154] X.-Y. Zhu *et al.*, "Z_2 topological edge state in honeycomb lattice of coupled resonant optical waveguides with a flat band", *Opt. Express* **26** (2018), no. 19, p. 24307-24317.
[155] M. L. N. Chen *et al.*, "Pseudospin-polarized topological line defects in dielectric photonic crystals", *IEEE Trans. Antennas Propagation* **68** (2019), p. 609-613.
[156] H. Zhong *et al.*, "Topological insulator properties of photonic kagome helical waveguide arrays", *Results Phys.* **12** (2019), p. 996-1001.
[157] H. Xiong *et al.*, "Polarization-resolved edge states in terahertz topological photonic crystal", *Opt. Express* **27** (2019), no. 16, p. 22819-22826.
[158] O. Gröning *et al.*, "Engineering of robust topological quantum phases in graphene nanoribbons", *Nature* **560** (2018), no. 7717, p. 209.
[159] A. P. Slobozhanyuk *et al.*, "Enhanced photonic spin Hall effect with subwavelength topological edge states", *Laser Photonics Rev.* **10** (2016), no. 4, p. 656-664.
[160] X.-C. Sun *et al.*, "Photonic topological states in a two-dimensional gyrotropic photonic crystal", *Crystals* **9** (2019), no. 3, p. 137.
[161] V. K. Kozin *et al.*, "Topological metamaterials based on polariton rings", *Phys. Rev. B* **98** (2018), no. 12, article ID 125115.
[162] R. E. Christiansen *et al.*, "Designing photonic topological insulators with quantum-spin-Hall edge states using topology optimization", *Nanophotonics* **8** (2019), p. 1363-1369.
[163] K. Y. Bliokh, D. Smirnova, F. Nori, "Quantum spin Hall effect of light", *Science* **348** (2015), no. 6242, p. 1448-1451.
[164] C. He *et al.*, "Acoustic topological insulator and robust one-way sound transport", *Nat. Phys.* **12** (2016), no. 12, p. 1124.
[165] S. S. Nanthakumar *et al.*, "Inverse design of quantum spin hall-based phononic topological insulators", *J. Mech. Phys. Solids* **125** (2019), p. 550-571.
[166] D. Jia *et al.*, "Pseudospin-dependent acoustic topological insulator by airborne sonic crystals with a triangular lattice", *Appl. Phys. Express* **12** (2019), no. 4, article ID 044003.
[167] H. Chen *et al.*, "Elastic quantum spin Hall effect in kagome lattices", *Phys. Rev. B* **98** (2018), no. 9, article ID 094302.

[168] F. Ju, Y. Cheng, X. Liu, "Acoustic spin Hall-like effect in hyperbolic metamaterials controlled by the helical wave", *Sci. Rep.* **8** (2018), no. 1, article ID 11113.
[169] B.-Z. Xia *et al.*, "Topological phononic insulator with robust pseudospin-dependent transport", *Phys. Rev. B* **96** (2017), no. 9, article ID 094106.
[170] Y. Liu, Y. Xu, W. Duan, "Phononic topological insulators with tunable pseudospin physics", *preprint*, arXiv:1809.05721 (2018).
[171] X.-F. Zhu *et al.*, "Topologically protected acoustic helical edge states and interface states in strongly coupled metamaterial ring lattices", *preprint*, arXiv:1508.06243 (2015).
[172] S. Wang, G. Ma, C. T. Chan, "Topological transport of sound mediated by spin-redirection geometric phase", *Sci. Adv.* **4** (2018), no. 2, article ID eaaq1475.
[173] A. Slobozhanyuk *et al.*, "Three-dimensional all-dielectric photonic topological insulator", *Nat. Photonics* **11** (2017), no. 2, p. 130.
[174] C. He *et al.*, "Photonic topological insulator with broken time-reversal symmetry", *Proc. Natl Acad. Sci. USA* **113** (2016), no. 18, p. 4924-4928.
[175] L.-y. Feng *et al.*, "Reconfigurable topological phononic crystal slabs", *Phys. Lett. A* **382** (2018), no. 39, p. 2880-2885.
[176] Z. Gao *et al.*, "Flexible photonic topological insulator", *Adv. Opt. Mater.* **6** (2018), no. 17, article ID 1800532.
[177] S. H. Mousavi, A. B. Khanikaev, Z. Wang, "Topologically protected elastic waves in phononic metamaterials", *Nat. Commun.* **6** (2015), p. 8682.
[178] Y. Yang, Z. H. Hang, "Topological whispering gallery modes in two-dimensional photonic crystal cavities", *Opt. Express* **26** (2018), no. 16, p. 21235-21241.
[179] Y. Li *et al.*, "Topological LC-circuits based on microstrips and observation of electromagnetic modes with orbital angular momentum", *Nat. Commun.* **9** (2018), no. 1, p. 4598.
[180] J. Mei, Z. Chen, Y. Wu, "Pseudo-time-reversal symmetry and topological edge states in two-dimensional acoustic crystals", *Sci. Rep.* **6** (2016), article ID 32752.
[181] Y. Deng *et al.*, "Observation of zone folding induced acoustic topological insulators and the role of spin-mixing defects", *Phys. Rev. B* **96** (2017), no. 18, article ID 184305.
[182] C. He *et al.*, "Topological phononic states of underwater sound based on coupled ring resonators", *Appl. Phys. Lett.* **108** (2016), no. 3, article ID 031904.
[183] H. Dai *et al.*, "Subwavelength acoustic topological edge states realized by zone folding and the role of boundaries selection", *J. Appl. Phys.* **124** (2018), no. 17, article ID 175107.
[184] S. Li *et al.*, "Observation of elastic topological states in soft materials", *Nat. Commun.* **9** (2018), no. 1, p. 1370.
[185] X.-D. Chen *et al.*, "Accidental double dirac cones and robust edge states in topological anisotropic photonic crystals", *Laser Photonics Rev.* **12** (2018), no. 11, article ID 1800073.
[186] Y. Zhou, P. R. Bandaru, D. F. Sievenpiper, "Quantum-spin-Hall topological insulator in a spring-mass system", *New J. Phys.* **20** (2018), no. 12, article ID 123011.
[187] A. B. Khanikaev *et al.*, "Photonic topological insulators", *Nat. Mater.* **12** (2013), no. 3, p. 233.
[188] M. Miniaci *et al.*, "Experimental observation of topologically protected helical edge modes in patterned elastic plates", *Phys. Rev. X* **8** (2018), no. 3, article ID 031074.
[189] E. Martini, M. G. Silveirinha, S. Maci, "Exact solution for the protected TEM edge mode in a PTD-symmetric parallel-plate waveguide", *IEEE Trans. Antennas Propagation* **67** (2018), no. 2, p. 1035-1044.
[190] M. G. Silveirinha, "P. T. D symmetry-protected scattering anomaly in optics", *Phys. Rev. B* **95** (2017), no. 3, article ID 035153.
[191] L.-H. Wu, X. Hu, "Scheme for achieving a topological photonic crystal by using dielectric material", *Phys. Rev. Lett.* **114** (2015), no. 22, article ID 223901.
[192] S. Yves *et al.*, "Crystalline metamaterials for topological properties at subwavelength scales", *Nat. Commun.* **8** (2017), article ID 16023.
[193] L. Wang *et al.*, "The existence of topological edge states in honeycomb plasmonic lattices", *New J. Phys.* **18** (2016), no. 10, article ID 103029.
[194] S. Barik *et al.*, "Two-dimensionally confined topological edge states in photonic crystals", *New J. Phys.* **18** (2016), no. 11, article ID 113013.
[195] Y. Yang *et al.*, "Visualization of a unidirectional electromagnetic waveguide using topological photonic crystals made of dielectric materials", *Phys. Rev. Lett.* **120** (2018), no. 21, article ID 217401.
[196] M. I. Shalaev *et al.*, "Robust topologically protected transport in photonic crystals at telecommunication wavelengths", *Nat. Nanotechnol.* **14** (2019), no. 1, p. 31.
[197] M. Honari-Latifpour, Y. Leila, "Topological plasmonic edge states in a planar array of metallic nanoparticles", *Nanophotonics* **8** (2019), p. 799-806.
[198] S. Wu, Y. Wu, J. Mei, "Topological helical edge states in water waves over a topographical bottom", *New J. Phys.* **20** (2018), no. 2, article ID 023051.

[199] R. Chaunsali, C.-W. Chen, J. Yang, "Experimental demonstration of topological waveguiding in elastic plates with local resonators", *New J. Phys.* **20** (2018), no. 11, article ID 113036.
[200] Y. Chen, X. Liu, G. Hu, "Topological phase transition in mechanical honeycomb lattice", *J. Mech. Phys. Solids* **122** (2019), p. 54-68.
[201] S.-Y. Yu *et al.*, "Elastic pseudospin transport for integratable topological phononic circuits", *Nat. Commun.* **9** (2018), no. 1, p. 3072.
[202] Z. Zhang *et al.*, "Topological creation of acoustic pseudospin multipoles in a flow-free symmetry-broken metamaterial lattice", *Phys. Rev. Lett.* **118** (2017), no. 8, article ID 084303.
[203] Z. Zhang *et al.*, "Experimental verification of acoustic pseudospin multipoles in a symmetry-broken snowflakelike topological insulator", *Phys. Rev. B* **96** (2017), no. 24, article ID 241306.
[204] Z.-G. Geng *et al.*, "Topologically protected edge transport of sound in coupled cavities of a modified honeycomb lattice", *J. Phys.: Condens. Matter* **30** (2018), no. 34, article ID 345401.
[205] S. Yves *et al.*, "Topological acoustic polaritons: robust sound manipulation at the subwavelength scale", *New J. Phys.* **19** (2017), no. 7, article ID 075003.
[206] B. Bradlyn *et al.*, "Topological quantum chemistry", *Nature* **547** (2017), no. 7663, p. 298.
[207] B. Orazbayev, R. Fleury, "Quantitative robustness analysis of topological edge modes in C6 and Valley-Hall metamaterial waveguides", *Nanophotonics* **8** (2019), p. 1433-1441.
[208] X.-T. He *et al.*, "A silicon-on-insulator slab for topological valley transport", *Nat. Commun.* **10** (2019), no. 1, p. 872.
[209] Z. Zhu *et al.*, "Negative refraction and partition in acoustic valley materials of a square lattice", *Phys. Rev. Appl.* **12** (2019), no. 2, article ID 024007.
[210] L. Ye *et al.*, "Observation of valley-selective microwave transport in photonic crystals", *Appl. Phys. Lett.* **111** (2017), no. 25, article ID 251107.
[211] X. Han *et al.*, "Experimental demonstration of acoustic valley hall topological insulators with the robust selection of C 3v-symmetric scatterers", *Phys. Rev. Appl.* **12** (2019), no. 1, article ID 014046.
[212] X. Wu *et al.*, "Direct observation of valley-polarized topological edge states in designer surface plasmon crystals", *Nat. Commun.* **8** (2017), no. 1, p. 1304.
[213] Y. Deng, Y. Jing, "A comparison study between topological insulators based on valley Hall and quantum spin Hall effects", *J. Acoust. Soc. Am.* **145** (2019), no. 3, p. 1762-1762.
[214] D. Song *et al.*, "Valley vortex states and degeneracy lifting via photonic higher-band excitation", *Phys. Rev. Lett.* **122** (2019), no. 12, article ID 123903.
[215] Z. Gao *et al.*, "Valley surface-wave photonic crystal and its bulk/edge transport", *Phys. Rev. B* **96** (2017), no. 20, article ID 201402.
[216] Q. Chen *et al.*, "Valley-Hall photonic topological insulators with dual-band kink states", *Adv. Optical Mater.* (2019), article ID 1900036.
[217] R. K. Pal, M. Ruzzene, "Edge waves in plates with resonators: an elastic analogue of the quantum valley Hall effect", *New J. Phys.* **19** (2017), no. 2, article ID 025001.
[218] C. He *et al.*, "Three-dimensional topological acoustic crystals with pseudospin-valley coupled saddle surface states", *Nat. Commun.* **9** (2018), no. 1, p. 4555.
[219] T.-W. Liu, F. Semperlotti, "Experimental evidence of robust acoustic valley Hall edge states in a nonresonant topological elastic waveguide", *Phys. Rev. Appl.* **11** (2019), no. 1, article ID 014040.
[220] T.-W. Liu, F. Semperlotti, "Tunable acoustic valley-Hall edge states in reconfigurable phononic elastic waveguides", *Phys. Rev. Appl.* **9** (2018), no. 1, article ID 014001.
[221] X. Wu *et al.*, "Interlayer topological transport and devices based on layer pseudospins in photonic valley-Hall phases", *Adv. Opt. Mater.* **7** (2019), article ID 1900872.
[222] J. Lu *et al.*, "Valley topological phases in bilayer sonic crystals", *Phys. Rev. Lett.* **120** (2018), no. 11, article ID 116802.
[223] J.-J. Chen *et al.*, "Topological valley transport of plate-mode waves in a homogenous thin plate with periodic stubbed surface", *AIP Adv.* **7** (2017), no. 11, article ID 115215.
[224] Y. Shen *et al.*, "Valley-projected edge modes observed in underwater sonic crystals", *Appl. Phys. Lett.* **114** (2019), no. 2, article ID 023501.
[225] H. Dai, B. Xia, D. Yu, "Temperature-controlled tunable underwater acoustic topological insulators", *J. Appl. Phys.* **125** (2019), no. 23, article ID 235105.
[226] J. Lu *et al.*, "Valley vortex states in sonic crystals", *Phys. Rev. Lett.* **116** (2016), no. 9, article ID 093901.
[227] J. Vila, R. K. Pal, M. Ruzzene, "Observation of topological valley modes in an elastic hexagonal lattice", *Phys. Rev. B* **96** (2017), no. 13, article ID 134307.
[228] H. Zhu, T.-W. Liu, F. Semperlotti, "Design and experimental observation of valley-Hall edge states in diatomic-graphene-like elastic waveguides", *Phys. Rev. B* **97** (2018), no. 17, article ID 174301.
[229] M. Miniaci *et al.*, "Valley-based splitting of topologically protected helical waves in elastic plates", *Phys. Rev. B* **100** (2019), no. 2, article ID 024304.

[230] Z. Yu, Z. Ren, J. Lee, "Phononic topological insulators based on six-petal holey silicon structures", *Sci. Rep.* **9** (2019), no. 1, p. 1805.
[231] Z.-G. Geng *et al.*, "Mirror-symmetry induced topological valley transport along programmable boundaries in a hexagonal sonic crystal", *J. Phys.: Condens. Matter* **31** (2019), no. 24, article ID 245403.
[232] B.-Z. Xia *et al.*, "Observation of valleylike edge states of sound at a momentum away from the high-symmetry points", *Phys. Rev. B* **97** (2018), no. 15, article ID 155124.
[233] C. Chen *et al.*, "Observation of topological locally resonate and Bragg edge modes in a two-dimensional slit-typed sonic crystal", *Appl. Phys. Express* **12** (2019), no. 9, article ID 097001.
[234] M. Chen *et al.*, "Tunable Dirac cones in two-dimensional acoustic metamaterials with matryoshka structure", *J. Acoust. Soc. Am.* **146** (2019), no. 1, p. 767-772.
[235] Y.-F. Tang *et al.*, "Topological phononic crystals with tunable interface state based on local resonance", *Appl. Phys. Express* **12** (2019), no. 9, article ID 094002.
[236] Y. Yang, Z. Yang, B. Zhang, "Acoustic valley edge states in a graphene-like resonator system", *J. Appl. Phys.* **123** (2018), no. 9, article ID 091713.
[237] G. G. Gentili *et al.*, "Towards topological protection based millimeter wave devices", *Phys. Rev. B* **100** (2019), no. 12, article ID 125108.
[238] M. Yan *et al.*, "On-chip valley topological materials for elastic wave manipulation", *Nat. Mater.* **17** (2018), no. 11, p. 993.
[239] F. Gao *et al.*, "Topologically protected refraction of robust kink states in valley photonic crystals", *Nat. Phys.* **14** (2018), no. 2, p. 140.
[240] Z. Wang *et al.*, "Guiding robust valley-dependent edge states by surface acoustic waves", *J. Appl. Phys.* **125** (2019), no. 4, article ID 044502.
[241] X.-D. Chen *et al.*, "Valley-contrasting physics in all-dielectric photonic crystals: orbital angular momentum and topological propagation", *Phys. Rev. B* **96** (2017), no. 2, article ID 020202.
[242] X. Liu, Q. Guo, J. Yang, "Tunable acoustic valley edge states in a flow-free resonator system", *Appl. Phys. Lett.* **115** (2019), no. 7, article ID 074102.
[243] H. Jiang *et al.*, "Acoustic valley edge states in a graphene-like system with sub-wavelength resonator", *J. Acoust. Soc. Am.* **146** (2019), no. 1, p. 736-741.
[244] X. Wen *et al.*, "Acoustic Dirac degeneracy and topological phase transitions realized by rotating scatterers", *J. Appl. Phys.* **123** (2018), no. 9, article ID 091703.
[245] D. Jia *et al.*, "Acoustic topological insulator by honeycomb sonic crystals with direct and indirect band gaps", *New J. Phys.* **20** (2018), no. 9, article ID 093027.
[246] J. Noh *et al.*, "Observation of photonic topological valley Hall edge states", *Phys. Rev. Lett.* **120** (2018), no. 6, article ID 063902.
[247] J. Lu *et al.*, "Observation of topological valley transport of sound in sonic crystals", *Nat. Phys.* **13** (2017), no. 4, p. 369.
[248] N. Laforge *et al.*, "Observation of topological gravity-capillary waves in a water wave crystal", *New J. Phys.* **21** (2019), no. 8, article ID 083031.
[249] J. K. Asbóth, B. Tarasinski, P. Delplace, "Chiral symmetry and bulk-boundary correspondence in periodically driven one-dimensional systems", *Phys. Rev. B* **90** (2014), no. 12, article ID 125143.
[250] V. Dal Lago, M. Atala, L. E. F. Foa Torres, "Floquet topological transitions in a driven one-dimensional topological insulator", *Phys. Rev. A* **92** (2015), no. 2, article ID 023624.
[251] M. Fruchart, "Complex classes of periodically driven topological lattice systems", *Phys. Rev. B* **93** (2016), no. 11, article ID 115429.
[252] N. H. Lindner, G. Refael, V. Galitski, "Floquet topological insulator in semiconductor quantum wells", *Nat. Phys.* **7** (2011), no. 6, p. 490.
[253] L. He *et al.*, "Floquet Chern insulators of light", *Nat. Commun.* **10** (2019), no. 1, p. 1-6.
[254] L. J. Maczewsky *et al.*, "Observation of photonic anomalous Floquet topological insulators", *Nat. Commun.* **8** (2017), article ID 13756.
[255] X.-L. Lü, H. Xie, "Topological phases and pumps in the Su–Schrieffer–Heeger model periodically modulated in time", *J. Phys.: Condens. Matter* **31** (2019), no. 49, article ID 495401.
[256] Q. Cheng *et al.*, "Observation of anomalous π modes in photonic Floquet engineering", *Phys. Rev. Lett.* **122** (2019), no. 17, article ID 173901.
[257] X. Liu, Q. Guo, J. Yang, "Miniaturization of Floquet topological insulators for airborne acoustics by thermal control", *Appl. Phys. Lett.* **114** (2019), no. 5, article ID 054102.
[258] L. He *et al.*, "Floquet Chern Insulators of Light", *preprint*, arXiv:1902.08560 (2019).
[259] C. M. Dai, W. Wang, X. X. Yi, "Photonic Floquet topological insulators with fluctuations and disorders", *Phys. Rev. A* **99** (2019), no. 3, article ID 033844.
[260] Y. Long, J. Ren, "Floquet topological acoustic resonators and acoustic Thouless pumping", *J. Acoust. Soc. Am.* **146** (2019), no. 1, p. 742-747.

[261] Y.-G. Peng, Z.-G. Geng, X.-F. Zhu, "Topologically protected bound states in one-dimensional Floquet acoustic waveguide systems", *J. Appl. Phys.* **123** (2018), no. 9, article ID 091716.
[262] Y.-G. Peng *et al.*, "Low-loss and broadband anomalous Floquet topological insulator for airborne sound", *Appl. Phys. Lett.* **110** (2017), no. 17, article ID 173505.
[263] W. Zhang, X. Chen, F. Ye, "Plasmonic topological insulators for topological nanophotonics", *Opt. Lett.* **42** (2017), no. 20, p. 4063-4066.
[264] S. Mukherjee *et al.*, "Experimental observation of anomalous topological edge modes in a slowly driven photonic lattice", *Nat. Commun.* **8** (2017), article ID 13918.
[265] M. Oudich *et al.*, "Space-time phononic crystals with anomalous topological edge states", *Phys. Rev. Res.* **1** (2019), no. 3, article ID 033069.
[266] Y. Zhang *et al.*, "Photonic Floquet topological insulators in atomic ensembles", *Laser Photonics Rev.* **9** (2015), no. 3, p. 331-338.
[267] H. Chen *et al.*, "Mechanical quantum Hall effect in time-modulated elastic materials", *Phys. Rev. Appl.* **11** (2019), no. 4, article ID 044029.
[268] M. C. Rechtsman *et al.*, "Photonic Floquet topological insulators", *Nature* **496** (2013), no. 7444, p. 196.
[269] R. Fleury, A. B. Khanikaev, A. Alu, "Floquet topological insulators for sound", *Nat. Commun.* **7** (2016), article ID 11744.
[270] M. Pasek, Y. D. Chong, "Network models of photonic Floquet topological insulators", *Phys. Rev. B* **89** (2014), no. 7, article ID 075113.
[271] P. Delplace, M. Fruchart, C. Tauber, "Phase rotation symmetry and the topology of oriented scattering networks", *Phys. Rev. B* **95** (2017), no. 20, article ID 205413.
[272] M. S. Rudner *et al.*, "Anomalous edge states and the bulk-edge correspondence for periodically driven two-dimensional systems", *Phys. Rev. X* **3** (2013), no. 3, article ID 031005.
[273] W. Hu *et al.*, "Measurement of a topological edge invariant in a microwave network", *Phys. Rev. X* **5** (2015), no. 1, article ID 011012.
[274] Y.-G. Peng *et al.*, "Experimental demonstration of anomalous Floquet topological insulator for sound", *Nat. Commun.* **7** (2016), article ID 13368.
[275] D. Leykam, M. C. Rechtsman, Y. D. Chong, "Anomalous topological phases and unpaired Dirac cones in photonic Floquet topological insulators", *Phys. Rev. Lett.* **117** (2016), no. 1, article ID 013902.
[276] M. Neupane *et al.*, "Observation of topological nodal fermion semimetal phase in ZrSiS", *Phys. Rev. B* **93** (2016), no. 20, article ID 201104.
[277] L. Xia *et al.*, "Observation of hourglass nodal lines in photonics", *Phys. Rev. Lett.* **122** (2019), no. 10, article ID 103903.
[278] M. Kim *et al.*, "Topologically nontrivial photonic nodal surface in a photonic metamaterial", *Phys. Rev. B* **99** (2019), no. 23, article ID 235423.
[279] W. Deng *et al.*, "Nodal rings and drumhead surface states in phononic crystals", *Nat. Commun.* **10** (2019), no. 1, p. 1769.
[280] H. Weng *et al.*, "Topological node-line semimetal in three-dimensional graphene networks", *Phys. Rev. B* **92** (2015), no. 4, article ID 045108.
[281] W. Gao *et al.*, "Experimental observation of photonic nodal line degeneracies in metacrystals", *Nat. Commun.* **9** (2018), no. 1, p. 950.
[282] H. C. Po, Y. Bahri, A. Vishwanath, "Phonon analog of topological nodal semimetals", *Phys. Rev. B* **93** (2016), no. 20, article ID 205158.
[283] L. Lu *et al.*, "Experimental observation of Weyl points", *Science* **349** (2015), no. 6248, p. 622-624.
[284] S.-Y. Xu *et al.*, "Discovery of a Weyl fermion semimetal and topological Fermi arcs", *Science* **349** (2015), no. 6248, p. 613-617.
[285] Y. Liu, Y. Xu, W. Duan, "Three-dimensional topological states of phonons with tunable pseudospin physics", *Research* **2019** (2019), article ID 5173580.
[286] M. Kim *et al.*, "Extremely broadband topological surface states in a photonic topological metamaterial", *Adv. Opt. Mater.* **7** (2019), article ID 1900900.
[287] L. Wang, S.-K. Jian, H. Yao, "Topological photonic crystal with equifrequency Weyl points", *Phys. Rev. A* **93** (2016), no. 6, article ID 061801.
[288] W. Ye *et al.*, "Photonic Hall effect and helical Zitterbewegung in a synthetic Weyl system", *Light: Sci. Appl.* **8** (2019), no. 1, p. 49.
[289] Y. Lu *et al.*, "Probing the Berry curvature and Fermi arcs of a Weyl circuit", *Phys. Rev. B* **99** (2019), no. 2, article ID 020302.
[290] H. Zhou *et al.*, "Observation of bulk Fermi arc and polarization half charge from paired exceptional points", *Science* **359** (2018), no. 6379, p. 1009-1012.
[291] A. A. Zyuzin, V. A. Zyuzin, "Chiral electromagnetic waves in Weyl semimetals", *Phys. Rev. B* **92** (2015), no. 11, article ID 115310.

[292] E. Goi *et al.*, "Observation of type I photonic Weyl points in optical frequencies", *Laser Photonics Rev.* **12** (2018), no. 2, article ID 1700271.
[293] Z. Yang, B. Zhang, "Acoustic type-II Weyl nodes from stacking dimerized chains", *Phys. Rev. Lett.* **117** (2016), no. 22, article ID 224301.
[294] B. Xie *et al.*, "Experimental realization of type-II Weyl points and Fermi arcs in phononic crystal", *Phys. Rev. Lett.* **122** (2019), no. 10, article ID 104302.
[295] X. Shi *et al.*, "Elastic Weyl points and surface arc states in three-dimensional structures", *Phys. Rev. Appl.* **12** (2019), no. 2, article ID 024058.
[296] Z. Song, X. Dai, "Hear the sound of Weyl fermions", *Phys. Rev. X* **9** (2019), no. 2, article ID 021053.
[297] Z. Yin *et al.*, "Tunable THz generalized Weyl points", *Opt. Express* **27** (2019), no. 2, p. 512-522.
[298] H. Ge *et al.*, "Experimental observation of acoustic weyl points and topological surface states", *Phys. Rev. Appl.* **10** (2018), no. 1, article ID 014017.
[299] M. Fruchart *et al.*, "Soft self-assembly of Weyl materials for light and sound", *Proc. Natl Acad. Sci. USA* **115** (2018), no. 16, p. E3655-E3664.
[300] D. Liu, J. Shi, "Circular phonon dichroism in Weyl semimetals", *Phys. Rev. Lett.* **119** (2017), no. 7, article ID 075301.
[301] T. Zhang *et al.*, "Double-weyl phonons in transition-metal monosilicides", *Phys. Rev. Lett.* **120** (2018), no. 1, article ID 016401.
[302] W. Gao *et al.*, "Photonic Weyl degeneracies in magnetized plasma", *Nat. Commun.* **7** (2016), article ID 12435.
[303] W.-J. Chen, M. Xiao, C. T. Chan, "Photonic crystals possessing multiple Weyl points and the experimental observation of robust surface states", *Nat. Commun.* **7** (2016), article ID 13038.
[304] S. M. Young *et al.*, "Dirac semimetal in three dimensions", *Phys. Rev. Lett.* **108** (2012), no. 14, article ID 140405.
[305] L. Lu *et al.*, "Symmetry-protected topological photonic crystal in three dimensions", *Nat. Phys.* **12** (2016), no. 4, p. 337.
[306] Y. Yang *et al.*, "Realization of a three-dimensional photonic topological insulator", *Nature* **565** (2019), no. 7741, p. 622.
[307] H.-X. Wang *et al.*, "Type-ii dirac photons", *NPJ Quantum Mater.* **2** (2017), no. 1, p. 54.
[308] Q. Guo *et al.*, "Three dimensional photonic Dirac points in metamaterials", *Phys. Rev. Lett.* **119** (2017), no. 21, article ID 213901.
[309] J. Y. Lin *et al.*, "Line nodes, Dirac points, and Lifshitz transition in two-dimensional nonsymmorphic photonic crystals", *Phys. Rev. B* **96** (2017), no. 7, article ID 075438.
[310] S. Borisenko *et al.*, "Experimental realization of a three-dimensional Dirac semimetal", *Phys. Rev. Lett.* **113** (2014), no. 2, article ID 027603.
[311] S. M. Young, C. L. Kane, "Dirac semimetals in two dimensions", *Phys. Rev. Lett.* **115** (2015), no. 12, article ID 126803.
[312] L. Lu *et al.*, "Weyl points and line nodes in gyroid photonic crystals", *Nat. Photonics* **7** (2013), no. 4, p. 294.
[313] M. Xiao *et al.*, "Synthetic gauge flux and Weyl points in acoustic systems", *Nat. Phys.* **11** (2015), no. 11, p. 920.
[314] F. Li *et al.*, "Weyl points and Fermi arcs in a chiral phononic crystal", *Nat. Phys.* **14** (2018), no. 1, p. 30.
[315] Q. Lin *et al.*, "Photonic Weyl point in a two-dimensional resonator lattice with a synthetic frequency dimension", *Nat. Commun.* **7** (2016), article ID 13731.
[316] M. G. Silveirinha, "Bulk-edge correspondence for topological photonic continua", *Phys. Rev. B* **94** (2016), no. 20, article ID 205105.
[317] S. Afzal, V. Van, "Topological phases and the bulk-edge correspondence in 2D photonic microring resonator lattices", *Opt. Express* **26** (2018), no. 11, p. 14567-14577.
[318] R.-J. Slager *et al.*, "Impurity-bound states and Green's function zeros as local signatures of topology", *Phys. Rev. B* **92** (2015), no. 8, article ID 085126.
[319] A. E. Hassan *et al.*, "Corner states of light in photonic waveguides", *Nat. Photon.* **13** (2019), no. 10, p. 697-700.
[320] B.-Y. Xie *et al.*, "Visualization of higher-order topological insulating phases in two-dimensional dielectric photonic crystals", *Phys. Rev. Lett.* **122** (2019), no. 23, article ID 233903.
[321] F. Liu, H.-Y. Deng, K. Wakabayashi, "Helical topological edge states in a quadrupole phase", *Phys. Rev. Lett.* **122** (2019), no. 8, article ID 086804.
[322] X. Zhang *et al.*, "Acoustic hierarchical topological insulators", *preprint*, arXiv:1811.05514 (2018).
[323] S.-y. Huo *et al.*, "Edge states and corner modes in second-order topological phononic crystal plates", *preprint*, arXiv:1905.09731 (2019).
[324] T. Mizoguchi, H. Araki, Y. Hatsugai, "Higher-order topological phase in a honeycomb-lattice model with anti-Kekulé distortion", *J. Phys. Soc. Japan* **88** (2019), no. 10, article ID 104703.
[325] H. Fan *et al.*, "Elastic higher-order topological insulator with topologically protected corner states", *Phys. Rev. Lett.* **122** (2019), no. 20, article ID 204301.
[326] W. A. Benalcazar, B. A. Bernevig, T. L. Hughes, "Quantized electric multipole insulators", *Science* **357** (2017), no. 6346, p. 61-66.
[327] S. Imhof *et al.*, "Topolectrical-circuit realization of topological corner modes", *Nat. Phys.* **14** (2018), no. 9, p. 925.

[328] C. W. Peterson *et al.*, "A quantized microwave quadrupole insulator with topologically protected corner states", *Nature* **555** (2018), no. 7696, p. 346.
[329] H. Xue *et al.*, "Acoustic higher-order topological insulator on a kagome lattice", *Nat. Mater.* **18** (2019), no. 2, p. 108.
[330] X. Ni *et al.*, "Observation of higher-order topological acoustic states protected by generalized chiral symmetry", *Nat. Mater.* **18** (2019), no. 2, p. 113.
[331] M. Serra-Garcia *et al.*, "Observation of a phononic quadrupole topological insulator", *Nature* **555** (2018), no. 7696, p. 342.
[332] X. Zhang *et al.*, "Second-order topology and multidimensional topological transitions in sonic crystals", *Nat. Phys.* **15** (2019), p. 582-588.
[333] S. A. A. Ghorashi *et al.*, "Second-order Dirac superconductors and magnetic field induced Majorana hinge modes", *Phys. Rev. B* **100** (2019), no. 2, article ID 020509.
[334] Y. Ota *et al.*, "Photonic crystal nanocavity based on a topological corner state", *Optica* **6** (2019), no. 6, p. 786-789.
[335] Y. Chen, X. Lu, H. Chen, "Effect of truncation on photonic corner states in a Kagome lattice", *Opt. Lett.* **44** (2019), no. 17, p. 4251-4254.
[336] B. Liu *et al.*, "Two-dimensional quadrupole topological insulator in γ-graphyne", *Nano Lett.* **19** (2019), no. 9, p. 6492-6497.
[337] L. Zhang *et al.*, "Higher-order photonic topological states in surface-wave photonic crystals", *preprint*, arXiv:1901.07154 (2019).
[338] S. N. Kempkes *et al.*, "Robust zero-energy modes in an electronic higher-order topological insulator", *Nat. Mater.* **18** (2019), p. 1292-1297.
[339] X.-D. Chen *et al.*, "Direct observation of corner states in second-order topological photonic crystal slabs", *Phys. Rev. Lett.* **122** (2019), no. 23, article ID 233902.
[340] Y. Volpez, D. Loss, J. Klinovaja, "Second-order topological superconductivity in π-junction rashba layers", *Phys. Rev. Lett.* **122** (2019), no. 12, article ID 126402.
[341] S.-B. Zhang, B. Trauzettel, "Detection of second-order topological superconductors by Josephson junctions", *Phys. Rev. Res.* **2** (2020), no. 1, article ID 012018.
[342] X.-L. Sheng *et al.*, "Two-dimensional second-order topological insulator in graphdiyne", *preprint*, arXiv:1904.09985 (2019).
[343] A. Agarwala, V. Juricic, B. Roy, "Higher Order Topological Insulators in Amorphous Solids", *preprint*, arXiv:1902.00507 (2019).
[344] S. Mittal *et al.*, "Photonic quadrupole topological phases", *Nat. Photonics* **13** (2019), p. 692-696.
[345] M. Weiner *et al.*, "Demonstration of a 3rd order hierarchy of higher order topological states in a three-dimensional acoustic metamaterial", *preprint*, arXiv:1903.00428 (2019).
[346] H. Xue *et al.*, "Realization of an acoustic third-order topological insulator", *Phys. Rev. Lett.* **122** (2019), no. 24, article ID 244301.
[347] X. Zhou *et al.*, "Optical isolation with nonlinear topological photonics", *New J. Phys.* **19** (2017), no. 9, article ID 095002.
[348] D. Leykam, Y. D. Chong, "Edge solitons in nonlinear-photonic topological insulators", *Phys. Rev. Lett.* **117** (2016), no. 14, article ID 143901.
[349] D. R. Gulevich *et al.*, "Exploring nonlinear topological states of matter with exciton-polaritons: edge solitons in kagome lattice", *Sci. Rep.* **7** (2017), no. 1, p. 1780.
[350] R. K. Pal *et al.*, "Amplitude-dependent topological edge states in nonlinear phononic lattices", *Phys. Rev. E* **97** (2018), no. 3, article ID 032209.
[351] B. G.-g. Chen, N. Upadhyaya, V. Vitelli, "Nonlinear conduction via solitons in a topological mechanical insulator", *Proc. Natl Acad. Sci. USA* **111** (2014), no. 36, p. 13004-13009.
[352] D. D. J. M. Snee, Y.-P. Ma, "Edge solitons in a nonlinear mechanical topological insulator", *Extreme Mech. Lett.* **76** (2019), article ID 100487.
[353] Y. Hadad, A. B. Khanikaev, A. Alu, "Self-induced topological transitions and edge states supported by nonlinear staggered potentials", *Phys. Rev. B* **93** (2016), no. 15, article ID 155112.
[354] Y. Hadad *et al.*, "Self-induced topological protection in nonlinear circuit arrays", *Nat. Electron.* **1** (2018), no. 3, p. 178.
[355] D. A. Dobrykh *et al.*, "Nonlinear control of electromagnetic topological edge states", *Phys. Rev. Lett.* **121** (2018), no. 16, article ID 163901.
[356] R. Chaunsali, T. Georgios, "Self-induced topological transition in phononic crystals by nonlinearity management", *Phys. Rev. B* **100** (2019), no. 1, article ID 014302.
[357] F. Zangeneh-Nejad, R. Fleury, "Nonlinear second-order topological insulators", *Phys. Rev. Lett.* **123** (2019), article ID 053902.
[358] A. Blanco-Redondo *et al.*, "Topological optical waveguiding in silicon and the transition between topological and trivial defect states", *Phys. Rev. Lett.* **116** (2016), no. 16, article ID 163901.

[359] L. Shen *et al.*, "Backscattering-immune one-way surface magnetoplasmons at terahertz frequencies", *Opt. Express* **23** (2015), no. 2, p. 950-962.
[360] H. Xu *et al.*, "Topological energy transfer in an optomechanical system with exceptional points", *Nature* **537** (2016), no. 7618, p. 80.
[361] Y.-X. Shen *et al.*, "Observation of low-loss broadband supermode propagation in coupled acoustic waveguide complex", *Sci. Rep.* **7** (2017), article ID 45603.
[362] Q. Wei *et al.*, "Experimental demonstration of topologically protected efficient sound propagation in an acoustic waveguide network", *Phys. Rev. B* **95** (2017), no. 9, article ID 094305.
[363] T. Jiang *et al.*, "Experimental demonstration of angular momentum-dependent topological transport using a transmission line network", *Nat. Commun.* **10** (2019), no. 1, p. 434.
[364] Y. Guo, T. Dekorsy, M. Hettich, "Topological guiding of elastic waves in phononic metamaterials based on 2D pentamode structures", *Sci. Rep.* **7** (2017), no. 1, article ID 18043.
[365] O. Oltulu *et al.*, "Topological insulator based locally resonant phononic crystals: wave propagation and acoustic band gaps", *Ferroelectrics* **499** (2016), no. 1, p. 123-129.
[366] R. Deshmukh *et al.*, "Long-range resonant energy transfer using optical topological transitions in metamaterials", *ACS Photonics* **5** (2018), no. 7, p. 2737-2741.
[367] C.-C. Chien *et al.*, "Topological quantization of energy transport in micromechanical and nanomechanical lattices", *Phys. Rev. B* **97** (2018), no. 12, article ID 125425.
[368] V. Peano *et al.*, "Topological phase transitions and chiral inelastic transport induced by the squeezing of light", *Nat. Commun.* **7** (2016), article ID 10779.
[369] S. A. H. Gangaraj, A. Nemilentsau, G. W. Hanson, "The effects of three-dimensional defects on one-way surface plasmon propagation for photonic topological insulators comprised of continuum media", *Sci. Rep.* **6** (2016), article ID 30055.
[370] A. P. Slobozhanyuk *et al.*, "Subwavelength topological edge states in optically resonant dielectric structures", *Phys. Rev. Lett.* **114** (2015), no. 12, article ID 123901.
[371] C.-Y. Ji *et al.*, "Transport tuning of photonic topological edge states by optical cavities", *Phys. Rev. A* **99** (2019), no. 4, article ID 043801.
[372] W.-M. Deng *et al.*, "Vortex index identification and unidirectional propagation in Kagome photonic crystals", *Nanophotonics* **8** (2019), no. 5, p. 833-840.
[373] M. He, L. Zhang, H. Wang, "Two-dimensional photonic crystal with ring degeneracy and its topological protected edge states", *Sci. Rep.* **9** (2019), no. 1, p. 3815.
[374] P. Wang, L. Lu, K. Bertoldi, "Topological phononic crystals with one-way elastic edge waves", *Phys. Rev. Lett.* **115** (2015), no. 10, article ID 104302.
[375] H. Dai *et al.*, "Observation of topological edge states of acoustic metamaterials at subwavelength scale", *J. Phys. D: Appl. Phys.* **51** (2018), no. 17, article ID 175302.
[376] Y. Jin, D. Torrent, B. Djafari-Rouhani, "Robustness of conventional and topologically protected edge states in phononic crystal plates", *Phys. Rev. B* **98** (2018), no. 5, article ID 054307.
[377] I. Kim, S. Iwamoto, Y. Arakawa, "Topologically protected elastic waves in one-dimensional phononic crystals of continuous media", *Appl. Phys. Express* **11** (2017), no. 1, article ID 017201.
[378] H. Liu *et al.*, "Thermally tunable topological edge states for in-plane bulk waves in solid phononic crystals", *Ultrasonics* **94** (2019), p. 227-234.
[379] B. Xie *et al.*, "Multiband asymmetric transmission of airborne sound by coded metasurfaces", *Phys. Rev. Appl.* **7** (2017), no. 2, article ID 024010.
[380] Z.-G. Chen *et al.*, "Multiple topological phase transitions in a gyromagnetic photonic crystal", *Phys. Rev. A* **95** (2017), no. 4, article ID 043827.
[381] S. A. Mann, D. L. Sounas, A. Alù, "Broadband delay lines and nonreciprocal resonances in unidirectional waveguides", *Phys. Rev. B* **100** (2019), article ID 020303.
[382] Y. V. Kartashov, D. V. Skryabin, "Two-dimensional topological polariton laser", *Phys. Rev. Lett.* **122** (2019), no. 8, article ID 083902.
[383] B. Bahari *et al.*, "Nonreciprocal lasing in topological cavities of arbitrary geometries", *Science* **358** (2017), no. 6363, p. 636-640.
[384] X.-C. Sun, X. Hu, "Topological ring-cavity laser formed by honeycomb photonic crystals", *preprint*, arXiv:1906.02464 (2019).
[385] C. Han *et al.*, "Lasing at topological edge states in a photonic crystal L3 nanocavity dimer array", *Light: Sci. Appl.* **8** (2019), no. 1, p. 40.
[386] J.-L. Xu *et al.*, "Ultrasensitive nonlinear absorption response of large-size topological insulator and application in low-threshold bulk pulsed lasers", *Sci. Rep.* **5** (2015), article ID 14856.
[387] H. Zhao *et al.*, "Topological hybrid silicon microlasers", *Nat. Commun.* **9** (2018), no. 1, p. 981.

[388] L. Pilozzi, C. Conti, "Topological cascade laser for frequency comb generation in PT-symmetric structures", *Opt. Lett.* **42** (2017), no. 24, p. 5174-5177.
[389] G. Harari *et al.*, "Topological insulator laser: theory", *Science* **359** (2018), no. 6381, article ID eaar4003.
[390] M. Hafezi *et al.*, "Robust optical delay lines with topological protection", *Nat. Phys.* **7** (2011), no. 11, p. 907.
[391] M. Hafezi *et al.*, "Imaging topological edge states in silicon photonics", *Nat. Photon.* **7** (2013), no. 12, p. 1001.
[392] M. A. Bandres *et al.*, "Topological insulator laser: experiments", *Science* **359** (2018), no. 6381, article ID eaar4005.
[393] F. Zangeneh-Nejad, R. Fleury, "Topological fano resonances", *Phys. Rev. Lett.* **122** (2019), no. 1, article ID 014301.
[394] A. Silva *et al.*, "Performing mathematical operations with metamaterials", *Science* **343** (2014), no. 6167, p. 160-163.
[395] A. Youssefi *et al.*, "Analog computing by Brewster effect", *Opt. Lett.* **41** (2016), no. 15, p. 3467-3470.
[396] F. Zangeneh-Nejad, R. Fleury, "Performing mathematical operations using high-index acoustic metamaterials", *New J. Phys.* **20** (2018), no. 7, article ID 073001.
[397] N. M. Estakhri, B. Edwards, N. Engheta, "Inverse-designed metastructures that solve equations", *Science* **363** (2019), no. 6433, p. 1333-1338.
[398] F. Zangeneh-Nejad, A. Khavasi, B. Rejaei, "Analog optical computing by half-wavelength slabs", *Opt. Commun.* **407** (2018), p. 338-343.
[399] F. Zangeneh-Nejad, A. Khavasi, "Spatial integration by a dielectric slab and its planar graphene-based counterpart", *Opt. Lett.* **42** (2017), no. 10, p. 1954-1957.
[400] F. Zangeneh-Nejad, R. Fleury, "Topological analog signal processing", *Nat. Commun.* **10** (2019), no. 1, p. 2058.
[401] M. Ezawa, "Topological switch between second-order topological insulators and topological crystalline insulators", *Phys. Rev. Lett.* **121** (2018), no. 11, article ID 116801.
[402] R. Süsstrunk, P. Zimmermann, S. D. Huber, "Switchable topological phonon channels", *New J. Phys.* **19** (2017), no. 1, article ID 015013.
[403] Y. Fan *et al.*, "Magnetization switching through giant spin-orbit torque in a magnetically doped topological insulator heterostructure", *Nat. Mater.* **13** (2014), no. 7, p. 699.
[404] J. Han *et al.*, "Room-temperature spin-orbit torque switching induced by a topological insulator", *Phys. Rev. Lett.* **119** (2017), no. 7, article ID 077702.
[405] N. H. D. Khang, Y. Ueda, P. N. Hai, "A conductive topological insulator with large spin Hall effect for ultralow power spin-orbit torque switching", *Nat. Mater.* **17** (2018), p. 808-813.
[406] J. Lee *et al.*, "All-fiberized, passively Q-switched 1.06 μm laser using a bulk-structured Bi_2Te_3 topological insulator", *J. Opt.* **16** (2014), no. 8, article ID 085203.
[407] Y. Chen *et al.*, "Large energy, wavelength widely tunable, topological insulator Q-switched erbium-doped fiber laser", *IEEE J. Sel. Top. Quantum Electron.* **20** (2013), no. 5, p. 315-322.
[408] H. Yu *et al.*, "Topological insulator as an optical modulator for pulsed solid-state lasers", *Laser Photonics Rev.* **7** (2013), no. 6, p. L77-L83.
[409] X. B. Wang *et al.*, "Topological-insulator-based terahertz modulator", *Sci. Rep.* **7** (2017), no. 1, article ID 13486.
[410] X. Xiao *et al.*, "All-electric spin modulator based on a two-dimensional topological insulator", *Appl. Phys. Lett.* **108** (2016), no. 3, article ID 032403.
[411] F. Hassler, A. R. Akhmerov, C. W. J. Beenakker, "Flat-lens focusing of electrons on the surface of a topological insulator", *Phys. Rev. B* **82** (2010), no. 12, article ID 125423.
[412] H. He *et al.*, "Topological negative refraction of surface acoustic waves in a Weyl phononic crystal", *Nature* **560** (2018), no. 7716, p. 61.
[413] T. Fujita, M. B. A. Jalil, S. G. Tan, "Topological insulator cell for memory and magnetic sensor applications", *Appl. Phys. Express* **4** (2011), no. 9, article ID 094201.
[414] L. Ye *et al.*, "Observation of acoustic valley vortex states and valley-chirality locked beam splitting", *Phys. Rev. B* **95** (2017), no. 17, article ID 174106.
[415] P. Qiu *et al.*, "Plasmonic valley chiral states in graphene based plasmonic crystals", *J. Phys. D: Appl. Phys.* **52** (2018), no. 1, article ID 015102.
[416] M. P. Makwana, R. Craster, S. Guenneau, "Novel topological beam-splitting in photonic crystals", *preprint*, arXiv:1902.00072 (2019).
[417] D. G. Rothe, E. M. Hankiewicz, "Tunable polarization in a beam splitter based on two-dimensional topological insulators", *Phys. Rev. B* **89** (2014), no. 3, article ID 035418.
[418] M. Makwana, R. Craster, S. Guenneau, "Topological beam-splitting in photonic crystals", *Opt. Express* **27** (2019), no. 11, p. 16088-16102.
[419] J. Lee *et al.*, "Passively Q-Switched 1.89-μm fiber laser using a bulk-structured Bi_2Te_3 topological insulator", *IEEE J. Sel. Top. Quantum Electron.* **21** (2014), no. 1, p. 31-36.
[420] H. Liu *et al.*, "Femtosecond pulse generation from a topological insulator mode-locked fiber laser", *Opt. Express* **22** (2014), no. 6, p. 6868-6873.
[421] Z.-C. Luo *et al.*, "2 GHz passively harmonic mode-locked fiber laser by a microfiber-based topological insulator saturable absorber", *Opt. Lett.* **38** (2013), no. 24, p. 5212-5215.

[422] M. Liu *et al.*, "Dual-wavelength harmonically mode-locked fiber laser with topological insulator saturable absorber", *IEEE Photonics Technol. Lett.* **26** (2014), no. 10, p. 983-986.
[423] P. Yan, R. Lin, H. Chen, H. Zhang, A. Liu, H. Yang, S. Ruan, "Topological insulator solution filled in photonic crystal fiber for passive mode-locked fiber laser", *IEEE Photonics Technol. Lett.* **27** (2014), no. 3, p. 264-267.
[424] F. Bernard *et al.*, "Towards mode-locked fiber laser using topological insulators", in *Nonlinear Photonics*, Optical Society of America, 2012.
[425] Z.-G. Geng *et al.*, "Acoustic delay-line filters based on largely distorted topological insulators", *Appl. Phys. Lett.* **113** (2018), no. 3, article ID 033503.
[426] Z. Zhang *et al.*, "Topological acoustic delay line", *Phys. Rev. Appl.* **9** (2018), no. 3, article ID 034032.
[427] K. Lai *et al.*, "Experimental realization of a reflections-free compact delay line based on a photonic topological insulator", *Sci. Rep.* **6** (2016), article ID 28453.
[428] Y. Wu *et al.*, "Applications of topological photonics in integrated photonic devices", *Adv. Optical Mater.* **5** (2017), no. 18, article ID 1700357.
[429] Y. Yang *et al.*, "Terahertz topological photonics for on-chip communication", *preprint*, arXiv:1904.04213 (2019).
[430] Z.-G. Chen *et al.*, "Acoustic frequency filter based on anisotropic topological phononic crystals", *Sci. Rep.* **7** (2017), no. 1, article ID 15005.
[431] F. Nathan, I. Martin, G. Refael, "Topological frequency conversion in a driven dissipative quantum cavity", *Phys. Rev. B* **99** (2019), no. 9, article ID 094311.
[432] Y. Wang *et al.*, "Topologically enhanced harmonic generation in a nonlinear transmission line metamaterial", *Nat. Commun.* **10** (2019), no. 1, p. 1102.
[433] C. Jürß, D. Bauer, "High-harmonic generation in Su–Schrieffer–Heeger chains", *Phys. Rev. B* **99** (2019), no. 19, article ID 195428.
[434] R. Ilan, F. De Juan, J. E. Moore, "Spin-based Mach-Zehnder interferometry in topological insulator p–n junctions", *Phys. Rev. Lett.* **115** (2015), no. 9, article ID 096802.
[435] V. Peano *et al.*, "Topological quantum fluctuations and traveling wave amplifiers", *Phys. Rev. X* **6** (2016), no. 4, article ID 041026.
[436] D. Malz, J. Knolle, A. Nunnenkamp, "Topological magnon amplification", *Nat. Commun.* **10** (2019), no. 1, p. 1-7.
[437] D. Leykam *et al.*, "Edge modes, degeneracies, and topological numbers in non-Hermitian systems", *Phys. Rev. Lett.* **118** (2017), no. 4, article ID 040401.
[438] K. Esaki *et al.*, "Edge states and topological phases in non-Hermitian systems", *Phys. Rev. B* **84** (2011), no. 20, article ID 205128.
[439] H. Zhao *et al.*, "Non-Hermitian topological light steering", *Science* **365** (2019), no. 6458, p. 1163-1166.
[440] M. S. Rudner, L. S. Levitov, "Topological transition in a non-hermitian quantum walk", *Phys. Rev. Lett.* **102** (2009), no. 6, article ID 065703.
[441] S. Longhi, D. Gatti, G. D. Valle, "Robust light transport in non-Hermitian photonic lattices", *Sci. Rep.* **5** (2015), article ID 13376.
[442] L. Li, C. H. Lee, J. Gong, "Geometric characterization of non-Hermitian topological systems through the singularity ring in pseudospin vector space", *Phys. Rev. B* **100** (2019), no. 7, article ID 075403.
[443] B. Midya, H. Zhao, L. Feng, "Non-Hermitian photonics promises exceptional topology of light", *Nat. Commun.* **9** (2018), no. 1, p. 2674.
[444] K. Y. Bliokh *et al.*, "Topological non-Hermitian origin of surface Maxwell waves", *Nat. Commun.* **10** (2019), no. 1, p. 580.
[445] A. Cerjan *et al.*, "Experimental realization of a Weyl exceptional ring", *Nat. Photon.* **13** (2019), p. 623-628.
[446] S. Malzard, C. Poli, H. Schomerus, "Topologically protected defect states in open photonic systems with non-Hermitian charge-conjugation and parity-time symmetry", *Phys. Rev. Lett.* **115** (2015), no. 20, article ID 200402.
[447] E. Edvardsson, F. K. Kunst, E. J. Bergholtz, "Non-Hermitian extensions of higher-order topological phases and their biorthogonal bulk-boundary correspondence", *Phys. Rev. B* **99** (2019), no. 8, article ID 081302.
[448] R. Chen *et al.*, "Finite-size effects in non-Hermitian topological systems", *Phys. Rev. B* **99** (2019), no. 15, article ID 155431.
[449] L. Xiao *et al.*, "Observation of topological edge states in parity-time-symmetric quantum walks", *Nat. Phys.* **13** (2017), no. 11, p. 1117.
[450] C. Sheng *et al.*, "Definite photon deflections of topological defects in metasurfaces and symmetry-breaking phase transitions with material loss", *Nat. Commun.* **9** (2018), no. 1, p. 4271.
[451] Ş. K. Özdemir *et al.*, "Parity-time symmetry and exceptional points in photonics", *Nat. Mater.* **18** (2019), p. 783-798.
[452] H. Shen, B. Zhen, L. Fu, "Topological band theory for non-Hermitian Hamiltonians", *Phys. Rev. Lett.* **120** (2018), no. 14, article ID 146402.
[453] Z. Gong *et al.*, "Topological phases of non-Hermitian systems", *Phys. Rev. X* **8** (2018), no. 3, article ID 031079.
[454] Y. Li *et al.*, "Waveguide metatronics: lumped circuitry based on structural dispersion", *Sci. Adv.* **2** (2016), no. 6, p. e1501790.

[455] H. M. Price *et al.*, "Four-dimensional quantum Hall effect with ultracold atoms", *Phys. Rev. Lett.* **115** (2015), no. 19, article ID 195303.
[456] M. Fremling *et al.*, "A Chern insulator in ln(8)/ln(3) dimensions", *preprint*, arXiv:1906.07387 (2019).
[457] Y. E. Kraus, Z. Ringel, O. Zilberberg, "Four-dimensional quantum Hall effect in a two-dimensional quasicrystal", *Phys. Rev. Lett.* **111** (2013), no. 22, article ID 226401.
[458] S.-C. Zhang, J. Hu, "A four-dimensional generalization of the quantum Hall effect", *Science* **294** (2001), no. 5543, p. 823-828.
[459] L. Yuan *et al.*, "Synthetic dimension in photonics", *Optica* **5** (2018), no. 11, p. 1396-1405.
[460] F. Mei *et al.*, "Topological insulator and particle pumping in a one-dimensional shaken optical lattice", *Phys. Rev. A* **90** (2014), no. 6, article ID 063638.
[461] E. Lustig *et al.*, "Photonic topological insulator in synthetic dimensions", *Nature* **567** (2019), no. 7748, p. 356.
[462] X.-W. Luo *et al.*, "Quantum simulation of 2D topological physics in a 1D array of optical cavities", *Nat. Commun.* **6** (2015), p. 7704.
[463] F. Mei *et al.*, "Simulating Z_2 topological insulators with cold atoms in a one-dimensional optical lattice", *Phys. Rev. A* **85** (2012), no. 1, article ID 013638.
[464] T. Ozawa, H. M. Price, "Topological quantum matter in synthetic dimensions", *Nat. Rev. Phys.* **1** (2019), p. 349-357.
[465] G. Salerno *et al.*, "Quantized Hall conductance of a single atomic wire: a proposal based on synthetic dimensions", *Phys. Rev. X* **9** (2019), no. 4, article ID 041001.
[466] C.-M. Jian, C. Xu, "Interacting topological insulators with synthetic dimensions", *Phys. Rev. X* **8** (2018), no. 4, article ID 041030.
[467] J. R. M. Silva *et al.*, "Phononic topological states in 1D quasicrystals", *J. Phys.: Condens. Matter* **31** (2019), article ID 505405.
[468] T. Ozawa *et al.*, "Synthetic dimensions in integrated photonics: from optical isolation to four-dimensional quantum Hall physics", *Phys. Rev. A* **93** (2016), no. 4, article ID 043827.
[469] D. J. Apigo *et al.*, "Observation of topological edge modes in a quasiperiodic acoustic waveguide", *Phys. Rev. Lett.* **122** (2019), no. 9, article ID 095501.
[470] Y. E. Kraus *et al.*, "Topological states and adiabatic pumping in quasicrystals", *Phys. Rev. Lett.* **109** (2012), no. 10, article ID 106402.
[471] M. Verbin *et al.*, "Observation of topological phase transitions in photonic quasicrystals", *Phys. Rev. Lett.* **110** (2013), no. 7, article ID 076403.
[472] Y. E. Kraus, O. Zilberberg, "Topological equivalence between the Fibonacci quasicrystal and the Harper model", *Phys. Rev. Lett.* **109** (2012), no. 11, article ID 116404.
[473] S. Ganeshan, K. Sun, S. D. Sarma, "Topological zero-energy modes in gapless commensurate Aubry–André–Harper models", *Phys. Rev. Lett.* **110** (2013), no. 18, article ID 180403.

Comptes Rendus

Physique

Objet de la revue

Les *Comptes Rendus Physique* sont une revue électronique évaluée par les pairs de niveau international, qui couvre l'ensemble des domaines de la physique et de l'astrophysique. Ils publient principalement des numéros thématiques, mais également des articles originaux de recherche, des annonces préliminaires, des articles de revue, des mises en perspective historiques, des textes à visée pédagogique ou encore des actes de colloque, sans limite de longueur, en anglais ou en français. Ils proposent également des numéros spéciaux consacrés à certains aspects récents et/ou significatifs de la discipline, dont les auteurs sont choisis parmi les chercheurs les plus actifs sur le sujet et dont la coordination est assurée par des rédacteurs en chef invités.

Les *Comptes Rendus Physique* sont diffusés selon une politique vertueuse de libre accès diamant, gratuit pour les auteurs (pas de frais de publications) comme pour les lecteurs (libre accès immédiat et pérenne).

À propos de la revue

Toutes les informations concernant la revue, y compris le texte des articles publiés qui est en accès libre intégral, figurent sur le site https://comptes-rendus.academie-sciences.fr/physique/.

Informations à l'attention des auteurs

Pour toute question relative à la soumission des articles, les auteurs peuvent consulter le site https://comptes-rendus.academie-sciences.fr/physique/.

Contact

Académie des sciences
23, quai de Conti, 75006 Paris, France
Tél. : (+33) (0)1 44 41 43 72
CR-Physique@academie-sciences.fr

Comptes Rendus
de l'Académie des sciences

Physique

Volume 21, nº 4-5, août-septembre 2020

Special issue / *Numéro thématique*
Metamaterials 1 / *Métamatériaux 1*

Guest editors / *Rédacteurs en chef invités*
Boris Gralak (CNRS, Institut Fresnel, Marseille, France)
Sébastien Guenneau (UMI2004 Abraham de Moivre, CNRS-Imperial College, London, UK)

1878-1535 (electronic)

Académie des sciences — Paris

COMPTES RENDUS
DE L'ACADÉMIE DES SCIENCES

Physique

Volume 21, nº 4-5, août-septembre 2020